



KATHOLIEKE UNIVERSITEIT LEUVEN
FACULTEIT INGENIEURSWETENSCHAPPEN
DEPARTEMENT CHEMISCHE INGENIEURSTECHNIEKEN
AFDELING TOEGEPASTE FYSISCHE SCHEIKUNDE EN
MILIEUTECHNOLOGIE
W. De Croylaan 46, B-3001 Leuven (Belgium)

INFLUENCE OF MEMBRANE CHARACTERISTICS ON FLUX DECLINE AND RETENTION IN NANOFILTRATION

Promotor:
Prof. dr. ir. B. Van der Bruggen
Prof. dr. C. Vandecasteele

Proefschrift voorgedragen tot
het behalen van het doctoraat
in de ingenieurswetenschappen

door

Katleen BOUSSU

Oktober 2007



KATHOLIEKE UNIVERSITEIT LEUVEN

FACULTEIT INGENIEURSWETENSCHAPPEN

DEPARTEMENT CHEMISCHE INGENIEURSTECHNIEKEN

AFDELING TOEGEPASTE FYSISCHE SCHEIKUNDE EN

MILIEUTECHNOLOGIE

W. De Croylaan 46, B-3001 Leuven (Belgium)

INFLUENCE OF MEMBRANE CHARACTERISTICS ON FLUX DECLINE AND RETENTION IN NANOFILTRATION

Examencommissie:

Prof. dr. ir. P. Van Houtte, voorzitter

Prof. dr. ir. B. Van der Bruggen, promotor

Prof. dr. C. Vandecasteele, promotor

Prof. dr. ir. I. Vankelecom, assessor

Prof. dr. ir. P. Van Puyvelde, assessor

Prof. dr. M. Nyström

(Lappeenranta University of Technology, Finland)

Prof. dr. ir. P. Van der Meeren

(Universiteit Gent, Belgium)

Proefschrift voorgedragen tot

het behalen van het doctoraat
in de ingenieurswetenschappen

door

Katleen BOUSSU

U.D.C. 66.06

Oktober 2007

© Katholieke Universiteit Leuven – Faculteit Ingenieurswetenschappen
Arenbergkasteel, B-3001 Leuven (Belgium)

Alle rechten voorbehouden. Niets uit deze uitgave mag worden vermenigvuldigd en/of openbaar worden gemaakt door middel van druk, fotocopie, microfilm, elektronisch of op welke andere wijze ook zonder voorafgaandelijke schriftelijke toestemming van de uitgever.

All rights reserved. No part of the publication may be reproduced in any form by print, fotoprint, microfilm or any other means without written permission from the publisher.

D/2007/7515/94

ISBN 978-90-5682-860-8

Dankwoord

Het resultaat van vier jaar onderzoek ligt op dit moment in uw handen. Het waren vier boeiende en leerrijke jaren, bestaande uit periodes met experimenteel labowerk afgewisseld met periodes met (al dan niet verplicht) interpretatie- en schrijfwerk. Dit boekje zou uiteraard niet tot stand zijn gekomen zonder de hulp van een heleboel mensen, tot wie ik op deze pagina een woord van dank zou willen richten.

In eerste instantie zou ik mijn promotoren, professor Bart Van der Bruggen en professor Carlo Vandecasteele, willen danken voor het aanreiken van dit onderwerp en het aanbieden van de vele kansen en mogelijkheden tijdens mijn doctoraat. Bart, onze vele discussies, de daaruit voortvloeiende nieuwe inzichten en je niet aflatende steun en wijze raad zullen me altijd bijblijven. Ook uit je geduldig lezen en corrigeren van de vele teksten heb ik veel bijgeleerd.

Ook wil ik mijn assessoren, professor Peter Van Puyvelde en professor Ivo Vankelecom, danken voor hun interesse in mijn werk en het zorgvuldig nalezen van deze tekst.

Verder wens ik het Instituut voor de Aanmoediging van Innovatie door Wetenschap en Technologie in Vlaanderen (IWT) te vermelden omwille van zijn genereuze financiële steun gedurende dit project.

Tijdens mijn doctoraat heb ik de kans gekregen om met verschillende mensen samen te werken. Deze contacten waren stuk voor stuk boeiend en lieten mij toe de membranen eens vanuit een ander standpunt te bekijken. Daarom een welgemeend dank je wel aan:

- Jérémie De Baerdemaeker (UGent) voor de PAS metingen en de vele discussies;
- professor Paul Van der Meeren en Jan Cocquyt (UGent) voor het ter beschikking stellen van de stromingspotential setup en voor het inwijden in de wereld van de colloïden;
- professor Chris Van Hasendonck, Alexander Volodin en Johan Snauwaert (KULeuven) voor de talloze AFM metingen;

- professor Diederik Depla (UGent) voor de XPS metingen en hun interpretatie;
- professor Ivo Vankelecom en Steliana Aldea (KULeuven) voor de ATR-FTIR metingen;
- professor Jan Delcour en Valerie Van Craeyveld (KULeuven) voor de GPC metingen.

De heer Luc Stubbe (zaakvoerder van Mr. Shine) en de collega's van KHKempen (Ward Colen en Guy Van Baelen) dank ik voor het wegwijs maken in de wereld van de carwash, voor de hulp bij de staalnames en voor de antwoorden op de vele vragen.

I would like to thank professor Charles Linder, Slava Freger and Yoram Oren from the Ben-Gurion University of the Negev (Israel) for the many interesting discussions about membrane synthesis, every time we met on a conference.

Bill Mickols (DOW/FilmTec) is acknowledged for supplying the membrane samples of NF270, NF90 and BW30XLE.

Niet alleen de samenwerking met andere onderzoeksgroepen, maar zeker ook het contact met naaste colleges maakte de voorbije vier jaar tot een boeiende en onvergetelijke periode. Stefanie (*l'astre de la maison*), Ben (*expert op het vlak van ontwijken van nieuwsgierige vragen én baby's*), Geert (*in den beginne bureaugenoot én membraancollega*), Adrian (*Thijn- en vogelfanaat*), Alexander (*†, woorden schieten tekort*), Agnieszka (*my teammate in membrane synthesis*), Leen (*van thesisbegeleidster naar toffe bureaugenote*), Tom (*dé specialist in BBQ*), Jo (*onze agenda*), Kathleen (*fan van Sesamstraat*), Jeroen (*helemaal naar Zuid-Korea én terug*), Johan (*taartjes of toch balkjes?*), Steven (*stille waters*), Dimitri en Daneel (*al even verdwenen, maar nog niet vergeten*): telkens zorgden zij voor een toffe werksfeer op het labo, voor levendige discussies over al dan niet wetenschappelijke onderwerpen en voor praktische ondersteuning tijdens mijn verboden-labo periodes.

Maar ook de hulp van Michèle, Christine, Elvira en Solvita was onmisbaar bij het uitvoeren van experimenten in het labo of bij het analyseren van het afvalwater. Ook Beatrice, Marie-Claude, Alena, Bart, Herman, Tony, Guido en Mark stonden altijd klaar om te helpen bij administratieve taken van de MaNaMa Milieu, (alweer dringende) bestellingen, rare pomp- of computerkuren of gewoon voor een deugddoende babbel.

Tijdens dit doctoraat heb ik ook samengewerkt met verschillende thesisstudenten. Bedankt Joachim, Céline, Aline, Inge en Karen voor het (soms vele) experimentele werk en de boeiende discussies. Het was fijn met jullie samen te werken.

Tenslotte wil ik zeker ook nog mijn hele familie in de bloemetjes zetten, die, ook al snapten ze niet altijd volledig wat ik daar allemaal in het *verre* Leuven uitspookte, toch keer op keer geïnteresseerd vroegen hoe het *op school* was. Ook mijn ouders, Karolien, Thierry en Sven verdienen een applausje, niet alleen voor hun hulp tijdens de laatste maanden, maar vooral voor hun morele en rustgevende steun.

En natuurlijk mogen mijn twee jongens zeker niet ontbreken in dit dankwoord! Philip, dank je wel om er altijd voor mij te zijn, niet alleen om mij te motiveren en te steunen, maar ook om mij soms (terecht) in te tomen in al mijn enthousiasme. Je bent er één uit de duizend, net zoals onze kleine Lucas! Jouw guitig en ondeugend lachje was de beste remedie om alle zorgen te relativeren en vergeten.

Voor stampertje

Katleen

Oktober 2007

List of symbols

a	colloid radius (m)
a	regression parameter
A	channel cross-sectional area for measurements of streaming potential (m ²)
A_i	photoelectron peak area (-)
$A_{membrane}$	membrane surface (m ²)
$b_1...b_p$	regression parameters
c_j	correction factor coefficient in calculation of log P (-)
C	concentration (mol L ⁻¹)
C_f	feed concentration (mol L ⁻¹)
C_i	atomic concentration percentage (-)
C_i	Cook's distance (-)
C_p	permeate concentration (mol L ⁻¹)
d	distance between colloids (m)
d	escape depth of emitted electrons (m)
E	positron energy (eV)
E	total interaction energy between colloids (J)
E_i	residue
f_i	fragment coefficient in calculation of log P (-)
F	Faraday constant (96,487 C mol ⁻¹)
h	Planck's constant (6.626·10 ⁻³⁴ J s)
H	Hamaker constant (J)
h_{ii}	leverage (-)
H_{11}	Hamaker constant of colloid (J)
H_{22}	Hamaker constant of water (J)
i	component i (-)
I	intensity (-)
J	water flux (L m ⁻² h ⁻¹)
J_p	permeate flux (L m ⁻² h ⁻¹)
J_w	pure water flux (L m ⁻² h ⁻¹)

List of symbols

k	Boltzmann constant ($1.38 \cdot 10^{-23} \text{ J K}^{-1}$)
$\log P$	logarithm of octanol-water partition coefficient (-)
L	channel length for measurements of streaming potential (m)
M_w	molecular mass (Da)
n_i	number of times a fragment occurs in the structure to calculate $\log P$ (-)
n_j	number of times a correction factor occurs in the structure to calculate $\log P$ (-)
N	number of data points (-)
q	adsorbed amount on membrane surface (mol m^{-2})
p	number of variables in regression model (-)
P	octanol-water partition coefficient (-)
r	pore size (m)
r_{PEG}	Stokes-Einstein radius of polyethylene glycol (m)
r_{50}	mean pore size (m)
R	universal gas constant ($8.31 \text{ J mol}^{-1} \text{ K}^{-1}$)
R	channel resistance for measurements of streaming potential (m^{-1})
R_a	resistance due to adsorption (m^{-1})
R_c	resistance due to cake formation (m^{-1})
R_{cp}	resistance due to concentration polarization (m^{-1})
R_f	fouling resistance (m^{-1})
R_g	resistance due to gel layer formation (m^{-1})
R_i	retention of component i (-)
R_i	resistance due to specific interactions between membrane and solute (m^{-1})
R_m	membrane resistance (m^{-1})
R_{rms}	root-mean-squared roughness (m)
R_p	resistance due to pore blocking (m^{-1})
R_{tot}	total resistance (m^{-1})
R^2	correlation coefficient (-)
S_{Ei}	variance of the residue
S_i	sensitivity factor (-)

List of symbols

S_{Mw}, S_p	measure for the distribution of the pore sizes (-)
T	temperature (K)
V	volume of feed solution (L)
V	volume of the pores (m ³)
V_p	permeate volume (L)
\bar{x}	average of all x_i values
$x_1 \dots x_p$	independent variables
Y	response variable
Y_i	observed variable
\bar{z}	average of all z_n values (m)
\bar{z}	mean positron implantation depth (m)
z_n	data point of roughness profile (m)
ΔC	concentration difference (mol L ⁻¹)
ΔE	difference in electric potential (V)
ΔE	streaming potential (V)
Δt	measurement time (s)
ΔT	temperature difference (K)
$\Delta \pi$	osmotic pressure (bar)
ΔP	transmembrane pressure difference (bar)
Δx	distance between membrane surface and plane of shear (m)
ϵ_o	vacuum dielectric permittivity ($8.85 \cdot 10^{-12}$ F m ⁻¹)
ϵ_r	relative dielectric permittivity (-)
ζ	zeta potential (V)
η	viscosity (Pa s)
θ	contact angle (°)
θ	analysis takeoff angle (°)
$\bar{\theta}$	average of all θ_n values (°)
θ_n	data point of the phase shift profile (°)
Θ	reflection angle (°)

List of symbols

θ_{rms}	root-mean-squared phase shift ($^{\circ}$)
κ^{-1}	Debye length (m)
κ	conductivity ($S\ m^{-1}$)
λ_e	mean free path for electrons (m)
μ	electrophoretic mobility ($m^2\ V^{-1}\ s^{-1}$)
ν	frequency of photons (s^{-1})
ρ	density ($kg\ m^{-3}$)
σ	retention (-)
τ	positron lifetime (s)
ψ	surface potential (V)

List of acronyms

AD	Adsorbed amount
ADJR ²	Adjusted Correlation Coefficient
AFM	Atomic Force Microscopy
ATR-FTIR	Attenuated Total Reflectance – Fourier Transform InfraRed
BE	Binding Energy of core electrons
BOD	Biological Oxygen Demand
C	Cyclone
CA	Cellulose Acetate
CMC	Critical Micelle Concentration
COD	Chemical Oxygen Demand
CP	Concentration Polarization
DBAR	Doppler Broadening of the Annihilation Radiation
DIPS	Diffusion Induced Phase Separation
DLVO	Derjaguin – Landau – Verwey – Overbeek
DMF	N,N-Dimethylformamide
DSC	Differential Scanning Calorimetry
DSR	Dynamic Stress Rheometer
D13	Laboratory-made membrane (32 % PES/DMF on FO2413)
D71	Laboratory-made membrane (32 % PES/DMF on FO2471)
FEG-SEM	Field Emission Gun – Scanning Electron Microscope
FIB	Focused Ion Beam
FTIR	Fourier Transform InfraRed
FWHM	Full-width half-maximum
HPLC	High Performance Liquid Chromatography
MCT	Mercury-Cadmium-Telluride
MF	Microfiltration
MWCO	Molecular Weight Cut-off (shortly cut-off)
NC-AFM	Non-Contact mode Atomic Force Microscopy
NF	Nanofiltration
NMP	N-Methyl-pyrrolidone

List of acronyms

N13	Laboratory-made membrane (30 % PES/NMP on FO2413)
N71	Laboratory-made membrane (30 % PES/NMP on FO2471)
o-Ps	Ortho-Positronium
PA	Polyamide
PALS	Positron Annihilation Lifetime Spectroscopy
PAS	Positron Annihilation Spectroscopy
PE	Polyethylene
PEG	Polyethylene glycol
PES	Polyethersulfone
PI	Polyimide
PP	Polypropylene
PPA	Polypiperazineamide
p-Ps	Para-Positronium
Ps	Positronium
RF	Relative Flux
RMS	Root-Mean-Squared
RO	Reverse Osmosis
SDBS	Sodium Dodecylbenzenesulfonate
SEM	Scanning Electron Microscopy
SF	Sand Filter
T-AFM	Tapping mode Atomic Force Microscopy
TFC	Thin Film Composite membranes
TGA	ThermoGravimetric Analysis
UF	Ultrafiltration
VIF	Variance Inflation number
XPS	X-ray Photoelectron Spectroscopy

Table of contents

Abstract.....	1
Nederlandstalige samenvatting.....	3
1 Membrane technology.....	17
1.1 Introduction	18
1.2 Pressure-driven membrane processes and nanofiltration	19
1.3 Principles and definitions	22
1.4 Flux decline and fouling	23
1.4.1 Mechanisms of flux decline	23
1.4.2 Fouling	26
1.5 Aim of this work and research approach	26
2 Methods and materials.....	29
2.1 Nanofiltration experiments	30
2.1.1 Filtration equipment	30
2.1.2 Selection of commercial membranes	33
2.2 Adsorption experiments	35
2.3 Synthesis of polyethersulfone membranes	36
2.4 Membrane characterization techniques	37
2.4.1 Atomic Force Microscopy	37
2.4.1.1 Theoretical background	37
2.4.1.2 Experimental conditions	40
2.4.2 Contact angle measurements	42
2.4.3 Determination of cut-off	43
2.4.4 Measurements of the streaming potential	43
2.4.5 Positron Annihilation Spectroscopy	45
2.4.5.1 Theoretical background	45
2.4.5.2 Experimental conditions	48
2.4.6 Attenuated Total Reflectance-Fourier Transform InfraRed	49

2.4.7 X-ray Photoelectron Spectroscopy	50
2.4.8 Scanning Electron Microscopy	51
2.4.9 Differential Scanning Calorimetry	52
2.4.10 Pre-treatment of membrane samples	53
2.5 Selection of feed components	53
2.5.1 Selection of organic components (uncharged and charged)	54
2.5.2 Selection and characterization of colloids	58
2.5.2.1 Characterization of colloids	58
2.5.2.2 DLVO theory	59
2.6 Chemical analysis of aqueous solutions	60
2.6.1 UV-VIS spectrophotometry	60
2.6.1.1 Analysis of saccharides	61
2.6.1.2 Analysis of amino acids	61
2.6.1.3 Analysis of surfactants	61
2.6.2 High Performance Liquid Chromatography	63
2.6.3 Determination of suspended and settleable solids, COD and BOD	64
2.7 Statistical methods: multiple linear regression	64
2.7.1 Principle of multiple linear regression	64
2.7.2 Selection of independent x variables	65
2.7.3 Diagnostics of the regression method	66
2.7.4 Experimental conditions	67
3 Synthesis of polyethersulfone membranes.....	69
3.1 Introduction	70
3.2 Preparation of membranes without support layer	73
3.2.1 Influence of the polymer concentration	74
3.2.2 Influence of the relative air humidity	76
3.2.3 Influence of additives to the polymer solution	78
3.2.4 Influence of additives to the non-solvent bath and the bath temperature	79
3.2.5 Influence of the solvent	80

3.2.6 Conclusion	82
3.3 Preparation of membranes on a support layer	82
3.3.1 Influence of the polymer concentration	83
3.3.2 Characterization of the membranes	86
3.3.3 Testing of the performance of the membranes	88
3.3.3.1 Evaluation of the retention of laboratory-made membranes	88
3.3.3.2 Evaluation of the relative flux of laboratory-made membranes	92
3.4 Conclusion	94
4 Physico-chemical characterization of nanofiltration membranes.....	95
4.1 Introduction	96
4.2 Chemical characterization of nanofiltration membranes	97
4.2.1 ATR-FTIR Spectroscopy	98
4.2.2 X-ray Photoelectron Spectroscopy	101
4.2.3 Conclusion	104
4.3 Physical characterization of nanofiltration membranes	104
4.3.1 Determination of the cut-off	104
4.3.2 Determination of the surface roughness	106
4.3.3 Determination of the surface hydrophobicity	110
4.3.4 Determination of the surface charge	112
4.3.5 Conclusion	113
4.4 Positron Annihilation Spectroscopy	114
4.4.1 <i>S</i> parameter	114
4.4.2 <i>R</i> parameter	115
4.4.3 Positron Annihilation Lifetime Spectroscopy	118
4.4.4 Comparison between cut-off and pore sizes obtained by PALS	121
4.5 Conclusion	124

5 Relation between characteristics and performance of nanofiltration membranes.....	125
5.1 Introduction	126
5.2 Nanofiltration performance during filtration of aqueous solutions containing dissolved organic components	126
5.2.1 Filtration of aqueous solutions containing dissolved uncharged organic components	128
5.2.1.1 Adsorption of uncharged organic components	131
5.2.1.2 Relative flux of uncharged organic components	133
5.2.1.3 Retention of uncharged organic components	135
5.2.1.4 Conclusion for uncharged organic components	137
5.2.2 Filtration of aqueous solutions containing dissolved charged organic components	139
5.2.2.1 Adsorption of charged organic components	142
5.2.2.2 Relative flux of charged organic components	143
5.2.2.3 Retention of charged organic components	147
5.2.2.4 Conclusion for charged organic components	149
5.3 Nanofiltration performance during filtration of colloidal dispersions	150
5.3.1 Introduction	150
5.3.2 Characterization of colloids	152
5.3.3 Influence of membrane characteristics on colloidal fouling	154
5.3.4 Influence of colloid characteristics on colloidal fouling	160
5.3.4.1 Influence of colloid charge	160
5.3.4.2 Influence of colloid size	161
5.3.4.3 Influence of colloid concentration	163
5.3.5 Influence of solution chemistry on colloidal fouling	165
5.3.5.1 Influence of pH	165
5.3.5.2 Influence of salt concentration	167
5.3.6 Conclusion for colloidal dispersions	169
5.4 General conclusion	169

6	Regeneration of carwash wastewater by nanofiltration.....	171
6.1	Introduction	172
6.2	Surfactant fouling of nanofiltration membranes	173
6.2.1	Introduction	173
6.2.2	Effect of the type of surfactant	176
6.2.2.1	Effect of the type of surfactant on adsorption and hydrophobicity	176
6.2.2.2	Effect of the type of surfactant on fouling and retention	180
6.2.3	Effect of the surfactant concentration	183
6.2.4	Effect of the addition of salt	184
6.2.4.1	Effect of the addition of salt on adsorption and hydrophobicity	184
6.2.4.2	Effect of the addition of salt on fouling and retention	186
6.2.5	Effect of pH of the surfactant solution	187
6.2.5.1	Effect of pH of the surfactant solution on adsorption and hydrophobicity	187
6.2.5.2	Effect of pH of the surfactant solution on fouling and retention	189
6.2.6	Effect of a mixture of surfactants	190
6.2.7	Conclusion	191
6.3	Applicability of nanofiltration in the carwash industry	192
6.3.1	Description of the selected carwash	192
6.3.1.1	Use of surfactants	192
6.3.1.2	Actual wastewater purification installation	193
6.3.2	Analysis of the wastewaters	194
6.3.3	Filtration experiments of the different wastewaters	197
6.3.3.1	Fouling results during filtration of carwash wastewater	198
6.3.3.2	Retention results during filtration of carwash wastewater	199

Table of contents

6.3.4 Cleaning procedure	201
6.4 Conclusion	203
Summary and general conclusions.....	205
References.....	211
Appendix I: Chemical structure of uncharged organic components..	235
Appendix II: Chemical structure of charged organic components....	237
List of publications.....	239
Curriculum vitae.....	243

Abstract

This dissertation investigates the influence of membrane characteristics on fouling and retention in nanofiltration. Laboratory-made nanoporous polyethersulfone membranes were studied, in addition to commercial nanofiltration membranes. A thorough physico-chemical characterization of the membranes allowed to distinguish two membrane classes, i.e., a polyamide and a polyethersulfone class. The pore size distribution in the skin layer of all commercial nanofiltration membranes was observed to be a bimodal instead of the well accepted log-normal function. Moreover, the cut-off did not correlate with the pore sizes, but rather with the ratio of the volume fraction of the large pores to the volume fraction of all pores.

Which membrane characteristic has the largest influence on the performance, depended on the characteristics of the (aqueous) feed solution. In the case that the feed solution contained dissolved organic components, a low volume fraction of small pores was desirable to minimize fouling. In addition, a large surface charge and a high hydrophilicity were favourable for filtration of charged components. For minimal colloidal fouling, a hydrophilic membrane surface was also the most important selection criterion. The retention of organic components was determined mainly by the cut-off of the commercial nanofiltration membranes; during filtration of charged organic components, the interplay between membrane and component charge was also crucial.

A case-study about recycling of wastewater in the carwash industry, indicated that a hydrophilic nanofiltration membrane with small pores should be selected, so that high permeate fluxes in combination with high retentions are obtained. Moreover, with this membrane, only a cleaning step with water appeared necessary to reach the original pure water flux.

Nederlandstalige samenvatting

Invloed van membraaneigenschappen op vervuiling en retentie in nanofiltratie

1 Inleiding

Nanofiltratie is een drukgedreven membraanproces waarbij kleine organische componenten (groter dan 200 Da) en multivalente ionen uit waterige oplossingen kunnen verwijderd worden. Een van de grote problemen bij de industriële implementatie van nanofiltratie is het optreden van membraanvervuiling, wat leidt tot een daling van de permeaatflux doorheen het membraan. Deze fluxdaling dient geminimaliseerd te worden, aangezien de flux doorheen het membraan bepalend is voor de benodigde membraanoppervlakte (en dus de kostprijs) bij filtratie van een bepaalde afvalstroom.

De doelstelling van dit werk was het bestuderen van de performantie (vervuiling en retentie) bij nanofiltratiemembranen op basis van de membraankarakteristieken. Dit zal toelaten om in een specifieke toepassing, het optimale membraan te selecteren.

2 Materiaal en Methoden

Tijdens de experimenten werd er gebruik gemaakt van een commerciële cross-flow nanofiltratie-eenheid op laboschaal (Amafilter, Test Rig PSSITZ), uitgerust met twee parallelle TZA 944 membraan modules. Met deze opstelling kan zowel de relatieve flux als de retentie van een bepaalde component bepaald worden. De relatieve flux is een maat voor de membraanvervuiling en is gedefinieerd als de verhouding van de permeaatflux ($L m^{-2} h^{-1}$) tot de flux van zuiver water; de retentie geeft weer hoeveel percent van een component wordt tegengehouden door het membraan. Een andere belangrijke membraanparameter is de waterpermeabiliteit, die de flux geeft per eenheid druk ($L m^{-2} h^{-1} bar^{-1}$).

In deze studie werden zowel commerciële als zelfaangemaakte (zie hoofdstuk 3) polymere membranen beschouwd. De membranen zijn dunne-film-composiet membranen, bestaande uit een dunne dense toplaag op een asymmetrische poreuze steunlaag. De volgende commerciële membranen werden geselecteerd: UTC20 (toplaag van polypiperazine amide); NF270, Desal51HL en Desal5DL (toplaag van polyamide); N30F en NFPES10 (toplaag van polyethersulfon); en NTR7450 (toplaag van gesulfoneerd polyethersulfon).

3 Synthese van polyethersulfon membranen

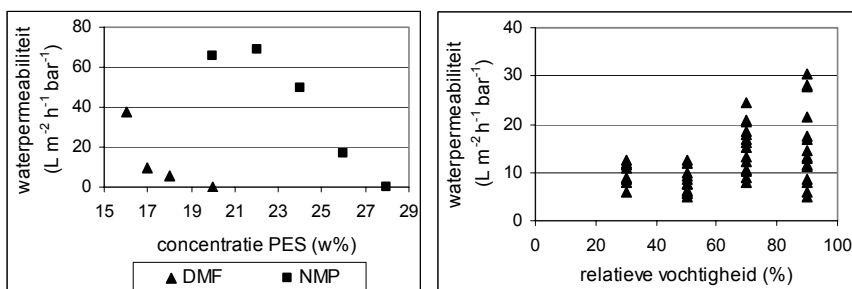
Een grondige kennis van membraaneigenschappen is noodzakelijk om membraanvervuiling beter te begrijpen. Aangezien de informatie gegeven door de membraanfabrikanten eerder beperkt is, werd er in deze studie geopteerd om zelf polyethersulfon membranen aan te maken met behulp van DIPS (Diffusie Geïnduceerde Fase Scheiding). Deze techniek houdt in dat een polymeeroplossing (van polyethersulfon (PES) opgelost in een solvent (N,N-dimethylformamide (DMF) of N-methyl-pyrrolidone (NMP)) wordt uitgestreken tot een dunne film op een steunlaag en vervolgens wordt ondergedompeld in een niet-solvent bad. Door een diffusiegedreven uitwisseling tussen solvent en niet-solvent, treedt er een fasescheiding op van de oorspronkelijk thermodynamisch stabiele polymeeroplossing in een polymeerrijke (de membraanmatrix) en een polymeearme fase (de poriën).

Synthese van membranen zonder steunlaag

Voor polyethersulfon membranen zonder steunlaag werden verschillende synthesefactoren geoptimaliseerd voor het verkrijgen van een nanoporeus membraan. De bestudeerde synthesefactoren waren de polymeerconcentratie, de relatieve vochtigheid, toevoeging van verschillende componenten aan het niet-solvent bad (bvb. alcohol) en aan de polymeeroplossing (bvb. niet-solvent, aceton), en de temperatuur van het niet-solvent bad.

De experimentele resultaten geven aan dat het beste nanoporeus membraan verkregen werd met een polymeeroplossing bestaande uit 17 % PES/DMF of 26 % PES/NMP (Figuur 1) in een atmosfeer met een relatieve vochtigheid gelijk aan

40 % (Figuur 1) en een niet-solvent bad van gedistilleerd water op 293 K. Deze membranen vertoonden een goede reproduceerbaarheid, een permeabiliteit vergelijkbaar met commerciële nanofiltratiemembranen en een retentie van 99 % voor congo rood (negatief geladen component met moleculaire massa 697 Da). Ook het gebruikte solvent (DMF of NMP) had een invloed op de membraanstructuur, zoals blijkt uit het verschil in waterpermeabiliteit (Figuur 1).



Figuur 1: Invloed van respectievelijk de polymerconcentratie en de relatieve vochtigheid (voor 17 % PES/DMF) op de waterpermeabiliteit (in dead-end)

Synthese van membranen met steunlaag

De optimale synthesefactoren werden vervolgens aangewend om polyethersulfon membranen aan te maken op een polymere steunlaag (FO2471 (PP/PE) of FO2413 (polyester)): **D13** en **D71** (voor een polymeeroplossing van 32 % PES in DMF op respectievelijk FO2413 en FO2471), en **N13** en **N71** (voor een polymeeroplossing van 30 % PES in NMP op respectievelijk FO2413 en FO2471).

De karakteristieken van deze membranen waren vergelijkbaar met deze van commerciële PES membranen (N30F en NFPES10), met uitzondering van de moleculaire gewichtscut-off (de moleculaire massa van een component met 90 % retentie, kortweg cut-off). Door de hogere cut-off van de zelfaangemaakte membranen (2000 Da in vergelijking met 1200 Da voor NFPES10) vertoonden deze membranen een lagere retentie voor raffinose (Tabel 1). Echter, voor negatief geladen componenten was de retentie vergelijkbaar; positief geladen componenten werden zelfs beter tegengehouden door de zelfaangemaakte membranen (vooral zichtbaar voor methyleenblauw). Een mogelijke verklaring hiervoor is de kleinere oppervlaktelading van de zelfaangemaakte membranen.

Tabel 1: Retentie (%) na twee uur filtratie in cross-flow met een voedingsconcentratie van 2 mmol L⁻¹ (raffinose) of 0.2 mmol L⁻¹ (andere componenten)

component	moleculaire massa (Da)	lading (neutrale pH)	N13	D71	NFPES10
raffinose	504	0	28	33	58
difenyaminsulfonzuur	271	-	82	75	87
congorood	697	-	100	99	100
methyleenblauw	320	+	80	80	32
janusgroen	511	+	96	99	95

4 Fysico-chemische karakterisatie van nanofiltratiemembranen

Zowel de commerciële als de zelfaangemaakte membranen werden gekarakteriseerd naar chemische samenstelling en enkele fysische karakteristieken, die bepalend (kunnen) zijn in het verklaren van membraanvervuiling. Bovendien werd er een voor nanofiltratie nieuwe techniek toegepast, met name PAS (Positron Annihilatie Spectroscopie), waarmee het mogelijk is om een beeld te krijgen van de dikte en de poriëngrootte van de toplaag.

Chemische karakterisatie van nanofiltratiemembranen

Een combinatie van de resultaten verkregen met ATR-FTIR (“Attenuated Total Reflectance-Fourier Transform InfraRed”) en XPS (“X-ray Photoelectron Spectroscopy”) toonde aan dat de membranen kunnen onderverdeeld worden in twee verschillende klassen: een polyamide klasse (bestaande uit Desal51HL, Desal5DL en NF270) en een polyethersulfon klasse (bestaande uit N30F, NFPES10, NTR7450, N13 en D71).

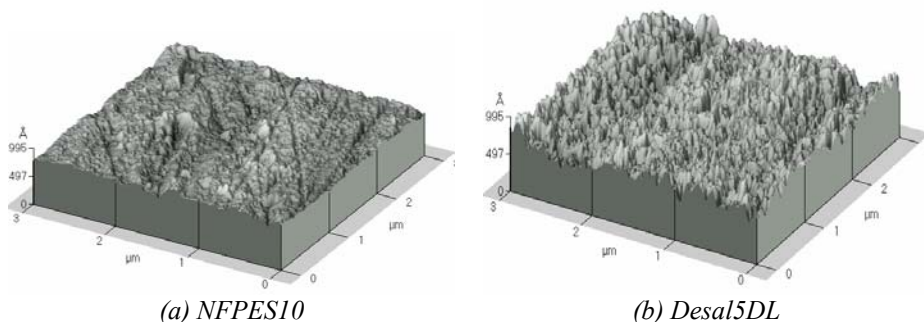
De structuur van de membranen uit de polyamide klasse is opgebouwd uit minimum drie lagen: (1) een dunne toplaag van polyamide, (2) een tussenlaag van poly(aryleensulfon ether) voor Desal5DL en NF270 of meer specifiek poly(fenyleensulfon ether) voor Desal51HL, en (3) een polyester steunlaag. Voor de polyethersulfon klasse werden slechts twee lagen geobserveerd: (1) een toplaag

van poly(fenyleensulfon ether) of de meer algemene structuur poly(aryleensulfon ether) in geval van NTR7450, en (2) een steunlaag van PP/PE of, in geval van NTR7450 en N13 een polyester steunlaag.

Fysische karakterisatie van nanofiltratiemembranen

Verscheidene fysische karakteristieken werden nagegaan voor de geselecteerde membranen, met name de cut-off, ruwheid, hydrofobiciteit en oppervlaktelading. De cut-off werd bepaald door het uitvoeren van filtratie-experimenten met een mengsel van polyethyleenglycolen, gevolgd door het fitten van de retentiecurve met het lognormaal model.

Zowel non-contact (Figuur 2) als tapping mode AFM (“Atomic Force Microscopy”) werden gebruikt ter bepaling van de ruwheid: de resultaten voor beide modes waren vergelijkbaar (met hogere ruwheden verkregen in tapping mode AFM), op voorwaarde dat hetzelfde scangebied beschouwd werd.



Figuur 2: Driedimensionale beelden verkregen met non-contact mode AFM van (a) een glad membraan, NFPE510 en (b) een ruw membraan, Desal5DL op een scangebied van 3 μm x 3 μm

De hydrofobiciteit van het membraanoppervlak werd nagegaan met behulp van de contacthoek en de faseverschuiving in tapping mode AFM, waaruit bleek dat een hydrofoob membraanoppervlak overeenkwam met een grote contacthoek en een kleine faseverschuiving.

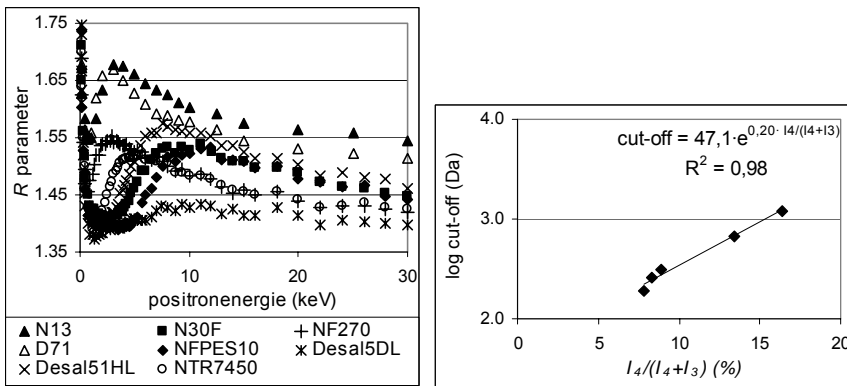
Een waarde van de zeta potentiaal (een maat voor de oppervlaktelading) werd verkregen door het uitvoeren van stromingspotentiaalmetingen in functie van de pH. Alle membranen zijn negatief geladen bij hoge pH en positief of neutral geladen bij lage pH.

Uit de resultaten van de fysische karakterisatie bleek dat dezelfde membraanklassen kunnen onderscheiden worden, aangezien de polyamide klasse de laagste cut-off en de meest ruwe en meest hydrofiele toplaag heeft.

Positron Annihilatie Spectroscopie (PAS)

De PAS techniek is gebaseerd op de studie van de annihilatiefenomenen na het implanteren van positronen in het membraan. Zowel de levensduur van de geïmplanteerde positronen (PALS, Positron Annihilatie Levensduur Spectroscopie) als de energiehuishouding van de annihilatie (*S* en *R* parameter) werden hierbij bestudeerd. De *S* parameter beschrijft de verbreding van de annihilatiepiek op 511 keV (DBAR, “Doppler Broadening of the Annihilation Radiation”) en geeft dus een indicatie van de chemie op de plaats van annihilatie.

De *R* parameter geeft de verhouding weer tussen 3 γ en 2 γ en bevat dus informatie over de grootte en de concentratie van de poriën: de lage porositeit in de toplaag van de membranen weerspiegelde zich in de lage waarde van de *R* parameter (Figuur 3) bij lage positronenergie. Op basis van het verloop van de *R* parameter, werd een positronenergie van 2 keV geselecteerd voor het uitvoeren van de PALS analyse op de toplaag van de commerciële membranen.



Figuur 3: R parameter (of de verhouding van 3 γ op 2 γ annihilatie) in functie van de positronenergie, en de correlatie tussen cut-off (Da) en $I_4 / (I_4 + I_3)$ (%)

In PALS is vooral de pick-off annihilatie van o-Ps (ortho-positronium) van belang, aangezien deze levensduur (τ_3) kan omgerekend worden naar een poriëngrootte

(r_3). De bijhorende spectrale intensiteit (I_3) is een maat voor de volumefractie van deze poriën. De resultaten van de PALS analyse zijn samengevat in Tabel 2. Uit de PALS resultaten volgde dat de distributie van de poriëngroottes in nanofiltratie eerder een bimodale functie was (in plaats van een lognormale functie). Bovendien gaf PALS aan dat een membraan met een hogere cut-off (of dus ook een grotere r_{50}) gekarakteriseerd werd door kleinere poriën (r_3 en r_4) in combinatie met een grotere volumefractie van de poriën (I_3 en I_4). De selectiviteit van een nanofiltratiemembraan werd dus niet bepaald door de poriëngrootte, maar eerder door de verhouding (Figuur 3) van de volumefractie van grote poriën (I_4) tot de volumefractie van alle poriën ($I_3 + I_4$).

Tabel 2: Selectieve samenvatting van de resultaten verkregen met PALS

	r_3 (nm)	r_4 (nm)	I_3 (%)	I_4 (%)	cut-off (Da)	r_{50} (nm)
Desal51HL	0,155	0,375	35,4	3,0	190	0,24
NFPES10	0,130	0,320	49,5	9,7	1200	0,46

In de toplaag van de zelfgemaakte membranen daarentegen, waren drie verschillende poriëngroottes aanwezig. Hiervan kwam de grootste poriëngrootte ($r_5 = 0,65$ nm) wel overeen met de gemiddelde poriëngrootte tijdens filtratie (r_{50}), aangezien deze membranen dichter bij ultrafiltratie aanleunen en het zeefeffect dus meer van belang wordt.

5 Relatie tussen de karakteristieken en de performantie van nanofiltratiemembranen

Zowel membraan- als voedingskarakteristieken bepalen de performantie van een membraan. Daarom werden drie verschillende voedingsoplossingen beschouwd:

- waterige oplossingen van opgeloste ongeladen organische componenten;
- waterige oplossingen van opgeloste geladen organische componenten;
- colloïdale dispersies.

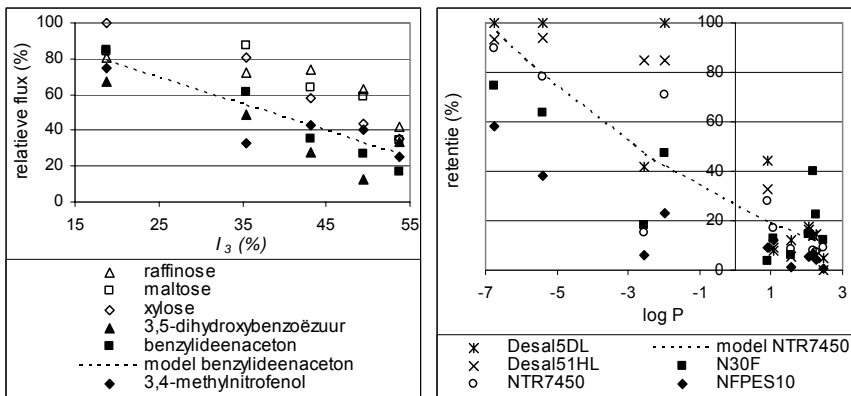
Telkens werden filtratie-experimenten uitgevoerd en werd met behulp van meervoudige lineaire regressie nagegaan welke membraan- of voedingskarakteristiek de meeste invloed had op de membraanprestatie (relatieve flux en retentie).

Filtratie van waterige oplossingen met opgeloste ongeladen organische componenten

Filtratie- en adsorptie-experimenten werden uitgevoerd met 11 ongeladen organische componenten. De hydrofobiciteit van deze componenten ($\log P$) bleek de belangrijkste variabele te zijn om de geadsorbeerde hoeveelheid en de retentie (Figuur 4) te verklaren. Ook bij de relatieve flux was deze variabele van belang. Dit impliceert dat met toenemende hydrofobiciteit, adsorptie en vervuiling toenemen terwijl de retentie afneemt.

Wat de membraanvariabelen betreft, was de volumefractie van de kleine poriën (I_3) uitermate belangrijk om fluxvermindering te minimaliseren (Figuur 4). De volumefractie van de grote poriën (I_4) en de cut-off bepaalden respectievelijk de geadsorbeerde hoeveelheid en de retentie.

De optimale membraankeuze gedurende filtratie van ongeladen organische componenten is dus een membraan met een lage volumefractie van poriën.



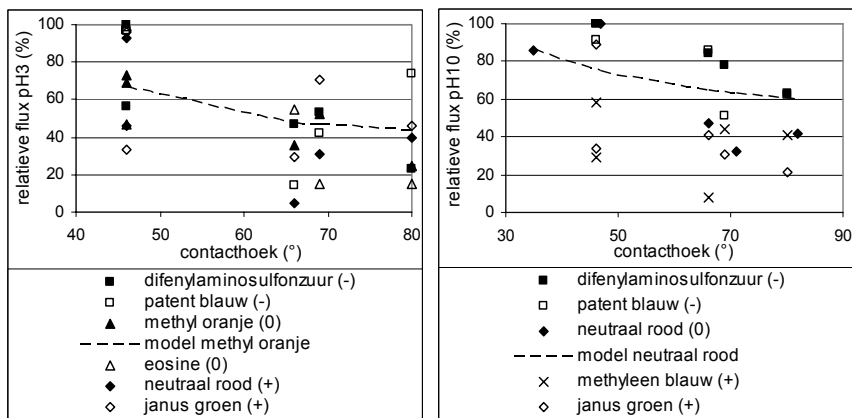
Figuur 4: Relatieve flux (%) en retentie (%) voor ongeladen organische componenten in functie van respectievelijk I_3 en $\log P$

Filtratie van waterige oplossingen met opgeloste geladen organische componenten

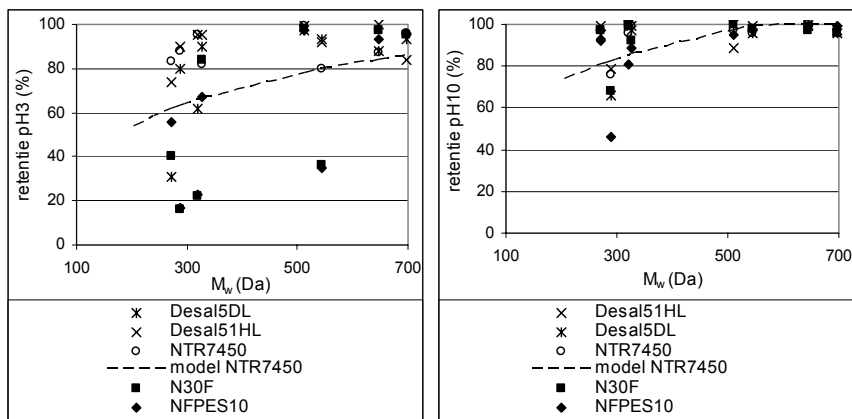
Filtratie- en adsorptie-experimenten werden uitgevoerd met 13 geladen organische componenten bij pH 3 en 10. Net zoals bij de ongeladen organische componenten, had de volumefractie van de kleine poriën (I_3) en de cut-off een invloed op respectievelijk de fluxvermindering en de retentie, als elke pH afzonderlijk werd beschouwd.

Gedurende filtratie van geladen organische componenten, bleek tevens de hydrofobiciteit van het membraanoppervlak (met name de contacthoek, Figuur 5) cruciaal te zijn in de beschrijving van de fluxvermindering. Dit is in tegenstelling met de ongeladen organische componenten, waar de contacthoek enkel belangrijk bleek te zijn na uitsluiting van I_3 en I_4 uit de statistische analyse. Omwille van elektrostatische interacties tussen het membraan en de geladen organische componenten, waren tevens de lading van membraan en component invloedrijk. De moleculaire massa van de componenten was zelfs de meest cruciale variabele in de verklaring van de retentie (Figuur 6).

De optimale membraankeuze tijdens filtratie van geladen organische componenten is dus een hydrofiel membraan met lage cut-off.



Figuur 5: Relatieve flux (%) voor geladen organische componenten in functie van de contacthoek bij pH 3 en pH 10

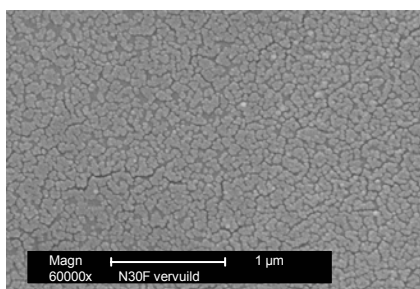


Figuur 6: Retentie (%) voor geladen organische componenten in functie van de moleculaire massa bij pH 3 en pH 10

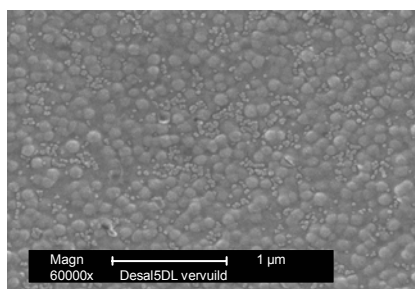
Filtratie van colloïdale dispersies

Uit filtratie-experimenten met 4 verschillende colloïdale dispersies bleek dat de contacthoek de meest invloedrijke factor was bij colloïdale vervuiling (onafhankelijk van lading en grootte van colloïd) door de vorming van uniforme, dense cake laag (Figuur 7) op het membraanoppervlak. Enkel tijdens filtratie van kleine colloïden met behulp van ruwe membranen (Figuur 7), speelde “valley clogging” een secundaire rol in membraanvervuiling.

De optimale membraankeuze tijdens filtratie van colloïdale dispersies is dus een hydrofiel, glad membraan.



N30F



Desal5DL

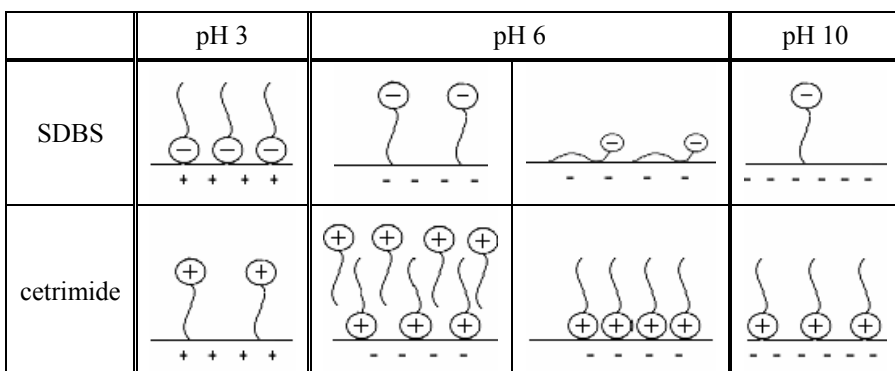
Figuur 7: Tweedimensionale beelden verkregen met SEM na filtratie van een Ludox CL dispersie (100 mg L^{-1} , neutrale pH, geen toevoeging van zout) met N30F (een hydrofoob membraan) en Desal5DL (een ruw membraan)

6 Regeneratie van afvalwater van de carwash met nanofiltratie

De implementatie van nanofiltratie om afvalwater in de carwash industrie te recyclen werd bestudeerd voor een typische automatische carwash. Omdat het afvalwater echter een complex mengsel is van verschillende componenten (waaronder surfactanten), werd de membraanperformantie eerst bestudeerd voor synthetische oplossingen van surfactanten.

Filtratie van waterige oplossingen met surfactanten

De fluxvermindering veroorzaakt door surfactanten was minimaal bij minimale adsorptie en indien de hydrofiële (geladen) kop van de surfactanten naar de oplossing was gericht waardoor het membraanoppervlak meer hydrofiel werd (Figuur 8). De minste fluxvermindering werd vastgesteld voor het anionisch surfactant (SDBS). Bij neutrale pH werd de meeste vervuiling vastgesteld voor het kationisch surfactant (cetrimide), omwille van de tegengestelde lading van membraan en surfactant. Zowel een hogere surfactantconcentratie als het toevoegen van een elektrolyet hadden een nadelige invloed op de fluxvermindering. Een verandering van de pH kon zowel een positieve als een negatieve invloed hebben op de membraanperformantie: voor cetrimide werd de hoogste relatieve flux geobserveerd bij lage pH, terwijl een hoge pH gunstig was voor SDBS.

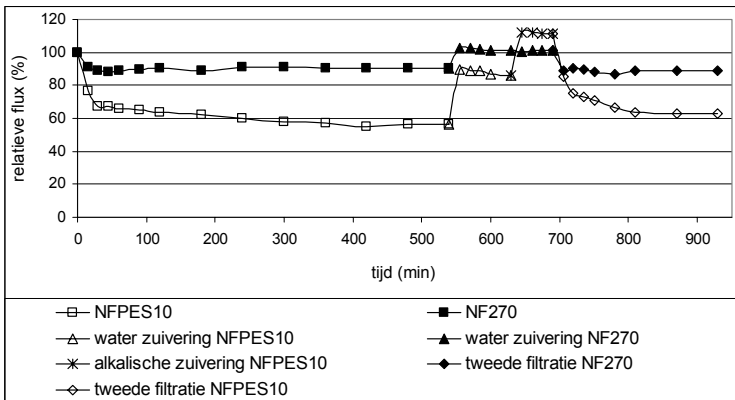


Figuur 8: Schema van de oriëntatie van SDBS (anionisch) en cetrimide (kationisch) aan het membraanoppervlak in functie van de pH

Filtratie van afvalwater van een automatische carwash

Momenteel wordt, met behulp van een cycloon, een lamellen- en een zandfilter, het afvalwater in de carwash gerecycleerd om de auto's te spoelen. Om dit afvalwater ook te kunnen gebruiken tijdens het wasproces, is een verdere zuivering noodzakelijk, waarvoor nanofiltratie een oplossing kan bieden. Hiervoor is een membraan met een hoge waterpermeabiliteit, een hoge relatieve flux en een hoge retentie vereist.

Dit werd het best verkregen met behulp van een hydrofiel membraan met kleine poriën (NF270, Figuur 9). Met dit hydrofiel membraan werd een permeaatflux bekomen van $45 \text{ L m}^{-2} \text{ h}^{-1} \text{ bar}^{-1}$, die slechts 5 % van de oorspronkelijke concentraties aan surfactanten en organische componenten bevatte. Een bijkomend voordeel van dit membraan was dat een reiniging met water gedurende 15 minuten reeds voldoende was om de oorspronkelijk flux van zuiver water terug te bereiken. Geen verdere chemische reiniging was vereist en er werd ook geen beschadiging of degradatie van het membraan vastgesteld na reiniging.



Figuur 9: Evolutie van de relatieve flux (%) voor NFPE10 en NF270 gedurende filtratie van afvalwater van de carwash (verzameld na de zandfilter), gedurende reiniging met water en alkalische producten (enkel voor NFPE10), en gedurende een tweede filtratie met hetzelfde afvalwater

Algemeen besluit

Dit onderzoek geeft aan dat het type voedingsoplossing tijdens filtratie de keuze van het meest geschikte nanofiltratiemembraan sterk beïnvloedt. Naast

componenteigenschappen (zoals hydrofobiciteit en lading), gaf meervoudige lineaire regressie aan dat de volgende membraankarakteristieken dienen gecontroleerd te worden voor een minimale fluxvermindering:

- de volumefractie van kleine poriën: tijdens filtratie van organische componenten;
- de hydrofobiciteit van het membraanoppervlak: tijdens filtratie van organische componenten en colloïdale dispersies;
- de oppervlaktelading: tijdens filtratie van geladen organische componenten;
- de oppervlakteruwheid: tijdens filtratie van dispersies met kleine colloïden.

Het retentiemechanisme van organische componenten bij NF was vooral afhankelijk van de cut-off en, bij geladen organische componenten, van de membraanlading.

Om deze vaststellingen te kunnen uitbreiden naar andere membranen, is een grondige (fysico-chemische) karakterisatie van de beschouwde membranen noodzakelijk, zoals uiteengezet in deze studie. Ook de aanmaak van PES membranen bleek nuttig in vergelijking met de karakteristieken en de membraanperformantie van commerciële PES membranen.

Bovendien bleek ook de beschouwde toepassing succesvol te zijn, aangezien de resultaten aantoonde dat nanofiltratie kan ingeschakeld worden om het afvalwater te recycleren in de carwash industrie.

Chapter 1

Membrane technology

1.1 Introduction

Membranes play a central role in our daily life. To say it with the words of Bowen (Yamazaki, 1998): “If you are tired of membranes, you are tired of life.” Biological membranes are hardly used in industrial applications, but separations with synthetic membranes have become increasingly important.

The heart of every membrane process is formed by the membrane itself, which can be considered as a permselective barrier or interface between two homogeneous phases (Figure 1.1). Separation is achieved because the membrane transports one component more readily than others due to differences in physical and/or chemical properties between the membrane and the permeating components.

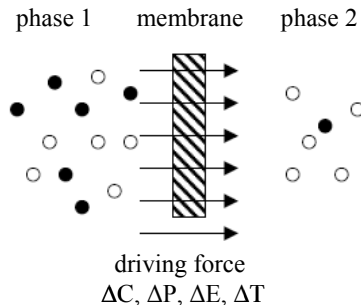


Figure 1.1: Schematic representation of a two-phase system separated by a membrane

Transport through the membrane only takes place when a driving force is applied to the feed. Possible driving forces are a pressure difference (ΔP), a concentration difference (ΔC), a temperature difference (ΔT) or a difference in electric potential (ΔE) across the membrane. Table 1.1 summarizes the different types of membrane processes and their respective driving forces (Mulder, 1996).

Table 1.1: Overview of membrane processes and their driving force

ΔP	ΔC	ΔT	ΔE
microfiltration	pervaporation	thermo-osmosis	electrodialysis
ultrafiltration	gas separation	membrane distillation	electro-osmosis
nanofiltration	dialysis		
reverse osmosis	liquid membranes		

As shown in Table 1.1, a large number of membrane processes are in use today. These processes have important advantages compared to traditional separation processes, such as continuous working mode, reduced energy consumption, easy scale-up and modular design of membrane installations allowing high flexibility (Mulder, 1996). Furthermore, no additional chemicals are required during the membrane process and combination with other separation techniques can lead to improved separations. The main disadvantages are loss of performance due to membrane fouling (section 1.4) and additional costs from membrane cleaning (which may need additional chemicals) and replacement.

1.2 Pressure driven membrane processes and nanofiltration

Pressure driven membrane processes are used to remove different types of solutes from a liquid feed stream. Generally, four different types are distinguished (Mulder, 1996): microfiltration (MF), ultrafiltration (UF), nanofiltration (NF) and reverse osmosis (RO). Figure 1.2 illustrates the separation possibilities of the four processes.

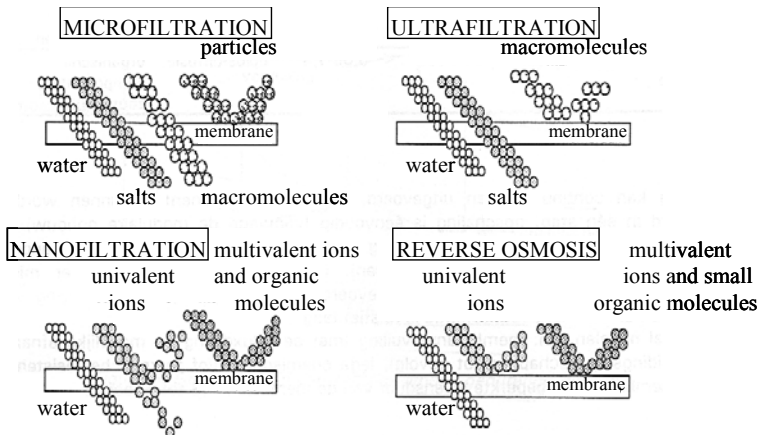


Figure 1.2: Schematic representation of microfiltration, ultrafiltration, nanofiltration and reverse osmosis

Microfiltration (MF) only retains particles by means of sieving. The average pore size ranges from 0.1 to 10 μm and low pressures (0.1 – 2 bar) are sufficient to obtain high permeabilities ($> 50 \text{ L m}^{-2} \text{ h}^{-1} \text{ bar}^{-1}$). Microfiltration is frequently used as a pre-treatment step for nanofiltration or reverse osmosis.

Ultrafiltration (UF) retains both particles and macromolecules by the same sieving mechanism as MF. UF membranes are characterized by their molecular weight cut-off (shortly cut-off), which is the molecular mass of a solute with 90 % retention. Components with a molecular mass above the cut-off have a high retention, whereas components with a molecular mass below the cut-off are retained only partially. The cut-off for UF lies typically between a few 1,000 and 100,000 Da, which corresponds with pore sizes between a few nanometer and 0.1 μm . Permeabilities between 10 and 50 $\text{L m}^{-2} \text{ h}^{-1} \text{ bar}^{-1}$ are obtained with pressures between 1 and 5 bar.

With reverse osmosis (RO) it is possible to retain small organic molecules and ions from a solution. As this process uses dense membranes which have a high hydrodynamic resistance, low permeabilities ($0.05 - 1.4 \text{ L m}^{-2} \text{ h}^{-1} \text{ bar}^{-1}$) are only realized with high-pressure gradients (10 – 100 bar). Instead of sieving, separation is obtained due to sorption and diffusion through the membrane.

Nanofiltration (NF) is situated between UF and RO. These membranes found their origin in the 1970s and the 1980s as modified RO membranes having high water fluxes. NF membranes require much lower pressures (5 – 20 bar) than RO, leading to significant energy savings. Moreover, NF combines a high permeability ($1.5 - 15 \text{ L m}^{-2} \text{ h}^{-1} \text{ bar}^{-1}$) with a high retention of dissolved organic molecules with a molecular mass above 200 Da. The cut-off of NF is situated between 150 and 1,000 Da. Due to charge interactions with the membrane, multivalent ions are also well retained.

Several polymeric NF membranes, made of cellulose acetate (CA), polyamide (PA), polypiperazineamide (PPA), polyimide (PI) or polyethersulfone (PES), are

nowadays commercially available. These polymeric membranes, with the exception of cellulose acetate and polyimide (which form symmetric membranes), are all thin film composite membranes (TFC, Figure 1.3) (Mulder, 1996).

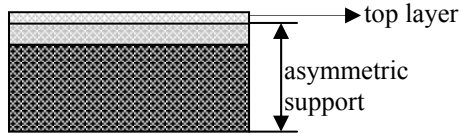


Figure 1.3: Schematic representation of a thin film composite membrane

This means that they have a thin dense top layer (tens to hundreds of nanometers) on an asymmetric support. The asymmetric support consists of a thin top layer (0.1 to 0.5 μm) supported by a porous sub layer (50 to 150 μm). Due to their structure, TFC membranes combine the high selectivity of a dense membrane with the high permeation rate of a very thin membrane. The top layer or skin determines the transport rate, while the porous sub layer acts only as a support to give the membrane its mechanical strength. Moreover, the top layer and the sub layer are composed of different polymers, so that each layer can be optimized independently to obtain the optimal selectivity, permeation rate and chemical and thermal stability.

Nanofiltration membranes are used in a wide range of applications:

- water softening (Cyna *et al.*, 2002; Schäfer *et al.*, 2001);
- removal of pesticides, endocrine disruptors and other organic micropollutants (Yoon *et al.*, 2007; Nghiem *et al.*, 2004);
- treatment of wastewater from the textile industry (Akbari *et al.*, 2006; De Florio *et al.*, 2005; Lopes *et al.*, 2005; Schoeberl *et al.*, 2005);
- purification of effluents from pulp and paper industry (Mänttari *et al.*, 2006; Nuortila-Jokinen *et al.*, 2004);
- water reuse in the brewery sector (Braeken *et al.*, 2004);
- purification of pharmaceutical broths (Capelle *et al.*, 2002);
- purification of process water in the food industry (Jiao *et al.*, 2004; Moresi and Lo Presti, 2003; Mänttari and Nyström, 2004).

1.3 Principles and definitions

As described in section 1.1, a membrane process is defined as a separation process in which a feed stream (liquid or gas) is divided into two streams: a retentate stream and a permeate stream (Figure 1.4). Either the permeate or the retentate stream can be the desired product. In the case of purification of wastewater, the permeate is desired.

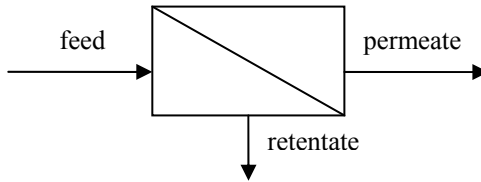


Figure 1.4: Schematic representation of a membrane process

The performance of a membrane process is characterized by three parameters: the selectivity, the flux through the membrane and the recovery (Koros *et al.*, 1996; Mulder, 1996).

For dilute aqueous mixtures, consisting of a solvent (water) and a solute, it is convenient to express the selectivity in terms of the retention towards the solute. The solute is partly or completely retained, while the solvent (water) molecules pass freely through the membrane. The retention (R_i) of component i can be calculated from its permeate ($C_{p,i}$) and feed concentration ($C_{f,i}$) by Equation 1.1. R_i is a dimensionless parameter and its value can vary between 100 % (component i completely retained) and 0 % (no retention of component i).

$$R_i = \left(1 - \frac{C_{p,i}}{C_{f,i}} \right) \cdot 100 \quad (1.1)$$

The flux is expressed as the volume flowing through the membrane per unit of time and per unit of membrane area ($\text{L m}^{-2} \text{h}^{-1}$). The permeability ($\text{L m}^{-2} \text{h}^{-1} \text{bar}^{-1}$) is defined as the flux per unit of pressure. A high water flux is preferable for an economic operation of the filtration process.

The recovery, which is defined as the ratio of the permeate stream to the feed stream, is mainly used for the design of industrial applications rather than a membrane characteristic. The recovery can be varied by the module design and typical values for industrial plants are near 80 %.

1.4 Flux decline and fouling

The water flux through the membrane is an important parameter for the design of a nanofiltration unit. The membrane area, needed to process a given water stream, is determined by the amount of water passing through the membrane per unit of pressure and surface. This implies that a high water flux is desirable to maintain the investment cost for the membranes as low as possible.

1.4.1 Mechanisms of flux decline

A commonly used model to describe flux decline is the resistance-in-series model (Schäfer *et al.*, 2005; Mulder, 1996). In this model the water flux (J) is written as a function of the driving force (ΔP), the viscosity (η) and the total resistance (R_{tot}):

$$J = \frac{\Delta P}{\eta \cdot R_{tot}} \quad (1.2)$$

When filtering pure water, the total resistance (R_{tot}) involves only the membrane resistance (R_m). This resistance is an intrinsic membrane characteristic that does not change during filtration or by changing the feed solution. It reflects the minimal resistance of the system against mass transport and determines thus the maximal water flux at a given pressure.

During filtration of a feed solution, the flux declines according to several mechanisms (Figure 1.5), like e.g., concentration polarization (R_{cp}), adsorption (R_a), formation of a gel layer (R_g) or a cake (R_c), or pore blocking (R_p). Flux decline can also be caused by the presence of specific interactions (R_i) between the membrane and the solute that can damage the membrane or change its properties.

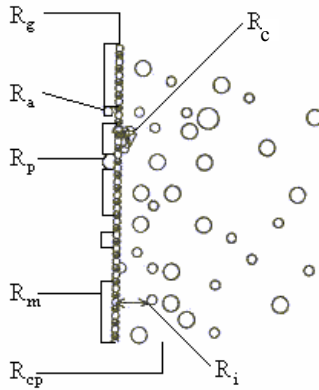


Figure 1.5: Mechanisms responsible for flux decline (Mulder, 1996)

All these individual resistances can be incorporated into a total fouling resistance (R_f), as formulated in Equation 1.3 (Schäfer *et al.*, 2005).

$$R_{tot} = R_m + R_f = R_m + R_{cp} + R_a + R_g + R_c + R_p + R_i \quad (1.3)$$

Concentration polarization (R_{cp}) is the process of accumulation of retained solutes in the membrane boundary layer, so that a high solute concentration at the membrane surface compared to the bulk solution is created. CP causes a reduction in flux predominantly due to the increased osmotic pressure or the formation of gels by retained organic components. Colloidal deposits can further increase CP by forming an unstirred layer that increases the boundary layer concentration. CP can be minimized by applying a turbulent flow on the feed side of the membrane, which was realized in this study by a high cross-flow velocity in the filtration experiments (around 6 m s^{-1}).

The osmotic pressure ($\Delta\pi$) is closely linked to CP, as an increased concentration of dissolved components at the membrane surface causes an increase in osmotic pressure. An osmotic pressure arises due to the concentration difference between feed and permeate side when dissolved components cannot pass through the membrane. As the osmotic pressure results in a decrease of the driving force, the permeate flux (J_p) should be corrected by a factor $\Delta P/(\Delta P - \Delta\pi)$. A rough calculation of the osmotic pressure ($\Delta\pi$) is provided by the Van 't Hoff equation:

$$\Delta\pi = (C_{f,i} - C_{p,i}) \cdot R \cdot T \quad (1.4)$$

where $C_{f,i}$ and $C_{p,i}$ are the concentration of component i in feed and permeate, respectively, R the universal gas constant and T the temperature.

Adsorption (R_a) results in the attachment of components to the membrane pores or to the membrane surface due to hydrophobic, polar or charge interactions. When adsorption occurs in the pores, the net pore opening decreases, resulting in flux decline. If the whole cross-section of the pore is filled by the adsorbed component, pores can even become blocked.

Formation of a gel layer (R_g) occurs when the concentration of solutes at the membrane surface reaches an upper limit, the gel layer concentration. This highly concentrated layer is in fact an extension of the concentration polarization phenomenon. The resistance against mass transport, exerted by the gel layer, is very high. However, as gel layer formation usually occurs during filtration of solutions containing macromolecules, it will not be considered further in this thesis.

Formation of a cake layer (R_c) can occur during filtration of colloidal dispersions, due to accumulation of particles on the membrane surface. A necessary condition for the cake to be built up, is that the colloidal particles are larger than the pores. Otherwise, the particles will penetrate into the membrane pores, resulting in pore blocking. For synthetic solutions containing (un)charged organic components, this resistance is of no importance.

Pore blocking (R_p) occurs when molecules of approximately the same size as the pore opening, fill the membrane pores and are prevented from further permeation, e.g., when the pore becomes narrower towards the end. Pore blocking does not only depend on the average pore size of the membrane, but also on the distribution of the pore sizes. When a single component solution is filtered, less flux decline is expected for a membrane with a wide pore size distribution, as only a fraction of the pores will be blocked.

Specific interactions (R_i), such as chemical binding of components to the membrane surface, can also influence the water flux. The most common interactions are, however, destructive and result in a flux increase instead of a flux decrease. This can be caused by the dissolving or the release of the top layer, so that the permeate can freely pass through the support layer. This phenomenon can only be prevented by avoiding solvents that are not compatible with the membrane material.

1.4.2 Fouling

Flux decline can be divided into a reversible and an irreversible fraction. The fraction of flux decline that is still present when pure water is applied as feed solution, is considered to be the irreversible part of flux decline or fouling (e.g., in the case a cake layer by colloidal particles is formed).

The fraction of flux decline that is not present anymore when pure water is applied, is due to the immediate presence of the feed solution used and is reversible (e.g., concentration polarization). Therefore, it cannot be considered as fouling.

1.5 Aim of this work and research approach

The aim of this work is to study the influence of membrane characteristics on flux decline and retention during nanofiltration, as flux decline is still one of the main research topics in membrane processes (Drioli, 2002). The results of this work allow to select an optimal membrane in a specific application. Moreover, this work will provide useful information in the field of membrane development, about which membrane characteristics to control for an optimal membrane performance.

The methods and materials used to this purpose are described in Chapter 2. Special attention is paid to the different membrane characterization techniques, as some of them are applied for the first time on nanofiltration membranes.

In addition to representative commercial nanofiltration membranes, laboratory-made membranes are also included in this study. The main reason for doing this was the scarcity of information given by the membrane manufacturers: no details were provided about the synthesis process or about possible additives or post-treatments. As this information is necessary to get a better insight into the performance of nanofiltration, synthesis of polyethersulfone membranes was carried out (Chapter 3). Both the search for optimal synthesis conditions as well as the characterization and performance of these laboratory-made polyethersulfone membranes were discussed.

A methodology for the physical and chemical characterization of the (commercial and laboratory-made) nanofiltration membranes is described in Chapter 4. Although non-contact mode AFM (for determination of the surface roughness) or measurements of the contact angle or the streaming potential (for determination of the hydrophobicity or the surface charge, respectively) are well-known characterization techniques, it is important to assemble these values for different membranes using the same setup, as this enhances an accurate comparison between the membranes.

Moreover, the surface roughness and the hydrophobicity of the membrane top layer were checked by a rather new method in nanofiltration: tapping mode AFM. PAS (Positron Annihilation Spectroscopy), on the other hand, is a novel characterization technique in the world of nanofiltration, in which the lifetime and the energy management of implanted positrons into the membrane are studied. In order to chemically characterize the top and support layer of the different membranes, ATR-FTIR and XPS were selected.

These characterization results were used as input to study which membrane characteristic is the most crucial to optimize flux decline and retention (Chapter 5). However, as it is known in literature that fouling is an interplay between membrane and feed properties (Bellona and Drewes, 2005; Van der Bruggen and Vandecasteele, 2001; Vrijenhoek *et al.*, 2001), the analysis was performed for three different feed solutions:

- aqueous solutions containing dissolved uncharged organic components;
- aqueous solutions containing dissolved charged organic components;
- colloidal dispersions.

For the dissolved organic components, previous work (Braeken, 2005; Van der Bruggen, 2000) already focused on the influence of the component properties on the membrane performance, so that for these two feed solutions attention is mainly paid to the membrane part of flux decline. However, for the colloidal dispersions, the influence of both membrane and colloid characteristics on membrane fouling was studied, and this in different conditions (i.e., with increasing colloid and salt concentration and at different pH).

Chapter 6 describes a potential application of nanofiltration: recycling of wastewater in the carwash industry. Because the carwash wastewater is a complex mixture of several components (among which surfactants), the interpretation of the obtained filtration results was hampered. Therefore, this chapter focuses firstly on the flux decline caused by (synthetic) surfactant solutions in different conditions, representative for the carwash wastewater.

Each chapter starts with an introduction, in which the state of the art about the respective subjects is elucidated.

Chapter 2

Methods and Materials

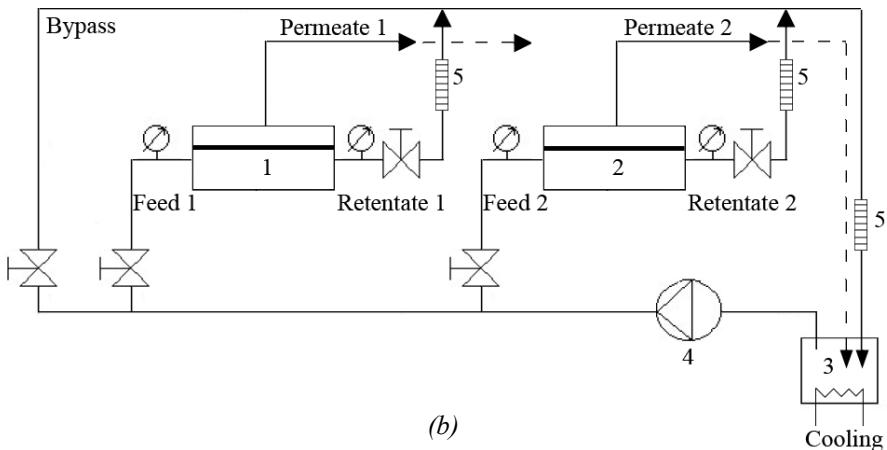
2.1 Nanofiltration experiments

2.1.1 Filtration equipment

Cross-flow filtration experiments were carried out on a laboratory scale filtration apparatus (Amafilter, Test Rig PSS1TZ, Figure 2.1a), equipped with two TZA 944 membrane modules in parallel. Figure 2.1b shows a schematic representation of the cross-flow nanofiltration unit.



(a)



(b)

Figure 2.1: Cross-flow nanofiltration unit: (a) picture and (b) schematic representation of the cross-flow nanofiltration unit (1 = module 1; 2 = module 2; 3 = feed tank; 4 = pump; 5 = flow meter)

The feed solution (3) is pumped to both membrane modules (1 and 2) by a three-stage membrane pump (4). The volume of the feed solution was 10 L, including 1.5 L in the tubes of the installation. Circular flat sheet membranes with a diameter of 9 cm and an effective filtration area ($A_{membrane}$) of 0.0059 m² were used in both membrane modules, of which the design is shown in Figure 2.2.



Figure 2.2: Design of the membrane module of the cross-flow nanofiltration unit

A constant feed composition was achieved by recycling the retentate and permeate stream to the feed tank. Samples of the feed and the permeate were taken to study the evolution of membrane performance as a function of time. During sampling, the permeate was collected in a graduated cylinder; the permeate flux (J_p) was calculated from the time (Δt) needed to obtain a certain permeate volume (V_p) by using Equation 2.1. As the permeate volume is always less than 20 mL and hence negligible compared to the feed solution of 10 L, the composition of the feed solution still remains constant.

$$J_p = \frac{V_p}{A_{membrane} \cdot \Delta t} \quad (2.1)$$

The pressure across the membrane can be varied from 0 to 60 bar; in all experiments the pressure was equal to 8 bar. Feed and retentate pressures can be set by using manual valves; the permeate pressure is equal to atmospheric pressure. A small pressure loss occurs in the membrane module causing a pressure difference between feed and retentate; the driving pressure was calculated as the average of feed and retentate pressures.

In all experiments, the flow and temperature of the feed were 500 L h^{-1} and 293 K , respectively. Because of the heat transfer of the pump, the temperature of the circulating solution increases which implies that cooling was necessary to maintain a constant temperature. Cooling was performed with an electronic circuit (OMRON E5AJ), which opens a cooling water valve and induces flow in the cooling coil if the temperature exceeds the setpoint.

For each experiment, a new membrane piece was used to eliminate the influence of previous experiments. Each membrane piece was firstly immersed in distilled water for at least 24 hours, to dissolve the conserving agents. Afterwards, the membrane was pressurized and the pure water flux was measured for each membrane piece (to take into account the variation between different membrane samples) after 15 minutes of filtration at 8 bar and at neutral pH. After switching to the feed solution, the permeate flux and the permeate concentration were determined after 15, 30, 45, 60, 90 and 120 minutes of operation. After two hours of filtration the experiment was stopped because, in most cases, both the permeate flux and the retention were stable.

To compare flux decline between different membranes, relative fluxes (in %) were defined as the ratio of the permeate flux to the (respective) pure water flux. The reproducibility or the absolute error on the relative flux was determined as 4 %. Due to the low feed concentrations (section 2.5), osmotic pressure was negligible. Only in the case of filtration of (colloidal or surfactant) solutions in the presence of NaCl, the relative flux was corrected for osmotic pressure.

To study the performance of the laboratory-made membranes without support layer (Chapter 3), *batch experiments* were performed with a dead-end filtration module (Sterlitech HP4750 Stirred Cell, Figure 2.3). This module can be used at pressures up to 69 bar for circular flat sheet membranes with a diameter of 4.3 cm and an effective filtration area of 0.00146 cm^2 . The feed solution of 300 mL is magnetically stirred to minimize concentration polarization. Pressure at the feed

side is supplied by an inert gas (N₂). Permeate fluxes were calculated using Equation 2.1.



Figure 2.3: Dead-end filtration module

2.1.2 Selection of commercial membranes

In addition to the laboratory-made membranes (Chapter 3), commercially available nanofiltration membranes were used in the experiments. These membranes were selected to cover the whole range of operation of nanofiltration (from ultrafiltration to reverse osmosis). A summary of the most important membrane characteristics, as given by the manufacturers, is given in Table 2.1.

Table 2.1: Overview of the characteristics of the commercial membranes, as given by the manufacturers

	manufacturer	cut-off ¹ (Da)	permeability (L m ⁻² h ⁻¹ bar ⁻¹)	max temp (K)	pH range
UTC20	Toray ²	180	15	318	3-10
NF270	Dow/FilmTec ³	200-300	11	318	3-10
Desal51HL	GE Osmonics ⁴	150-300	9	323	3-10
Desal5DL	GE Osmonics ⁴	150-300	9	363	1-11
N30F	Nadir ⁵	400	1-1.75*	368	1-14
NTR7450	Nitto-Denko ⁶	600-800	12	313	2-11
NFPES10	Nadir ⁵	1,000	5-10*	368	1-14

¹cut-off = molecular mass of a component with 90 % retention; ²Toray Ind. Inc., Tokyo, Japan; ³Dow/FilmTec, Edina, USA; ⁴GE Osmonics, Le Mee sur Seine, France; ⁵Nadir Filtration GmbH, Wiesbaden, Germany; ⁶Nitto-Denko, Basel, Switzerland; * test conditions at 40 bar, 293 K, stirred cell with 700 rpm

All membranes are thin film composite membranes. According to the information given by the manufacturer, UTC20 has a polypiperazineamide top layer; NF270, Desal51HL and Desal5DL have a crosslinked aromatic polyamide top layer; N30F and NFPE10 have a permanently hydrophilic polyethersulfone top layer; NTR7450 has a sulfonated polyethersulfone top layer. The chemical structures of the different membrane top layers are given in Figure 2.4a to 2.4c.

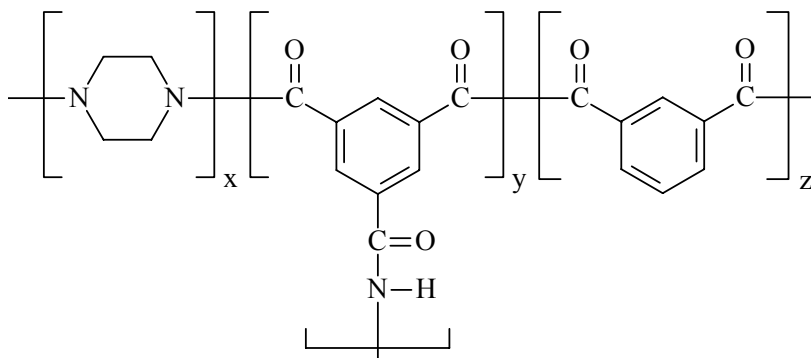


Figure 2.4a: Chemical structure of a polypiperazineamide top layer (UTC20)

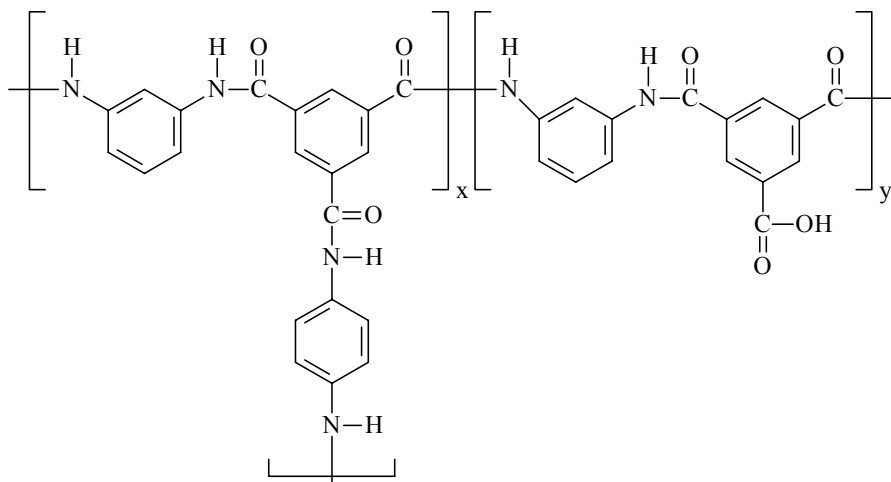


Figure 2.4b: Chemical structure of a crosslinked aromatic polyamide top layer (NF270, Desal51HL and Desal5DL)

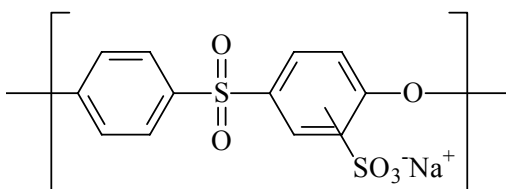


Figure 2.4c: Chemical structure of a sulfonated polyethersulfone top layer (NTR7450)

2.2 Adsorption experiments

Batch experiments were used to study adsorption of organic components on the membrane surface. In these experiments (Figure 2.5), the membrane top layer was exposed to 50 mL (V) of an aqueous feed solution containing uncharged or charged organic components in a concentration of 2 mmol L^{-1} or 0.2 mmol L^{-1} , respectively. For the (colored) charged components, a lower feed concentration was selected because of cleaning problems of the equipment. Adsorption of the surfactants on the membrane surface was studied for a feed concentration of 1.6 mmol L^{-1} (around 600 mg L^{-1}).



Figure 2.5: Setup used to measure the adsorbed amount on the membrane surface

The concentration decrease of the organic components was determined after 90 minutes. This duration was determined in a preliminary experiment where the adsorbed amount on the membrane surface (q) was measured as a function of time for all membranes. Saturation was obtained after approximately 90 minutes. The concentration difference before (C_f) and after 90 minutes (C) in a batch cell was determined. The concentration difference in a batch cell without the membrane

$((C_f - C_b)$; C_b is the concentration after 90 minutes without membrane) was subtracted to compensate for adsorption on the container walls or evaporation of the component of interest. The adsorbed amount per unit of membrane area (q) was calculated from V , C_f , C_b and the membrane surface ($A_{membrane}$) using Equation 2.2. The relative error on the adsorbed amount, calculated by error analysis using various membrane pieces of a given kind, was lower than 15 %.

$$q = \frac{[(C_f - C) - (C_f - C_b)] \cdot V}{A_{membrane}} = \frac{(C_b - C) \cdot V}{A_{membrane}} \quad (2.2)$$

The above described methodology was used to study the adsorbed amount on the membrane top layer. As diffusion of the feed components into the membrane is also an intrinsic phenomenon, sorption into the sub layer cannot be avoided. However, the fact that the adsorbed amount does not change anymore after 90 minutes (Braeken, 2005), indicates that all available adsorption places are reached by the feed components. Moreover, diffusion of feed components through the membrane does not occur on a time scale of hours, but rather on a time scale of several days/weeks (Geens *et al.*, 2005).

2.3 Synthesis of polyethersulfone membranes

Polyethersulfone (PES) from Solvay Belgium (Radel A-100) was used, which according to the manufacturer also contains titanium dioxide (0 – 6 w%) and carbon black (0 – 1 w%). This polymer was dissolved in two different solvents (N,N-dimethylformamide (DMF) or N-methyl-pyrrolidone (NMP)) by heavy stirring during several days to obtain a homogeneous solution. The viscosity of the polymer solutions was measured with a DSR (Dynamic Stress Rheometer from Rheometrics) in a nitrogen atmosphere at 303 K.

A thin film of the polymer solution with a thickness of 150 μm was cast on a support with a filmograph (K4340 Automatic Film Applicator, Elcometer) at a speed of 20 mm s^{-1} in an atmosphere with controlled relative air humidity. The

support was either a glass plate or a glass plate with a non-woven support layer taped on it. The non-woven support layers FO2471 (PP/PE, air permeability at 2 mbar: $300 \text{ dm}^3 \text{ m}^{-2} \text{ s}^{-1}$) and FO2413 (polyester, air permeability at 2 mbar: $150 \text{ dm}^3 \text{ m}^{-2} \text{ s}^{-1}$) were obtained from Freudenberg Vliesstoffe KG (Germany). To prevent the polymer solution of intruding in the pores of these support layers, the support layer was wetted with the appropriate solvent prior to casting (Tsai *et al.*, 1995). The casting thickness was increased to $250 \mu\text{m}$ to obtain a defect-free membrane.

The casted polymer film was immersed in a non-solvent bath of distilled water at 293 K (unless otherwise mentioned), in which phase separation starts and the membrane is formed. The membrane was afterwards repeatedly washed with distilled water and wet stored. For each set of process parameters, three identical membrane sheets were synthesized and tested to obtain a mean value of the flux and the retention.



Figure 2.6: Setup used to synthesize polyethersulfone membranes: (a) the filmograph and (b) the membrane box, in which an atmosphere with controlled relative air humidity could be established

2.4 Membrane characterization techniques

2.4.1 Atomic Force Microscopy (AFM)

2.4.1.1 Theoretical background

Atomic Force Microscopy (AFM) probes the surface of a sample with a sharp tip, located at the free end of a cantilever (Wiesendanger, 1994). Forces between the

tip and the sample surface cause the cantilever to bend. This cantilever deflection is detected optically by focusing a laser beam onto the back of the reflective cantilever. As the tip scans the surface of the sample, moving up and down with the contour of the surface, the laser beam is deflected off the attached cantilever into a dual element photodiode (the beam-bounce method). This photodetector measures the difference in light intensities between the upper and lower photodiodes and converts this signal into a voltage. This method enables a computer to generate a three-dimensional map of the surface topography.

There are three commonly used AFM techniques: contact mode, non-contact mode and tapping mode. In *contact mode*, the tip scans the sample in close contact with the surface. This means that the interatomic force between the sample and the tip is repulsive with a typical value of 10^{-7} N. Problems with contact mode are caused by excessive tracking forces applied by the probe to the sample. Therefore, contact mode AFM cannot be applied to soft surfaces, such as polymeric membranes.

In situations where tip contact might alter the sample, *non-contact mode* is used. In this mode the tip moves about 5 - 15 nm above the sample surface. Attractive interatomic forces between the tip and the sample are detected, and topographic images are constructed by scanning the tip above the surface. The attractive forces from the sample are, however, substantially weaker (10^{-13} N) than the forces used in contact mode. Therefore, the cantilever is driven to vibrate near its resonance frequency by means of a piezoelectric element and changes in the resonance frequency as a result of tip-surface force interaction are measured (dynamic detection method). Problems with non-contact mode can be caused by a contaminant layer (present on the sample) which interferes with the cantilever oscillation and results in a low resolution.

Tapping mode AFM allows high-resolution topographic imaging of sample surfaces by alternately bringing the tip in contact with the surface to provide high resolution and then lifting it off the surface to avoid dragging the tip across the surface. Tapping mode imaging is again implemented by oscillating the cantilever

assembly at or near the cantilever's resonance frequency using a piezoelectric crystal. The piezo motion causes the cantilever to oscillate with a large amplitude (typically greater than 20 nm) when the tip is not in contact with the surface. The oscillating tip is then moved towards the surface until it begins to gently touch, or tap the surface. During scanning, the vertically oscillating tip alternately contacts the surface and lifts off, generally at a frequency of 50,000 to 500,000 cycles per second. As the oscillating cantilever begins to intermittently contact the surface, the cantilever oscillation is reduced due to energy loss caused by the tip contacting the surface. The reduction in oscillation amplitude is used to identify and measure surface features.

A powerful extension of tapping mode AFM is *phase imaging*. In phase imaging, the phase shift is derived from the difference in phase angle between the freely oscillating cantilever in air and the cantilever oscillation during scanning. The convention of phase scaling is based on the freely resonating cantilever in air. The phase shift is zero when there is no interaction between the tip or the cantilever and the sample surface. However, in the case of a tip - sample interaction, a phase lag is induced if the interaction is attractive and a phase advance appears if the interaction is repulsive. The phase shift is hence very sensitive to local variations in the material properties. Moreover, by using a hydrophilic silicon tip, one can observe whether the interactions between the tip and the sample are hydrophilic or hydrophobic. A hydrophilic surface interacts strongly with a hydrophilic tip, resulting in a large phase shift. A hydrophobic surface does not interact strongly with a hydrophilic tip, resulting in a small phase shift.

AFM allows to image insulators and semiconductors as well as electrical conductors and has many applications (Santos and Castanho, 2004) such as analysing ionic crystals, DNA and RNA (Round and Miles, 2004; Wu *et al.*, 2004), red blood cells (Zachee *et al.*, 1996), etc. AFM has also been used to study the roughness of polymeric (Davey *et al.*, 2004; Bowen *et al.*, 2002; Freger *et al.*, 2002; Khulbe and Matsuura, 2000) and ceramic membranes (Vilaseca *et al.*, 2004; Marchese *et al.*, 2000). For ultrafiltration and microfiltration membranes AFM can

be used, not only to measure the roughness, but also to study the size and the shape of pores on the surface (Gumi *et al.*, 2003; Väisänen *et al.*, 2002; Huisman *et al.*, 2000; Ho *et al.*, 1999).

For the smaller pores of nanofiltration and reverse osmosis, however, great care is needed in the interpretation of pore diameters (obtained by AFM) because of convolution effects between the tip and the pore (Bowen and Doneva, 2000; Kwak *et al.*, 1997). Another application of AFM in the membrane field is the direct measurement of the force of adhesion between a particle (like silica or polystyrene) and the membrane surface by immobilizing the particle at the end of the cantilever, which allows to predict fouling without process measurements (Bowen *et al.*, 2002; Hilal and Bowen, 2002; Bowen and Doneva, 2000).

2.4.1.2 Experimental conditions

Non-contact mode AFM was performed with an M5 AFM system (VEECO). The cantilever was made from Si with a spring constant of 3.2 N m^{-1} and a nominal tip apex radius of 10 nm. After scanning, the images were flattened with a second order polynomial approximation to remove AFM scanner-induced curvature and slope from the image. After flattening, the RMS roughness (R_{rms} , root-mean-squared roughness) was calculated, which represents the standard deviation of the data:

$$R_{rms} = \sqrt{\frac{\sum_{n=1}^N (z_n - \bar{z})^2}{N}} \quad (2.3)$$

where z_n is a data point of the roughness profile, \bar{z} the average of all z_n values within the given area and N the number of data points within the given area.

Other definitions can also be used to characterize the roughness like the mean roughness (the mean value of the surface relative to the center plane) or the peak-to-valley distance (the distance between the highest and lowest data point of the surface). However, these definitions are less accurate than the RMS roughness. In the peak-to-valley distance only two points of the scanned surface (i.e., the highest

and the lowest) are taken into account, which is not representative for the whole surface; the mean roughness is not able to distinguish between surfaces that differ in shape or spacing. Hence the RMS roughness is the most accurate and will be used in the rest of this thesis.

Tapping mode AFM images as well as AFM phase images were obtained with a Nanoscope III scanning probe microscope (Digital Instruments, Santa Barbara, California). The SPM probe used was a SiO₂ non-contact SPM probe (Nanosensors) with a spring constant of 40 N m⁻¹, a resonance frequency of 190 kHz and a typical radius of 10 nm. After scanning the images were flattened with a second order polynomial approximation and the RMS value of the roughness was calculated by Equation 2.3. The RMS value was also calculated for the phase shift Θ_{rms} by using Equation 2.4.

$$\Theta_{rms} = \sqrt{\frac{\sum_{n=1}^N (\theta_n - \bar{\theta})^2}{N}} \quad (2.4)$$

where θ_n is a data point of the phase shift profile, $\bar{\theta}$ the average of all θ_n values within the given area and N the number of data points within the given area.

For non-contact mode AFM as well as for tapping mode AFM, the analyses were carried out on a dry sample in an atmosphere with a relative humidity of 30 %. Measuring a dry sample has two advantages compared to measuring a wet surface:

- It is easier to make a distinction between a hydrophobic and a hydrophilic surface by measuring a dry surface (with a hydrophilic tip). Only on a hydrophilic dry surface, the relative humidity will deliver an additional capillary force, which would not be present on a wet surface. Because of the absence of the capillary force when a wet surface is measured, it is not possible to distinguish between a hydrophobic and a hydrophilic surface.
- Measuring a wet surface takes 5 to 10 times longer than measuring a dry surface.

For non-contact mode AFM as well as for tapping mode AFM, the roughness and the phase shift were measured for five different scan areas: $0.5\ \mu\text{m} \times 0.5\ \mu\text{m}$, $1\ \mu\text{m} \times 1\ \mu\text{m}$, $3\ \mu\text{m} \times 3\ \mu\text{m}$, $5\ \mu\text{m} \times 5\ \mu\text{m}$ and $10\ \mu\text{m} \times 10\ \mu\text{m}$. The first scan was always made for the largest area ($10\ \mu\text{m} \times 10\ \mu\text{m}$). Then the area was reduced until the smallest area ($0.5\ \mu\text{m} \times 0.5\ \mu\text{m}$) was reached. In the case of non-contact mode AFM, each measurement was done three times on two different areas to obtain a mean value of the RMS roughness. The standard deviation of the different measurements was lower than 10 %.

2.4.2 Contact angle measurements

When a liquid droplet is applied on a membrane surface, the droplet will take a specific shape resulting in a specific contact angle with the membrane (Figure 2.7a). The value of the contact angle theoretically ranges from 0° to 180° . The higher the affinity between the water droplet and the membrane surface, the smaller the contact angle and the higher the degree of wetting. Contact angles measured with water are used to study the degree of hydrophilicity/hydrophobicity: hydrophilic surfaces show a small value for the contact angle, whereas hydrophobic surfaces show a large contact angle.

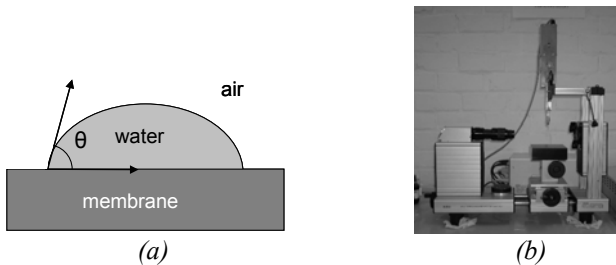


Figure 2.7: Contact angle measurements: (a) the principle and (b) the setup

Contact angle measurements were performed with a Drop Shape Analysis System DSA 10 Mk2 (Krüss, Figure 2.7b) in a three-phase system consisting of the membrane surface, air and water droplets of $2\ \mu\text{L}$. The sessile drop method was chosen and the contact angle was measured in an equilibrium mode: a droplet of water is placed on the membrane surface, after which the contact angle between the droplet and the membrane surface is calculated. Each contact angle was measured

50 times and an average value was calculated. The contact angle of the wet, clean membrane was determined for all membranes.

2.4.3 Determination of cut-off

The cut-off is considered in literature as a measure for the size of the pores and is defined as the molecular mass of a component that is retained for 90% by the membrane. This parameter is often used, especially for ultrafiltration membranes (Aimar *et al.*, 1990), but it cannot be considered as an absolute parameter. Although the cut-offs are specified by the manufacturer for the considered commercial membranes (Table 2.1), a comparison is hampered because the value of the cut-off strongly depends on experimental conditions (e.g., the pressure applied, the concentration and the nature of the feed solution) (Bellona *et al.*, 2004).

Therefore, the cut-off was experimentally determined for each commercial membrane by filtration in the cross-flow setup with the same feed solution under the same conditions (293 K, 8 bar, 600 L h⁻¹). As feed solution, a mixture of polyethylene glycols (PEG) with different molecular mass (from 150 to 3,000 Da) in a concentration of 1 g L⁻¹ was selected (Cleveland *et al.*, 2002). Analysis of the concentration of PEG in feed and permeate was done with Gel Permeation Chromatography (Shodex OHpak SB-803 HQ). By fitting the obtained retention curve with the log-normal model (Van der Bruggen *et al.*, 2000b), the cut-off was calculated as the molecular mass of PEG with 90% retention. The relative error on the obtained values of the cut-off is lower than 10 %.

2.4.4 Measurements of the streaming potential

Measurements of the streaming potential are frequently used to characterize the charge properties of membranes. Membranes acquire a charge when brought into contact with an aqueous solution due to dissociation of functional groups or adsorption of ions from the solution. Because this surface charge is compensated by the attraction of counterions from the solution, an electrical double layer is

formed. When the ions within this electrical double layer are forced to move along with a flow, a streaming potential is generated.

From the streaming potential (ΔE), the zeta potential (ζ), which is defined as the potential at the plane of shear between the surface and the solution, is calculated by using the Helmholtz-Smoluchowski equation (Childress and Elimelech, 1996):

$$\zeta = \frac{\Delta E \cdot \eta}{\Delta P \cdot \varepsilon_o \cdot \varepsilon_r} \cdot \frac{L}{A} \cdot \frac{1}{R} \quad (2.5)$$

where η is the viscosity of the solution, ΔP the applied pressure, ε_o the vacuum dielectric permittivity, ε_r the relative dielectric permittivity, L the channel length, A the channel cross-sectional area and R the channel resistance.

The ratio L/A was determined using the Fairbrother and Mastin approach (Fairbrother and Mastin, 1924). For solutions with low surface conductivity (i.e., electrolyte concentration larger than 10^{-3} M), this ratio is given by:

$$\frac{L}{A} = \kappa \cdot R \quad (2.6)$$

where κ is the conductivity. With this expression, Equation (2.5) reduces to its usable form (Möckel *et al.*, 1998; Kim *et al.*, 1996; Nyström *et al.*, 1989):

$$\zeta = \frac{\Delta E \cdot \eta \cdot \kappa}{\Delta P \cdot \varepsilon_o \cdot \varepsilon_r} \quad (2.7)$$

Streaming potential measurements can be carried out both through the membrane pores and along the membrane surface. However, the interpretation of measurements through the membrane is difficult in the case of nanofiltration membranes, because the Helmholtz-Smoluchowski equation does not hold for pore sizes as small as 1 nm (the ratio of pore radius to electrical double layer thickness must be large), and because the influence of the support layer is not well incorporated.

The experimental setup is shown schematically in Figure 2.8. The electrolyte solution is pumped through the cell, which consists of two membranes with a

spacer in between. This way, only the charge characteristics on the exterior surface of the membrane were determined. The membrane samples had dimensions of 76 mm x 26 mm and were glued on to glass plates. The applied pressure difference was set at 0.4 bar. The cell potential was measured continuously by two Pt electrodes. Data acquisition took place with a computer. When the valve at the inlet of the cell was closed, the solution stopped flowing through the cell (non-flow mode). The flow started again when the valve was opened (flow mode). The difference in potential between flow and non-flow mode gives the streaming potential.

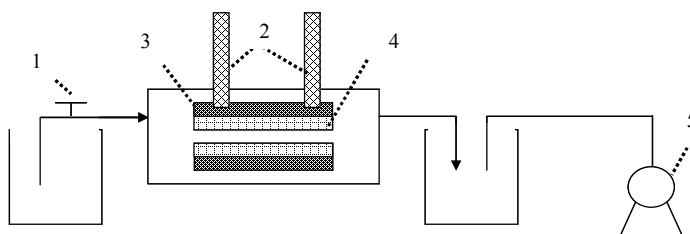


Figure 2.8: Schematic representation of the experimental setup for the streaming potential measurements (1 = feed valve; 2 = Pt electrodes; 3 = glass plate; 4 = membrane; 5 = vacuum pump)

For the determination of the zeta potential, a 0.01 M KCl solution was used. The pH of the solution ranged from 3 to 12 and was set by adding NaOH and HCl. A lower pH would give difficulties in interpreting the data because of the high contribution of hydrogen ions to the conductivity of the solution. The streaming potential difference was measured 10 times and a mean value was calculated. The relative error on the measured values was below 10 %. Only around the iso-electric point (when the surface charge is very small), the relative error increased up to 30 %.

2.4.5 Positron Annihilation Spectroscopy (PAS)

2.4.5.1 Theoretical background

Positron Annihilation Spectroscopy (PAS) is a relatively novel technique in membrane science and is based on the study of the annihilation phenomena after

implanting positrons in the sample. Both the lifetime of the implanted positrons (Positron Annihilation Lifetime Spectroscopy, PALS) and the energy management of the annihilation (both Doppler Broadening of the Annihilation Radiation, DBAR and the Compton to peak relation or the R parameter) were studied. A summary of the PAS technique is given in Table 2.2.

The energy of the incident positrons (E) determines the mean positron implantation depth (\bar{z}) according to Equation 2.8:

$$\bar{z} = \frac{C \cdot E^n}{\rho} \quad (2.8)$$

where C and n are constants and ρ the density of the polymer. The values of C and n are $2.8 \text{ mg cm}^{-2} \text{ keV}^{-n}$ and 1.7, respectively (Algers *et al.*, 2003).

Table 2.2: Summary of the PAS technique

		type of annihilation	lifetime (ns)	DBAR at 511 keV	R parameter
positron		free	0.44	yes	2γ
positronium (Ps)	p-Ps	self	0.124	no	2γ
	o-Ps	pick-off	1 – 6	yes	2γ
		self	142	-	3γ

Positron Annihilation Lifetime Spectroscopy (PALS)

After injection of the positrons in the sample, the positrons either diffuse into the polymer and are annihilated as a free positron with an electron in about 0.44 ns (free positron annihilation), or capture an electron from the material and form a hydrogen-like quasi-stable atom, known as positronium (Ps). The para-Ps (p-Ps), in which the spins of two particles are antiparallel, has a mean lifetime of 0.124 ns (self-annihilation of p-Ps), whereas the ortho-Ps (o-Ps), in which the spins are parallel, has an intrinsic lifetime of 142 ns in vacuum (self-annihilation of o-Ps). In polymers, the o-Ps atom preferentially gets localized within the free volume cavities, where it moves in the internal regions and collides frequently with the molecules of the walls. During a collision, o-Ps may annihilate with an electron

other than its bound partner and with opposite spin, with the consequence that the (mean) o-Ps lifetime decreases from its value in a vacuum to the low ns-range (1-6 ns, pick-off annihilation) (Jean *et al.*, 2003). The smaller the cavity is, the higher the frequency of collisions and the shorter the o-Ps lifetime is. Assuming a spherical shape of the holes, the mean hole radius (r_i) can be calculated from the mean o-Ps lifetime (τ_i) using the equation of Tau-Eldrup (Equation 2.9):

$$\tau_i = \frac{1}{2} \cdot \left[1 - \frac{r_i}{r_i + \delta r} + \left(\frac{1}{2\pi} \right) \cdot \sin \left(\frac{2\pi r_i}{r_i + \delta r} \right) \right]^{-1} \quad (2.9)$$

from which the volume of the pores (V_i) can be calculated using Equation 2.10:

$$V_i = \frac{4}{3} \cdot \pi \cdot r_i^3 \quad (2.10)$$

Equation 2.9 is derived from a semi-empirical model (Satyanarayana *et al.*, 2006; Dlubek *et al.*, 2005), which assumes that o-Ps is localized in an infinitely high potential well with radius $r_i + \delta r$ where r_i is the hole radius. The empirically determined $\delta r = 0.166$ nm describes the penetration of the Ps wave function into the cavity walls (Dlubek *et al.*, 2005; Jean *et al.*, 2003). The spectral intensity associated with the o-Ps lifetime component is related to the volume fraction of these free volume cavities, if no Ps-quenching functional groups exist in the molecular structure, as is the case in the present study (Abbe *et al.*, 1981).

Compton to peak relation (R parameter) and Doppler Broadening of the Annihilation Radiation (DBAR)

The different types of annihilation of the implanted positrons and positroniums do not only result in a different lifetime, but also in a different annihilation energy. Due to the requirement of conservation of energy, annihilation results in the formation of two γ rays at 511 keV. Only during self-annihilation of o-Ps, three γ rays are formed (Table 2.2), which predominantly contribute to the energy region below 511 keV.

The relation of 3γ to 2γ or the Compton to peak relation is represented by the R parameter. This parameter describes the fraction of the surface under the total low energy region (Compton region) of the annihilation spectrum to that under the 511 keV line. The R parameter hence contains information about the size and the concentration of the different pores.

Another parameter, the S parameter describes the line shape of the annihilation at 511 keV. Due to the electron momentum in the propagation direction of the (two) γ rays, the annihilation line at 511 keV is broadened (DBAR). Therefore, the S parameter is defined as the ratio of the number of counts in a central window (511 ± 0.81 keV) to the total number of counts in the annihilation peak (511 ± 6.46 keV). This parameter hence probes the momentum distribution of the electrons surrounding the site of annihilation and is an indication for the chemistry and the structural defects at the site of annihilation.

Applications of PAS

In recent years, PAS has found increasing interest and growing application in studies of the local free (empty) volume cavities in polymeric materials. Such cavities play a crucial role in the general mechanical and rheological properties of polymers (Kilburn *et al.*, 2005; Faupel *et al.*, 2004; Algers *et al.*, 2003; Dlubek and Alam, 2002; Cao *et al.*, 1999). Concerning membrane characterization, PAS has mainly been used in the past to study membranes for gas separation (Kruse *et al.*, 2005; Winberg *et al.*, 2005; Wang *et al.*, 2004; Shimazu *et al.*, 2003; Merkel *et al.*, 2002). Only a few manuscripts report on the use of PAS applied to reverse osmosis membranes (Kim *et al.*, 2005; Shimazu *et al.*, 2000) or pervaporation membranes (Satyanarayana *et al.*, 2006). To the best knowledge of the author, PAS has not yet been applied to NF membranes.

2.4.5.2 Experimental conditions

The depth selective positron lifetime measurements (PALS) were performed using the lifetime setup of the magnetically guided positron beam at Washington State University (Szpala *et al.*, 2002). The magnetically guided slow positron beam is

used to probe surfaces and thin films using positrons with an energy of 1 keV up to an energy of 60 keV. When a positron hits the sample, secondary electrons are created. The detection of these secondary electrons by the microchannel-plate detector creates the start signal while the detection of one of the annihilation γ 's by the photomultiplier tube creates the stop signal of the lifetime measurement. To avoid charging of the membrane samples, a 10 nm gold layer was deposited on the membrane surface.

In order to decompose the lifetime spectra, a MATLAB program was available, which allows the use of a specific resolution function consisting of 2 identical Gaussian distributions which are shifted from each other by a few ns and of which the second distribution is only a fraction of about 9 % from the first distribution. During the analysis, the p-Ps lifetime was fixed to 0.124 ns (τ_l) and the intensities of the different positronium components were analyzed using the constraint that $\Sigma I_{o-Ps} = 3 \cdot I_{p-Ps}$. From the obtained o-Ps lifetimes (τ_i), the radii of the pores (r_i), which are considered to be free volume elements, can be calculated using Equation 2.9. The relative error on the measured intensities and lifetimes was 0.5 % and 5 %, respectively.

In addition to the lifetime experiments, the energy of the annihilation radiation was studied using a high-purity Ge-detector with a resolution of 1.4 keV at 511 keV (Puglisi *et al.*, 2001). The detector is situated perpendicular to the beam direction. At each selected energy, a spectrum was collected with approximately $1 \cdot 10^6$ counts in the total spectrum. This setup allows to determine the Doppler Broadening of the Annihilation Radiation (DBAR, given by the S parameter) and the ratio of annihilation in 3γ to the annihilation in 2γ (given by the R parameter).

2.4.6 Attenuated Total Reflectance–Fourier Transform InfraRed (ATR-FTIR)

In ATR-FTIR, the sample is exposed to infrared radiation with a wave number between 4,000 and 400 cm^{-1} . Molecules absorb this radiation at characteristic vibration frequencies. An infrared spectrum represents the absorbance as a function

of the wave number; the observed peaks can be identified with the functional groups within a molecule. ATR-FTIR (Attenuated Total Reflectance, Figure 2.9) means that the sample with refractive index n_1 is placed on a crystal with a (high) refractive index n_2 . If the relation of n_1 to n_2 is smaller than the sine of the reflection angle (θ), the infrared radiation is not able to penetrate deeply into the sample (in contrast to FTIR, where the radiation passes through the sample).

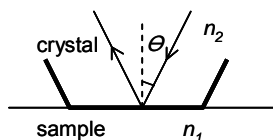


Figure 2.9: Principle of ATR-FTIR

ATR-FTIR spectra were measured in a vertical ATR cell using a Bruker IFS66v/S vacuum FTIR spectrometer with an operating vacuum lower than 3 mbar inside the spectrometer. The internal reflection elements were KRS-5 IRE trapezoidal-shaped crystals (S.A.F.I.R., Belgium, 52 mm x 20 mm x 2 mm) with 25 internal reflections. Due to the fact that the crystal was not totally covered by the membrane, not all the reflections were active. The FTIR spectrometer was equipped with a liquid nitrogen cooled MCT detector and a KBr beam splitter. A total of 512 scans were signal averaged using an optical resolution of 2 cm^{-1} .

2.4.7 X-ray Photoelectron Spectroscopy (XPS)

In XPS, the sample is exposed to an X-ray photon bombardment, resulting in the release of electrons due to the photoelectric effect. Subtracting the kinetic energy of the released electrons from the energy of the photons ($h\nu$, with h the Planck's constant and ν the photon frequency), the binding energy of the core electrons (BE) is obtained. An XPS spectrum represents the number of photoelectrons as a function of the binding energy.

Since the number of photoelectrons for a chemical element depends on the atomic concentration of that element in the sample, the atomic concentration percentages (C_i) were calculated from the photoelectron peak area (A_i) and the sensitivity factor

(S_j) using Equation 2.11. The sensitivity factor is equal to 0.296 for C_{1s} , 0.711 for O_{1s} , 0.477 for N_{1s} and 0.570 for S_{2p} .

$$C_i = \frac{A_i/S_i}{\sum_n^m A_j/S_j} \quad (2.11)$$

Moreover, because the binding energy is a constant for each chemical element (except for hydrogen and helium) and also depends on the chemical environment of this element, the different peaks were assigned by fitting to the different element core levels.

XPS measurements were performed with a Perkin Elmer Phi ESCA 5500 system equipped with a monochromated 450 W Al $K\alpha$ source, which emits at 1486.6 eV. The base pressure of the ESCA system was below $1 \cdot 10^{-7}$ Pa. C_{1s} , O_{1s} , N_{1s} and S_{2p} core levels were collected at an analysis takeoff angle between membrane surface and analyzer of 54° . A flood gun was used for charge neutralization on the non-conductive membranes. Before analysis, the membranes were sputtered during 6 seconds to remove the contaminant layer on the membrane surface. The C_{1s} core level taken at 285 eV (aliphatic carbon) is used as binding energy reference.

The analysis of the binding energy was performed with the XPS Peak 4.1 program (XPS Peak 4.1, 2001). After subtracting a Shirley-type background from the signals, the recorded spectra were fitted with Gauss-Lorentz curves and with a similar FWHM (full-width half-maximum) for all peaks of one chemical element. For C_{1s} , the binding energy region between 277 eV and 286 eV was studied. This implies that the $\pi \rightarrow \pi^*$ shake-up satellite, characteristic for the presence of aromatic rings in the polymer, was neglected (Gardella *et al.*, 1986).

2.4.8 Scanning Electron Microscopy (SEM)

In SEM, a two-dimensional image of the membrane surface or cross-section is obtained by radiation of the sample with an electron beam; the image is determined by the reflected, secondary electrons.

The setup used to visualize the (surface and cross-sections of the) laboratory-made membranes and the surfaces of the commercial membranes was a Philips Scanning Electron Microscope XL30 FEG with an accelerating voltage of 20 keV. To avoid charging of the membrane material by the electron beam, a conductive gold coating was applied on the samples. A clear cross-section was obtained by fracturing the membranes after immersing in liquid nitrogen.

Cross-sections of the commercial membranes were visualized using a FEI Nova Nanolab dualbeam, which combines a high resolution Scanning Electron Microscope (FEG-SEM) with a Focused Ion Beam (FIB). With this setup, a small cross-section is made by scanning the sample with a gallium ion beam. To avoid damaging of the surface and in order to obtain a clean straight cut, a layer of platinum is deposited in situ on the membrane surface. To prevent charging of the samples during both FIB and SEM operation of the dualbeam, a thin (< 10 nm) gold layer was deposited on the membranes prior to loading of the samples into the dualbeam system.

2.4.9 Differential Scanning Calorimetry (DSC)

DSC measurements were performed with a DSC2920 of T.A. Instruments. The membrane samples (around 6 mg) were placed in aluminum pans, which were rinsed with nitrogen at 50 mL min⁻¹. The testing procedure consists of heating from room temperature to 323 K, holding the temperature at 323 K for 15 minutes to remove the moisture, heating to 623 K, holding the temperature at 623 K for 3 minutes and cooling to 273 K. Heating and cooling were done at a speed of 10 K min⁻¹.

The upper limit of 623 K was determined to prevent degradation of the membrane and was based on TGA (ThermoGravimetric Analysis) measurements by using an SDT Q600. The membranes, placed in aluminum oxide pans, were heated at a speed of 5 K min⁻¹. The pans were rinsed with nitrogen at a flow of 100 mL min⁻¹.

2.4.10 Pre-treatment of membrane samples

The described characterization techniques do not always allow to perform a measurement on a wet membrane, e.g., when the technique has to be performed in a vacuum atmosphere (e.g., XPS or SEM) or when the presence of water would complicate or hinder a reliable interpretation of the results (e.g., ATR-FTIR or PAS).

Therefore, it was necessary to perform some characterization techniques on a dry membrane surface. Because the drying protocol also has an influence on the membrane structure, the membranes were all treated in the same way. Firstly, the membranes were placed in distilled water for at least 24 hours. This step is necessary to leach conserving agents out of the membrane. Afterwards, the membrane was taken with a pair of tweezers to avoid contamination of the top layer of the membranes and to dry them to the air in a separate room with the top layer up for at least 48 hours, prior to the characterization test. The characterization techniques were performed on several membrane pieces on several moments and gave rise to the same results, which implies that the drying procedure used was reproducible.

2.5 Selection of feed components

In the cross-flow setup, filtration experiments were performed with aqueous feed solutions, which contained either uncharged organic components (at neutral pH and in a concentration of 2 mmol L^{-1}) or charged organic components (at pH 3 or pH 10 and in a concentration of 0.2 mmol L^{-1}). For the (colored) charged components, a lower feed concentration was selected because of cleaning problems of the equipment. Filtration experiments were also performed with colloidal dispersions (in a concentration of 100 mg L^{-1}) in different conditions. To study the applicability of nanofiltration to recycle wastewater in the carwash industry (Chapter 6), aqueous solutions with surfactants (in a typical concentration of 40 mg L^{-1}) were used as feed solution. Unless otherwise mentioned, the feed solution contained only one single component.

2.5.1 Selection of organic components (uncharged and charged)

Uncharged organic components were selected in order to cover a large range of molecular mass (M_w) and hydrophobicity ($\log P$), as summarized in Table 2.3. The chemical structure of the components is represented in Appendix I.

Table 2.3: Characteristics of the selected dissolved uncharged organic components

	M_w (Da)	$\log P$
benzonitrile	103	1.54
benzylalcohol	108	1.08
p-tolualdehyde	120	2.26
benzylidene acetone	146	2.04
xylose	150	-1.98
xylitol	152	-2.56
3,4-methylnitrophenol	153	2.46
3,5-dihydroxybenzoic acid	154	0.91
4,3-chloronitrobenzaldehyde	185	2.17
maltose	342	-5.42
raffinose	504	-6.76

The hydrophobic properties of an uncharged component are generally described by the octanol-water partition coefficient P , which represents the ratio of the concentration of a component in the octanol-phase to the concentration in the aqueous phase of a two-phase system at equilibrium. Since the measured values range from 10^{-4} to 10^{+8} , the logarithm of the octanol-water partition coefficient is commonly used as a measure for the hydrophobicity of a component.

The values of $\log P$ were calculated on the basis of a group contribution method (Syracuse Research Corporation, 2003; Meylan and Howard, 2000), according to Equation 2.12:

$$\log P = \sum (f_i \cdot n_i) + \sum (c_j \cdot n_j) + 0.229 \quad (2.12)$$

where f_i is the fragment coefficient, n_i the number of times a fragment occurs in the structure, c_j the correction factor coefficient and n_j the number of times a factor

occurs in the structure. The constant (0.229) is generated by the statistical analysis of Meylan and Howard (2000) for correspondence between the estimates and the experimentally measured values of log P.

As an example, Table 2.4 indicates the calculation of log P for 3,4-methylnitrophenol; the structure of 3,4-methylnitrophenol is given in Figure 2.10. The experimental value of log P for 3,4-methylnitrophenol (i.e., 2.48, as determined by Schwarzenbach *et al.* (1988)), corresponds well with the calculated value, as is also shown in Figure 2.11 for the other uncharged organic components.

Table 2.4: Calculation of the logarithm of the octanol-water partition coefficient ($\log P$) of 3,4-methylnitrophenol

type	number	fragment description	coefficient	total
f_i	1	-CH ₃ [aliphatic carbon]	0.547	0.547
f_i	6	aromatic carbon	0.294	1.764
f_i	1	-OH [hydroxy, aromatic attach]	-0.480	-0.480
f_i	1	-NO ₂ [nitro, aromatic attach]	-0.182	-0.182
c_j	1	ring reaction → -NO ₂ with -OH	0.578	0.578
constant		equation constant		0.229
log P				2.456

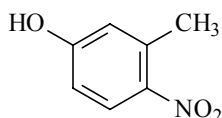


Figure 2.10: Structure of 3,4-methylnitrophenol

As the filtration experiments with dissolved charged organic components were performed at pH 3 and pH 10, the molecular mass (M_w) and the component charge at these pH values were used as selection criteria, as summarized in Table 2.5. The chemical structure of the charged components is represented in Appendix II. For these components, the value of log P was not determined as this parameter only correctly describes the partition coefficient of neutral components.

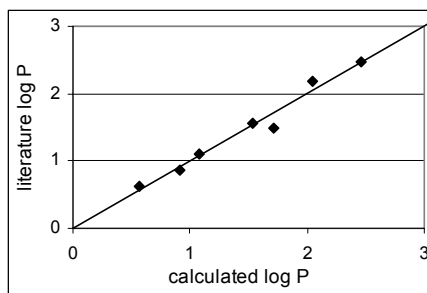


Figure 2.11: Correspondence between the calculated and the experimental values of $\log P$

Table 2.5: Characteristics of the selected dissolved charged organic components

	M_w (Da)	charge		
		pH 3	neutral pH	pH 10
serine	105	+	0	-
isoleucine	131	+	0	-
glutamine	146	+	0	-
phenylalanine	165	+	0	-
tryptophane	204	+	0	-
diphenylaminosulfonic acid	271	-	-	-
neutral red	288	+	+	0
methylene blue	319	++	+	+
methyl orange	327	0	-	-
janus green	511	+	+	+
patent blue	543	-	-	-
eosine	645	0	--	--
congo red	696	0	--	--

The charge of the components was estimated at each pH based on their pKa values. As an example, Figure 2.12 shows the structure of the amino acid phenylalanine, which carries a weak acid carboxyl group ($-COOH$) and a weak basic amine group ($-NH_2$). At pH 10, a larger fraction of the carboxyl group is dissociated as compared to the protonation of the amine group ($pK_{a2} = 9.4$), resulting in a

negative charge of phenylalanine. At pH 3, a larger fraction of the amine group is protonated than the dissociation of the acid group ($pK_{a1} = 2.4$), resulting in a positively charged component.

In the case of eosine and congo red, the presence of two strongly acid groups is responsible for the double negative charge at neutral pH and pH 10.

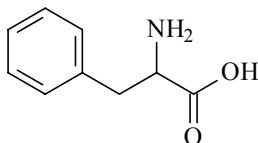


Figure 2.12: Structure of phenylalanine

In addition to these dissolved organic components, three surfactants were selected to study the applicability of nanofiltration in the carwash industry: an ethoxylated alcohol (neodol 91-5E, nonionic), sodium dodecylbenzenesulfonate (SDBS, anionic) and hexadecyltrimethylammonium bromide (cetrimide, cationic). These surfactants have a similar molecular mass, as given in Table 2.6. The chemical structure is represented in Appendix II.

Table 2.6: Characteristics of the three selected surfactants

		neodol	SDBS	cetrimide
type		nonionic	anionic	cationic
M_w (Da)		387	348	364
CMC (mg L^{-1})	water	300	2,320	1,320
	0.1 M NaCl	-	1,600	700

For SDBS and cetrimide, the critical micelle concentration (CMC) was determined by conductivity measurements as a function of the surfactant concentration. Solutions with increasing surfactant concentration show increasing conductivity. Because only monomers contribute to the conductivity of the solution, the increase of the conductivity as a function of the surfactant concentration stops once the CMC is reached. From that point on, the monomer concentration is constant, while the number of micelles increases (Goodwin, 2004). The CMC was determined for

SDBS and cetrimide, both in distilled water and in the presence of 0.1 M NaCl, as indicated in Table 2.6. The value of the CMC of neodol was taken from Xiarchos and Doulia (2006).

2.5.2 Selection and characterization of colloids

Four different commercial colloidal dispersions were selected: VP Disp. W7520 (20 w%) and Aerodisp W630 (30 w%) (from Degussa), and Ludox CL (30 w%) and Ludox HS-30 (30 w%) (from Sigma-Aldrich). According to the manufacturer, VP Disp. W7520 and Aerodisp W630 have a mean aggregate size of 120 nm and 140 nm, respectively, while Ludox CL and Ludox HS-30 have a size smaller than 100 nm. Not only the size, but also the composition of the colloids differs.

VP Disp. W7520 and Aerodisp W630 are made of silica and alumina, respectively. Ludox HS-30 is a colloidal silica dispersion, while Ludox CL is a colloidal silica where each particle is coated with a layer of alumina. The colloid concentrations were determined with a turbidimeter (DRT-15CE, Scientific Inc.).

2.5.2.1 Characterization of colloids

The electrophoretic mobility (μ) of the particles was determined using a Zetasizer IIc instrument (Malvern) at 293 K. The colloid concentration was 20 $\mu\text{L mL}^{-1}$ in the case of Ludox HS-30 and Ludox CL, 4.4 $\mu\text{L mL}^{-1}$ in the case of Aerodisp W7520 and 0.5 $\mu\text{L mL}^{-1}$ in the case of Aerodisp W630. The pH was controlled by adding NaOH or HCl. The applied electric field was typically 2,000 V m^{-1} . The zeta potential (ζ) was derived from the electrophoretic mobility (μ) by using Equation 2.13 (Oshima, 2001):

$$\zeta = \frac{3 \cdot \eta \cdot \mu}{2 \cdot \varepsilon_0 \cdot \varepsilon_r} \cdot \left[1 + \frac{1}{2 \cdot \left[1 + \frac{2.5}{\kappa \cdot a \cdot (1 + 2 \cdot \exp(-\kappa \cdot a))} \right]^3} \right]^{-1} \quad (2.13)$$

where η is the viscosity, ε_0 the vacuum dielectric permittivity, ε_r the relative dielectric permittivity, κ^{-1} the Debye length and a the radius of the colloid.

The hydrodynamic radius of the colloids was determined by Dynamic Light Scattering using the ALV/CGS-3 Compact Goniometer (ALV-GmbH, Germany). Measurements were performed on diluted colloidal solutions at a scattering angle of 90° and at a temperature of 295 K. Data analysis was performed by cumulant analysis.

2.5.2.2 DLVO theory

The total interaction energy (E) between colloids of radius a in a monovalent electrolyte can be calculated as the sum of the repulsion energy and the attraction energy by using the DLVO theory (Van der Meeren *et al.*, 2004; Hoek *et al.*, 2003; Brant and Childress, 2002; Howell *et al.*, 1993), as formulated in Equation 2.14:

$$E = \frac{64 \cdot \pi \cdot \varepsilon \cdot a^2}{d + 2 \cdot a} \cdot \left(\frac{R \cdot T}{F} \right)^2 \cdot \left[\tanh \left(\frac{F \cdot \psi}{4 \cdot R \cdot T} \right) \right]^2 \cdot \exp(-\kappa \cdot d) \quad (2.14)$$

$$- \frac{H}{6} \cdot \left(\frac{2}{S^2 - 4} + \frac{2}{S^2} + \ln \frac{S^2 - 4}{S^2} \right)$$

where d is the distance between colloids, R the universal gas constant, T the temperature, F the Faraday constant, ψ the surface potential, H the Hamaker constant and $S = (d + 2 \cdot a)/a$.

The surface potential (ψ) is calculated from the zeta potential (ζ), which is generally considered to be the potential at 0.2 nm (Δx) from the surface (i.e., the plane of shear), by using the Eversole and Boardman equation:

$$\tanh \left(\frac{F \cdot \psi}{4 \cdot R \cdot T} \right) = \exp \left(\ln \left[\tanh \left(\frac{F \cdot \zeta}{4 \cdot R \cdot T} \right) \right] + \kappa \cdot \Delta x \right) \quad (2.15)$$

The Hamaker constant (H) is calculated from the Hamaker constant of the colloid (H_{11}) and the Hamaker constant of water (H_{22}) as $H = (\sqrt{H_{11}} - \sqrt{H_{22}})^2$. H_{11} is equal to $6.6 \cdot 10^{-20}$ J or $15.2 \cdot 10^{-20}$ J in the case of silica or alumina colloids, respectively (Médout-Marère, 2005), while H_{22} is equal to $3.8 \cdot 10^{-20}$ J (Van der Meeren *et al.*, 2004).

The interaction energy (E) has to be compared with the driving force of the Brownian motion of the colloids, which is proportional to $k \cdot T$, with k the Boltzmann constant. When the ratio $(E/(k \cdot T))$ is larger than 20, no coagulation occurs and the stability of the dispersion is guaranteed.

2.6 Chemical analysis of aqueous solutions

Various analytical techniques were used to determine the solute concentration in both the filtration and the adsorption experiments. All feed solutions were prepared using distilled water. UV-VIS spectrophotometry was used to analyze samples containing components with aromatic ring structures. Samples containing saccharides, amino acids or surfactants need a pre-treatment reaction to form colored components, before analysis with the spectrophotometer was possible. The concentration of the organic component xylitol was analyzed using High Performance Liquid Chromatography (HPLC).

For the application with carwash wastewater, a more extensive analysis was necessary. Both the suspended and settleable solids were determined; the COD (chemical oxygen demand) and BOD (biological oxygen demand) were used as a measure for the concentration of organic components.

2.6.1 UV-VIS spectrophotometry

A Shimazu UV-1601 double beam spectrophotometer was used to analyze the concentration of single aromatic components. Most of them were analyzed by measuring the absorption of UV-light, with exception of dyes which absorb light in the visible region. For each component, the light spectrum was scanned to find the wavelength with the highest absorption peak. At this wavelength, calibration curves were made (for each condition of pH and salt concentration), based on the law of Lambert-Beer, which assumes a linear relation between the solute concentration and the absorbance.

2.6.1.1 Analysis of saccharides

The concentration of mono- and oligosaccharides, or their derivatives, were determined colorimetrically by adding phenol and sulfuric acid to the samples. Due to a condensation reaction, an orange-yellow colored product was formed with an absorbance maximum between 470 nm and 490 nm (Dubois *et al.*, 1956).

The procedure consists of adding 1 mL of a 5 w% phenol solution to 1 mL of the sugar sample in a test tube. In a thermostatically controlled water bath at 303 K, 5 mL of concentrated sulfuric acid (98 %) was added to the test tube, which was then covered with parafilm. After exactly 10 minutes the test tube was shaken; after exactly 30 minutes reaction, the absorption was measured at 485 nm with the spectrophotometer.

2.6.1.2 Analysis of amino acids

The concentration of amino acids was determined by the ninhydrin method. This spectrophotometric method is based on the formation of a blue color by reaction of ninhydrin and components having free amino groups (Colowick and Kaplan, 1957).

The procedure consists of adding 1 mL of the ninhydrin solution to 0.1 mL of the amino acid sample (at pH 5) in a test tube. The ninhydrin solution is a combination of two solutions and was prepared, e.g., for 50 samples, by adding 0.04 g of $\text{SnCl}_2 \cdot 2\text{H}_2\text{O}$ to 25 mL of a 0.2 M citrate buffer at pH 5 and by adding 1 g of ninhydrin to 25 mL of methyl cellosolve. The test tube was covered with an aluminum cap and the content was mixed. A rack of tubes was heated for 20 minutes in an oil bath at 373 K. Afterwards, 5 mL of diluent (a mixture of equal volumes of water and n-propanol) was added to each tube and the content was mixed. The tubes were transferred to a dry rack and readings were taken on the spectrophotometer at 569 nm, starting 15 minutes after the tubes had been removed from the oil bath. The color is stable for at least one hour.

2.6.1.3 Analysis of surfactants

The concentration of nonionic surfactants in solution was determined by using a two phase titration with sodium tetrakis(4-fluorophenyl)borate (Tsubouchi *et al.*,

1985). This method is based on the formation of cationic complexes between the nonionic surfactant and the positive sodium ion. The ionic pair of the cationic complex together with the anion tetrakis(4-fluorophenyl)borate, can be extracted in dichloroethane. At the end, when no free nonionic surfactants are present anymore to form an ionic pair with, the anion tetrakis(4-fluorophenyl)borate forms an ionic pair with the Victoria blue indicator as a result of which the color of the organic solution turns from red to purple.

The methylene blue method was used for the analysis of anionic surfactants of the sulfonate type. Anionic surfactants can form a complex with the cationic dye (methylene blue) in acidic solution, which can be extracted with chloroform (Clesceri *et al.*, 1989). The amount of formed complex can be determined spectrophotometrically at a wavelength of 653 nm.

Cationic surfactants were determined with a cuvet test (Hach Lange, Germany). In this cuvet, a complex is formed between a cationic surfactant and bromophenol blue. This complex is extracted with chloroform and determined with the spectrophotometer at a wavelength of 413 nm.

To determine the amount of surfactant in a mixture of surfactants (like e.g., in the wastewater of the carwash), each analysis method was checked for influences from the presence of other surfactants. Therefore, seven aqueous solutions with one or more surfactants were made and the concentration of each surfactant in each mixture was determined. The results are given in Table 2.7.

The two phase titration for the determination of nonionic surfactants works well in the presence of anionic surfactants, as there is only a small overestimation of the concentration of nonionic surfactants in mixture 2 and 4. However, in the presence of cationic surfactants, the concentration of nonionic surfactants is overestimated largely, even if there is no nonionic surfactant present in the solution (mixture 3 and 6). This should be taken into account when discussing the concentration of nonionic surfactants in mixtures of surfactants.

Table 2.7: Surfactant analysis in a mixture of surfactants

mixture	real concentration (mg L ⁻¹)			measured concentration (mg L ⁻¹)		
	nonionic	anionic	cationic	nonionic	anionic	cationic
1	10	0	0	10.6	0	0
2	0	10	0	0.5	11.5	0
3	0	0	10	23.7	0	11.5
4	10	10	0	11.0	11.5	0
5	10	0	10	33.0	0	11.5
6	0	10	10	24.6	1.1	4.3
7	10	10	10	36.0	0.9	4.4

The analysis method for the anionic and cationic surfactants is not influenced by the presence of nonionic surfactants. Only when both anionic and cationic surfactants are present in the mixture (mixture 6 and 7), they interact with each other in the form of flakes. As these flakes are not determined by the respective analysis methods, a lower concentration of anionic and cationic surfactants is obtained in mixture 6 and 7.

2.6.2 High Performance Liquid Chromatography (HPLC)

HPLC is a chromatographic technique using a liquid as the mobile phase. Components are distributed between the stationary phase in the column and the mobile phase depending on their affinity for each phase.

This technique was only used for the uncharged organic component xylitol, for which the analyses were carried out with a Waters TM 600S controller equipped with a Waters TM 626 pump. The column used was a Shodex RS pack KC-811 column with a length of 300 mm and an inner diameter of 8 mm; this column is packed with ion-exchange resin gels of sulfonated styrene divinylbenzene copolymer. HPLC measurements for xylitol were performed at a temperature of 313 K and with a flow of 1 mL min⁻¹. As mobile phase, 0.1 v% H₃PO₄ was used; acetic acid was selected as internal standard. Detection occurred with a UV-detector at a wavelength of 193 nm.

2.6.3 Determination of suspended and settleable solids, COD and BOD

The suspended solids (in mg L^{-1}) are those solids that can be separated from the wastewater with a filter of glass fibre (Whatmann GF/C) with pore sizes of $0.45 \mu\text{m}$ (Norm NBN 366). The settleable solids (in mL L^{-1}) are that part of the suspended solids that settle down in an Imhoff cone during a period of two hours (Norm NBN 312).

The chemical oxygen demand (COD, in $\text{mg O}_2 \text{L}^{-1}$) is a measure for the degree of organic pollution in wastewater, as it expresses the amount of oxygen needed to oxidize chemically (with potassium dichromate) the organic matter present in the wastewater (Norm NBN T91-201). The biochemical oxygen demand (BOD, in $\text{mg O}_2 \text{L}^{-1}$) expresses the amount oxygen that micro-organisms need for the biochemical oxidation of organic biodegradable components in wastewater (Norm NBN 470).

2.7 Statistical methods: multiple linear regression

2.7.1 Principle of multiple linear regression

In a multiple linear regression model, the response variable Y is expressed as a function of several independent variables x_1, x_2, \dots, x_p (Carbonez, 2004; Hubert, 2004):

$$Y_i = a + b_1 \cdot x_{1,i} + b_2 \cdot x_{2,i} + \dots + b_p \cdot x_{p,i} + E_i \quad (i = 1, \dots, N) \quad (2.16)$$

where E_i is the residue and N the number of data.

This regression model supposes that the variables x_i are experimentally determined without a measurement error and that E_i is independent and normally distributed with a mean value equal to zero and a constant variance. The observed values Y_i are considered as a spot check out of a normal population; the parameters a and b_1, \dots, b_p need to be estimated.

To check whether the obtained regression model is valid, it is necessary to study whether the parameters b_1, \dots, b_p are significantly different from zero. With ($b_1 = b_2 = \dots = b_p = 0$) as null hypothesis and with the F test ($F_{p, N-p-1}$), the probability (p value) to find a more extreme value of F is calculated. If this p value is larger than 0.05, the null hypothesis is accepted implying that all b parameters are equal to zero and that there is no regression.

To test whether each b_j ($j = 1, \dots, p$) parameter is equal to zero, the Student t test (t_{N-p-1}) is useful. The null hypothesis is in this case formulated as ($b_j = 0$).

For multiple linear regression, the goodness of fit is represented by means of an adjusted correlation coefficient ($ADJR^2$). This coefficient takes into account the number of independent variables and is calculated from the correlation coefficient (R^2) using Equation 2.17.

$$ADJR^2 = 1 - \frac{(1 - R^2)}{(N - 1) \cdot (N - p - 1)} \quad (2.17)$$

2.7.2 Selection of independent x variables

Several independent x variables can be used to explain the response variable Y . However, it is necessary to compose a regression model with as few possible x variables with as much as possible information (high $ADJR^2$).

Starting from m x variables, an optimal subset of p x variables was obtained by using the stepwise selection method. This method starts from a model without variables and continues by adding variables to the model, according to a specific criterion. However, added variables do not remain necessarily into the model. When a variable is added, the stepwise selection method checks according to a specific criterion, if, among all variables already present in the model, no variable could be deleted from the model.

The criterion used for adding or deleting variables is the F test, which is developed in the stepwise selection method to study if a group of x variables has a significant influence.

2.7.3 Diagnostics of the regression method

When the multiple linear regression model is formulated with an optimal subset of p x variables, special data points need to be detected and minimized to enhance the reliability of this regression model (Rousseeuw and Leroy, 2003). Special data points can be classified into three categories.

The first category consists of outliers, which are data points with a large residue (outlying in Y). Outliers have an absolute value of the studentized residual larger than 2; the studentized residual is defined as the relation of the residue (E_i) to the variance of the residue (s_{Ei}).

The second category consists of leverage points, which are x_i variables with a very large or very small value (outlying in X). As a measure of distance between x_i and \bar{x} (the average of all x_i values), the leverage h_{ii} is used. An observation x_i is a leverage point, if his leverage h_{ii} is larger than $\frac{2 \cdot (p+1)}{N}$.

The third category consists of influential data points, which combine a large residue with a very large or very small x value (outlying in Y and X). Therefore, the Cook's distance (C_i) is defined as the distance between an observation Y_i and a chosen regression model; an observation is influential if the Cook's distance (C_i) is larger than the 50th percentile of the F distribution ($F_{p+1, N-p-1}$).

If some of these special data points are found in the formulated regression model, the estimation of the model parameters is disturbed. Therefore, another regression model has to be searched for or the special data points (especially the influential data points) have to be deleted from the data set.

In addition to the special data points, the collinearity of the x variables is studied. If one variable is a combination of other variables, this is reflected in a value of the variance inflation number (VIF) larger than 10. This problem can be solved by deleting or replacing variables.

2.7.4 Experimental conditions

Statistical analysis was performed for the relative flux, the retention and the adsorbed amount (response variables Y) as a function of membrane and component properties (variables x) with the computer program SAS. The purpose was to formulate a multiple linear regression model, with the least number of variables in combination with the highest correlation coefficient ($ADJR^2$) and without (too many) special data points or collinearity between the different variables.

Chapter 3

Synthesis of polyethersulfone membranes

Adapted from: Polymer 47 (2006) 3464-3476

3.1 Introduction

As fouling is an interplay between the membrane and the feed components, it is important to have a good understanding of the properties of the membranes. However, information given by the membrane manufacturers is generally rather scarce; in some cases the composition of the top layer is not even known. Polyethersulfone and polyamide are among the most applied polymers for nanofiltration, but these may e.g., contain unknown additives. Therefore, laboratory-made membranes with a well-known composition were prepared and used for comparison with commercial membranes.

Among the different membrane preparation techniques, asymmetric polyethersulfone membranes are commonly prepared by Diffusion Induced Phase Separation, DIPS (Zhang *et al.*, 2005; Kim *et al.*, 2002; Lin *et al.*, 2002; Vankelecom, 2002; Kastelan-Kunst *et al.*, 1996; McHugh and Miller, 1995). In this process, a thin layer of the polymer dissolved in an appropriate solvent is cast on a suitable support and phase separation is induced by a non-solvent. This phase inversion can be obtained in several ways (Osmonics Inc., 2000; Van de Witte *et al.*, 1996; Gelman Sciences Inc., 1993; Petersen, 1993), of which immersion precipitation is most efficient. In this process, phase inversion is induced by immersing the polymer solution film in a non-solvent bath.

Due to the immersion, a diffusion driven exchange between solvent and non-solvent starts: the non-solvent diffuses into the polymer solution and the solvent diffuses into the non-solvent bath. Because of this diffusion process, the composition of the polymer solution changes and moves into the binodal region of the ternary phase diagram (composed of polymer, solvent and non-solvent, Figure 3.1), so that the polymer solution is separated into two phases: a polymer-rich phase and a polymer-poor phase. At a certain stage during phase demixing, the polymer-rich phase solidifies, whereas the polymer-poor phase gives rise to the pores.

Both kinetics and thermodynamics play an important role during membrane formation and were for polyethersulfone extensively studied in literature (Baik *et al.*, 2001; Barth and Wolf, 2000; Kim *et al.*, 2000; Barton *et al.*, 1997; Han *et al.*, 1995; Han and Bhattacharyya, 1994; Swinyard and Barrie, 1988; Tkacik and Zeman, 1987). Changing the preparation conditions influences hence both kinetics and thermodynamics, resulting in a different membrane structure and a different membrane performance.

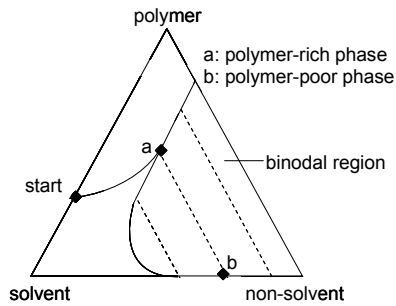


Figure 3.1: Ternary phase diagram for Diffusion Induced Phase Separation (Mulder, 1996)

For example, an increase in the polymer concentration leads to a lower porosity of the membrane and hence to a lower water flux (Mosqueda-Jimenez *et al.*, 2004; Baik *et al.*, 2001; Barth *et al.*, 2000b). To increase the water flux, pore-forming agents, such as polyvinyl-pyrrolidone (Marchese *et al.*, 2003; Han and Nam, 2002; Lafreniere *et al.*, 1987), polyethylene glycol (Kim and Lee, 1998) or an acid (Chaturvedi *et al.*, 2001; Linder and Kedem, 2001; Han *et al.*, 1999) can be added to the polymer solution. When on the other hand a volatile component like acetone is added to the polymer solution, a denser top layer will develop, resulting in higher retentions (Barth *et al.*, 2000b).

Not only to the polymer solution, but also to the non-solvent bath, components like an alcohol (Han and Bhattacharyya, 1994; Swinyard and Barrie, 1988) or a solvent (Baik *et al.*, 2001) can be added to change the membrane structure. Another factor that may influence membrane synthesis, is the temperature of the non-solvent bath: increasing this temperature may either lead to an increase (Chaturvedi *et al.*, 2001)

or to a decrease (Spricigo *et al.*, 2002) of the water flux depending on the polymer system studied. The polyethersulfone system is also sensitive to the relative air humidity (Han *et al.*, 1995). By changing all these factors, an optimized membrane for a specific purpose can be obtained.

From this literature overview, it is clear that up to now studies concerning membrane formation are rather focused on the principle of the formation process and on the influence of *some* preparation factors on the membrane structure without considering the membrane performance. Because the formation process of a membrane is a complex phenomenon, most studies are limited to the influence of only one or two preparation factors on the thermodynamics and kinetics of the formation process. If the influence on the membrane performance is at all studied, the studies are generally limited to a dead-end setup in which only the pure water flux and the retention of one specific component are measured.

A thorough testing of the membrane performance in a cross-flow setup is currently missing. Also a thorough characterization of the membrane surface properties, which are important to explain fouling phenomena, can hardly be found in literature. Therefore, this chapter gives a systematic and complete overview of the synthesis of polyethersulfone membranes by the phase inversion technique, focusing on the membrane performance rather than on the formation process.

In a first part of this chapter, *several* preparation factors were studied experimentally to find the optimal conditions to obtain a nanoporous polyethersulfone membrane. Membranes without support layer were chosen initially for two reasons:

- At least one factor, the support layer, could be excluded.
- These membranes without support layer could be tested in a dead-end setup that allows to test the performance of the membranes in a shorter time with a smaller piece of membrane.

The knowledge gained in this first part can be (partially) used in the second part of the chapter, in which membranes on a support layer were prepared. These

membranes were then characterized and tested in detail for their performance in a cross-flow setup, both for uncharged and charged components, as listed in Table 3.1.

Table 3.1: Summary of the properties of the components used to test the performance of the laboratory-made membranes

	M_w (Da)	charge at neutral pH
raffinose	504	0
diphenylaminosulfonic acid	271	-
methyl orange	327	-
congo red	697	--
neutral red	289	+
methylene blue	320	+
janus green	511	+

3.2 Preparation of membranes without support layer

Membranes were made on a glass plate without support to study the influence of different preparation factors to obtain the optimal conditions for a nanoporous polyethersulfone membrane. The preparation factors include a non-solvent bath of distilled water at 293 K, a relative air humidity of 40 % and no addition of components either to the non-solvent bath or to the polymer solution. As solvent, N,N-dimethylformamide (DMF) or N-methyl-pyrrolidone (NMP) were used. The influence of the polymer concentration and the relative air humidity were studied firstly. Then, different components were added to the non-solvent bath and to the polymer solution. Of the non-solvent bath, not only the influence of the additives, but also the influence of the bath's temperature on the membrane performance was investigated.

The purpose of the synthesis was to obtain a nanoporous polyethersulfone membrane. To verify if this criterion was fulfilled, the membrane performance (the pure water permeability and the retention of two components) was studied and

compared with the performance of commercial nanofiltration membranes. As it was the goal in this stage to obtain a quick view of the membrane performance, only aqueous solutions containing congo red and raffinose were selected as feed; a detailed study of the membrane performance is carried out in section 3.3.

For the commercial membranes, the pure water permeability ranges between 1.5 and 15 $\text{L m}^{-2} \text{h}^{-1} \text{bar}^{-1}$ (Table 4.3). The retention of congo red (a negatively charged component) is about 98 % for all commercial nanofiltration membranes (Table 5.4 and Table 5.5), while for raffinose (uncharged component) the retention differs strongly from membrane to membrane (Table 5.1).

3.2.1 Influence of the polymer concentration

The influence of the polymer concentration on the water permeability for both PES/DMF and PES/NMP membranes is shown in Figure 3.2. The pure water permeability decreases when the polymer concentration increases.

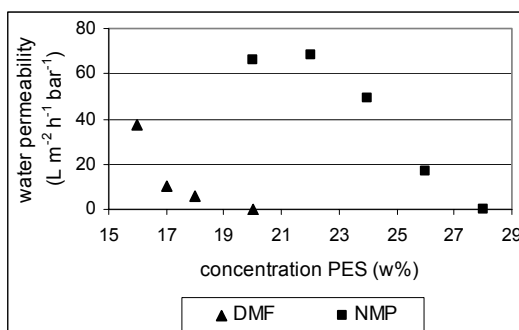


Figure 3.2: Influence of the polymer concentration on the pure water permeability ($\text{L m}^{-2} \text{h}^{-1} \text{bar}^{-1}$) (dead-end measurements)

This is explained by the observed increase in the viscosity of the polymer solution. For example, in the case of PES/NMP, the viscosity of a 26 % polymer solution was 2.15 Pa s, while a viscosity of 6.11 Pa s was measured for a 30 % polymer solution. This increase in viscosity hampers the diffusional exchange between solvent and non-solvent and leads to a higher polymer concentration at the interphase between polymer solution and non-solvent bath and hence to a lower porosity and a lower permeability of the membrane.

SEM images of the cross-section of a PES/DMF membrane with different polymer concentrations are shown in Figure 3.3. A comparison between these images indicates that a high polymer concentration results in a less porous membrane (top layer) with less fingerlike pores (called macrovoids).

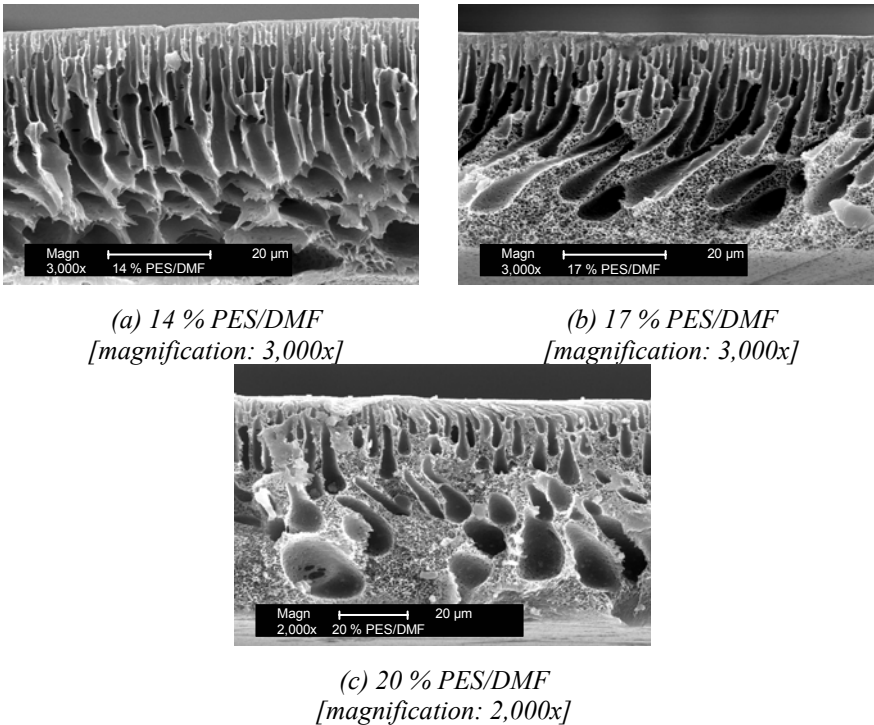


Figure 3.3: Influence of the polymer concentration on the membrane structure [Figure (c) has a lower magnification due to its larger membrane thickness]

The polymer concentration also influences the final thickness of the membrane. Starting from a 150 µm casting thickness, the final thickness of the membranes made with a 14 % PES/DMF and a 20 % PES/DMF solution is 50 µm and 60 µm, respectively. In both cases, a reduction in thickness is observed because the transport of non-solvent (distilled water) into the polymer solution (PES/DMF) is slower than the transport of the solvent (DMF) into the non-solvent (water). This phenomenon is related to the good miscibility of solvent and non-solvent and to the hydrophobic nature of the polymer, if water is used as non-solvent.

By increasing the polymer concentration and hence the viscosity, both the rate of solvent into the non-solvent and the rate of non-solvent into the polymer solution decrease, resulting in less contraction and hence in a thicker membrane. The same trend was observed for the PES/NMP membranes.

The decreasing porosity with increasing polymer concentration has not only an influence on the permeability (as shown in Figure 3.2), but also on the retention of the membranes. For congo red (feed concentration = 0.02 mmol L^{-1}), the retention increases from 91 % (for 20 % PES/NMP) to 99 % (for 26 % PES/NMP) and from 93 % (for 16 % PES/DMF) to 99 % (for 17 % PES/DMF). The retention of raffinose (feed concentration = 2 mmol L^{-1}) was in all cases very low (below 5 %). From these data, it was seen that there is a large difference between the retention of raffinose and congo red. This was explained by the fact that raffinose is uncharged while congo red carries a negative charge. Because the membrane surface is also negatively charged at neutral pH (section 3.3.2), congo red experiences a repulsion force, resulting in a high retention of this component.

This paragraph proves that the polymer concentration has a large influence on the membrane performance and structure. To study the influence of the other preparation factors, an optimal polymer concentration was selected, namely 17 % PES in the case of DMF and 26 % PES in the case of NMP. These concentrations were chosen in such a way that a nanoporous structure was obtained: congo red was retained very well (99 %) and the water permeability was in the nanofiltration range ($10 \text{ L m}^{-2} \text{ h}^{-1} \text{ bar}^{-1}$ for 17 % PES/DMF and $19 \text{ L m}^{-2} \text{ h}^{-1} \text{ bar}^{-1}$ for 26 % PES/NMP).

3.2.2 Influence of the relative air humidity

To study the influence of the relative air humidity on the water permeability, 15 membranes were synthesized at relative humidities of 30, 50, 70 and 90 %, respectively. The results are given in Figure 3.4 for a 17 % PES/DMF membrane; the results for PES/NMP (not shown) were similar.

Figure 3.4 shows that a higher relative humidity gives rise to a larger variation (higher standard deviation) on the measured water permeability. In literature, Chaturvedi *et al.* (2001) reported that exposure to higher humidity gives more porous membranes with higher water permeation rates for the system PES/DMF and PES/NMP, but they tested only two different humidities (55 % and 90 %) and no standard deviations of the experimental water fluxes were given.

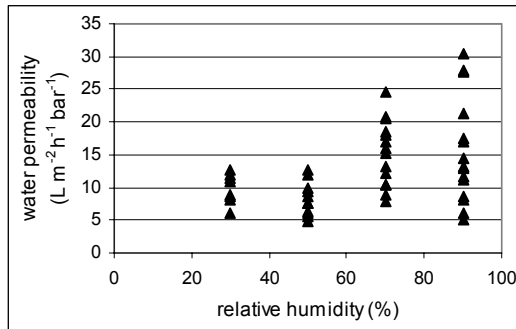


Figure 3.4: Influence of the relative air humidity on the pure water permeability ($L m^{-2} h^{-1} bar^{-1}$) of a 17 % PES/DMF membrane. Each point represents the water permeability of a membrane at a specific relative air humidity.

The relative humidity influences the membrane performance, as during the casting of the polymer solution to a film, the composition of the cast film varies by water vapour sorption. Water vapour sorption occurs rather than evaporation of the solvent, since DMF and NMP are highly hygroscopic and non-volatile solvents. Due to this water vapour sorption, phase separation occurs on some places on the membrane surface, prior to the phase separation that occurs when the cast film is placed in the non-solvent bath of distilled water. The relative humidity can thus solely have an influence on the top layer of the membrane surface, as the underlying layers of the membrane are only formed at the moment of immersion in the non-solvent bath.

SEM images of the cross-section of the membranes at low and high relative humidity were similar and comparable with Figure 3.3b. A change in the top layer of the membrane should have an influence on the observed retentions, but the

effects were small: congo red is almost completely retained at all humidities, while the retention of raffinose is always very small (below 5 %).

This paragraph proves that, to enhance the reproducibility, membranes should be prepared in an atmosphere with a low relative humidity. Because of the presence of a non-solvent bath of distilled water, there are restrictions on the minimal relative humidity. A relative humidity of 40 % could be maintained in all experiments.

3.2.3 Influence of additives to the polymer solution

Different components were added to the polymer solution, such as acetone (a volatile additive) or distilled water (non-solvent). No pore-forming agents were added, because according to literature (Marchese *et al.*, 2003; Han and Nam, 2002; Chaturvedi *et al.*, 2001; Han *et al.*, 1999; Kim and Lee, 1998), these additives would drastically enlarge the pores resulting in undesired low retentions of both congo red and raffinose.

When volatile components are added to the polymer solution, they can evaporate during the casting of the polymer film, resulting in the formation of a membrane with a top layer containing smaller pores (and hence lower permeabilities and higher retentions). Just as with the relative humidity, a volatile additive is thought to have only an influence on the top layer of the membrane. However, by adding up to 8 % acetone, the permeability for the 17 % PES/DMF membrane increased from $10 \text{ L m}^{-2} \text{ h}^{-1} \text{ bar}^{-1}$ to $13 \text{ L m}^{-2} \text{ h}^{-1} \text{ bar}^{-1}$ and there was no effect on the observed retentions of congo red and raffinose. So, adding acetone to the polymer solution did not provide a large improvement in the membrane performance.

By adding water (non-solvent) to the polymer solution, the starting polymer solution (which is normally located in the stable region) moves closer to the unstable binodal region in the ternary phase diagram of the polymer system. By immersing this polymer solution in the non-solvent bath, only small amounts of water are needed for phase separation to occur. This results in the formation of a porous membrane with a thin top layer and hence with a high water permeability.

This phenomenon was observed for the 17 % PES/DMF system where the water permeability increases from $10 \text{ L m}^{-2} \text{ h}^{-1} \text{ bar}^{-1}$ to $20 \text{ L m}^{-2} \text{ h}^{-1} \text{ bar}^{-1}$ when 0.9 % of distilled water is added. As, at the same time the retention of congo red decreases from 99 % to 94 %, adding water to the polymer solution did not seem to improve the membrane performance.

3.2.4 Influence of additives to the non-solvent bath and the bath temperature

The influence of adding an alcohol to the non-solvent bath of distilled water was investigated for the PES/DMF and the PES/NMP system. Increasing the alcohol concentration (isopropanol or ethanol) in the distilled water bath from 0 % to 40 % causes a decrease in the water permeability for the 17 % PES/DMF membrane from $10 \text{ L m}^{-2} \text{ h}^{-1} \text{ bar}^{-1}$ to $4 \text{ L m}^{-2} \text{ h}^{-1} \text{ bar}^{-1}$. When the non-solvent bath consisted of pure isopropanol, the water flux was reduced to zero for both the PES/DMF and the PES/NMP system. Although the influence of adding alcohol to the non-solvent bath on the water permeability was remarkable, congo red was in all cases retained for 99 % (except for the case of a pure alcohol bath, where no flux was measured and hence no permeate sample could be collected).

This phenomenon was explained in literature (Swinyard and Barrie, 1988) by the fact that, if an alcohol is used as non-solvent, the binodal region in the ternary phase diagram shrinks significantly. This implies that more non-solvent (alcohol) is needed to diffuse into the polymer solution before this solution reaches the binodal region and phase separation can occur. This results in a membrane with a thicker dense layer, which can explain the decrease of the water flux.

A decrease of the water flux was also observed when the temperature of the distilled water bath for both the PES/DMF and the PES/NMP system was increased, as shown in Table 3.2. Increasing the bath temperature not only decreased the water permeability but also slightly decreased the retention of congo red.

This effect can again be explained by the shrinkage of the binodal region in the ternary phase diagram, when increasing the bath temperature, as reported by Swinyard and Barrie (1988). Moreover, when the bath temperature increases, the

polymer solution becomes less viscous, resulting in an increased diffusivity of the solvent through both the internal polymer phase as well as through the interface between the developing membrane and the non-solvent bath. This results in a faster concentration of the polymer in the film, giving a thicker dense layer and hence a smaller flux. In addition, when the bath temperature is increased, the solubility of the polymer in the solvent increases, so that the polymer is kept in solution at a higher water concentration without phase separation and again a thicker dense film is generated.

Table 3.2: Influence of the temperature of the non-solvent bath on the water permeability ($L m^{-2} h^{-1} bar^{-1}$) and on the retention (%) of congo red (for a feed concentration of $0.02 mmol L^{-1}$)

temperature (K)	17 % PES/DMF		26 % PES/NMP	
	permeability	retention	permeability	retention
285	13	99	24	99
293	10	99	19	99
320	3	94	1	92

3.2.5 Influence of the solvent

The solvent (DMF or NMP) also influences strongly the membrane performance. This effect was particularly obvious for the water permeability (as shown in Figure 3.2). The explanation for this large difference in water permeability was found in the membrane structure. Figure 3.5 presents SEM images of the cross-sections and of the top layers of a 32 % PES/DMF and a 30 % PES/NMP membrane.

From Figure 3.5 (left), it is seen that the PES/NMP membrane is thicker than the PES/DMF membrane (85 μm and 60 μm , respectively) and that the PES/NMP membrane has longer and narrower macrovoids in comparison with the PES/DMF membrane. Also the thickness of the top layer differs for both membranes (Figure 3.5 (right)), as the PES/NMP membrane has a top layer of about 0.5 μm , whereas a top layer of about 3 μm is observed for the PES/DMF membrane. When

SEM images of membranes prepared with a lower polymer concentration are studied, the same conclusions could be drawn.

From this SEM study, it becomes clear that the PES/DMF membranes are characterized by a thicker top layer than the PES/NMP membranes. Because the water flux is inversely proportional with the thickness of a membrane (Hagen-Poiseuille) and because the sub layer of the PES/DMF and the PES/NMP membranes is very porous with many macrovoids, the main resistance for the water flux is located in the top layer. So, the thicker the top layer, the more resistance and the lower the water flux, which was observed for the PES/DMF membranes.

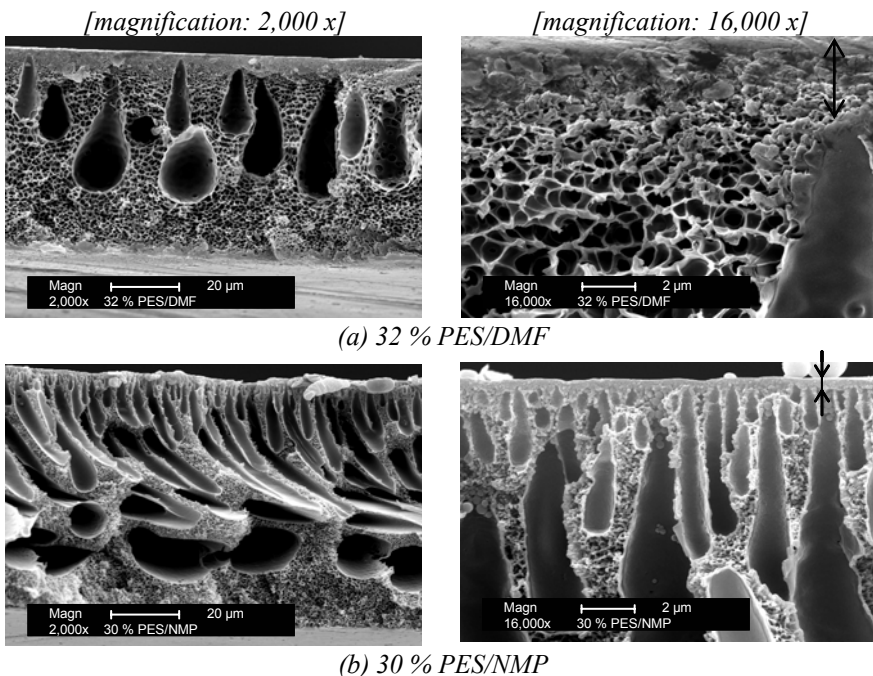


Figure 3.5: SEM images of (a) 32 % PES/DMF and (b) 30 % PES/NMP with a zoom on the top layer

The presence of the thicker top layer in PES/DMF membranes was explained both by thermodynamics and kinetics. By performing viscosity measurements, it became clear that the DMF solution is less viscous than the NMP solution

(4.81 Pa s for 32 % PES/DMF versus 6.11 Pa s for 30 % PES/NMP). This lower viscosity of the PES/DMF solution increases the diffusivity of DMF versus NMP through both the polymer solution as well as through the interface between the developing membrane and the non-solvent bath. DMF also has a higher enthalpy of solution in water than NMP as was seen from DMF's solubility parameter ($50.7 \text{ (J mL}^{-1})^{0.5}$ versus $47.3 \text{ (J mL}^{-1})^{0.5}$ for NMP).

These two facts imply that DMF has a higher gradient into the water phase than NMP and that the transport of DMF into water is faster than the transport of NMP into water, while the uptake of water into both polymer solutions is more similar. This will result in a faster concentration of the polymer in the PES/DMF film, giving a thicker dense top layer.

3.2.6 Conclusion

By changing the preparation conditions for PES membranes (without support layer), it is proven that the polymer concentration and the relative humidity are the most important preparation factors to obtain a reproducible membrane with a good performance. The choice of the solvent also plays an important role in the formation of the membrane.

This knowledge will be used in the study of the synthesis of polyethersulfone membranes on a support layer, which allows to study the performance of the membranes in a more realistic way. However, when polyethersulfone membranes are prepared on a support, the influence of this support layer on the membrane performance also has to be taken into account (Aerts *et al.*, 2006).

3.3 Preparation of membranes on a support layer

Two different support layers (FO2413 and FO2471) and two different solvents (DMF and NMP) were used, resulting in four different types of membranes. To prevent the polymer solution of intruding in the pores of the support layers, the support layer was wetted with the appropriate solvent prior to casting. As non-solvent, a distilled water bath at 293 K was used. No components were added to

the non-solvent bath or to the polymer solution. During casting of the polymer solution, the relative air humidity was 40 %. After synthesis, the membranes were characterized and tested for their performance in the cross-flow setup.

3.3.1 Influence of the polymer concentration

Figure 3.6 shows the influence of the polymer concentration on the water permeability for the four different membranes. Just as without support layer (paragraph 3.2.1), the water permeability decreases with increasing polymer concentration. Besides the polymer concentration, the support layer used is also important, as the more porous support FO2413 gives rise to a higher water permeability than the denser support FO2471. This effect is also reported by Barth *et al.* (2000b) and explained by Aerts *et al.* (2006) by the shrinkage effect. Due to the fact that the polymer solution can intrude more in the more porous support FO2413, shrinkage of the polyethersulfone film is less, resulting in a higher water permeability.

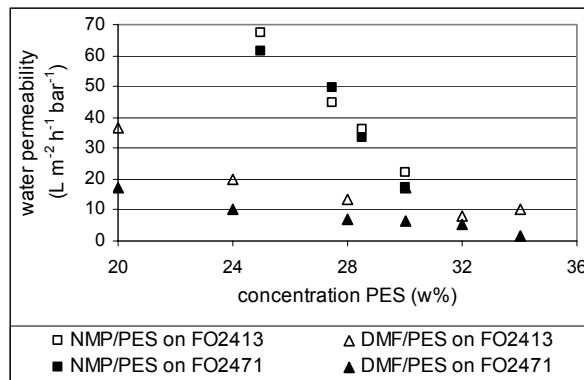


Figure 3.6: Influence of the polymer concentration on the water permeability ($L m^{-2} h^{-1} bar^{-1}$), measured in cross-flow

To characterize and to test the performance of the membranes, an optimal polymer concentration should be selected, so that a reasonable water flux is combined with a good retention of an uncharged component (raffinose). In the experiments, it was observed that the retention of raffinose increases with increasing polymer

concentration, e.g., from 23 % in the case of 20 % PES to 31 % in the case of 34 % PES when PES/DMF membranes were cast on FO2413.

So, a high polymer concentration would be advantageous for the retention, but disadvantageous for the water permeability. There are also practical limitations, as a very high polymer concentration would result in a very viscous solution. This hampers the defect-free casting of the solution on the support layer.

Taking into account these practical limitations and the experimental values of the water permeability and the retention, the optimal concentrations were determined as 32 % PES for DMF and 30 % PES for NMP. The membranes prepared with these concentrations will be studied in the rest of the manuscript and will be referred to as: **D13** and **D71** (for a 32 % PES/DMF solution cast on FO2413 and FO2471, respectively) versus **N13** and **N71** (for a 30 % PES/NMP solution cast on FO2413 and FO2471, respectively). Their water permeability was determined as 17.0 and 22.2 L m⁻² h⁻¹ bar⁻¹ for N71 and N13, respectively, while D71 and D13 have a water permeability of 4.7 and 9.4 L m⁻² h⁻¹ bar⁻¹, respectively. The retention of raffinose (feed concentration = 2 mmol L⁻¹) was almost equal for all membranes and was about 27 % (as described in more detail in paragraph 3.3.3.1).

A comparison between the membranes without support layer (paragraph 3.2) and with support layer (this paragraph) indicates that the latter ones have higher water permeabilities and also higher retentions of uncharged components. The good retention of raffinose was explained by the higher polymer concentrations used for making membranes on the support layer. The difference in water permeability was related to the way the membranes are placed in the non-solvent bath.

When casting on a support layer, this support is taped on a glass plate and the casting solution is then applied as a wet film. By immersing the solution in non-solvent, phase separation occurs and propagates from the top surface of the wet film into the bulk, forming an integrally skinned dense layer on the top surface of the remaining porous structure. On the other hand, when the wet film is cast directly on the glass plate and then immersed in the non-solvent bath, the

membrane may rapidly lift of the glass plate with a considerable amount of solvent remaining in the membrane. With non-solvent (or distilled water in this case) on both sides of the developing membrane, a solvent gradient on the backside of the membrane is also established. A less porous layer will hence be formed on the backside of the asymmetric membrane, which in combination with the (very dense) top layer results in a lower water flux.

This mechanism was confirmed by comparing SEM images of membranes made from a 32 % PES/DMF or a 30 % PES/NMP solution on a glass plate (Figure 3.5) or on a support layer (Figure 3.7). A comparison between Figure 3.5 and 3.7 indicates that the backside of the membranes made on a glass plate is less porous than the backside of the membranes made on a support. In the latter case, the macrovoids appear all through the polyethersulfone layer towards the support layer.

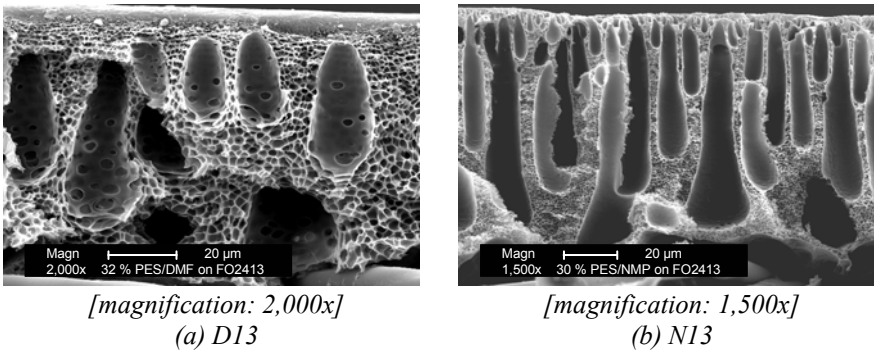


Figure 3.7: SEM images of the cross-sections of the polyethersulfone layer of (a) D13 and (b) N13

Figure 3.7 again shows the difference in membrane structure when using DMF or NMP as solvent. The influence of the solvent, when making a membrane on a support layer, is however twofold. Firstly, there is an influence when the solvent is used to dissolve the polymer, which was clearly seen in Figure 3.7. Secondly, when making a membrane on a support layer, the solvent is also used to wet the support layer prior to casting, so that intruding of the polymer solution in the pores

of the support layer is prevented. Mostly, the same solvent as the one used to dissolve the polymer, is used.

When different solvents are applied, the water permeability will be influenced. For instance, when wetting the support layer with DMF prior to casting a PES/NMP solution, the water permeability decreases for N71 from 17.0 to 11.2 L m⁻² h⁻¹ bar⁻¹ and for N13 from 22.2 to 10.2 L m⁻² h⁻¹ bar⁻¹. In contrary, when casting a PES/DMF solution on a support layer wetted with NMP, the water permeability increases from 4.7 to 6.3 L m⁻² h⁻¹ bar⁻¹ for D71 and from 9.4 to 10.7 L m⁻² h⁻¹ bar⁻¹ for D13.

Apparently, using DMF as solvent either to dissolve the polymer or to wet the support layer has a disadvantageous effect on the water permeability. Using NMP as solvent however seems to have an advantageous effect on the water flux.

3.3.2 Characterization of the membranes

Table 3.3 summarizes the characteristics of the four laboratory-made membranes on a support layer. The characteristics of two commercial polyethersulfone nanofiltration membranes (NFPES10 and N30F) are also included in Table 3.3 for reference (as described in more detail in Chapter 4).

Table 3.3: Characteristics of the laboratory-made membranes and commercial polyethersulfone nanofiltration membranes

		N71	N13	D71	D13	NFPES10	N30F
permeability (L m ⁻² h ⁻¹ bar ⁻¹)		17.0 (± 3.4)	22.2 (± 3.1)	4.7 (± 1.4)	9.4 (± 2.6)	15.4 (± 2.8)	3.8 (± 0.8)
contact angle (°)		67 (± 3)	67 (± 3)	73 (± 2)	73 (± 2)	72 (± 4)	88 (± 2)
roughness ¹ (nm)		3.7	4.4	3.9	3.7	2.4	3.4
zeta potential (mV)	pH 4	-7	-4	-3	-2	-2	-5
	pH 7	-12	-10	-13	-8	-12	-15
	pH 10	-17	-14	-13	-12	-15	-18
cut-off (Da)		2,200	2,100	2,000	1,900	1,200	680

¹ roughness measured in non-contact mode AFM on a scan area of 3 μm x 3 μm

To test the reproducibility, 15 different membrane samples were prepared; the water permeability was measured for each sample. The standard deviations on the water permeability (given in Table 3.3) were not significantly different from the commercial membranes, which indicate that the laboratory-made membranes are as reproducible as the commercial membranes.

Contact angle measurements were performed to study the hydrophobicity of the membrane surfaces. Table 3.3 shows that the commercial membrane N30F has the most hydrophobic membrane surface, while the hydrophobicity of the other membranes is comparable.

The roughness of the membrane surface is visualized in Figure 3.8 for D71 and N13. As can be seen from Table 3.3, the roughness values are similar for all membranes. NFPES10 has the smoothest membrane surface.

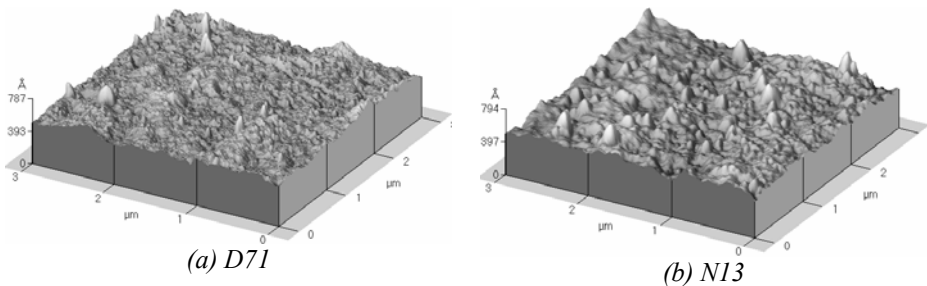


Figure 3.8: Non-contact mode AFM images of (a) D71 and (b) N13 on a scan area of $3 \mu\text{m} \times 3 \mu\text{m}$

From the behavior of the zeta potential as a function of pH, it becomes clear that all polyethersulfone membranes are negatively charged at high pH and that this negative charge diminishes when the pH decreases. The iso-electric point, defined as the pH for which the net charge of the membrane is equal to zero, is located around 3 for all membranes. This behavior of the charge as a function of the pH can be explained by the adsorption of anions or by the presence of sulfonic groups ($-\text{SO}_3^-$) on the surface. These sulfonic groups are strongly acidic and are completely dissociated at a pH above 2.

The fact that the hydrophobicity, the surface charge and the roughness are almost similar for the laboratory-made and the commercial membranes indicates that the top layer of all membranes is composed of the same polymer. However, there is a difference between the laboratory-made and the commercial membranes as was seen in the cut-off. The cut-off or the molecular mass of polyethylene glycol with 90 % retention, is higher for the laboratory-made membranes (about 2,000 Da). The lower cut-off of the commercial membranes can probably be explained by different preparation conditions or the presence of additives during synthesis or by a post-treatment after synthesis.

3.3.3 Testing of the performance of the membranes

The performance of the laboratory-made membranes was tested in a cross-flow setup, by filtering a feed solution of uncharged (feed concentration = 2 mmol L⁻¹) and charged components (feed concentration = 0.2 mmol L⁻¹) during two hours. For the (colored) charged components, a lower feed concentration was selected because of cleaning problems of the equipment. To have a reference, the same experiments were repeated for the commercial membranes.

3.3.3.1 Evaluation of the retention of laboratory-made membranes

The results of the retention after two hours filtration for both the laboratory-made and the commercial membranes are summarized in Table 3.4. A difference in retention of the laboratory-made membranes, depending on the charge of the component, was observed. The uncharged component raffinose has the lowest retention, which is due to the absence of charge interactions between the component and the membrane surface. The higher cut-off of the laboratory-made membranes in comparison with the commercial membranes causes the retention of raffinose to be lower for the laboratory-made membranes.

When the components carry a negative charge, the retention increases considerably, even for small components like diphenylaminosulfonic acid ($M_w = 271$ Da) or methyl orange ($M_w = 327$ Da). Strong repulsion forces between the negatively charged membrane and the negatively charged component can explain

this phenomenon. These repulsion forces are even so strong that the retention of the laboratory-made membranes is only a little lower than the one of the commercial membranes, in spite of the higher cut-off of the former ones. For congo red, a large negative component ($M_w = 697$ Da), the same retention was observed for the different membranes after two hours filtration.

Table 3.4: Retention (%) after 2 h of filtration in cross-flow with a feed concentration of 2 mmol L⁻¹ (raffinose) or 0.2 mmol L⁻¹ (other components)

	N71	N13	D71	D13	NFPES10	N30F
raffinose	22	28	33	26	58	75
diphenylaminosulfonic acid	84	82	75	74	87	93
methyl orange	55	55	72	69	76	88
congo red	100	100	99	99	100	99
neutral red	72	75	55	76	50	61
methylene blue	79	80	80	79	32	35
janus green	96	96	99	98	95	95

However, this was not the case during the whole duration of the filtration experiment. The retention of congo red by the commercial membrane N30F was only 70 % after 15 minutes of filtration and reaches a stable value (of 100 %) only after one hour. In contrast, the retention of the laboratory-made membranes was already stable from the beginning of the experiment. Also for diphenylaminosulfonic acid, a very low retention of 30 % and 55 % was observed for N30F and NFPES10, respectively, during the first hour of filtration. This phenomenon was not only observed for negatively charged components, but also for positively charged components like janus green. Unlike the stable retention of the laboratory-made membranes, janus green was only retained for 40 % and 80 % by N30F and NFPES10, respectively, in the beginning of the filtration experiment. Only after 90 minutes, a stable value of the retention (95 %) was observed.

Another remarkable phenomenon is that janus green, even after reaching a stable retention, is less retained by the commercial membranes than by the laboratory-

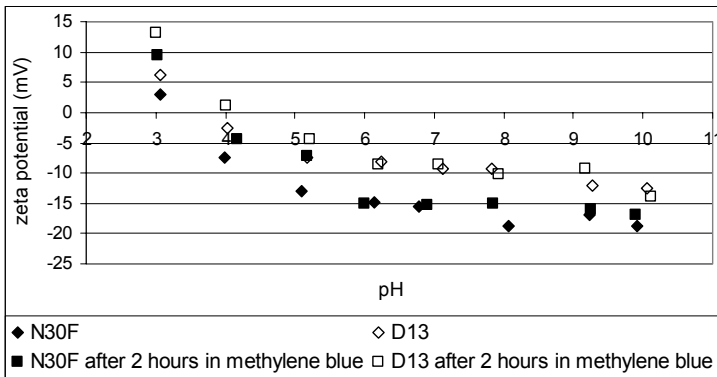
made membranes. Five percent of janus green is passed through the commercial membranes, while D71 and D13 let pass only one or two percent of janus green. For N71 and N13 a retention of 96 % or a passage of 4 % of janus green was measured. This discrepancy between the commercial and the laboratory-made membranes gets even larger when filtering small positively charged components like neutral red ($M_w = 289$ Da) or methylene blue ($M_w = 320$ Da). Especially for methylene blue, this effect is remarkable: methylene blue is retained only for 32 % or 35 % by the commercial membranes, while retentions up to 80 % were measured for the laboratory-made membranes.

This remarkably higher retention of positively charged components by the laboratory-made membranes was explained by studying the surface charge of the membranes, before and after the membrane has been in contact with the feed solution. The same procedure was performed in literature by Susanto and Ulbricht (2005). Surface charge measurements were performed for the unused membrane and for the same membrane after immersion during two hours (i.e., the duration of a cross-flow experiment) in a feed solution of 0.2 mmol L^{-1} of methylene blue or janus green. For janus green, the surface charge of the membrane after 15 minutes immersion was also measured. The data are given in Figure 3.9 for D13 and N30F; the results were similar for the other membranes. Because the filtration experiments were performed at near neutral pH (pH 6), the discussion is limited to this pH.

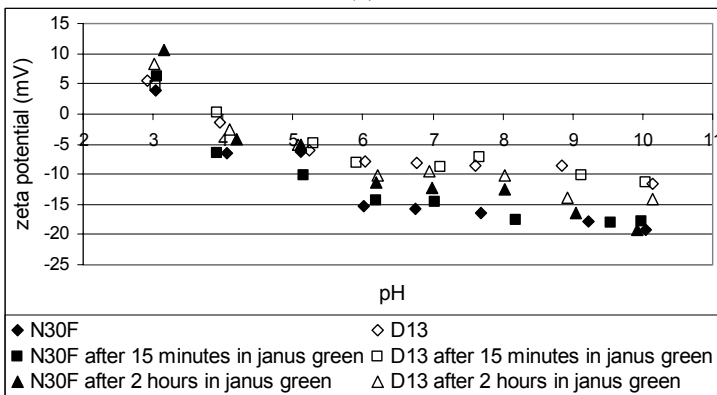
Figure 3.9a shows that for methylene blue, no difference in surface charge is observed between the unused and the immersed membrane. This effect is seen both for the commercial and the laboratory-made membranes. Starting from Figure 3.9a, the lower retention of methylene blue by the commercial membranes could be explained by the large negative surface charge. Between the positively charged component and the negatively charged surface, an electrostatic attraction force acts, resulting in an increased concentration of the component at the membrane surface and hence in a lower retention. Because the laboratory-made membranes are less negatively charged than the commercial membranes, the attraction force

between component and surface is smaller and hence a higher retention of methylene blue is obtained.

For janus green (Figure 3.9b), the surface charge of the commercial membrane N30F did not change during the first 15 minutes. Only after two hours, the membrane surface became less negatively charged, probably due to adsorption of janus green. In contrast, no decrease in the surface charge of the laboratory-made membranes was observed. The surface charge of D13 remained almost the same after 15 minutes immersion and even became a little more negatively charged after two hours immersion. The latter is probably due to inaccuracies during measuring.



(a)



(b)

Figure 3.9: Zeta potential as a function of pH for D13 and N30F, before and after immersion in (a) methylene blue and (b) janus green

From the observations given in Figure 3.9b, two conclusions can be drawn. The first conclusion is that the time dependency of the surface charge corresponds to the time dependency of the retention of janus green. As mentioned previously, low retentions of janus green for the commercial membranes were observed during the beginning of the filtration, because the membrane surface is then still very negatively charged. Only after two hours, when the surface has become less negative, the electrostatic attraction force between component and surface diminishes resulting in a higher retention. Unlike the commercial membranes, the laboratory-made membranes had a stable high retention from the beginning of the filtration, which is in agreement with the fact that almost the same surface charge was observed before and after immersing these membranes in a solution of janus green. A second conclusion that was drawn from Figure 3.9b, is that the surface charge of both the commercial and the laboratory-made membranes is almost equal after immersion during two hours in janus green. This could explain the similar retention of janus green for these membranes.

From this description of the influence of the component charge on the retention, it is clear that the laboratory-made membranes have the highest retention for charged components, independently of the sign of the charge. In contrast, the retention for the commercial membranes is dependent on the sign of the component charge as the lowest retention was observed for small positively charged components. Besides the influence of the component charge, there is also an influence of the molecular mass as larger components are better retained.

The only exception to this is methyl orange, which shows a too small retention for its molecular mass for all membranes. The lower retention can possibly be explained by its molecular geometry (Appendix II); this topic is not further considered in this thesis, but is in literature (Santos *et al.*, 2006) already observed for uncharged organic components.

3.3.3.2 Evaluation of the relative flux of laboratory-made membranes

The relative fluxes and the permeate fluxes (measured after two hours filtration) for both the laboratory-made and the commercial membranes are summarized in

Table 3.5. Because the relative flux is defined as the ratio of the permeate flux to the pure water flux, the relative flux is a measure for the degree of flux decline (due to the presence of the solute). The flux decline of all membranes for all feed solutions is in the same order, with some exceptions.

Table 3.5: Relative flux (a, in %) and permeate flux (b, in $L m^{-2} h^{-1}$) after 2 h of filtration in cross-flow with a feed concentration of $2 mmol L^{-1}$ (raffinose) or $0.2 mmol L^{-1}$ (other components)

	N71	N13	D71	D13	NFPE10	N30F
raffinose	70	86	58	71	63	42
diphenylaminosulfonic acid	69	72	79	81	53	29
methyl orange	70	53	59	7	59	34
congo red	36	85	32	75	55	43
neutral red	56	54	63	11	49	17
methylene blue	52	52	84	63	60	57
janus green	55	52	83	60	53	46

(a)

	N71	N13	D71	D13	NFPE10	N30F
raffinose	9.6	15.8	1.9	7.2	8.7	1.6
diphenylaminosulfonic acid	9.1	14.4	4.8	7.0	9.3	1.0
methylene blue	8.2	12.1	3.2	5.5	10.5	1.5

(b)

For example, raffinose and diphenylaminosulfonic acid have lower relative fluxes for the commercial membranes in comparison with the laboratory-made membranes. However, the low relative flux of diphenylaminosulfonic acid for the commercial membranes was not observed during the whole duration of the filtration experiment: only after one hour, the permeate flux decreased considerably.

Very low permeate fluxes were also observed when filtering methyl orange or neutral red solutions with D13 or N30F. Especially for D13, specific interactions between these components and the membrane caused the flux through the membrane to decrease by 90 %. Of the tested positively charged components,

neutral red was the only one resulting in a strong flux decline on some membranes. This implies that the good retention of the positively charged components by the laboratory-made membranes does not result in more flux decline, as the degree of flux decline is comparable for the laboratory-made and the commercial membranes. The D71 membrane even showed the highest relative flux for methylene blue and janus green in comparison with the other membranes. The highest (absolute) permeate fluxes (Table 3.5b) were observed for N13 and N71.

3.4 Conclusion

Nanoporous polyethersulfone membranes with a performance similar to commercial membranes can be prepared using the phase inversion technique. A compromise between a high retention of a reference component (congo red or raffinose) and a high water permeability was obtained through proper choice of the concentration of the polymer. The relative air humidity during casting should also be as low as possible to improve the reproducibility. Besides these two preparation factors, it was shown that the membrane structure and hence the membrane performance are strongly dependent on the casting solvent, as PES/NMP membranes have a higher water permeability than PES/DMF membranes.

The physical characteristics of these laboratory-made membranes were similar to the characteristics of commercial polyethersulfone nanofiltration membranes, with exception of the cut-off. In spite of the higher cut-off for the laboratory-made membranes, the retention of charged components was remarkably high. This phenomenon was in particular observed when filtering small, positively charged components. In spite of these high retentions, the flux decline for the laboratory-made membranes was comparable to the commercial membranes, which in combination with the higher pure water permeability, leads to higher permeate fluxes. The fact that there is more and more pure permeate flux, makes the laboratory-made membranes interesting when filtering aqueous solutions of charged components.

Chapter 4

Physico-chemical characterization of nanofiltration membranes

*Adapted from: Chem. Phys. Chem. 8 (2007) 370-379
Desalination 191 (2006) 245-253
J. Colloid Interface Sci. 286 (2005) 632-638*

4.1 Introduction

Membrane fouling is an interplay between feed composition, membrane characteristics and operating conditions. The former two are interrelated, as the composition of the feed determines which membrane characteristics are crucial to prevent fouling (Chapter 5). For example, an aqueous solution containing organic components (e.g., pesticides) should be filtered with a nanofiltration (NF) membrane with a low hydrophobicity (Bellona *et al.*, 2004; Kiso *et al.*, 2001). Membrane fouling can be minimized by a good choice of operating conditions. Using a cross-flow setup with a high feed velocity (Hoek *et al.*, 2002) and an optimal cleaning frequency (Ang *et al.*, 2006; Wang *et al.*, 2005) can already reduce some of the negative effects of fouling. Both the composition of the feed and the operating conditions have to be optimized in each particular case. The membrane characteristics, on the other hand, can be determined independently from the application, with the advantage that this information can then be applied in future membrane fouling studies.

This chapter describes a methodology for the physical and chemical characterization of nanofiltration membranes. In addition to some physical characteristics (cut-off, roughness, hydrophobicity and surface charge), the porosity and the chemical composition of the membrane top layer are discussed. Seven typical commercial NF membranes (UTC20, NF270, Desal51HL, Desal5DL, N30F and NFPES10) were selected, of which the characteristics given by the manufacturers are summarized in Table 2.1. These membranes are all thin film composite membranes, which means that they consist of a thin top layer (e.g., polyethersulfone or polyamide) on top of a porous support, made from different polymers. In this chapter, the top layer is further divided into an upper part, called the skin layer, and into a lower more porous part, called the sub layer.

For reference, two laboratory-made membranes with well-known chemical composition are also included: D71 and N13 (Chapter 3, section 3.3). D71 is synthesized by casting a top layer of polyethersulfone, dissolved in N,N-

dimethylformamide (DMF), on the support layer FO2471 (made of PP/PE); N13 is composed of a top layer of polyethersulfone, dissolved in N-methyl-pyrrolidone (NMP), and a polyester support layer (FO2413).

Although in literature, membrane fouling is mostly related to well-known physical characteristics (like e.g., the roughness, the hydrophobicity or the surface charge), the influence of both the porosity and the chemical composition of the membrane should not be underestimated. The porosity of the top layer of a membrane determines to which extent e.g., organic foulants can intrude into and block or foul the pores.

Information about the chemical composition is also crucial for the fouling phenomenon for several reasons. Firstly, the chemical composition of the top layer is (directly or indirectly) related to the physical characteristics. The polymer (or monomer) used has a direct influence on e.g., the surface charge, while it determines indirectly the choice of the membrane preparation technique and hence e.g., the thickness of the top layer. Secondly, fouling is in some cases dependent on specific interactions between the feed components and the membrane surface; these specific interactions are not taken into account in the (more general) physical characteristics.

4.2 Chemical characterization of nanofiltration membranes

The chemical composition of top and support layer of the selected commercial and laboratory-made membranes was studied with two different techniques: ATR-FTIR (Attenuated Total Reflectance - Fourier Transform InfraRed) and XPS (X-ray Photoelectron Spectroscopy). In ATR-FTIR, molecular vibrations are studied by exposing the membrane to infrared radiation (section 2.4.6), while in XPS the chemical composition is deduced by exposing the sample to X-rays and measuring the kinetic energy of the emitted electrons (section 2.4.7).

4.2.1 ATR-FTIR Spectroscopy

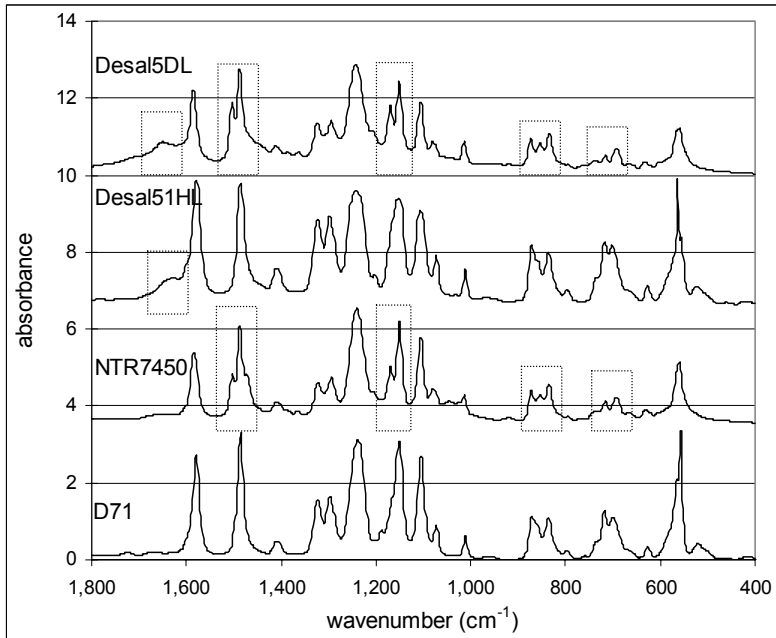
ATR-FTIR spectra of the top layer of the laboratory-made membrane D71 and of the commercial membranes Desal5DL, Desal51HL and NTR7450 and ATR-FTIR spectra of the support layers FO2413 and FO2471 are given in Figure 4.1. As it was the goal to obtain general information about the polymer structure, the peaks in the spectra were not analyzed individually, but rather compared with spectra of known polymers in literature (Pavia *et al.*, 1996; Hummel and Scholl, 1978).

The spectrum of the top layer of D71 (Figure 4.1a) was identical to the spectrum of the other laboratory-made membrane N13 (not shown) and to the spectra of N30F and NFPES10 (not shown). These commercial membranes (N30F and NFPES10) only had an additional peak at 1670 cm^{-1} , which may originate from additives (e.g., a copolymer like polyvinylpyrrolidone, as reported by Wang and Chung (2005b) and Ernst *et al.* (2000)) or from residual products (e.g., solvent, as reported by Pihlajamäki *et al.* (1998)) used during membrane synthesis. Comparing these spectra with the spectra given by Hummel and Scholl (1978), indicates that the top layer of all four membranes (D71, N13, N30F and NFPES10) is composed of poly(phenylenesulfone ether), as given in Figure 4.2a.

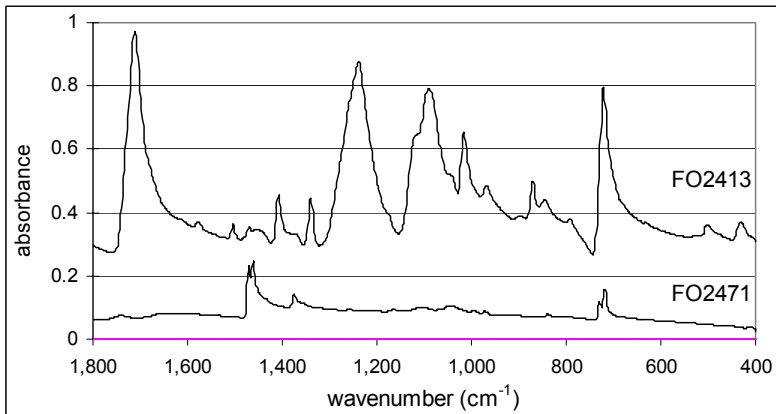
The spectrum of the top layer of the commercial membrane NTR7450, made of sulfonated polyethersulfone (Table 2.1) according to the manufacturer, shows some differences with the former spectra: the peaks at 1500 cm^{-1} and at 1150 cm^{-1} are split, between 900 cm^{-1} and 800 cm^{-1} three peaks are visible (instead of two peaks for D71) and between 720 cm^{-1} and 650 cm^{-1} only very small peaks are visible. These differences are all indications that the top layer of NTR7450 is composed of a more hydrophobic polyethersulfone, generally called poly(arylenesulfone ether), as shown in Figure 4.2b and reported also by Pihlajamäki *et al.* (1998).

The spectra of Desal51HL and D71 are very similar, although their top layer is composed of a different polymer (Table 2.1). The only difference between the two spectra is an additional small peak at 1630 cm^{-1} , which can be, according to Freger

et al. (2002), assigned to the presence of polyamide (amide I peak). Desal5DL, another commercial membrane with a top layer made of polyamide, also shows this additional peak at 1630 cm^{-1} . However, the spectrum of Desal5DL resembles more the spectrum of NTR7450 instead of D71, as indicated in Figure 4.1a. The spectrum of NF270 (not shown) was similar to Desal5DL.



(a)



(b)

Figure 4.1: ATR-FTIR spectra of (a) the top layer of Desal5DL, Desal51HL, NTR7450 and D71 and (b) the support layers FO2413 and FO2471

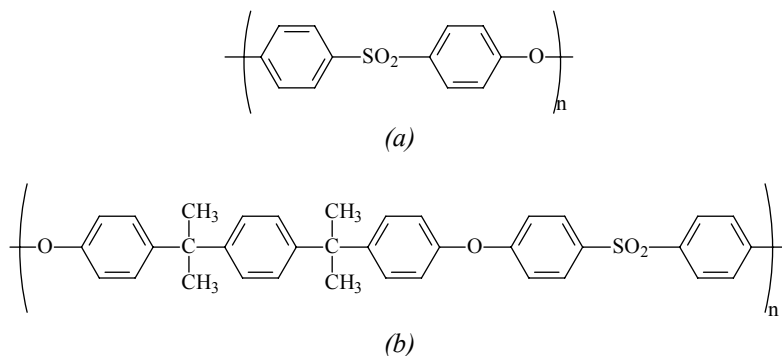


Figure 4.2: Chemical structure of (a) poly(phenylenesulfone ether) and (b) poly(arylenesulfone ether)

The fact that the spectra of these membranes (Desal51HL, Desal5DL and NF270) are not typical for polyamide, possibly means that the infrared radiation penetrates too deep (typically around 1 μm , according to Freger *et al.* (2002)) into the membrane for the polyamide top layer to be seen exclusively. Commercial polyamide membranes are traditionally made by the interfacial polymerization process, which results in a very thin top layer (around 50 nm) in contrast to the thicker top layer of polyethersulfone membranes obtained by the phase inversion process.

The ATR-FTIR spectra of the two known support layers (FO2471 and FO2413) are shown in Figure 4.1b. The spectra of the support layers of the commercial membranes (not shown) were compared with these two spectra to derive their composition. As indicated by the peaks at 1465 cm^{-1} and 720 cm^{-1} , FO2471 is composed of PP and PE, which was also the case for the support layers of D71, N30F and NFPES10. FO2413 is characterized by peaks at wavenumbers of 1700 cm^{-1} and 1230 cm^{-1} , which can be assigned to the presence of polyester. The other (large) peaks at 1100 cm^{-1} , 1000 cm^{-1} and 720 cm^{-1} probably indicate the presence of ionic sulphate groups ($-\text{RSO}_3^-$) in the polyester. The support layers of N13, Desal51HL, Desal5DL, NTR7450 and NF270 (not shown) are also (mainly) composed of polyester, as their spectra were similar to the spectrum of FO2413.

4.2.2 X-ray Photoelectron Spectroscopy (XPS)

Performing XPS measurements has the advantage that the X-rays do not penetrate too deeply into the membrane. Using an analysis takeoff angle between membrane surface and analyzer (θ) of 54° in XPS, 95 % of the emitted electrons comes from an escape depth $d \leq 3 \cdot \lambda_e \cdot \sin \theta = 7.5 \text{ nm}$, considering a value for the mean free path (λ_e) of the C_{1s} electrons in polyamide of 3.2 nm (Ariza *et al.*, 2002; Ariza *et al.*, 2000). This implies that the chemical information obtained through XPS originates only from the top layer of the nanofiltration membranes.

This is also seen from Table 4.1, in which the atomic concentration percentages of C_{1s} , O_{1s} , N_{1s} and S_{2p} of the different membranes are given. As shown in Table 4.1, the percentages of C_{1s} and O_{1s} are comparable for all membranes in contrast to the percentages of N_{1s} and S_{2p} . The membranes with a top layer of polyamide (NF270, Desal51HL and Desal5DL) obviously have a higher percentage of N_{1s} , while the polyethersulfone membranes (N30F, NFPES10, D71 and N13) have more S_{2p} than N_{1s} in their top layer.

Table 4.1: Atomic concentration percentages (%) of C_{1s} , O_{1s} , N_{1s} and S_{2p} obtained by XPS on commercial and laboratory-made membranes

	C_{1s}	O_{1s}	N_{1s}	S_{2p}
NF270	72.0	17.0	10.9	0.1
Desal51HL	75.9	12.6	10.7	0.8
Desal5DL	72.4	17.6	9.5	0.5
NTR7450	72.1	19.2	5.2	3.5
N30F	79.9	14.4	1.8	3.9
NFPES10	77.3	16.8	2.4	3.5
D71	77.0	16.3	2.6	4.1
N13	79.7	14.4	2.3	3.6

The atomic concentration percentages of these membranes agree well with other data reported in literature (Kim *et al.*, 2005; Benavente and Vazquez, 2004; Wavhal and Fisher, 2002). Small amounts of sulfur (nitrogen) in polyamide (polyethersulfone) membranes are in literature (Benavente and Vazquez, 2004;

Pihlajamäki *et al.*, 1998) attributed to environmental contamination or residual products from membrane manufacturing (like e.g., preservatives). Only for the top layer of NTR7450 both elements are present, with even more N_{1s} than S_{2p}. This nitrogen can originate from a post-treatment of the membrane or from additives used during the synthesis process.

More information about the chemical environment of carbon, oxygen, nitrogen and sulfur is obtained by deconvoluting the respective XPS spectra. The results of the different contributions are given in Table 4.2 for three typical commercial membranes: NFPE10 (comparable to N30F, D71 and N13), NTR7450 and Desal51HL (comparable to Desal5DL and NF270).

Table 4.2: Binding energies (BE, in eV) and peak areas (%) for C_{1s}, O_{1s}, N_{1s} and S_{2p} XPS spectra for three selected commercial membranes

	NFPE10		NTR7450		Desal51HL		assignment
	BE	area	BE	area	BE	area	
C _{1s}	285	74	285	68	285	66	C-C
	285.7	15	285.7	13	-	-	C-S
	286.9	12	286.7	14	286.2	25	C-O, C-N
	-	-	288.3	4	287.9	9	C=N, O=C-N, C=O
O _{1s}	532.1	62	531.9	65	531.7	75	C=O, O=C-N, C-O, O=S=O
	533.4	38	533.4	35	533.3	25	H···O=C-N, O=C-O
N _{1s}	-	-	400.2	100	399.9	100	C-N, C=N, O=C-N
S _{2p3/2}	168.3	60	168.3	75	-	-	O=S=O
	164.2	40	164.3	25	-	-	-S-

For all membranes, the core level C_{1s} spectrum contains a major peak at 285 eV (reference energy), associated with aliphatic/aromatic C-C bonding. For NFPE10, two minor components with a shift of 0.7 eV and 1.9 eV (relative to the reference energy at 285 eV) are attributed to the carbon-sulfur and carbon-oxygen groups, respectively (Figure 4.3a). These components are also found for NTR7450,

together with an additional smaller component at a 3.3 eV shift, which forms an indication for the presence of a double bond between carbon and nitrogen and between carbon and oxygen. Due to the absence of sulfur in the top layer of Desal51HL, the contribution of the carbon-sulfur group at a shift of 0.7 eV is missing.

The O_{1s} spectrum is for all membranes deconvoluted into two different components (Figure 4.3b), while the N_{1s} spectrum for NTR7450 and Desal51HL only contains one major peak at 400 eV. In literature, similar deconvolutions for the C_{1s} , O_{1s} and N_{1s} peaks were performed by Kull *et al.* (2005), Benavente and Vazquez (2004), Wavhal and Fisher (2002) and Beamson and Briggs (1992).

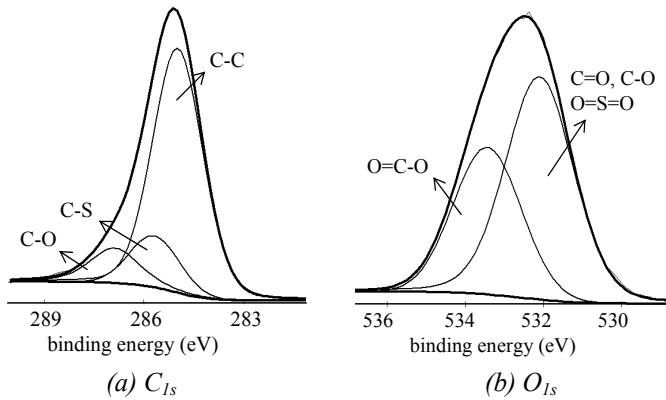


Figure 4.3: Deconvolution into different components for (a) the C_{1s} and (b) the O_{1s} peak for NFPE10

For NFPE10 and NTR7450, the S_{2p} spectrum is composed of two separate peaks at a distance of 4 eV from each other. Each of these S_{2p} peaks is deconvoluted in two peaks, i.e. $2p_{3/2}$ en $2p_{1/2}$, with a typical doublet separation of 1 eV and with a fixed relation between their peak surfaces of 2:1 (Beamson and Briggs, 1992). The $S_{2p_{3/2}}$ peak at 168 eV and 164 eV is assigned to sulfur present in a sulfone group and in a sulfide group, respectively. The fact that there is a sulfide group means that the sulfone group in the top layer of the membranes is transformed during sputtering of the membrane surfaces (section 2.4.7), as was concluded also by Marletta *et al.* (1991) and Kaul (1987). XPS measurements without sputtering indeed indicated only one doublet with $2p_{3/2}$ at 168 eV, which proves the presence of a sulfone group in the polymer of the top layer.

4.2.3 Conclusion

Combining the results of ATR-FTIR with XPS permits to determine the overall chemical composition of the membranes. Two different membrane classes could be distinguished: a class of membranes with a polyamide top layer (Desal51HL, Desal5DL, NF270) and a class of membranes with a polyethersulfone top layer (N30F, NFPES10, NTR7450, D71, N13).

The membrane structure of the first class consisted of (minimum) three layers: (1) a thin top layer of polyamide, (2) an intermediate layer of poly(arylenesulfone ether) in the case of Desal5DL and NF270 or more specifically poly(phenylenesulfone ether) in the case of Desal51HL, and (3) a polyester support layer.

For the second membrane class, only two layers were observed: (1) a top layer of poly(phenylenesulfone ether) or the more general poly(arylenesulfone ether) in the case of NTR7450, and (2) a support layer of PP/PE or, in the case of NTR7450 and N13, a support layer of polyester. In this second membrane class, small chemical differences were observed between the commercial and the laboratory-made membranes, which were attributed to the use of additives or post-treatments by the manufacturers.

4.3 Physical characterization of nanofiltration membranes

Several physical characteristics of the commercial and laboratory-made membranes were studied. In addition to the cut-off, the membrane surface was characterized for roughness, hydrophobicity and surface charge. An overview of the results of these characterization techniques is given in Table 4.3. The porosity and the thickness of the skin layer using PAS is discussed in section 4.4.

4.3.1 Determination of the cut-off

In literature, the cut-off is considered as a measure for the size of the pores and is defined as the molecular mass of a component with 90 % retention. The cut-off is strongly dependent on the component used and the filtration conditions.

Table 4.3: Overview of the physical characteristics of the commercial and laboratory-made membranes

		UTC20	NF270	Desal51HL	Desal5DL	NTR7450	N30F	NFPES10	D71	N13
cut-off ¹ (Da)		160	170	190	260	310	680	1,200	2,000	2,100
cut-off ² (Da)		180	200-300	150-300	150-300	600-800	400	1,000	-	-
water permeability (L m ⁻² .h ⁻¹ .bar ⁻¹)		10.3 (± 1.2)	8.3 (± 0.5)	11.4 (± 1.1)	3.7 (± 0.9)	5.7 (± 1.0)	3.8 (± 0.8)	15.4 (±2.8)	4.7 (± 1.4)	22.2 (±3.1)
roughness (nm)	NC-AFM ²	4.6	4.2	5.9	9.8	1.5	3.4	2.4	3.9	4.4
	T-AFM ³	5.6	-	6.4	13.2	2.1	3.9	2.2	-	-
hydrophobicity (°)	contact angle	36 (± 4)	27 (± 4)	47 (± 4)	44 (± 3)	70 (± 4)	88 (± 2)	72 (± 4)	73 (± 2)	67 (± 3)
	phase shift T-AFM ³	4.1	-	6.6	3.6	2.3	1.8	3.0	-	-
zeta potential (mV)	pH 4	5	-2	-4	-1	-3	-5	-2	-3	-4
	pH 7	-8	-19	-14	-18	-17	-15	-12	-13	-10
	pH 10	-17	-24	-17	-21	-19	-18	-15	-13	-14

¹cut-off, as experimentally obtained by using a mixture of PEG; ²cut-off, as given by the manufacturer; ³NC-AFM: non-contact mode AFM on 3 µm x 3 µm; ⁴T-AFM: tapping mode AFM on 3 µm x 3 µm

Therefore, the cut-off was determined for each membrane in the same conditions (293 K, 8 bar, 600 L h⁻¹) with the same feed solution (mixture of polyethylene glycols (PEG)), as described in section 2.4.3. By plotting the observed retention for each PEG in the mixture against its molecular mass, a retention curve was obtained. Fitting this curve with the log-normal model (as was done also by Van der Bruggen *et al.* (2000b)) led to the determination of the cut-off (i.e., the molecular mass of PEG with 90 % retention). The experimental data and the fitted model are shown in Figure 4.4 for some commercial membranes.

The experimental cut-offs (summarized in Table 4.3) agree well with the cut-offs given by the manufacturer (Table 2.1 and repeated in Table 4.3), with the exception of N30F and NTR7450, which have a higher and lower cut-off, respectively, than specified by the manufacturer.

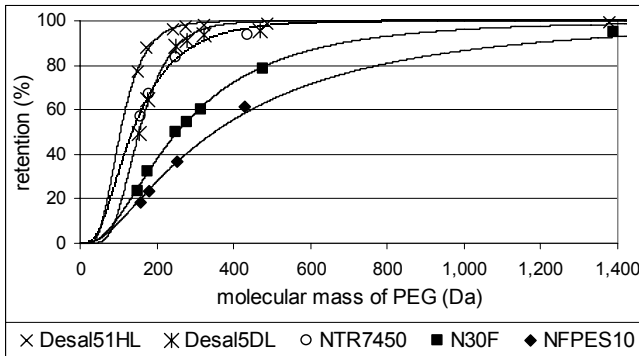


Figure 4.4: Determination of the cut-off by fitting the retention curve with the log-normal model

4.3.2 Determination of the surface roughness

The surface roughness was analyzed by non-contact mode and tapping mode AFM (section 2.4.1) on five different scan areas. The results are given in Table 4.4 and are of the same order of magnitude as the roughness values observed in literature (Bowen *et al.*, 2002; Bowen and Doneva, 2000).

From these results it is seen that the scanned area plays a significant role: the larger the scanned area, the higher the roughness. Figure 4.5 illustrates this effect for

Desal5DL, for which the surface roughness is visualized with non-contact mode AFM on four different scan areas.

Table 4.4: RMS roughness (nm) of the top layer of the commercial membranes, measured with non-contact mode AFM (NC) and tapping mode AFM (T) on different scan areas

	0.5 μm x		1 μm x		3 μm x		5 μm x		10 μm x	
	0.5 μm		1 μm		3 μm		5 μm		10 μm	
	NC	T	NC	T	NC	T	NC	T	NC	T
UTC20	2.2	-	2.6	2.8	4.6	5.6	4.8	4.8	6.8	8.8
NF270	2.1	-	2.8	-	4.2	-	4.6	-	-	-
Desal51HL	2.6	3.7	3.0	5.9	5.9	6.4	6.2	9.3	11.2	11.8
Desal5DL	5.2	6.8	5.7	10.8	9.8	13.2	10.9	13.9	12.8	14.7
NTR7450	0.8	0.5	0.9	0.7	1.5	2.1	1.8	2.3	3.1	3.2
N30F	1.3	0.9	2.5	1.6	3.4	3.9	3.9	4.1	5.5	4.9
NFPES10	0.8	0.8	1.3	1.1	2.4	2.2	2.7	2.5	3.8	3.5

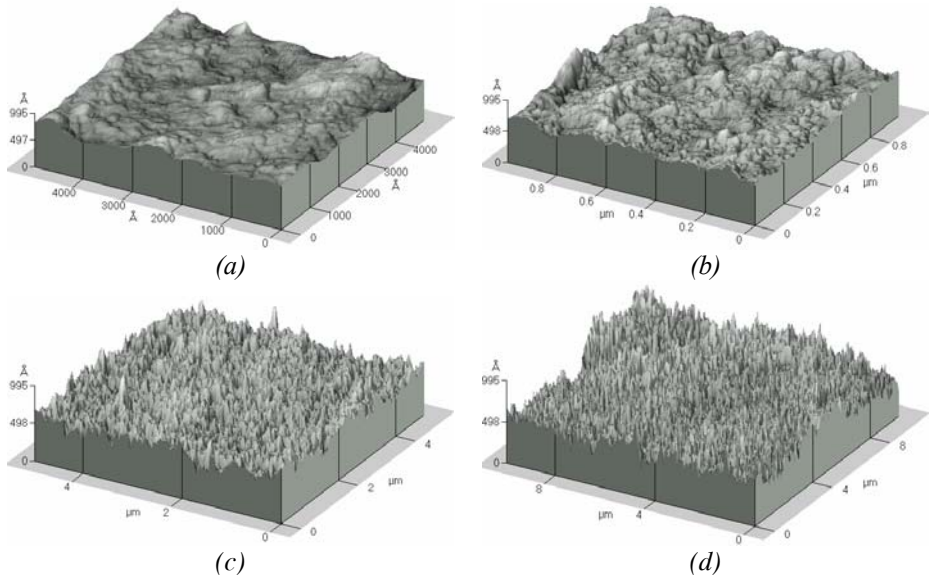


Figure 4.5: Non-contact mode AFM images of Desal5DL for four different scan areas: (a) 0.5 μm x 0.5 μm , (b) 1 μm x 1 μm , (c) 5 μm x 5 μm , (d) 10 μm x 10 μm

This phenomenon of increasing roughness with increasing scan area is related to the dependency of the roughness on the spatial wavelength of the scanned area or the frequency. For a small surface area, only the roughness of the ‘higher’ frequencies is measured. When scanning a larger surface area, the roughness caused by additional lower frequencies also has to be taken into account. This results in a higher roughness value when scanning a larger surface area. Or, in other words, when the scan size is changed, it is possible to measure a different surface topography resulting in a different roughness.

Therefore, it is crucial that the same scan size range is used when comparing the surface roughness of different samples. Considering the same scan range in Table 4.4, it becomes clear that, for non-contact mode as well as for tapping mode AFM, NTR7450 and NFPE10 are the smoothest membranes, while Desal5DL has the roughest top layer. In order to visualize the difference in roughness, non-contact mode and tapping mode AFM images of a very smooth (NFPE10) and a very rough membrane (Desal5DL) are shown in Figure 4.6 and 4.7, respectively.

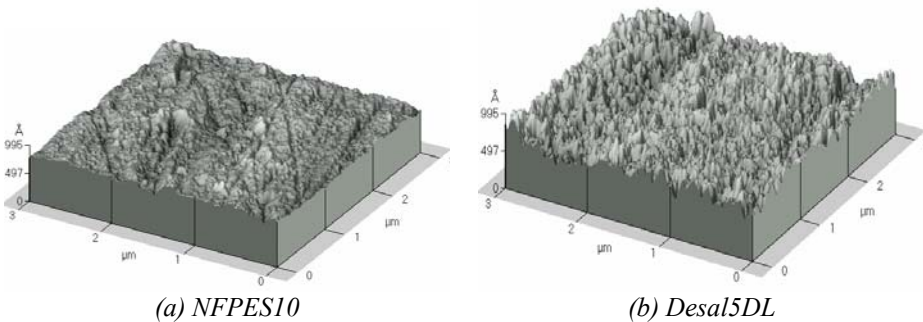


Figure 4.6: Non-contact mode AFM images of (a) a smooth membrane, NFPE10 and of (b) a rough membrane, Desal5DL on a scan area of 3 μm x 3 μm

Although non-contact mode and tapping mode AFM predict the same order of roughness for the different membranes, tapping mode AFM leads to a larger difference between the roughness values of the different membranes. For example, on a scan area of 0.5 μm x 0.5 μm , Table 4.4 indicates that the roughness varies from 0.8 nm to 5.2 nm in non-contact mode and from 0.5 nm to 6.8 nm in tapping mode AFM. A comparison between the roughness values, obtained in both AFM

modes, e.g., on a scan area of $0.5 \mu\text{m} \times 0.5 \mu\text{m}$, is also visualized in Figure 4.8. For the smoother membranes, the roughness measured in tapping mode AFM is smaller than in non-contact mode, while the opposite is observed for the rougher membranes Desal51HL and Desal5DL.

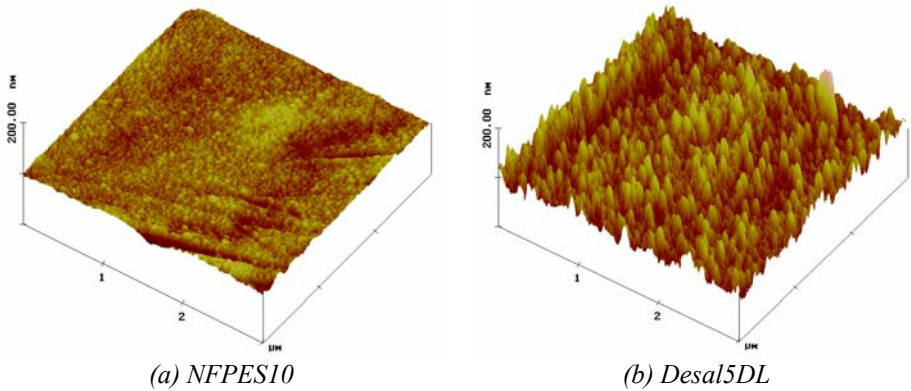


Figure 4.7: Tapping mode AFM images of (a) a smooth membrane, NFPE510 and of (b) a rough membrane, Desal5DL on a scan area of $3 \mu\text{m} \times 3 \mu\text{m}$

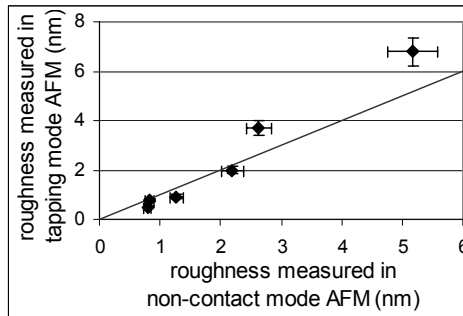


Figure 4.8: Comparison between the roughness values (nm) measured in non-contact mode and in tapping mode AFM for a scan area of $0.5 \mu\text{m} \times 0.5 \mu\text{m}$, together with the bisector of the graph

This phenomenon is intrinsic to the measuring method in tapping mode AFM, where the tip (attached to the cantilever) taps the scanned surface in contrast to non-contact mode AFM, where the distance between the tip and the surface is approximately 10 nm. When a contaminant layer (e.g., a few monolayers of condensed water) covers the surface, an AFM operating in tapping mode penetrates this layer to image the underlying surface. In non-contact mode, however, the

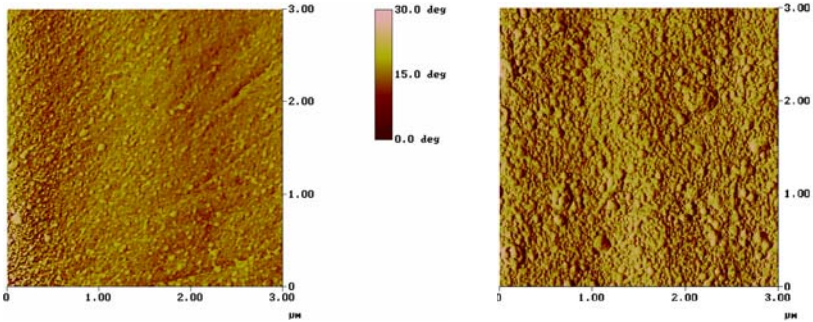
AFM tip cannot penetrate the contaminant layer and hence images the surface of the contaminant layer. This also implies that, although tapping mode AFM is more time consuming, it gives more realistic results than non-contact mode AFM. An additional advantage of tapping mode AFM is the simultaneous measurement of the phase shift (section 4.3.3).

4.3.3 Determination of the surface hydrophobicity

Determination of the contact angle is a well-known method (Roudman and DiGiano, 2000) to study the hydrophobicity of a membrane surface. Table 4.3 lists the measured contact angles and shows that NF270 and UTC20 are the most hydrophilic membranes while N30F has the most hydrophobic membrane surface.

An alternative method to study the hydrophobicity of a membrane surface is by using tapping mode AFM. While the reduction in oscillation amplitude of the AFM tip was used for the roughness study, the hydrophobicity of the membrane surface was deduced from the phase shift of the AFM tip (section 2.4.1). This phase shift is derived from the difference in phase angle between the freely oscillating cantilever in air and the cantilever oscillation during scanning. The phase shift is zero when there is no interaction between the tip or the cantilever and the membrane. However, in the case of a tip-membrane interaction, a phase lag is induced if the interaction is attractive and a phase advance appears if the interaction is repulsive. Areas in a phase image exhibiting a phase lag with respect to the free oscillation are shown darkened, regions of advanced phase are lightened. Figure 4.9 shows a two-dimensional phase image of NFPES10 and Desal51HL.

The results of the measured RMS phase shifts for the different membranes and for the different scan areas are given in Table 4.5. Because the AFM measurements were carried out with a hydrophilic silicon tip, one can observe whether the interaction between the tip and the sample is hydrophilic or hydrophobic. A hydrophilic surface interacts strongly with a hydrophilic tip, resulting in a large phase shift. A hydrophobic surface only interacts weakly with a hydrophilic tip, resulting in a small phase shift.



(a) NFPE510

(b) Desal51HL

Figure 4.9: Phase images of (a) NFPE510 and (b) Desal51HL for a scan area of $3 \mu\text{m} \times 3 \mu\text{m}$

Table 4.5: RMS phase shift ($^\circ$) obtained with tapping mode AFM on the top layer of the commercial membranes on different scan areas

	0.5 $\mu\text{m} \times$ 0.5 μm	1 $\mu\text{m} \times$ 1 μm	3 $\mu\text{m} \times$ 3 μm	5 $\mu\text{m} \times$ 5 μm	10 $\mu\text{m} \times$ 10 μm
UTC20	-	2.2	4.1	8.0	6.6
NF270	-	-	-	-	-
Desal51HL	4.6	4.4	6.6	2.9	9.5
Desal5DL	1.7	2.5	3.6	3.7	6.5
NTR7450	1.3	1.4	2.3	3.2	5.2
N30F	0.9	0.9	1.8	3.0	3.6
NFPE510	1.7	2.9	3.0	2.8	6.8

From Table 4.5, it becomes clear that NTR7450, N30F and NFPE510 are characterized by a more hydrophobic top layer as given by the smaller phase shift (small interaction between membrane and tip). More interaction (and hence larger phase shifts) occurs between the tip and the other membranes (Desal5DL, Desal51HL and UTC20).

Similar to the RMS roughness (Table 4.4), the RMS phase shifts increase with increasing scan area. This can be explained by the fact that with increasing scan area, the roughness and hence the contact area between tip and sample increase. This implies that there can be more interaction between tip and sample, resulting in a larger phase shift.

A comparison between the phase shifts and the contact angles (Figure 4.10) confirms the expectation that a large contact angle corresponds to a small phase shift. The only exception is Desal51HL, which shows a very large phase shift (for all scanned areas) compared to the contact angle, indicating a very strong specific interaction between the hydrophilic silicon tip and the Desal51HL membrane.

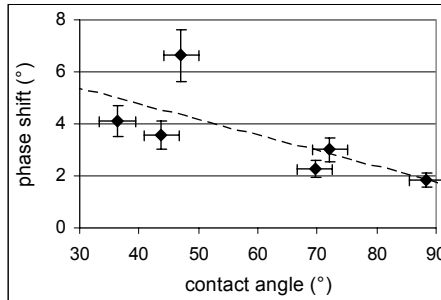


Figure 4.10: Comparison between the RMS phase shift (measured in tapping mode AFM on a scan area of $3\ \mu\text{m} \times 3\ \mu\text{m}$) and the contact angle

4.3.4 Determination of the surface charge

In addition to the roughness and the hydrophobicity, the top layer of each membrane is characterized for surface charge. The zeta potential as a function of pH is given in Figure 4.11; the values at pH 4, 7 and 10 for all membranes are summarized in Table 4.3.

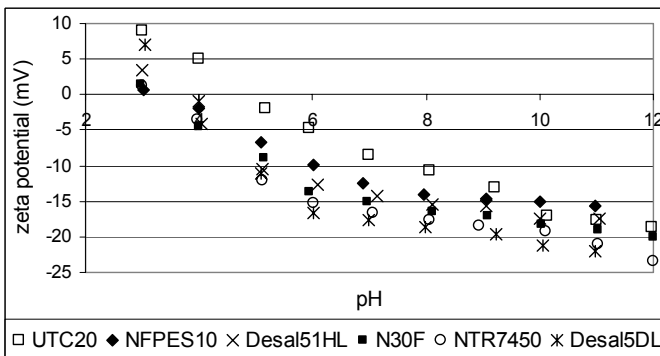


Figure 4.11: Zeta potential (mV) as a function of pH for the different commercial membranes

At low pH, the membranes are slightly positively charged and they become negatively charged at high pH. This behavior of the surface charge as a function of pH is also observed for other membranes in literature (Fievet *et al.*, 2004; Schaepe and Vandecasteele, 2001; Kim *et al.*, 1996). As indicated in Figure 4.11, the iso-electric point, i.e., the pH at which the net charge of the membrane is equal to zero, is located between 3 and 4 for all the membranes. Only the UTC20 membrane with a polypiperazineamide top layer, has an iso-electric point close to pH 5.

This behavior of the charge as a function of pH can be explained, for membranes with a top layer of polyethersulfone (NFPE10, N30F, NTR7450, D71 and N13) by the adsorption of anions or by the presence of sulfonic groups ($-SO_3^-$) on the surface. These sulfonic groups are strongly acidic and are completely dissociated at a pH above 2.

The other membranes (UTC20, NF270, Desal51HL and Desal5DL) have a top layer of polyamide and possesses both carboxylic and amine functional groups on the membrane surface (Figure 2.4a and 2.4b). Carboxylic groups ($-COO^-$) are weakly acidic and are not dissociated at low pH, while amine groups give the membrane surface a positive charge in acid medium ($-NH_3^+$ is only weakly charged, while $-N^+R_3$ is completely dissociated and thus positively charged over the entire pH range).

4.3.5 Conclusion

The results of the physical characterization indicate the presence of the two same membrane classes as those identified by chemical characterization (section 4.2.3), i.e., a polyamide class (Desal51HL, Desal5DL, NF270 and UTC20) and a polyethersulfone class (N30F, NFPE10, NTR7450, D71 and N13). The membranes of the polyamide class have the lowest cut-off and the roughest and most hydrophilic membrane surface.

4.4 Positron Annihilation Spectroscopy (PAS)

To study the porosity of the top layer of different membranes, PAS measurements (section 2.4.5) were performed to obtain the energy of annihilation (given by the S and the R parameter) and the lifetime of the implanted positrons (given by the PALS results).

4.4.1 S parameter

The S parameter is a tool to characterize the line shape of the Doppler Broadening of Annihilation Radiation (DBAR) at 511 keV and forms an indication for the chemistry and the structural defects at the site of annihilation.

Figure 4.12 shows the evolution of the S parameter as a function of the positron energy (0 - 60 keV) for the commercial and the laboratory-made membranes. For positrons with a low energy, which annihilate in the top layer of the membranes, the S parameter is rather similar for all membranes, indicating that the polymers used in the top layer of the different membranes have the same affinity for the formation of positronium. Only for the commercial membrane Desal5DL and for a positron energy below 5 keV, the S parameter is very small. For very low positron energy (below 1 keV), many variations in the S parameter are detected for all membranes due to surface effects (or the back diffusion of positronium and positrons near the surface), as studied by Bas *et al.* (2004) and Cao *et al.* (1999).

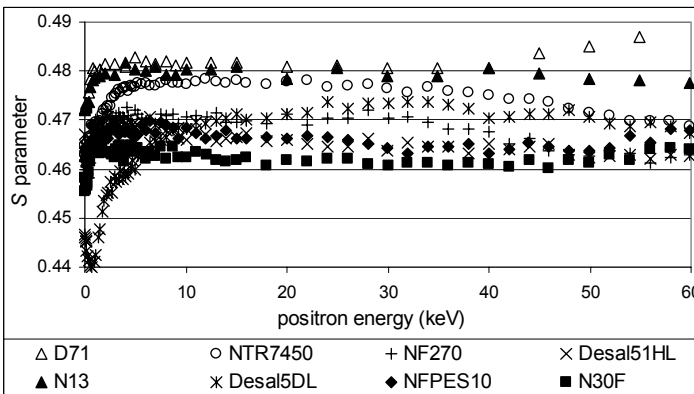


Figure 4.12: S parameter (derived from DBAR measurements) as a function of the positron energy for the commercial and the laboratory-made membranes

The difference in pore size between top and support layer was clearly seen in the increase of the S parameter from low to high energy. It is also interesting to note that a similar evolution of the S parameter for D71 at a positron energy above 40 keV (i.e., increasing S parameter with increasing energy) was observed for the commercial membranes N30F and NFPES10. This indicates that the support layers of these membranes are similar, as already concluded from the ATR-FTIR measurements (section 4.2.1). The evolution of the S parameter also shows that the support layer of N13 is similar to the one of the other commercial membranes (NTR7450, NF270, Desal5DL and Desal51HL).

4.4.2 R parameter

The R parameter or the relation of 3γ to 2γ describes the fraction of the surface under the total low energy region (Compton region) of the annihilation spectrum to that under the 511 keV line and contains information about the size and the concentration of the different pores.

Figure 4.13 shows the evolution of the R parameter as a function of the positron energy (0 - 30 keV) for the commercial and the laboratory-made membranes. At low positron energy (above 0.5 eV), the R parameter is very small, which forms an indication of the small porosity of the skin layer. The R parameter subsequently increases and then again decreases with increasing energy. The increase in R is an indication for the increase in porosity in the transition of the dense skin layer to the porous sub layer. The decrease in R is rather due to positronium related phenomena than to a decreased porosity, as explained in more detail by Jean *et al.* (2003).

From the evolution of the R parameter as a function of the positron energy, the thickness of the skin layer of the different membranes was compared. The transition between skin and sub layer is, however, not observed sharply in Figure 4.13. This is explained in literature (Algers *et al.*, 2003; He *et al.*, 2003; Dlubek and Alam, 2002) not only by the fact that positronium diffuses in the membrane, but primarily by the fact that the positron has an implantation-stopping profile.

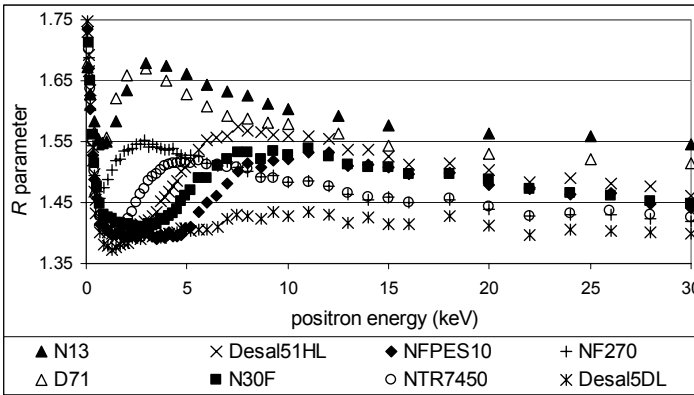


Figure 4.13: *R* parameter (or the ratio of 3γ to 2γ annihilation) as a function of the positron energy for the commercial and the laboratory-made membranes

If the transition between skin and sub layer is approximated by the positron energy at half of the slope between the regions of small and large *R* parameters, and assuming the densities are similar, Figure 4.13 indicates that the commercial membranes with a top layer of polyethersulfone (NFPE10 and N30F) have a thicker skin layer than Desal51HL, Desal5DL and NF270.

This can be explained by the different preparation processes for both types of membranes. As already indicated in section 4.2.1, polyethersulfone membranes are traditionally prepared by phase inversion while interfacial polymerisation is used to prepare polyamide membranes. Because the latter technique results in a thinner top layer, the skin layer (or the upper part of the top layer) can also be thinner. This is however not the case for the commercial membrane NTR7450, for which the thickness of the skin layer is situated between Desal5DL and NF270. Also for the laboratory-made membranes D71 and N13, the skin layer is very thin, especially in comparison with the commercial polyethersulfone membranes N30F and NFPE10.

SEM images of the cross-sections of the different membranes were used to study visually the difference in porosity between skin and sub layer and also the thickness of the skin layer. Figure 4.14 shows SEM images of the membranes NFPE10 and NF270, both on a scale of $3\ \mu\text{m}$ and $100\ \text{nm}$. On the images with a scale of $3\ \mu\text{m}$, a platinum layer, which was needed to protect the surface of the

membranes during the FIB cross-sectioning, was seen. These images clearly indicate the difference in porosity of the sub layers of both membranes.

Zooming in on the skin layer of the membranes (images with a scale of 100 nm) reveals the thickness of the skin layer to be 190 nm for NFPE10 and only 25 nm for NF270. The thickness of the skin layers of the other membranes is situated between these two extremes.

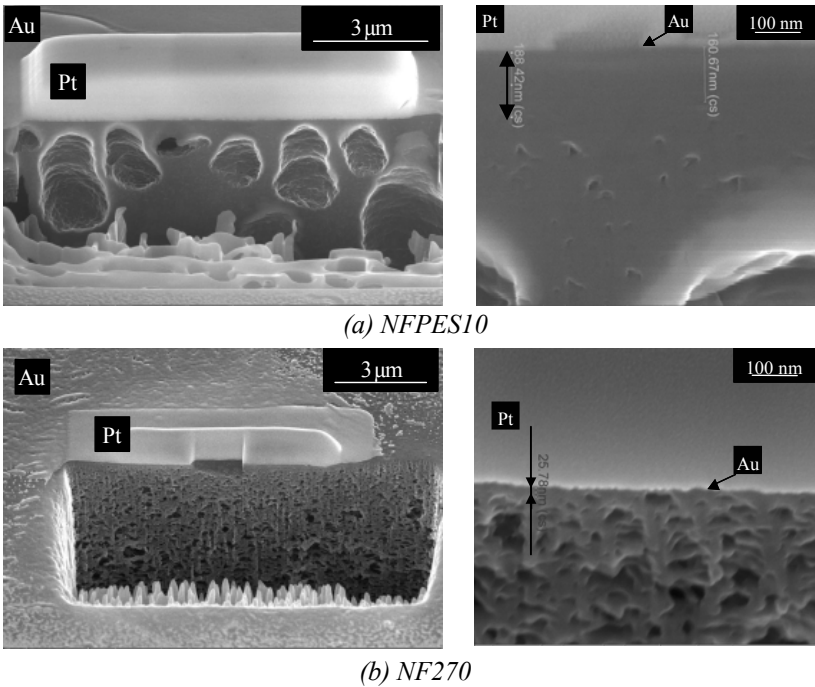


Figure 4.14: SEM images of the cross-sections of the commercial membranes (a) NFPE10 and (b) NF270, with a zoom on the skin layer

In addition to the evolution of the porosity and the thickness of the skin layer, the R parameter also gives useful information about the selection of the positron energy for the PALS measurements. As it was the aim of PALS to determine the lifetime of the positrons in the skin layer of the membranes, a positron energy corresponding with an implantation depth (Equation 2.8) situated in the skin layer, should be selected.

Figure 4.13 indicates that a positron energy of 2 keV matches this condition for the commercial membranes, except for NF270, for which it was not possible to

perform PALS measurements because of the very thin skin layer. For the laboratory-made membranes D71 and N13, a positron energy of 1 keV was selected for the lifetime experiments.

4.4.3 Positron Annihilation Lifetime Spectroscopy (PALS)

Typical positron lifetime spectra for a commercial (NTR7450) and a laboratory-made (N13) membrane are shown in Figure 4.15. Such a spectrum is a sum of decaying exponentials corresponding to the number of positron states in the material, convoluted with the instrumental resolution function (that is responsible for the initial increasing part of the spectrum).

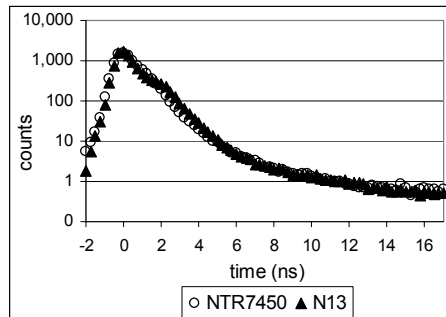


Figure 4.15: Typical positron annihilation lifetime spectra for a commercial (NTR7450) and a laboratory-made (N13) membrane

The lifetime spectra for the commercial membranes were analyzed in terms of four (mean) lifetime components: τ_1 due to p-Ps annihilation (0.124 ns), τ_2 due to free positron annihilation (around 0.44 ns), τ_3 and τ_4 due to o-Ps annihilation. The latter two lifetimes are the most relevant, as τ_3 and τ_4 can be converted into pore radii r_3 and r_4 or pore volumes V_3 and V_4 using Equation 2.9 and 2.10, respectively. Each lifetime also has an intensity I_i . Because the formation probability of positronium is similar for the different membranes (section 4.4.1), the intensity (I_3 and I_4) corresponds with the volume fraction of the involved pores. The relation of the intensity I_3 and I_4 to the pore volume V_3 and V_4 is a measure for the number of pores with size r_3 and r_4 , respectively. The results for the lifetimes, the pore sizes and the intensities are given in Table 4.6.

Table 4.6 shows two different types of pores: pores in which the positronium shows a lifetime shorter than 1 ns (τ_3) and pores in which the positronium shows a lifetime longer than 2 ns (τ_4). In literature (Dlubek *et al.*, 2005), an intermediate lifetime of around 1 ns in polymers is attributed to the formation of o-Ps in the existing crystals of the polymer. To check whether the short lifetimes (τ_3) in this study are a result of the crystallinity of the polymer, or rather an indication for the presence of small pores, DSC measurements were performed. If the short lifetimes are due to the (semi-)crystallinity of the polymer in the top layer, a crystallinity peak of the top layer should be observed during the DSC experiment.

Table 4.6: The results of the PALS analysis performed on commercial nanofiltration membranes ($\tau_1 = 0.124$ ns and τ_2 around 0.44 ns)

	Desal51HL	Desal5DL	NTR7450	N30F	NFPES10
τ_3 (ns)	0.94	0.90	0.78	0.81	0.82
τ_4 (ns)	3.20	3.51	2.50	2.48	2.39
r_3 (nm)	0.155	0.150	0.125	0.130	0.130
r_4 (nm)	0.375	0.395	0.330	0.325	0.320
I_1 (%)	12.9	6.9	15.8	20.7	19.8
I_2 (%)	48.7	72.6	36.9	17.3	21.1
I_3 (%)	35.4	18.8	43.1	53.7	49.5
I_4 (%)	3.0	1.7	4.2	8.3	9.7
I_3/V_3	2,271	1,330	5,271	5,838	5,381
I_4/V_4	13.59	6.59	27.92	57.75	70.71

Figure 4.16 shows a DSC measurement of a support layer (FO2471) and of a commercial membrane (NFPES10). As the top layer of NFPES10 is thin in comparison with the support layer, the two measurements almost look the same: during heating, two melting peaks were observed due to melting of PE (at 130 °C) and PP (at 160 °C), while during cooling, the peak at 115 °C corresponds with the crystallization of PE and PP (ATHAS Data Bank, 1994).

The glass transition temperatures of PP and PE are situated below 0 °C (typically around -18 °C and -100 °C, respectively) and are hence not visible in Figure 4.16.

However, when both measurements are compared in more detail, a difference at 220 °C is revealed, which is due to the glass transition of polyethersulfone, forming the top layer of NFPEs10. No melting peak or crystallinity peak (Blackadder *et al.*, 1979) of polyethersulfone was observed in Figure 4.16.

This was explained by the fact that phase inversion (used for preparation of polyethersulfone membranes) is a very fast process, which implies that the polymer has no time to form crystals. This means that, for the interpretation of the PALS data, the short lifetimes (τ_3) are not a result of the crystallinity, but rather an indication for the presence of small pores.

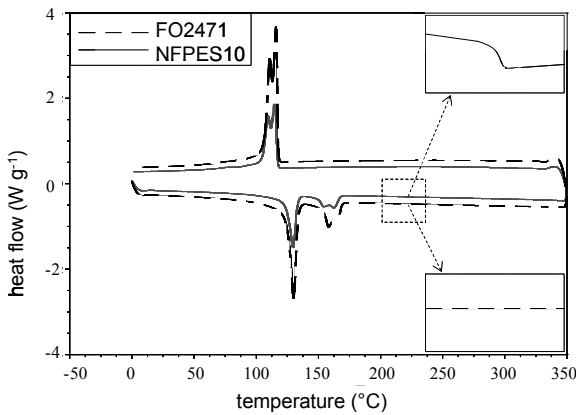


Figure 4.16: DSC measurement of a support layer (FO2471) and a commercial membrane (NFPEs10), with zoom on 220 °C

Considering both the small (τ_3) and the large pores (τ_4), Table 4.6 indicates that Desal51HL and Desal5DL are characterized by a larger pore size (r_3 and r_4) and a smaller volume fraction of the pores (I_3 and I_4) in comparison with the other commercial membranes. The relation of the intensity to the pore volume (I_i/V_i) forms an indication for the number of pores, for which Table 4.6 proves that much more small pores (I_3/V_3) are present than large pores (I_4/V_4) and that the membranes Desal51HL and Desal5DL are characterized by less pores (both small and large ones) in comparison with the other commercial membranes. This means that, taking into account that the lifetime is related to the smallest diameter of a pore, both pores are available for water (water has a typical molecular diameter of

0.275 nm (Beckstein and Sansom, 2004)). As a consequence, the cut-off seems not to be correlated with the size of the pores (section 4.4.4).

Starting from these PALS data, the porosity of the top layer of the membranes can be defined in several ways. Either the number of large pores (I_4/V_4) or the total number of pores ($I_3/V_3 + I_4/V_4$) can be used as a measure for the porosity, or the volume fraction of the large pores (I_4) and the small pores (I_3), or the volume fraction of all pores ($100-I_2$). As porosity is mostly defined as the fraction of pores within a given volume (Mulder, 1996), it is best presented by the values of the intensities (I_3 and I_4). The highest porosity is observed for the skin layer of NFPE10 and N30F, while the skin layer of the commercial membrane Desal5DL is the least porous.

The same lifetime analysis could be carried out for the laboratory-made membranes N13 and D71. However, as these membranes have a very thin skin layer (Figure 4.13), a lower positron energy (1 keV instead of 2 keV for the commercial membranes) was selected for the PALS experiments to make sure that the porosity of the skin layer (and not the porosity of the sub layer) was studied. The obtained lifetime spectra could only be fitted using five different lifetimes, of which τ_1 , τ_2 , τ_3 and τ_4 were similar to the lifetimes of the commercial membranes (Table 4.6). However, only the longest lifetime ($\tau_5 = 10$ ns) could be determined accurately, because of the poor resolution function at low energy (seen as an extra bump in Figure 4.15 for N13). This lifetime, which corresponds with a pore size of 0.65 nm, forms an indication for the presence of very large pores in the skin layer of these laboratory-made membranes.

4.4.4 Comparison between cut-off and pore sizes obtained by PALS

Table 4.7 summarizes the results of the pore sizes from PALS (r_3 , r_4 and r_5) and the results from the filtration experiments with PEG (cut-off and r_{50}). As described in section 4.3.1, the cut-off or the molecular mass of PEG with 90 % retention, was

obtained by fitting the retention curve (retention as a function of molecular mass of PEG: Figure 4.4) with the log-normal model, according to Equation 4.1:

$$\sigma(M_w^*) = \int_0^{M_w^*} \frac{1}{S_{M_w} \cdot \sqrt{2\pi}} \cdot \frac{1}{M_w} \cdot \exp\left(-\frac{[\ln(M_w) - \ln(MWCO) + 0.56 \cdot S_{M_w}]^2}{2 \cdot S_{M_w}^2}\right) dM_w \quad (4.1)$$

where σ is the retention of PEG with molecular mass M_w^* and S_{M_w} a measure for the distribution of the pore sizes.

Table 4.7: Summary of the results obtained by PALS (r_3 , r_4 and r_5) and obtained by filtration experiments with PEG (cut-off and r_{50}) for the commercial and the laboratory-made membranes

	Desal51HL	Desal5DL	NTR7450	N30F	NFPES10	D71
r_3 (nm)	0.155	0.150	0.125	0.130	0.130	~ 0.14
r_4 (nm)	0.375	0.395	0.330	0.325	0.320	~ 0.35
r_5 (nm)	-	-	-	-	-	0.65
cut-off (Da)	190	260	310	680	1,200	2,000
r_{50} (nm)	0.24	0.30	0.28	0.39	0.46	0.65

The retention curve can also be calculated as a function of the Stokes-Einstein radius of PEG (r_{PEG}), by using Equation 4.2 (Tam and Tremblay, 1991). The Stokes-Einstein radius is only an approximation of the effective radius of PEG, as it represents the radius of a hard sphere that diffuses at the same rate as PEG.

$$r_{PEG} = 0.262 \cdot \sqrt{M_w} - 0.3 \quad (4.2)$$

By fitting this retention curve in the same way with Equation 4.3, a value of the mean pore size (r_{50}) was obtained for each membrane.

$$\sigma(r_c) = \int_0^{r_c} \frac{1}{S_p \cdot \sqrt{2\pi}} \cdot \frac{1}{r} \cdot \exp\left(-\frac{[\ln(r) - \ln(r_{50})]^2}{2 \cdot S_p^2}\right) dr \quad (4.3)$$

where σ is the retention of PEG with radius r_c and S_p a measure for the distribution of the pore sizes. The mean pore size represents the size of a molecule with 50 % retention and was used for comparison with r_3 , r_4 and r_5 .

Concerning the commercial membranes, no correlation was observed between the pore sizes determined by PALS (r_3 and r_4) and the cut-off (or r_{50}): membranes with the lowest cut-off even have the largest pore size (r_3 and r_4). On the other hand, Figure 4.17 indicates a correlation between the cut-off and the ratio $I_4 / (I_4 + I_3)$, which is the volume fraction of the large pores to the total volume fraction of all pores. The correlation was also confirmed by performing a statistical analysis of the cut-off (as a function of all membrane characteristics) with linear regression using the computer program SAS.

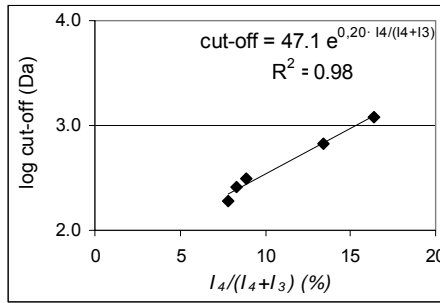


Figure 4.17: Correlation between cut-off (Da) and $I_4 / (I_4 + I_3)$ (%) for commercial nanofiltration membranes

These observations have consequences for the understanding of the transport mechanism through nanofiltration. As nanofiltration is situated in between ultrafiltration and reverse osmosis, both the sieving mechanism by size exclusion as in ultrafiltration (like reported by Ren *et al.* (2006)) and solution - diffusion as in reverse osmosis (like reported by Paul (2004)) play a role. Up to now, most models in literature that describe nanofiltration (Santos *et al.*, 2006; Wang and Chung, 2005b; Hilal *et al.*, 2004; Bowen and Welfoot, 2002b) consider it to be more a sieving process, a transition model between pore flow and solution-diffusion is recently introduced by Robinson *et al.* (2005).

The results of this section indicate that the mechanism of nanofiltration is not governed by the absolute size of the pores, but rather by the relation between the different pores. The presence of more and more smaller pores to the total porosity hinders the transport of molecules through the membrane exponentially.

For the laboratory-made membranes (D71 and N13), the largest pore size obtained from PALS (r_5) is equal to the mean pore size obtained from the filtration experiments (r_{50}). As these membranes are already closer to the ultrafiltration region, the sieving mechanism becomes more important, resulting in a similarity between the PALS and the filtration experiments.

4.5 Conclusion

Characterization of the membranes has indicated that all membranes were constructed of different layers with a different chemical composition. For the first membrane class (the polyamide class), at least three layers were present in their membrane structure: a thin top layer of polyamide, an intermediate layer of polyethersulfone and a support layer of polyester. No intermediate layer was observed for the second membrane class (the polyethersulfone class); their membrane structure consisted only of a poly(arylenesulfone ether) top layer and a support layer (PP/PE or polyester).

This chemical composition is related to the physical characteristics and the results of the PAS experiments as it was shown that the polyethersulfone class has the highest cut-off, the smoothest and most hydrophobic membrane surface and the thickest skin layer. The difference between the two membrane classes can also be confirmed statistically by using principal component analysis or cluster analysis; however, such an analysis falls behind the scope of this thesis.

In the skin layer of the commercial membranes, two different pore sizes were observed for all commercial membranes with pore sizes between 0.125 – 0.155 nm and 0.320 – 0.395 nm, respectively (depending on the membrane type). This indicates that the pore size distribution in nanofiltration is not a log-normal function, as usually assumed, but rather a bimodal function. Moreover, the cut-off of the commercial membranes correlates with the ratio of the volume fraction of the large pores to the volume fraction of all pores, indicating that transport through nanofiltration membranes depends more on the relation between the different pores than on the absolute pore sizes.

Chapter 5

Relation between characteristics and performance of nanofiltration membranes

*Adapted partly from: J. Membr. Sci. 289 (2007) 220-230
J. Membr. Sci. 278 (2006) 418-427*

5.1 Introduction

In order to understand and to explain membrane performance on the basis of membrane characteristics (Chapter 4), the experimental filtration results were statistically analyzed by multiple linear regression. This allows to select the most influential membrane and component characteristic(s) to explain and to describe membrane performance. As membrane performance depends highly upon the feed solution, three different types of feed solutions are considered in this chapter:

- filtration of aqueous solutions containing dissolved uncharged organic components;
- filtration of aqueous solutions containing dissolved charged organic components;
- filtration of colloidal dispersions.

To evaluate the membrane performance, both the adsorbed amount, the relative flux and the retention were considered. Although the permeate fluxes are also very crucial (e.g., in the design of a nanofiltration unit), the goal of this chapter was to focus on membrane fouling which is represented by the relative flux. Therefore, the relative flux (and not the absolute permeate flux) was included in the statistical analysis.

To obtain a sufficiently large data set, the statistical analysis was also not performed separately for the two membrane classes, but for all commercial nanofiltration membranes together.

5.2 Nanofiltration performance during filtration of aqueous solutions containing dissolved organic components

A partial or total retention of individual organic pollutants (such as pesticides (Shaan *et al.*, 2007; Kiso *et al.*, 2001), endocrine disrupting components or pharmaceutical residues (Yoon *et al.*, 2007; Nghiem *et al.*, 2005)) is becoming an important concern during water and wastewater treatment with nanofiltration. The

main limitation, however, remains permeate flux decline as a function of time, as a result of membrane fouling.

In literature, it is suggested by several researchers that fouling during filtration of dissolved (uncharged) organic components is mainly related to adsorption on the membrane material (Braeken *et al.*, 2005c; Violleau *et al.*, 2005; Van der Bruggen *et al.*, 2002). Both phenomena were explained on the basis of the component properties as a correlation was found between the octanol-water partition coefficient ($\log P$) and adsorption; adsorption is also related to the dipole moment and the water solubility (Van der Bruggen *et al.*, 2002). Concerning the membrane characteristics, the hydrophobicity of the top layer is believed to cause the most flux decline (Susanto and Ulbricht, 2005; Song *et al.*, 2004; Kimura *et al.*, 2003; Van der Bruggen *et al.*, 2002).

When filtering charged organic components, electrostatic attraction or repulsion forces between the component and the membrane influence the degree of fouling. A necessary condition for this is that the membrane surface charge is large enough; otherwise hydrophobic forces overcome the electrostatic forces resulting in more fouling of hydrophobic membranes (Mänttari *et al.*, 2000).

Physical sieving by pores is believed to be one of the main driving factors in the retention of organic components, with a molecular mass larger than the cut-off of the membranes (Bellona *et al.*, 2004). For smaller uncharged components, molecular mass in combination with $\log P$ determine the retention (Agenson *et al.*, 2003): hydrophobic (small) components are not well retained by nanofiltration membranes. As these components have less polar groups than hydrophilic components, they are less solvated. Due to their smaller size, they can enter more easily in the membrane pores and permeate through the membrane (Braeken *et al.*, 2005b). For these hydrophobic components, an influence of adsorption on retention was also observed in literature (Kimura *et al.*, 2003; Nghiem *et al.*, 2002), as a breakthrough in permeate concentration occurred, after saturation of the membrane, resulting in a lower retention in steady state.

For charged components, both size exclusion and electrostatic interactions are responsible for separation (Mänttari *et al.*, 2000; Van der Bruggen *et al.*, 1999; Nyström *et al.*, 1995).

This section aims to determine the most influential membrane characteristic(s) to explain adsorption, relative flux and retention of both uncharged and charged components on commercial nanofiltration membranes, as such a systematic and complete analysis is currently missing in literature. Therefore, in each case, a multiple linear regression model (section 2.7) was formulated with the adsorbed amount, the relative flux or the retention as response variable (Y) and with both membrane and component characteristics as input variables (x_1, \dots, x_p). The goal of this statistical analysis was to obtain a regression model with the least number of variables in combination with the highest correlation coefficient ($ADJR^2$).

5.2.1 Filtration of aqueous solutions containing dissolved uncharged organic components

Table 5.1 summarizes the adsorbed amount, the relative flux and the retention (Y) during the experiments with dissolved uncharged organic components at neutral pH. Table 5.1 also indicates the molecular mass (M_w) and the hydrophobicity ($\log P$) of each component, which were used as component variables (x) to formulate the regression model.

The molecular mass is an easy to determine and available parameter to describe the size of a component (Van der Bruggen *et al.*, 1999). Other parameters, such as the Stokes diameter, the equivalent molecular diameter, the molecular width, a calculated molecular diameter or shape were not included.

The hydrophobicity of a component can also be expressed by its water solubility or dipole moment. However, these parameters are less useful than $\log P$ (Braeken, 2005): the water solubility is infinite for certain components, whereas the dipole moments are usually determined in apolar solvents. These dipole moments differ significantly from those in water and are therefore not representative.

Table 5.1: Summary of the adsorbed amount (AD , in mmol m^{-2}), the relative flux (RF , in %) and the retention (R , in %) during experiments with dissolved uncharged organic components (feed concentration = 2 mmol L^{-1} , neutral pH , values of relative flux and retention after 2 hours of filtration)

	M_w (Da)	log P	Desal51HL			Desal5DL			NTR7450			N30F			NFPES10		
			AD	RF	R	AD	RF	R	AD	RF	R	AD	RF	R	AD	RF	R
benzonitrile	103	1.54	8.3	88	5	9.8	99	12	9.9	63	8	14.8	44	6	13.7	69	1
benzylalcohol	108	1.08	4.8	<i>11</i>	9	2.5	80	8	3.9	32	17	7.2	11	13	7.5	1	12
p-tolualdehyde	120	2.26	8.9	76	6	7.2	53	14	9.8	50	8	14.1	38	23	14.5	43	5
benzylidene acetone	146	2.04	9.2	61	17	5.1	85	18	7.5	35	15	14.9	17	15	18.1	27	6
xylose	150	-1.98	1.6	81	85	<i>2.4</i>	100	<i>100</i>	0	58	71	0	35	47	0	44	23
xylitol	152	-2.56	-	99	85	-	97	42	-	73	<i>15</i>	-	77	18	-	88	6
3,4-methylnitrophenol	153	2.46	10.7	33	<i>0</i>	<i>1.6</i>	75	5	4.5	43	9	16.1	25	12	18.3	40	0
3,5-dihydroxybenzoic acid	154	0.91	1.1	49	33	0.2	67	44	0.3	28	28	2.1	34	4	2.9	13	9
4,3-chloronitrobenzaldehyde	185	2.17	11.8	36	14	2.3	100	14	6.9	23	8	15.0	12	<i>40</i>	17.5	16	7
maltose	342	-5.42	0	87	94	0.8	<i>84</i>	100	0	64	78	0	34	64	0.8	59	<i>38</i>
raffinose	504	-6.76	0	72	93	<i>1.3</i>	<i>81</i>	100	0	74	90	<i>0</i>	<i>42</i>	75	<i>1.3</i>	63	58

Note: the *italic* values are outliers or leverage points for the regression models, formulated in section 5.2.1

The membrane variables (x) used are summarized in Table 5.2; for the experiments with the uncharged organic components, only the values at pH 6 were taken into account. As a measure for the porosity of the top layer, the volume fraction of the large (I_4) and the small (I_3) pores measured with PAS were selected. The results of non-contact mode AFM on a scan area of $3 \mu\text{m} \times 3 \mu\text{m}$ and the contact angles represent the roughness and the hydrophobicity of each membrane, respectively. Values of the zeta potential were used to characterize the charge properties of the membrane.

Table 5.2: Summary of the membrane characteristics at different pH values, used in the statistical analysis of the experiments with dissolved (un)charged organic components or colloidal dispersions

		Desal51HL	Desal5DL	NTR7450	N30F	NFPES10
cut-off (Da)	pH 3	220	290	-	590	1,300
	pH 6	190	260	310	680	1,200
	pH 10	220	270	-	630	1,300
I_3 (%)	pH 6	35.4	18.8	43.1	53.7	49.5
I_4 (%)	pH 6	3.0	1.7	4.2	8.3	9.7
roughness ¹ (nm)	pH 3	5.0	9.5	1.2	1.7	2.0
	pH 6	5.9	9.8	1.5	3.4	2.4
	pH 10	8.5	13.3	1.2	2.1	2.0
contact angle (°)	pH 3	46	46	66	80	69
	pH 6	47	44	70	88	72
	pH 10	35	47	71	82	66
water permeability ($\text{L m}^{-2} \text{bar}^{-1} \text{h}^{-1}$)	pH 3	12.0	4.1	3.2	2.9	9.6
	pH 6	11.4	3.7	5.7	3.8	15.4
	pH 10	10.7	4.1	4.9	2.5	15.1
zeta potential (mV)	pH 3	4	7	1	1	1
	pH 6	-13	-17	-15	-14	-10
	pH 10	-17	-21	-19	-18	-15

¹ roughness measured in non-contact mode AFM on a scan area of $3 \mu\text{m} \times 3 \mu\text{m}$

5.2.1.1 Adsorption of uncharged organic components

From the results in Table 5.1, it becomes clear that the most adsorption occurred for N30F and NFPE10: hydrophobic, smooth membranes with a high cut-off and a porous top layer (indicated by a large value of I_3 and I_4).

The empirical correlation that provided the best fit of the experimental results for the adsorption of dissolved uncharged organic components was formulated with multiple linear regression (based upon 50 data points) as:

$$\sqrt{\text{adsorbed amount}} = 0.78 + 0.62 \cdot \log P + 0.073 \cdot (\log P)^2 + 0.12 \cdot I_4 \quad (5.1)$$

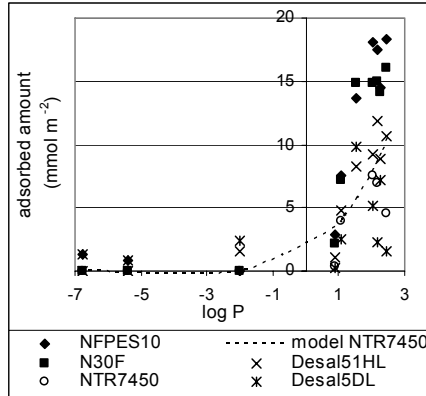
in which $\log P$, $(\log P)^2$ and I_4 explained 56 %, 11 % and 7 %, respectively, of the experimental results ($ADJR^2 = 72$ %). The square root was needed to obtain positive values of the adsorbed amount.

From Equation 5.1, it was concluded that the hydrophobicity of the component ($\log P$) clearly influences the adsorbed amount, in correspondence with literature (Van der Bruggen *et al.*, 2002). This is shown in Figure 5.1a.

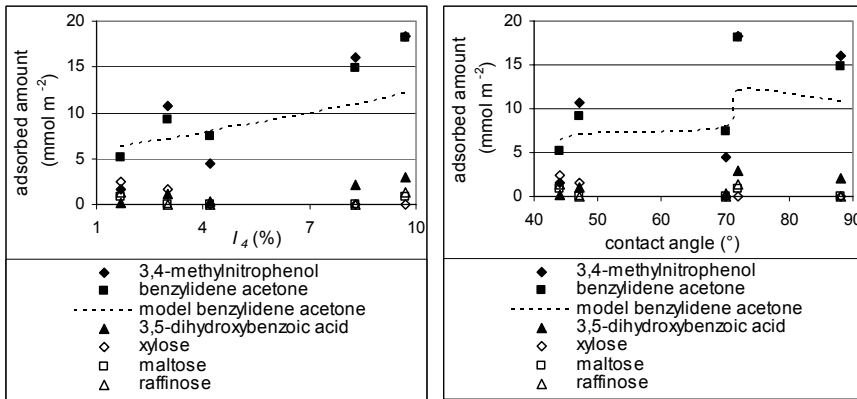
Among the membrane characteristics, the volume fraction of the large pores (I_4) and not the contact angle is the most influential. Excluding I_4 from the statistical analysis, results in the cut-off to be the most influential membrane characteristic. In other words, the cut-off is an alternative parameter to describe the effect of pore size on adsorption, but the relation is less univocal. The volume fraction of the small pores (I_3) is a further possible parameter, again less univocal as a descriptor for adsorption.

Figure 5.1b and 5.1c show the adsorbed amount as a function of I_4 and the contact angle, respectively, for a selection of uncharged components. A first group of components was selected based on their similar molecular mass and increasing hydrophobicity: xylose ($\log P = -1.98$), 3,5-dihydroxybenzoic acid ($\log P = 0.91$), benzylidene acetone ($\log P = 2.04$) and 3,4-methylnitrophenol ($\log P = 2.46$). The selection of the second component group was based on their similar

hydrophobicity and increasing molecular mass: xylose ($M_w = 150$ Da), maltose ($M_w = 342$ Da) and raffinose ($M_w = 504$ Da).



(a)



(b)

(c)

Figure 5.1: Adsorbed amount (mmol m^{-2}) of dissolved uncharged organic components on Desal51HL, Desal5DL, NTR7450, N30F and NFPE10 as a function of (a) log P, (b) I_4 and (c) the contact angle (feed concentration = 2 mmol L^{-1} , neutral pH)

The influence of I_4 on the adsorbed amount (Figure 5.1b) can be explained by the fact that if many large pores are present in the top layer of a membrane, organic components can adsorb both on the membrane surface and onto the pore walls, resulting in a high adsorption. Moreover, the membranes with the most adsorption (N30F and NFPE10) also have the thickest top layer (section 4.4.2), which in combination with its high porosity implies that the organic components can indeed

adsorb in the membrane. For the other membranes, made of polyamide, the top layer is less porous (section 4.4.3) and also very thin, so that adsorption mainly occurs on the membrane surface. In contrast with the conclusions of Kimura *et al.* (2003), the contact angle is not a good descriptor for the adsorption of uncharged organic components, as it does not allow to describe the difference in adsorption between NTR7450 and NFPE10 (given by the bump in Figure 5.1c).

5.2.1.2 Relative flux of uncharged organic components

Table 5.1 indicates that the lowest relative fluxes occur for N30F and NFPE10, for which in section 5.2.1.1 also the highest amount of adsorption was observed. This means that adsorption of dissolved uncharged organic components is related to flux decline, as visualized in Figure 5.2.

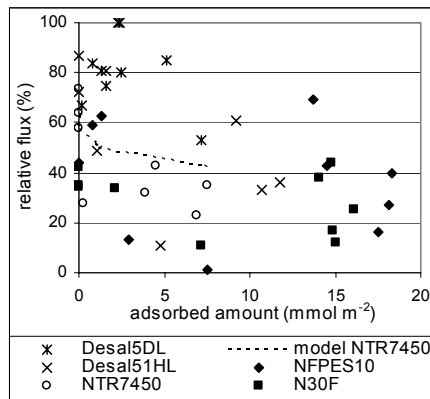


Figure 5.2: Relative flux (%) as a function of the adsorbed amount for dissolved uncharged organic components (feed concentration = 2 mmol L⁻¹, neutral pH)

Although the same membranes (N30F and NFPE10) have the highest amount of adsorption and the lowest relative fluxes, linear regression (based upon 55 data points) showed that flux decline is not influenced by the same (membrane) variables as adsorption. The empirical mode equation providing the best fit was:

$$\text{relative flux} = 113.07 - 1.49 \cdot I_3 - 3.10 \cdot \log P \quad (5.2)$$

in which I_3 and $\log P$ explained 45 % and 13 %, respectively, of the experimental results ($ADJR^2 = 56$ %).

In contrast to adsorption, where the component hydrophobicity ($\log P$) was the most influential variable, flux decline is determined mainly by the volume fraction of small pores (I_3 , shown in Figure 5.3a). The volume fraction of the large pores (I_4 , shown in Figure 5.3b) or the membrane hydrophobicity (shown in Figure 5.3c) cannot fully explain the experimental results of flux decline. This can be explained by the fact that small pores, present in the top layer of a membrane, can more easily be blocked totally by organic components (and especially by hydrophobic organic components, Figure 5.3d) in comparison with large pores, which implies that a membrane with a high value of I_3 is more susceptible to flux decline.

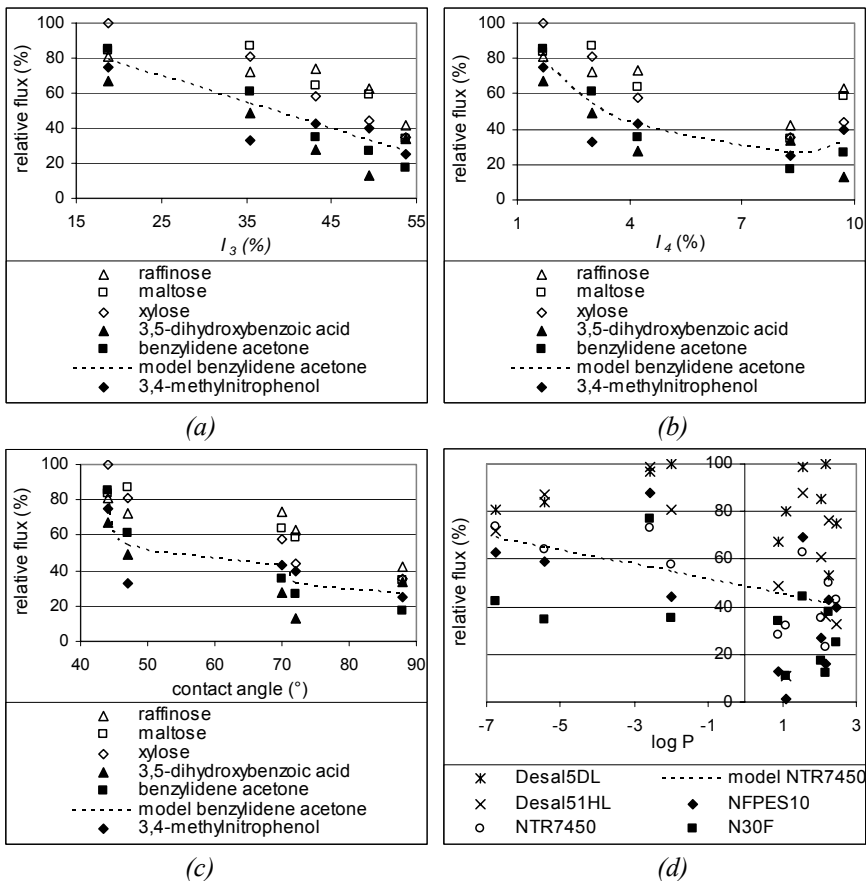


Figure 5.3: Relative flux (%) of dissolved uncharged organic components for Desal51HL, Desal5DL, NTR7450, N30F and NFPES10 as a function of (a) I_3 , (b) I_4 , (c) the contact angle and (d) $\log P$ (feed concentration = 2 mmol L^{-1} , neutral pH)

If, however, I_3 was excluded from the statistical analysis, linear regression pointed out that the volume fraction of the large pores (I_4) explains the most the results of relative flux. Excluding both I_3 and I_4 results in the contact angle to be the most influential membrane characteristic.

5.2.1.3 Retention of uncharged organic components

The experimental retentions (Table 5.1) indicate that dissolved uncharged organic components are the best retained by Desal51HL and Desal5DL, which are hydrophilic membranes with a low cut-off and a slightly porous top layer (low values of I_3 and I_4). The other membranes (NTR7450, N30F and NFPES10) show a lower retention for these components.

Formulating a linear regression model (based upon 55 data points) for the retention data yields:

$$\sqrt{\text{retention}} = 5.73 - 0.71 \cdot \log P - 0.002 \cdot \text{cut} - \text{off} \quad (5.3)$$

in which $\log P$ and cut-off explained 65 % and 8 %, respectively, of the experimental results ($ADJR^2 = 72$ %). The square root was needed to obtain positive values for the retention.

Similar to the adsorbed amount, the hydrophobicity of the component is the most crucial variable for the retention data in the regression model: the lowest retention was observed for hydrophobic components (Figure 5.4a). This is explained in literature (Braeken *et al.*, 2005b) by the fact that hydrophobic components have less interaction with the water phase (through which these components permeate more in the membrane phase) and are less solvated with water molecules in comparison with hydrophilic components.

This implies that hydrophobic components give rise to a high amount of adsorption (Figure 5.1a) in combination with a low retention, as visualized in Figure 5.4b. This is explained in literature by the breakthrough effect (Braeken *et al.*, 2005b; Kimura *et al.*, 2003), which means that an adsorbed component, after (quick)

saturation of the membrane, can pass through the membrane by diffusion and/or convection.

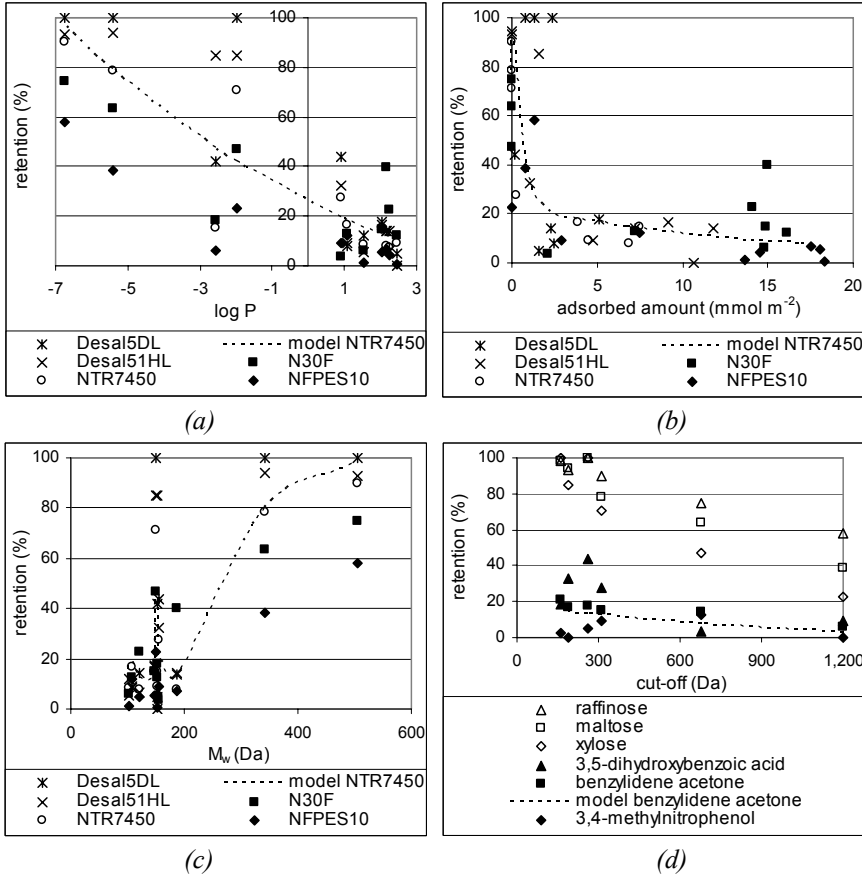


Figure 5.4: Retention (%) of dissolved uncharged organic components for Desal51HL, Desal5DL, NTR7450, N30F and NFPE10 as a function of (a) log P , (b) the adsorbed amount, (c) the molecular mass and (d) the cut-off (feed concentration = 2 mmol L^{-1} , neutral pH)

Although it is expected that the molecular mass also plays a role in the description of the retention, it is not indicated by multiple linear regression as one of the most influential parameters. As shown in Figure 5.4c, retention increases with increasing molecular mass. However, there is a bump around 150 Da, which appears from the difference in retention between hydrophilic and hydrophobic components with a similar molecular mass (e.g., xylose and 3,4-methylnitrophenol, respectively).

Moreover, as the larger components (such as maltose or raffinose) are characterized by a very small value of log P in combination with high experimental retentions, linear regression selected log P as the most influential component variable. The presence of experimental retention results for large, hydrophobic components might possibly change this conclusion; however, these components are hard to find due to their limited water solubility.

The cut-off, derived from PEG retention measurements (section 4.3.1), is the most relevant membrane characteristic to describe the retention of uncharged organic components (Figure 5.4d). This was also concluded by Kimura *et al.* (2003). The volume fraction of the large pores (I_4) was the most influential membrane variable when the cut-off was excluded from the regression model.

5.2.1.4 Conclusion for uncharged organic components

The selection of membrane and component variables by multiple linear regression for uncharged organic components is summarized in Table 5.3. The hydrophobicity (log P) of uncharged organic components plays a major role to explain the adsorbed amount and the retention of commercial nanofiltration membranes. Log P is also of importance when the relative flux is considered. This implies that with increasing hydrophobicity, adsorption increases while the relative flux and the retention decrease.

Table 5.3: Summary of membrane and component variables, selected by multiple linear regression to explain the adsorbed amount, the relative flux and the retention of dissolved uncharged organic components

	adsorption	relative flux	retention
membrane	I_4	I_3	cut-off
component	log P	log P	log P

Note: the **bold** values are the most crucial variables

Concerning the membrane variables, the volume fraction of the small pores (I_3) is extremely important to minimize flux decline. The volume fraction of the large pores (I_4) and the cut-off determine the adsorbed amount and the retention,

respectively. As described in section 4.4.4, the cut-off correlates with the ratio of the volume fraction of the large pores (I_4) to the total volume fraction of all pores ($I_4 + I_3$). This implies that, although not the same membrane variables are important when considering the adsorbed amount, the relative flux or the retention, membranes with a high volume fraction of (small and/or large) pores are characterized by a high amount of adsorption, a low relative flux and a low retention.

Figure 5.2, Figure 5.4b and Figure 5.5 show the relative flux and the retention as a function of the adsorbed amount and the relative flux as function of the retention, respectively. The regression model for NTR7450, shown in these figures, is obtained by combining Equations 5.1, 5.2 and 5.3. This implies that, when purification of wastewater is the goal of the membrane process, membranes with a low volume fraction of pores (e.g., Desal51HL or Desal5DL) should be selected as they combine a high retention with a high relative flux. In this case, the presence of hydrophobic components in the wastewater can worsen the picture.

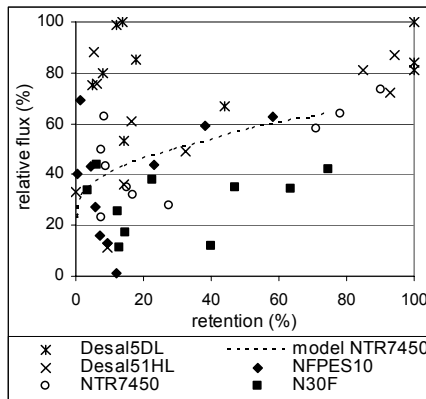


Figure 5.5: Relative flux (%) as a function of the retention for dissolved uncharged organic components (feed concentration = 2 mmol L⁻¹, neutral pH)

5.2.2 Filtration of aqueous solutions containing dissolved charged organic components

Table 5.4 and 5.5 summarize the adsorbed amount, the relative flux and the retention (Y) during the experiments with charged organic components at pH 3 and pH 10, respectively. Table 5.4 and 5.5 also indicate the molecular mass (M_w) and the charge of each component at both pH values, which were used as component variables (x) to formulate the regression model. No influence of pH is assumed on the molecular mass.

The membrane variables at pH 3 and pH 10, which are used in multiple regression, are summarized in Table 5.2. Taking into account the relative fault on the cut-off (i.e., 10 %), no significant influence of pH was observed, in agreement with literature (Ozaki and Li, 2002). The volume fractions of (both small and large) pores at pH 3 and pH 10 were assumed to be equal to the values at pH 6, as it was not possible to obtain a value of I_3 or I_4 at low or high pH due to the limited access to the PALS setup.

Table 5.2 also indicates that the top layer of the polyethersulfone membranes (NTR7450, N30F and NFPE10) is the roughest and the most hydrophobic at neutral pH, as was also observed by Mänttari *et al.* (2006b). In spite of the more hydrophilic character at pH 3, a decrease of the water permeability was observed for NTR7450 and NFPE10 at this pH. When changing the pH, the polyamide membranes (Desal51HL and Desal5DL) are less susceptible to variations in the contact angle (only Desal51HL becomes more hydrophilic at pH 10), although the roughness of these membranes increases with increasing pH. The behavior of the zeta potential as a function of pH is already described in section 4.3.4: the membranes were positively and negatively charged at pH 3 and pH 10, respectively.

Table 5.4: Summary of the adsorbed amount (*AD*, in mmol m^{-2}), the relative flux (*RF*, in %) and the retention (*R*, in %) during experiments with dissolved charged organic components at pH 3 (feed concentration = 0.2 mmol L^{-1} , values of relative flux and retention after 2 hours of filtration)

pH 3	M_w (Da)	com- ponent charge	Desal51HL			Desal5DL			NTR7450			N30F			NFPES10		
			AD	RF	R	AD	RF	R	AD	RF	R	AD	RF	R	AD	RF	R
serine	105	+	0.8	68	89	0	132	26	1.5	33	50	2.4	51	20	2.6	36	17
isoleucine	131	+	0.6	94	92	2.1	106	59	0	32	76	1.5	75	34	0	51	19
glutamine	146	+	0	59	97	0	112	39	1.2	27	75	0.2	47	40	0	49	18
phenylalanine	165	+	4.4	77	93	1.5	68	39	3.7	33	46	1.1	59	31	2.2	66	14
tryptophane	204	+	0.7	81	95	0.4	92	36	1.0	20	45	0	55	9	1.3	61	5
diphenylaminosulfonic acid	271	-	5.0	56	74	1.8	151	31	1.9	47	83	3.7	23	40	2.8	53	56
neutral red	289	+	4.1	93	90	7.1	46	80	41.1	5	88	7.9	40	16	7.6	31	17
methylene blue	320	+	0	89	95	0	37	62	0.3	8	95	0.3	72	22	2.5	45	23
methyl orange	327	0	1.5	69	95	0	73	90	9.5	36	82	8.5	25	84	0	52	67
janus green	511	+	0	96	99	5.5	33	97	6.5	29	99	3.4	46	98	3.8	71	97
patent blue	544	-	5.8	97	92	0.2	97	93	4.5	14	80	6.1	74	36	5.8	42	35
eosine	646	0	0	47	100	0	99	88	0.2	55	87	0.3	15	97	1.4	15	93
congo red	697	0	1.4	78	84	0	102	93	0	81	96	0.8	27	95	0	39	96

Note: the *italic* values are outliers or leverage points for the regression models, formulated in section 5.2.2

Table 5.5: Summary of the adsorbed amount (AD, in mmol m⁻²), the relative flux (RF, in %) and the retention (R, in %) during experiments with dissolved charged organic components at pH 10 (feed concentration = 0.2 mmol L⁻¹, values of relative flux and retention after 2 hours of filtration)

pH 10	M _w (Da)	com- ponent charge	Desal51HL			Desal5DL			NTR7450			N30F			NFPES10		
			AD	RF	R	AD	RF	R	AD	RF	R	AD	RF	R	AD	RF	R
serine	105	-	0	63	89	1.5	128	52	0	70	39	1.6	56	59	2.0	69	35
isoleucine	131	-	1.6	77	92	0	127	39	2.3	98	39	0.3	41	55	3.4	77	34
glutamine	146	-	0	60	87	0	131	31	0.6	89	31	1.0	82	52	0	98	29
phenylalanine	165	-	4.7	90	95	0.8	138	84	2.9	82	91	1.3	60	86	0	84	85
tryptophane	204	-	0.8	95	96	0.5	152	91	0.2	110	91	0.3	64	92	0.6	85	77
diphenylaminosulfonic acid	271	-	4.3	109	99	1.5	111	95	2.1	84	97	2.9	63	97	2.5	78	92
neutral red	289	0	1.1	86	79	9.5	126	66	22.6	32	76	12.7	42	68	17.9	47	46
methylene blue	320	+	9.4	58	99	1.4	29	100	1.7	8	96	19.3	41	100	0.4	44	81
methyl orange	327	-	0	77	99	0	32	97	0.5	42	99	0.3	40	92	1.6	20	89
janus green	511	+	0	89	89	0	34	100	2.8	41	97	2.4	21	100	0.6	31	95
patent blue	544	-	2.7	91	99	0.4	122	96	1.9	86	96	3.9	62	98	4.1	51	97
eosine	646	--	7.9	77	99	1.4	114	100	1.7	94	100	1.5	59	97	1.7	51	99
congo red	697	--	0.7	81	97	0.6	101	96	0.7	101	97	1.3	40	96	0.7	39	99

Note: the *italic* values are outliers or leverage points for the regression models, formulated in section 5.2.2

5.2.2.1 Adsorption of charged organic components

The experimental results of the adsorbed amount at pH 3 (Table 5.4) and pH 10 (Table 5.5) indicate that charged organic components do not adsorb much on the membrane surfaces. This was also stated by Kimura *et al.* (2003). Even no difference in adsorbed amount was observed, when component and membrane are equally or oppositely charged.

For example, the positively charged component janus green and the negatively charged component patent blue show the same low amount of adsorption at pH 10. A very high amount of adsorption, comparable with the adsorption of hydrophobic uncharged components (Table 5.1), is only observed in some specific cases:

- neutral red on NTR7450 at pH 3 and pH 10;
- neutral red on N30F and NFPES10 at pH 10;
- methylene blue on N30F at pH 10.

As neutral red and methylene blue have a rather similar component structure (Figure 5.6), it may mean that in these cases a specific interaction occurs between the components and the polyethersulfone membrane surfaces.

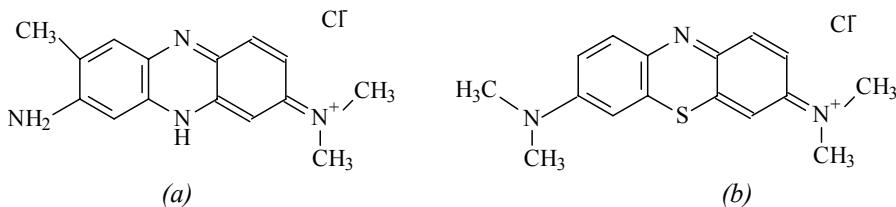


Figure 5.6: Structure of (a) neutral red and (b) methylene blue

Because the charged organic components do not adsorb sufficiently on the nanofiltration membranes (with exception of neutral red and methylene blue), it was not possible to obtain a valuable regression model (residues were not normally distributed). This is also visualized in Figure 5.7 for a selection of charged components. Both small and large components were selected carrying a positive, a negative or no charge at pH 3 and pH 10 (if available). Figure 5.7 shows that no correlation could be observed between the adsorbed amount and I_4 (which was the most important membrane characteristic for the adsorption of uncharged organic

components in section 5.2.1.1). The very low adsorption also implies that, in contrast with uncharged organic components, adsorption will not play a significant role in the flux decline or the retention of these charged organic components.

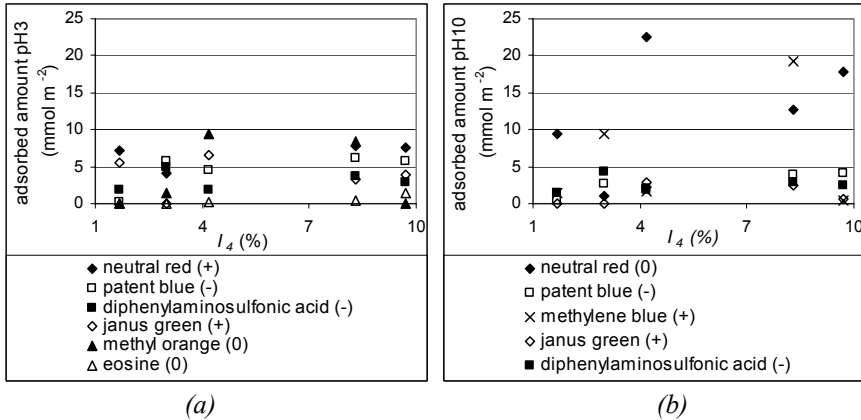


Figure 5.7: Adsorbed amount (mmol m⁻²) of dissolved charged organic components on Desal51HL, Desal5DL, NTR7450, N30F and NFPE10 at (a) pH 3 and (b) pH 10 as a function of I₄ (feed concentration = 0.2 mmol L⁻¹)

5.2.2.2 Relative flux of charged organic components

The lowest relative fluxes at pH 3 and pH 10 were obtained for N30F and NFPE10 (Table 5.4 and 5.5), just as in the case with the uncharged organic components (section 5.2.1.2).

The high relative fluxes of Desal5DL were removed from the data set (influential data points), so that the following linear regression model was obtained for the experimental results both at pH 3 and pH 10 (based upon 117 data points):

$$\text{relative flux} = 33.74 - \frac{10.59}{\text{membrane charge}} + \frac{1637}{\text{contact angle}} - 5.58 \cdot \text{component charge} \quad (5.4)$$

in which the membrane charge, the contact angle and the component charge explained 18 %, 8 % and 4 %, respectively, of the experimental results ($ADJR^2 = 28 \%$).

To increase the adjusted correlation coefficient ($ADJR^2$), a regression model was formulated separately at pH 3 (based upon 61 data points) and pH 10 (based upon 56 data points), respectively.

$$\text{at pH 3: relative flux} = 1.06 + \frac{3612}{\text{contact angle}} - \frac{126.95}{I_3} \quad (5.5)$$

in which the contact angle and I_3 explained 33 % and 11 %, respectively, of the experimental results ($ADJR^2 = 41 \%$).

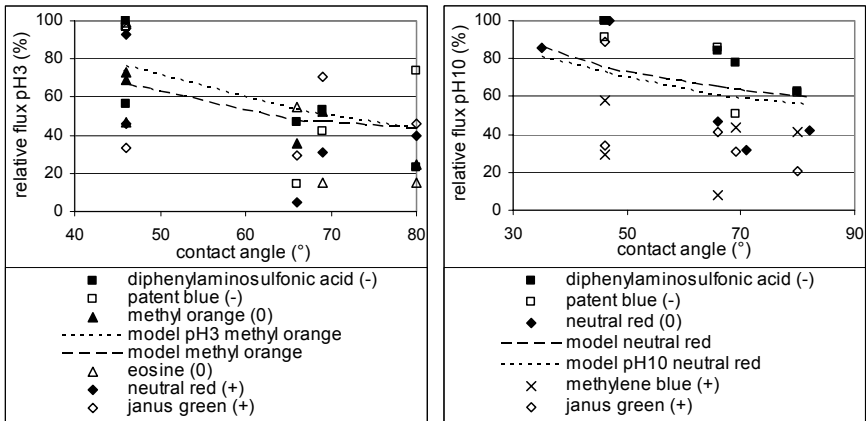
$$\begin{aligned} \text{at pH 10: relative flux} = & 22.54 - 12.62 \cdot \text{component charge} \\ & + \frac{1523}{\text{contact angle}} + \frac{90.05}{I_3} \end{aligned} \quad (5.6)$$

in which the component charge, the contact angle and I_3 explained 23 %, 11 % and 6 %, respectively, of the experimental results ($ADJR^2 = 36 \%$).

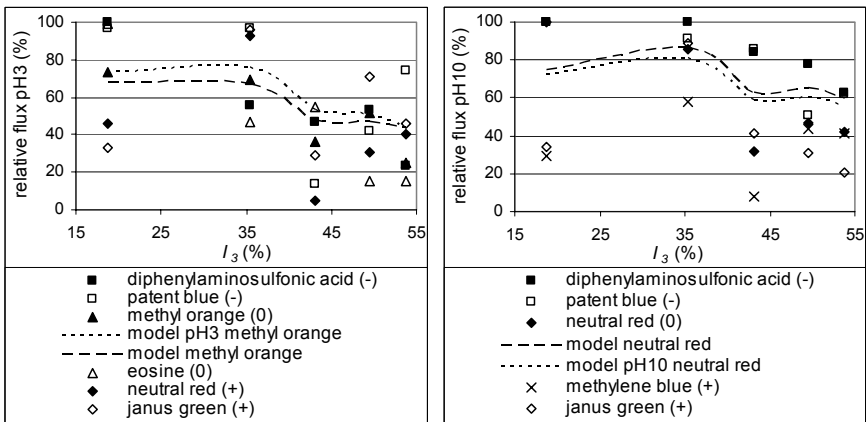
The relative fluxes at pH 3 and pH 10 are shown in Figure 5.8 as a function of membrane and component characteristics. Starting from the regression models at each pH separately (Equations 5.5 and 5.6), the hydrophobicity of the membrane surface (the contact angle) is the most influential membrane characteristic for flux decline at pH 3 and pH 10 (Figure 5.8a), which is consistent with the finding in literature (Song *et al.*, 2004) that a more hydrophobic top layer gives rise to lower relative fluxes. Similar to the uncharged organic components, the volume fraction of the small pores (I_3) also has a negative influence on flux decline (Figure 5.8b).

When linear regression was applied only on the values of the relative fluxes at pH 3 (Equation 5.5), no component characteristic appears into the model. This implies that the same relative fluxes were predicted for one membrane, independently from the molecular mass or the charge of the component (Figure 5.8c). At pH 3, this assumption can be motivated by the fact that the membrane surfaces carry only a small positive charge at pH 3, so that electrostatic interactions between the membrane and the charged components are weak.

However, due to the larger membrane surface charge at pH 10 (in absolute value), electrostatic interactions become more important, as suggested by the presence of the component charge as explaining variable in Equation 5.6. Figure 5.8c on the right-hand shows that positively charged components are more susceptible to flux decline than negatively charged components, which can be explained by electrostatic attraction forces between the negatively charged membrane surface and the positively charged components.



(a)



(b)

Figure 5.8 (to be continued): Relative flux (%) of dissolved charged organic components for Desal51HL, Desal5DL, NTR7450, N30F and NFPES10 at pH 3 (left) and pH 10 (right) as a function of (a) the contact angle, (b) I_3 , (c) the component charge and (d) the membrane surface charge (feed concentration = 0.2 mmol L^{-1})

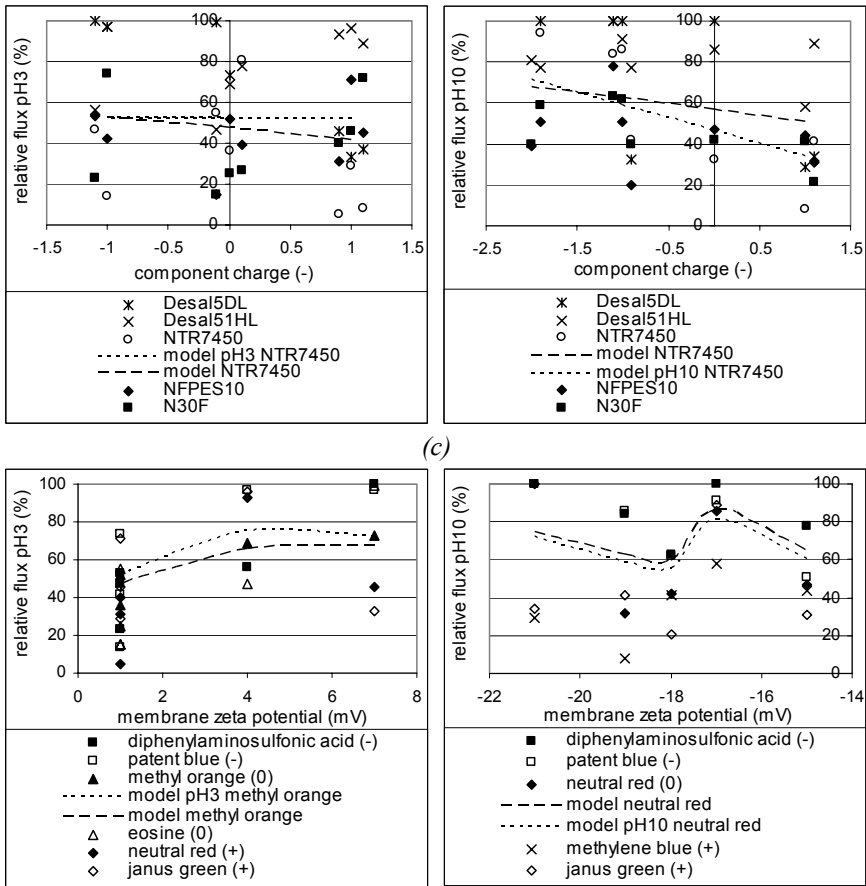


Figure 5.8 (continued): Relative flux (%) of dissolved charged organic components for Desal51HL, Desal5DL, NTR7450, N30F and NFPES10 at pH 3 (left) and pH 10 (right) as a function of (a) the contact angle, (b) I_3 , (c) the component charge and (d) the membrane surface charge (feed concentration = 0.2 mmol L^{-1})

Just as in the case of uncharged organic components (Equation 5.2), the membrane charge does not determine the flux decline when only the relative fluxes at one pH are considered. If the relative fluxes at both pH 3 and pH 10 are considered (Equation 5.4), the membrane charge (Figure 5.8d) in combination with the component charge, comes into the picture. Teixeira *et al.* (2005) came to similar conclusions. This means that the difference in flux decline between pH 3 and pH 10 can be explained by electrostatic interactions between membrane and

component. Lower relative fluxes were obtained at pH 3, as shown in Figure 5.8 and also observed by Mänttari *et al.* (2000).

5.2.2.3 Retention of charged organic components

The highest retentions at pH 3 and pH 10 were observed for Desal51HL (Table 5.4 and 5.5). This was also the case when filtering dissolved uncharged organic components (section 5.2.1.3).

Performing multiple linear regression on the retention values at both pH 3 and pH 10 (based upon 130 data points) yields:

$$\text{retention} = -82.75 + 26.13 \cdot \ln(M_w) + \frac{5053}{\text{cut-off}} - \frac{18.54}{\text{membrane charge}} \quad (5.7)$$

in which $\ln(M_w)$, the membrane charge and the cut-off explained 31 %, 16 % and 7 %, respectively, of the experimental results ($ADJR^2 = 53$ %).

Equation 5.7 indicates that it can be shown by multiple linear regression that the membrane charge (Figure 5.9a) is the most important membrane characteristic to describe the retention of charged organic components. As shown in Figure 5.9, charged components are better retained at pH 10 than at pH 3. Bellona and Drewes (2005) and Qin *et al.* (2003) concluded the same from their experimental results. Just as in the case with the dissolved uncharged organic components (Equation 5.3), the cut-off is an important membrane characteristic to describe the experimental retention results (Figure 5.9b).

A comparison between the retention results of an uncharged and a charged component with the same molecular mass indicates that the highest retention is observed for charged components. Van der Bruggen *et al.* (1999) and Timmer *et al.* (1998) came to similar conclusions. For example, for glutamine (negatively charged at pH 10) and benzylidene acetone (uncharged), which are components with the same molecular mass (i.e., 146 Da), the retention with NFPES10 is 29 % (Table 5.5) and 6 % (Table 5.1), respectively.

Although the component charge plays a role in retention, Equation 5.7 pointed out that, for nanofiltration membranes at pH 3 and pH 10, the component charge is less influential than the molecular mass. Independent of the component charge, a higher retention was observed for larger components (Figure 5.9c). This was also observed by Schaep *et al.* (1998).

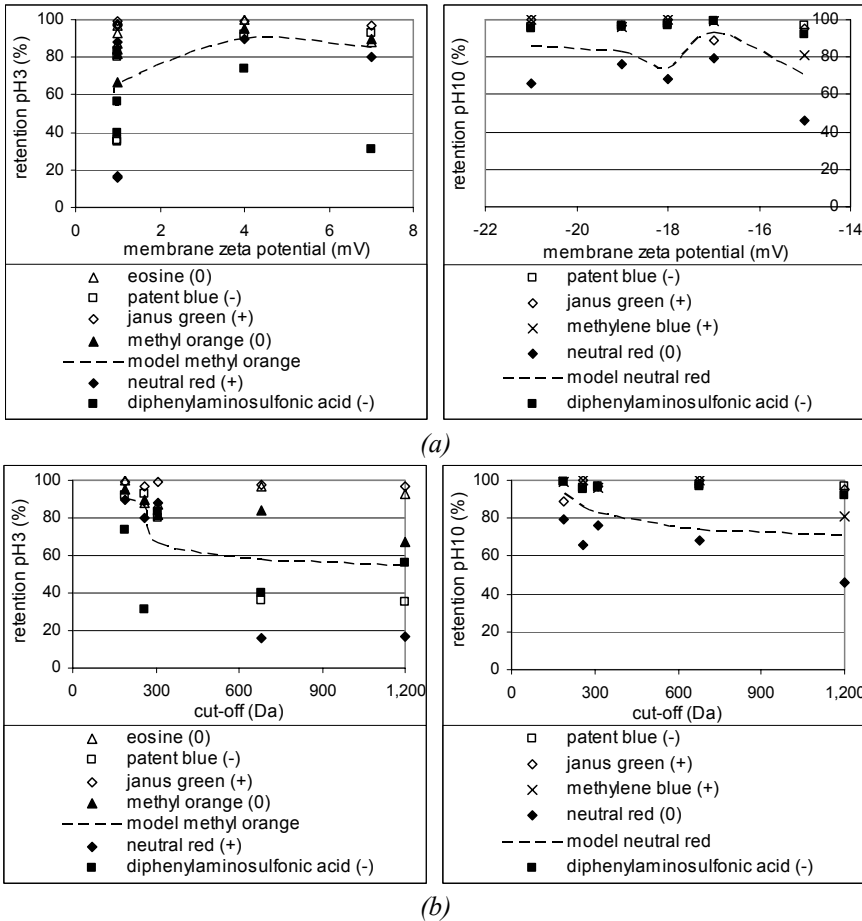
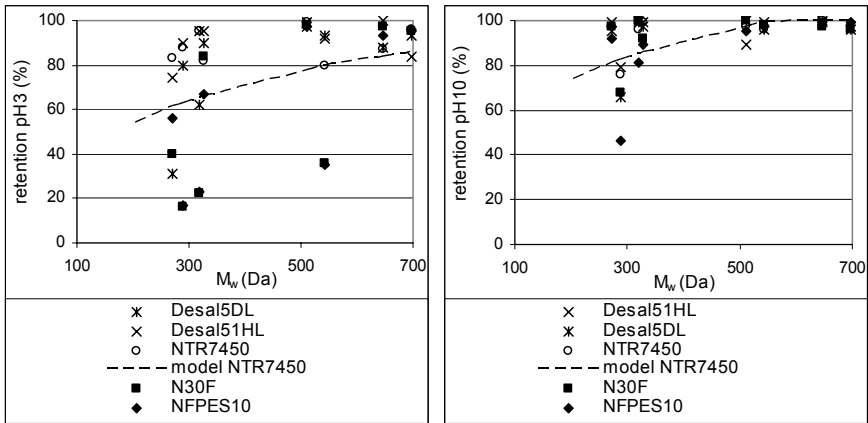


Figure 5.9 (to be continued): Retention (%) of dissolved charged organic components for Desal51HL, Desal5DL, NTR7450, N30F and NFPES10 at pH 3 (left) and pH 10 (right) as a function of (a) the membrane surface charge, (b) the cut-off and (c) the molecular mass (feed concentration = 0.2 mmol L⁻¹)



(c)

Figure 5.9 (continued): Retention (%) of dissolved charged organic components for Desal51HL, Desal5DL, NTR7450, N30F and NFPES10 at pH 3 (left) and pH 10 (right) as a function of (a) the membrane surface charge, (b) the cut-off and (c) the molecular mass (feed concentration = 0.2 mmol L^{-1})

5.2.2.4 Conclusion for charged organic components

The selection of membrane and component variables by multiple linear regression for charged organic components is summarized in Table 5.6. Just as in the case of the dissolved uncharged organic components (Table 5.3), the volume fraction of the small pores (I_3) and the cut-off have an influence on flux decline and retention of the nanofiltration membranes (at one pH value), respectively.

Table 5.6: Summary of membrane and component variables, selected by multiple linear regression to explain the adsorbed amount, the relative flux and the retention of dissolved charged organic components at pH 3 and pH 10

	relative flux			retention
	pH 3	pH 10	pH 3 and 10	pH 3 and 10
membrane	contact angle	contact angle	charge	charge
	I_3	I_3	contact angle	cut-off
component	-	charge	charge	molecular mass

Note: the **bold** values are the most crucial variables

However, when filtering dissolved charged organic components, the hydrophobicity of the membrane surface is crucial to describe flux decline, in

contrast with the uncharged components (where the contact angle came only into the picture after excluding both I_3 and I_4 from the statistical analysis). Due to electrostatic interactions between the membrane and the charged components, both the component charge and the membrane surface charge have an influence on the membrane performance. The molecular mass was the most crucial variable to explain the retention results for charged organic components.

This implies that, for purification of wastewater, the best membrane performance (high relative flux in combination with a high retention) can be obtained by selecting a hydrophilic membrane with a low cut-off in combination with a feed solution composed mainly of large, negatively charged components.

5.3 Nanofiltration performance during filtration of colloidal dispersions

5.3.1 Introduction

Colloidal particles are ubiquitous in natural waters. Colloids cover a wide size range, from a few nanometers to a few micrometers. Aquatic colloids comprise clay minerals, colloidal silica, iron, aluminum, and manganese oxides, organic colloids and suspended matter, and calcium carbonate precipitates (Norde, 2003). In membrane water treatment processes, fouling by these colloidal particles is one of the major categories of performance deterioration. Despite the vast efforts to reduce membrane fouling by improving membrane properties, optimizing operational conditions and pretreatment of the feed water, fouling is unavoidable (Liikanen *et al.*, 2002; Shaalan, 2002).

Therefore, understanding fouling phenomena is critical for the development of membrane-based water treatment technologies. Depending on the relative size of colloidal particles and membrane pores, fouling may occur due to either accumulation of particles on the membrane surface and build-up of a cake or by

penetration within the membrane pores (Lee *et al.*, 2005; Tarabara *et al.*, 2004; Warczok *et al.*, 2004; Elimelech *et al.*, 1997; Zhu and Elimelech, 1997). This section focuses on the former aspect of colloidal fouling, which occurs for nanofiltration (NF) membranes.

As fouling is an interplay between membrane and feed solution, the characteristics of both the membrane and the colloids, together with the feed solution chemistry, are needed to explain and to control membrane fouling. For the membrane characteristics, it is assumed in literature that colloidal fouling is related to the roughness of the membrane surface (Hoek *et al.*, 2003; Vrijenhoek *et al.*, 2001; Elimelech *et al.*, 1997; Zhu and Elimelech, 1997). Because of the ridge-and-valley structure of rough membrane surfaces, colloids are thought to be preferentially transported into the valleys (path of least resistance), which results in “valley clogging” and hence in a more severe flux decline in comparison with smooth membranes. However, other researchers (Van der Bruggen *et al.*, 2004; Van der Bruggen *et al.*, 2004b) did not observe any correlation between colloidal fouling and surface roughness, and the surface hydrophobicity seemed to be the most critical membrane characteristic to control colloidal fouling. Another important membrane property is reported to be the permeability (Costa and de Pinho, 2005; Zhang and Song, 2000; Zhu and Elimelech, 1997), since a higher flux can bring more colloids to the membrane surface in a given time period, resulting in a faster growth of the cake layer.

For the colloid characteristics, both the size, the charge and the concentration of the colloids may influence fouling. An increase in colloid concentration mostly leads to an increase in fouling (Singh and Song, 2005; Chun *et al.*, 2002; Zhang and Song, 2000; Zhu and Elimelech, 1997), while larger colloids either cause more (Zhang and Song, 2000) or less (Tarabara *et al.*, 2004; Yiantsios and Karabelas, 1998) fouling in comparison with smaller colloids.

For the solution chemistry, adapting the pH changes the charge of both membrane surface and colloids and hence the electrostatic interaction forces between

membrane and colloid on the one hand and between colloids on the other hand (Van der Meeren *et al.*, 2004; Faibish *et al.*, 1998). In addition, the ionic strength of the solution is also a critical parameter that affects membrane fouling, as the fouling potential increases with ionic strength (Lee *et al.*, 2005; Singh and Song, 2005; Lee *et al.*, 2004). The increase is attributed to the compression of the double layer formed around the colloids at increased strength. This well accepted theory has been reported to be true for silica particles larger than 50 nm (Singh and Song, 2005).

From this literature overview, it appears clearly that membrane fouling by colloids is influenced by many factors. Up to now, fouling phenomena are studied by considering only a limited number of fouling factors with (mostly) only one membrane in combination with (mostly) only one colloidal dispersion.

This study aims to investigate several representative NF membranes (Desal51HL, Desal5DL, NTR7450, N30F and NFPE10) when filtering several colloids (VP Disp. W7520, Aerodisp W630, Ludox CL and Ludox HS-30, section 2.5.2) with a different solution chemistry. This approach not only allows to obtain a (qualitative) global fouling study in which both membrane and colloid characteristics are emphasized, but it also allows to check whether the same membrane characteristics are determining during filtration of these representative colloidal dispersions. This reinforces not only the reliability of the conclusions made, but it also facilitates the selection of a proper membrane during filtration of an arbitrary colloidal dispersion (e.g., in a specific application).

5.3.2 Characterization of the colloids

The zeta potential of the different colloids as a function of pH is given in Figure 5.10, together with the approximate borders of the colloid stability region. These borders are taken in this case at about ± 30 mV (in conditions of very low ionic strength), as it is suggested in literature (Rabinovich-Guilatt *et al.*, 2004) that such an absolute value of the zeta potential is needed to ensure the colloid stability by electrostatic repulsion according to the DLVO theory.

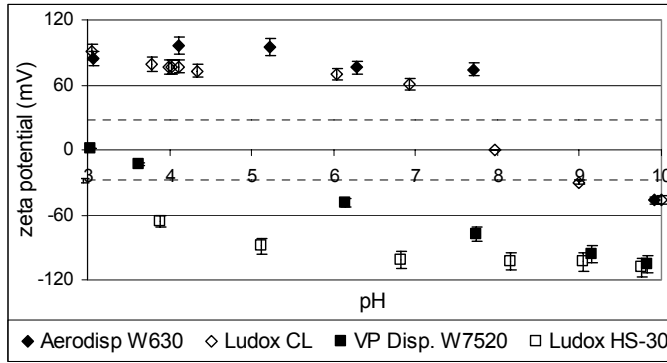


Figure 5.10: Zeta potential (mV) as a function of pH for the different colloids

Figure 5.10 clearly shows the difference in colloid composition. The two silica colloids (VP Disp. W7520 and Ludox HS-30) are negatively charged at a pH above 3. These results correspond with the results from Van der Meeren *et al.* (2004) and Kosmulski (2003). The other two colloids (Aerodisp W630 and Ludox CL) are positively charged at low and intermediate pH, have an iso-electric point between pH 8 and 9 and are negatively charged at high pH. At high pH, however, the zeta potential is low inside the colloid instability region, implying that aggregation is possible. The iso-electric points of both the alumina colloid (Aerodisp W630) and the alumina-coated silica colloid (Ludox CL) correspond well with literature data (Van der Meeren *et al.*, 2004; Kuan *et al.*, 2000; Zhu and Elimelech, 1995). Comparing Figure 5.10 with Figure 4.11 also indicates that the colloid zeta potentials are substantially larger in magnitude than the membrane zeta potentials at intermediate pH.

The hydrodynamic radii of the colloids at different pH conditions and in different NaCl concentrations are given in Table 5.7. At intermediate pH, it is clear that for Ludox CL and Ludox HS-30, the radii are much smaller than for Aerodisp W630 and VP Disp. W7520. Changing the pH or adding NaCl had no significant influence on the colloid size, with exception of Ludox CL and Aerodisp W630 at high pH, where severe coagulation took place close to their iso-electric point (Figure 5.10). Although for the same reasons, some coagulation could be expected for Ludox HS-30 and VP Disp. W7520 at low pH, this was not observed. A

possible explanation could be that the zeta potentials of these colloids at low pH are very close to the borders of the colloid stability region (e.g., Ludox HS-30 at pH 3 in Figure 5.10), so that still some electrostatic repulsion forces occur between these silica colloids.

Table 5.7: Hydrodynamic radius (nm) of the different colloids as a function of pH and NaCl concentration

	Ludox CL	Aerodisp W630	Ludox HS-30	VP Disp. W7520
pH 3	30	77	10	68
pH 5	28	84	8	69
pH 10	233	104	8	68
0.05 M NaCl	41	80	9	67
0.1 M NaCl	42	85	9	67

Combining Figure 5.10 with Table 5.7 indicates the differences between the four selected colloids. At neutral pH, VP Disp. W7520 and Aerodisp W630 are large, negatively and positively charged colloids, respectively, whereas Ludox HS-30 and Ludox CL are small, negatively and positively charged colloids, respectively.

5.3.3 Influence of membrane characteristics on colloidal fouling

Figure 5.11 presents the evolution of the relative flux as a function of filtration time for the different membranes when filtering a 100 mg L⁻¹ Ludox CL dispersion. Similar observations were made for the other colloids (not shown). Figure 5.11 shows that after 15 minutes of filtration the relative flux already becomes stable for all membranes, except for NTR7450.

The stable relative flux as a function of filtration time implies that the colloid fouling cake on the membrane surface is formed instantaneously and that no cake growth takes place. This was also observed by Chun and Park (2004) and by Van der Bruggen *et al.* (2004b). Only for NTR7450, the fouling cake on the membrane surface seems to grow as a function of time, as reflected by the continuously decreasing relative flux. The decrease of the relative flux for NTR7450 was

observed to be similar with all colloidal dispersions, except for VP Disp. W7520 for which a stable relative flux was observed.

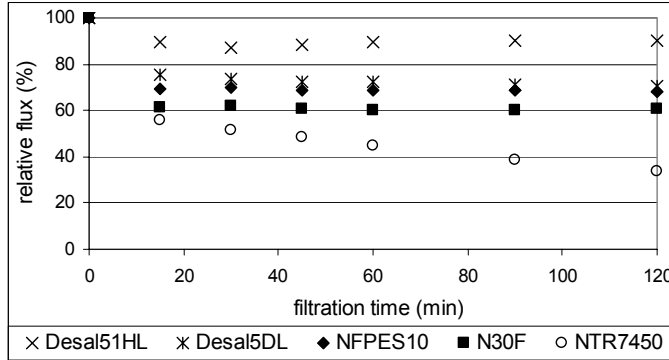


Figure 5.11: Evolution of the relative flux (%) as a function of filtration time for Ludox CL (feed concentration = 100 mg L^{-1} , neutral pH, without salt addition)

The results for the relative fluxes after two hours of filtration with a colloid concentration of 100 mg L^{-1} are given in Table 5.8. The lowest relative fluxes were observed for the more hydrophobic polyethersulfone membranes NTR7450, N30F and NFPES10. Because of the continuous decrease of the relative flux as a function of filtration time (Figure 5.11), NTR7450 showed the lowest relative fluxes except when filtering VP Disp. W7520. In that case, the relative flux remained stable as a function of filtration time as mentioned before. As the fouling results of NTR7450 were outliers among the other membranes, this membrane has been left aside in the following discussions.

The more hydrophilic membranes Desal51HL and Desal5DL have the highest relative fluxes and no significant difference was observed between these membranes when filtering large colloids (Aerodisp W630 and VP Disp. W7520). However, the small colloids (Ludox HS-30 and Ludox CL) foul these membranes in a different way: the lowest relative fluxes were found for Desal5DL. As the characteristics of Desal51HL and Desal5DL are very similar except for their roughness (Desal51HL is smoother, Table 4.3), this implies that the surface roughness also plays a (secondary) role in the fouling phenomenon.

Table 5.8: Relative fluxes (%) after 2 hours of filtration with colloidal dispersions for the different commercial nanofiltration membranes (feed concentration = 100 mg L⁻¹, neutral pH, without salt addition)

	Desal51HL	Desal5DL	NTR7450	N30F	NFPES10
Ludox CL	90	70	34	60	68
Aerodisp W630	87	91	51	50	69
Ludox HS-30	96	84	19	82	89
VP Disp. W7520	96	95	92	92	87

These results indicate that the hydrophobicity of the membrane surface is the most important parameter for colloidal fouling. The surface roughness has a minor influence and only when filtering small colloids. However, it should be kept in mind that this conclusion is based only on two different types of nanofiltration membranes, i.e., polyethersulfone and polyamide membranes. Other polymers (e.g., polyimide) or other types of membranes (e.g., anorganic membranes) are not considered in this study.

No influence on the fouling results was observed for the cut-off, the surface charge or the water permeability. This is illustrated by the different fouling degrees of Desal5DL and NTR7450 (nearly the same cut-off), Desal51HL and N30F (similar surface charge at neutral pH), and Desal51HL and NFPES10 (similar permeability). To check the influence of the permeability in more detail, the hydraulic resistance due to fouling (R_f , section 1.4.1) is calculated using Equation 5.8 and summarized in Table 5.9.

$$R_f = \frac{\Delta P}{\eta} \cdot \left(\frac{1}{J_p} - \frac{1}{J_w} \right) \quad (5.8)$$

where ΔP is the applied pressure, η the viscosity, J_p the permeate flux and J_w the pure water flux of the membrane used.

Because of the low initial permeability, higher resistances due to fouling (after two hours of filtration) were observed for Desal5DL, N30F and NTR7450. Just as with the relative flux, a different resistance due to fouling was observed for membranes

with the same permeability (Desal51HL and NFPES10). However, as the amount of solution filtered can also be critical in fouling phenomena, resistances due to fouling were also calculated after collection of a permeate volume of 100 mL (case 2). The resistances due to fouling were in both cases very similar, except for NTR7450 (Figure 5.11).

Table 5.9: Fouling resistance (m^{-1}) of the different membranes after two hours of filtration of colloidal dispersions (case 1) and after collection of 100 mL permeate (case 2) (feed concentration = 100 mg L⁻¹ of Ludox CL, neutral pH, without salt addition)

	Desal51HL	Desal5DL	NTR7450	N30F	NFPES10
case 1	$4 \cdot 10^{12}$	$40 \cdot 10^{12}$	$161 \cdot 10^{12}$	$53 \cdot 10^{12}$	$8 \cdot 10^{12}$
case 2	$4 \cdot 10^{12}$	$36 \cdot 10^{12}$	$100 \cdot 10^{12}$	$52 \cdot 10^{12}$	$7 \cdot 10^{12}$

To visualize the fouling effects, SEM images of the membrane surfaces were taken before and after fouling, as illustrated in Figure 5.12 for the membranes Desal5DL and N30F in combination with Ludox CL. For the rough membrane Desal5DL, the (small) colloids are situated mainly in the valleys of the surface after filtration; i.e., “valley clogging” has taken place. However, in the case of N30F, the colloids are distributed over the entire membrane surface due to hydrophobic interactions between the colloids and the membrane surface and a uniform, dense cake layer is formed. Research by Brant and Childress (2002) led to the same conclusion.

The resistance of this cake layer seems to be larger than the resistance of “valley clogging” by the small colloids, since the hydrophobic membrane N30F has a lower relative flux than the rough membrane Desal5DL (Table 5.8). Due to the absence of hydrophobic interactions (no dense cake layer) and due to the presence of a smooth surface (no “valley clogging”), the highest relative flux during filtration of *small* colloids was found for Desal51HL.

However, the similar relative flux of Desal51HL and Desal5DL after filtration of *large* colloids indicates that the effect of “valley clogging” by large colloids is very small (as described in more detail in section 5.3.4.2). Hydrophobic interactions

between colloids and the membrane surface (e.g., N30F) seem to be the most influential and also the only fouling mechanism in the case of filtration of large colloids; “valley clogging” only seems to play a (secondary) role in the case of filtering small colloids.

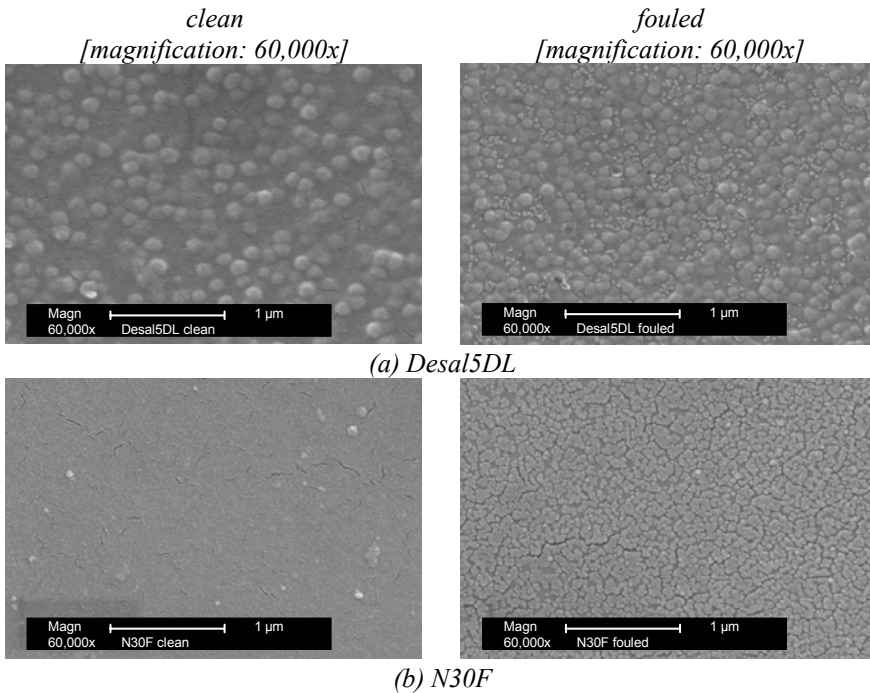


Figure 5.12: SEM images of the surfaces of (a) Desal5DL and (b) N30F, in clean and in fouled state (after filtering a dispersion of Ludox CL of 100 mg L^{-1} at neutral pH without salt addition)

In addition to SEM, non-contact mode AFM experiments were performed to obtain a topographic image and to calculate the roughness of the membrane surface before and after fouling. The RMS roughness of Desal5DL and NFPES10 before and after filtration with colloidal dispersions are given in Table 5.10 for two different scan areas ($1 \mu\text{m} \times 1 \mu\text{m}$ and $3 \mu\text{m} \times 3 \mu\text{m}$). A comparison between both scan areas shows that the roughness is the highest on the largest scan area ($3 \mu\text{m} \times 3 \mu\text{m}$) in all cases, as discussed in section 4.3.2.

Table 5.10: RMS roughness (nm) of Desal5DL and NFPES10 for the clean surface, after filtration with water and after filtration with different colloidal dispersions on two different scan areas (feed concentration = 100 mg L⁻¹, neutral pH, without salt addition)

		Desal5DL		NFPES10	
		1 μm x 1 μm	3 μm x 3 μm	1 μm x 1 μm	3 μm x 3 μm
		clean		5.7	9.8
after filtra- tion with	water	9.8	11.8	1.8	2.6
	Ludox CL	9.7	10.8	2.7	2.7
	Aerodisp W630	8.1	9.1	8.2	6.1
	Ludox HS-30	6.0	9.3	2.6	2.9
	VP Disp. W7520	8.9	12.1	8.7	11.9

To check whether the roughness increases or decreases after filtration with colloidal dispersions, an appropriate reference should be selected. Table 5.10 indicates that the roughness increases (for both scan areas) after filtration with distilled water when compared to the clean unused membrane. A possible explanation for this could be the change in compaction of the membrane, caused by the applied pressure, through which the membrane surface gets more and deeper/higher valleys/hills. Therefore, the only appropriate reference is the roughness value after filtration with distilled water.

Typical AFM images of Desal5DL and NFPES10 after filtration with water and after filtration with Aerodisp W630 are shown in Figure 5.13. For Desal5DL, a few of the large Aerodisp W630 colloids are found in the valleys of the membrane surface, but the effect is rather limited. This sharply contrasts with NFPES10, for which the membrane surface is changed drastically after colloidal fouling.

These visual observations are also reflected by the roughness values in Table 5.10: the roughness either decreases or increases for both scan areas due to colloidal fouling of Desal5DL or NFPES10, respectively. The decrease in roughness for Desal5DL was explained by the presence of colloids in the valleys of the surface,

through which the AFM tip ‘sees’ less deep valleys on the membrane surface, which results in a lower roughness value. The membrane surface of NFPES10 becomes rougher after filtration with colloids due to the formation of a cake layer, of which the presence is confirmed both by SEM (Figure 5.12) and AFM (Figure 5.13) images.

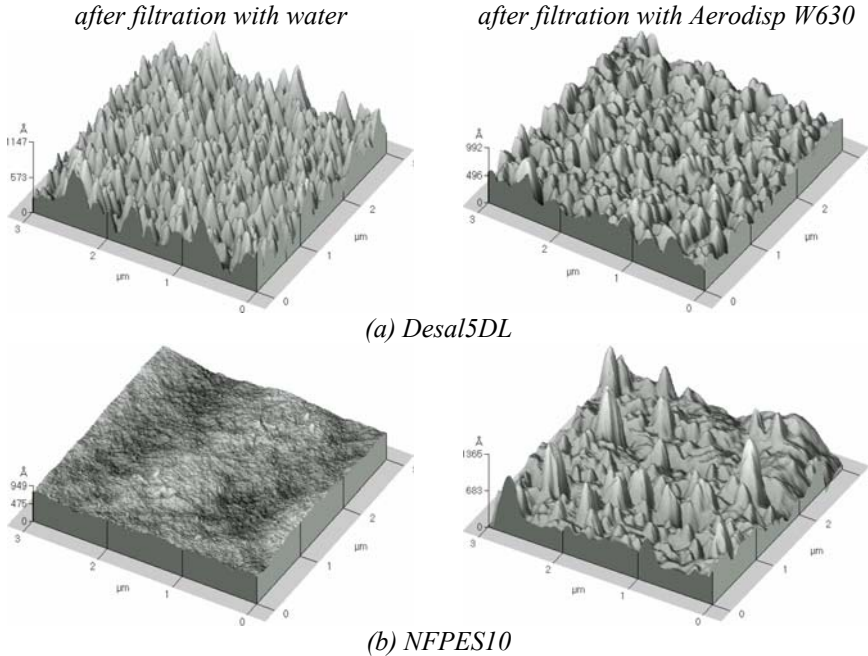


Figure 5.13: Non-contact mode AFM images of (a) Desal5DL and (b) NFPES10 on a scan area of $3 \mu\text{m} \times 3 \mu\text{m}$, after filtration with water (left) and after filtration with Aerodisp W630 (right) (feed concentration = 100 mg L^{-1} , neutral pH, without salt addition)

5.3.4 Influence of colloid characteristics on colloidal fouling

5.3.4.1 Influence of colloid charge

The influence of colloid charge on fouling was understood by comparing the relative fluxes of Ludox CL and Ludox HS-30 on the one hand and Aerodisp W630 and VP Disp. W7520 on the other hand (Table 5.8). The size of the colloids is in both cases comparable (Table 5.7), implying that the influence of colloid size can be neglected. Table 5.8 indicates that the negatively charged colloids (Ludox HS-30 and VP Disp. W7520) foul the membranes less than the

positively charged colloids (Ludox CL and Aerodisp W630, respectively), NTR7450 with Ludox CL and Ludox HS-30 being the only exceptions.

This lower fouling tendency was explained by electrostatic repulsion forces between the negatively charged colloids and the negatively charged membrane surfaces at neutral pH. The influence of the colloid charge is in particular observed for the hydrophobic membranes N30F and NFPES10, although their surface charges (and hence electrostatic forces) are similar to the charges of the other membranes. A possible explanation for this can be the hydrophobicity of the colloids, since it is mentioned in literature (Brant and Childress, 2002) that alumina or alumina-coated colloids are more hydrophobic than silica colloids. Therefore, Ludox CL and Aerodisp W630 would experience more hydrophobic interactions than Ludox HS-30 and VP Disp. W7520, and this especially in combination with a more hydrophobic membrane surface like N30F or NFPES10.

5.3.4.2 Influence of colloid size

The influence of colloid size on fouling was understood by comparing the relative fluxes of Ludox CL and Aerodisp W630 on the one hand and Ludox HS-30 and VP Disp. W7520 on the other hand. These colloids are in both cases similarly charged (Figure 5.10), implying that the influence of colloid charge can be neglected. Table 5.8 indicates that the small colloids (Ludox CL and Ludox HS-30) have lower relative fluxes than the large colloids (Aerodisp W630 and VP Disp. W7520, respectively), which is especially visible for the rough membrane Desal5DL. In section 5.3.3, this was attributed to the phenomenon of “valley clogging”, which seems to occur preferentially for small colloids.

The difference in hydrodynamic forces between large and small colloids can also explain this phenomenon. An analogy was made with media filtration, in which a suspended particle has to leave the streaming pattern of the filtered water to reach the surface of a grain. As described by Crittenden *et al.* (2005), this can happen by diffusion (small colloids) or impaction (large colloids). Although the streaming patterns in nanofiltration run along the membrane surface instead of through the

medium (as in media filtration), the principle is analogous to media filtration. By means of diffusion, small colloids can reach and get attached to the membrane surface. In the case of a rough membrane, these colloids are released more difficultly and hence “valley clogging” occurs. The impaction of large colloids, on the other hand, is counteracted by the high feed velocity applied in the membrane module. This implies that the probability of a large colloid to reach the membrane surface is lower than the probability of a small colloid, through which “valley clogging” mainly occurs for small colloids.

The colloid size does not only have an influence on the membrane – colloid interactions, but also on the colloid – colloid interactions as given by the DLVO theory (Van der Meeren *et al.*, 2004; Hoek *et al.*, 2003; Brant and Childress, 2002). With this theory, the relation of the total interaction energy between colloids (E) to the driving force of the Brownian motion of the colloids ($k \cdot T$) is calculated (section 2.5.2.2) and given in Figure 5.14 for the different colloids.

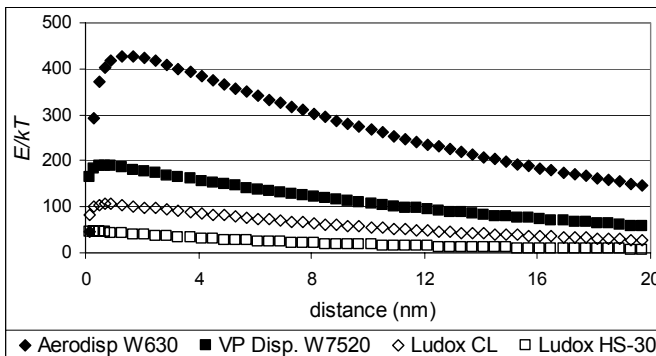


Figure 5.14: DLVO interaction energy diagram of different colloids at pH 6 (electrolyte concentration = 0.3 mol m^{-3} and 293 K)

The interaction energy between colloids is influenced by both the size, the (absolute value of the) surface charge density and the surface composition of the colloids. The most repulsion is observed between the Aerodisp W630 colloids, as these colloids are large (Table 5.7) and have a large surface charge (Figure 5.10).

Figure 5.14 also indicates that the least repulsion is observed between the smallest colloids (Ludox CL and Ludox HS-30), which possibly explains their “valley clogging” on rough membranes. Between the large colloids, the repulsion forces are much larger which means that the probability that two large colloids come together in a small valley on a rough membrane is much smaller.

The DLVO theory can also be applied to study the interaction energy between a surface (in this case the membrane) and colloids, as described by Hoek and Agarwal (2006) and Bhattacharjee and Elimelech (1997). Unlike the DLVO analysis for colloid-colloid interactions, the calculation of membrane-colloid interactions requires extensive computational work and the value of (currently) unknown data (e.g., Hamaker constant of a membrane). This analysis is beyond the scope of this thesis.

5.3.4.3 Influence of colloid concentration

In addition to colloid size and charge, the colloid concentration also plays a role in membrane fouling. Figure 5.15 presents the relative fluxes for NFPES10 and NTR7450 after filtration of the colloidal dispersions in different concentrations. The results for the other membranes were comparable to the results for NFPES10. The role of the colloid concentration on membrane fouling is limited for NFPES10, as the relative flux does not change with increasing concentration. This agrees with the observations of Chun and Park (2004). Only for VP Disp. W7520, a higher colloid concentration causes more membrane fouling.

The opposite tendency is, however, observed for NTR7450, for which membrane fouling decreases with increasing concentration for all studied colloids. The reason why this membrane forms an exception is not clear; the combination of the small pore size with the high hydrophobicity probably causes this uncommon phenomenon. NTR7450 is also the only membrane where a decrease of the relative flux as a function of time was observed in all experiments (except for VP Disp. W7520, section 5.3.3).

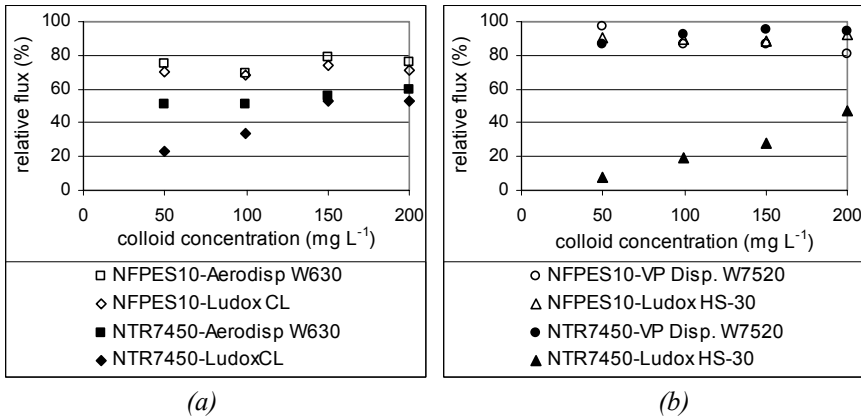


Figure 5.15: Influence of the colloid concentration on the relative flux (%) of NFPE10 and NTR7450 after filtration of (a) Aerodisp W630 and Ludox CL and (b) VP Disp. W7520 and Ludox HS-30 (neutral pH, without salt addition)

As the colloid concentration only has a minor influence on fouling (except for NTR7450), a sufficiently large data set was obtained for multiple linear regression to verify the influence of the different membrane characteristics on colloidal fouling (as described in section 5.3.3). Both the membrane (Table 5.2) and the colloid characteristics at neutral pH (i.e., size (Table 5.7) and zeta potential (Figure 5.10)) were used as input variables.

The low relative fluxes of NTR7450 were removed from the data set (influential data points), so that the following model was obtained based upon 62 data points:

$$relative\ flux = 134.67 - 0.64 \cdot contact\ angle - \frac{509.03}{colloid\ charge} - 1.96 \cdot roughness \quad (5.9)$$

in which the contact angle, the colloid charge and the membrane surface roughness explained 32 %, 28 % and 7 %, respectively, of the experimental results ($ADJR^2 = 66\%$).

This statistical analysis confirms that, in addition to colloid characteristics, the membrane hydrophobicity in the first place (Figure 5.16a) and the roughness in the second place (Figure 5.16b) are the most relevant membrane characteristics.

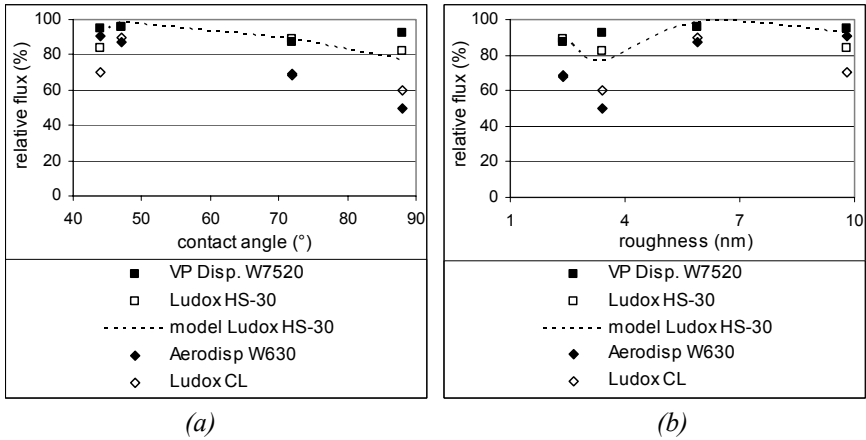


Figure 5.16: Relative flux (%) of different colloidal dispersions for Desal51HL, Desal5DL, NTR7450 and NFPE510 as a function of (a) the contact angle and (b) the roughness (feed concentration = 100 mg L⁻¹, neutral pH, without salt addition)

5.3.5 Influence of solution chemistry on colloidal fouling

5.3.5.1 Influence of pH

The influence of pH on the relative flux for the different colloidal dispersions is shown in Figure 5.17 for Desal51HL and NFPE510. The results for the other membranes (N30F and Desal5DL) were comparable. A distinction has to be made between the alumina and the silica colloids.

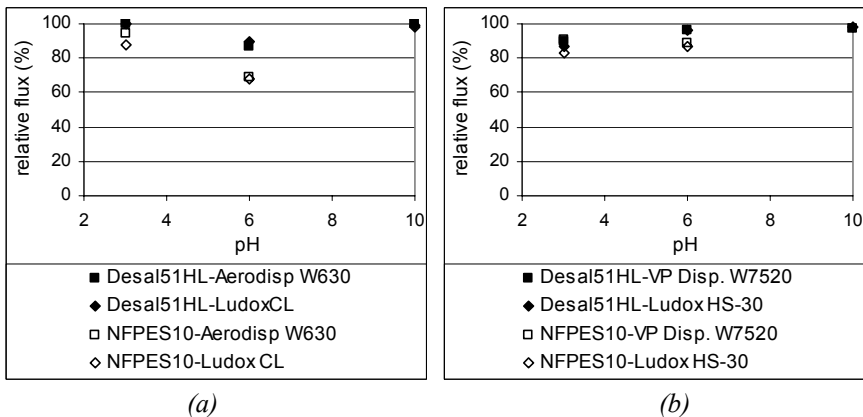


Figure 5.17: Influence of pH on the relative flux (%) after filtration of (a) Aerodisp W630 and Ludox CL and (b) VP Disp. W7520 and Ludox HS-30 (feed concentration = 100 mg L⁻¹, without salt addition)

For the alumina colloids (Ludox CL and Aerodisp W630, Figure 5.17a), the lowest relative flux was observed at pH 6 because of electrostatic attraction forces between the negatively charged membrane and the positively charged colloid. At pH 3 and 10, electrostatic repulsion forces between the equally charged membranes and colloids result in less fouling. This implies that the observed coagulation of the alumina colloids at pH 10 (Table 5.7) does not give rise to the formation of significant deposits on the membrane surface, but rather to the formation of very porous fractal aggregates, in agreement with the results of Van der Meeren *et al.* (2004).

For NFPES10 (and also for N30F, not given), Figure 5.17a indicates a difference between the relative fluxes of the alumina colloids at pH 3 and pH 10. This was explained by the fact that the iso-electric point of these membranes is close to pH 3, so that only limited interaction forces between the membrane surface and the colloids occur. Due to the strong repulsion forces between the alumina colloids at pH 3 (shown for Ludox CL in Figure 5.18), fouling is, however, limited.

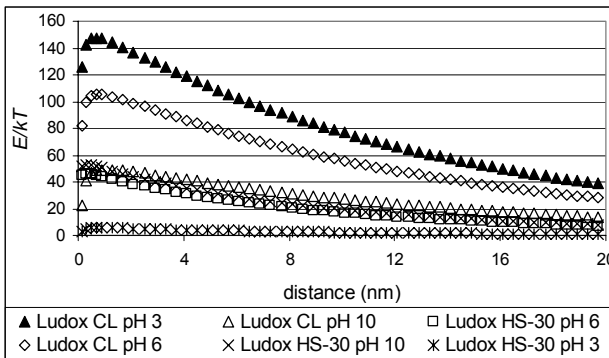


Figure 5.18: DLVO interaction energy diagram of Ludox CL and Ludox HS-30 at different pH values (electrolyte concentration = 0.3 mol m^{-3} and 293 K)

For the silica colloids (Ludox HS-30 and VP Disp. W7520, Figure 5.17b), the relative fluxes increase with increasing pH. This was explained by the fact that, not only the membrane, but also (and especially) the colloid surface gets more negatively charged. As there is no influence of membrane charge on fouling (section 5.3.3), the increase in relative flux with increasing pH is related to the (major) increase in colloid charge. This results in stronger electrostatic repulsion

forces between the membrane surface and the colloids on the one hand and between the colloids on the other hand (Figure 5.18) and hence in less fouling.

5.3.5.2 Influence of salt concentration

Table 5.11 presents the relative fluxes of Desal51HL, N30F and NFPE10 after filtration of solutions with different salt concentrations, with and without the addition of colloids. Both in the absence and the presence of colloids, the relative flux of Desal51HL decreases, while the relative flux of N30F and NFPE10 increases with increasing salt concentration.

Table 5.11: Relative fluxes (%) for Desal51HL, N30F and NFPE10 as a function of NaCl concentration (M) after filtration of NaCl solutions without colloids and after filtration of NaCl solutions with Ludox HS-30 and Aerodisp W630 (feed concentration = 100 mg L⁻¹, neutral pH)

M NaCl	no colloid			Ludox HS-30			Aerodisp W630		
	0.01	0.05	0.1	0	0.05	0.1	0	0.05	0.1
Desal51HL	89	90	82	96	85	78	87	93	81
N30F	64	91	101	82	86	93	50	92	94
NFPE10	96	104	106	89	96	94	69	94	94

In the absence of colloids, the explanation for the decreasing flux of Desal51HL on the one hand and the increasing flux of N30F and NFPE10 on the other hand with increasing salt concentration is twofold, starting from the basis that an increasing salt concentration leads to a thinner electrical double layer of the membrane. Due to the obtained shielding effect of the membrane charge, the repulsion in the pores decreases, which results in lower fluxes, observed for Desal51HL (Table 5.11).

However, for membranes with larger pores (N30F and NFPE10) the electroviscous effect comes into the picture, as described in literature by Huisman *et al.* (1997). This effect is dependent on the membrane pore size (i.e., larger pore sizes give larger electroviscous effect) and is based on the fact that, with increasing salt concentration, the thinner double layer and the smaller membrane charge offer less resistance to water passage which hence results in higher (relative) fluxes. This

implies that the lowest relative flux should be expected for a feed solution without salt addition, in contradiction with the results of Table 5.11. The electroviscous effect hence forms only a partial explanation for the behavior of N30F and NFPE10. To understand this phenomenon better, additional experiments should be performed, which however falls behind the scope of this work.

The discussion about the difference in behavior of the relative flux for Desal51HL on the one hand and N30F and NFPE10 on the other hand is also supported by the data, shown in Figure 5.19. The pore size of Desal51HL is independent of the salt concentration (as given by the constant sugar retention). However, for N30F, the sugar retention decreases with increasing salt concentration; the same phenomenon is also observed by Bargeman *et al.* (2005). This indicates that the pores of N30F seem to get larger. Whether this is related to a real increase in pore diameter or rather to a decrease in pore hydration, is not clear from these experiments.

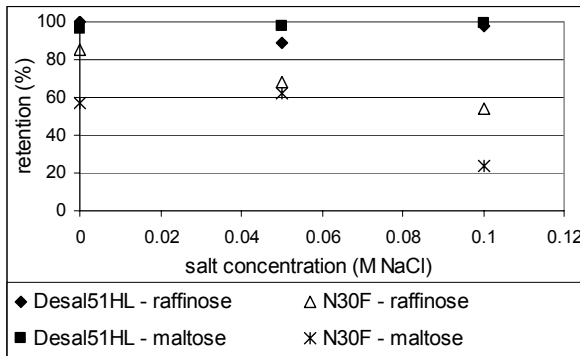


Figure 5.19: Retention (%) of raffinose and maltose for Desal51HL and N30F as a function of NaCl concentration after filtration of NaCl solutions without colloids (neutral pH)

In the presence of colloids, Table 5.11 indicates that the behavior of the relative flux is similar to the behavior of the relative flux without colloids. However, a comparison between the relative fluxes in both situations reveals that the colloids cause an extra fouling resistance in addition to the salt (as indicated by the lower relative fluxes in the presence of colloids and NaCl).

5.3.6 Conclusion for colloidal dispersions

The hydrophobicity of nanofiltration membranes seems to be the most influential factor in colloidal fouling, independent of colloid size or charge. Only when small colloids are filtered with rough membranes, “valley clogging” plays an additional secondary role in membrane fouling. Therefore, the optimal membrane choice to minimize fouling is a membrane with a hydrophilic, smooth surface.

For the influence of the colloids, the least membrane fouling was observed (at neutral pH and without the addition of salt) for large, negatively charged colloids. The colloid concentration does not play any role in the case of filtering small or positively charged colloids; only during filtration of large, negatively charged colloids, the colloid concentration should be as low as possible for a minimal fouling result. Depending on the pore size of the membrane, increasing the ionic strength of the solution (at neutral pH) could also be advantageous to minimize colloidal fouling.

5.4 General conclusion

The performance of (polyethersulfone and polyamide) nanofiltration membranes depends on both membrane and feed properties, as it was shown that changing the type of the (aqueous) feed solution implies the selection of another optimal membrane.

To minimize fouling of nanofiltration membranes, a low volume fraction of small pores (I_3) is desirable if the feed solution contains dissolved uncharged or charged organic components. In the latter case, it was shown that a large surface charge and a high hydrophilicity are also favourable. A hydrophilic membrane surface was also the most important selection criterion for minimal colloidal fouling. Only during filtration of small colloids, a (hydrophilic) nanofiltration membrane with a smooth top layer is required.

Not only the membrane, but also the feed characteristics control the degree of fouling. Hydrophilic components guarantee the best results during filtration of dissolved uncharged components at neutral pH, while negatively charged

components guarantee the best results during filtration of dissolved charged components at high pH. For a given membrane, minimal fouling is obtained in the case of large, negatively charged colloids.

The retention of dissolved organic components is determined mainly by the cut-off of the nanofiltration membranes, which correlates with the relation of the volume fraction of the large pores to the total volume fraction of the pores. If the dissolved organic components are uncharged, their hydrophobicity should be low for a maximal retention.

These results indicate that for each type of feed solution, a specific membrane needs to be selected. However, a real waste water can be a mixture of several dissolved (un)charged organic components and colloids. Due to interactions between these components, the membrane performance can improve or get worse. This means that filtration experiments with (representative) mixtures of components need to be performed in the future to fine-tune the understanding of membrane performance in real applications. Moreover, experiments with other nanofiltration membranes (other polymeric ones or anorganic ones) are needed to extend the conclusions made to the whole nanofiltration world.

Chapter 6

Regeneration of carwash wastewater by nanofiltration

*Adapted from: Sep. Purif. Technol. 54 (2007) 139-146
Chem. Phys. Chem. 8 (2007) 1836-1845*

6.1 Introduction

Water is one of the most valuable raw materials on earth. It is necessary to life and seems to be inexhaustible. The earth surface is covered for 70 % with water, of which 97 % is seawater and more than 2 % is ice. Taking into account polluted water and water on very deep places, only 0.003 % of the total amount of water is available for drinking water supply. But like every raw material, water or the “blue gold” is not inexhaustible. Water scarcity has to be handled both through rational water consumption as well as through water re-use and water recycling in the industry. In Flanders, the industry counts for 60 % of the total water consumption. By using new technologies, such as nanofiltration, a large amount of water can possibly be saved. In this chapter, the application of nanofiltration for water recycling in the carwash industry is investigated.

A carwash is defined as a non-domestic installation for external cleaning of cars. Three types of carwashes occur: the roll-over (in which the washing installation moves over the car), the automatic carwash (in which the car is pulled through the washing installation) and the self-carwash. In Belgium, e.g., the (around 400) automatic carwashes have the highest capacity (on average 30,000 cars a year) in combination with the highest water consumption (on average 400 L a car) (Huybrechts *et al.*, 2002). As the problem of water recycling is the most prominent in this type of carwash, a typical automatic carwash was selected in this study (section 6.3.1).

The carwash industry is conscious of the need of water recycling, as in some European countries water recycling in carwashes is already regulated by law. In Germany and Austria, a recycling percentage of minimal 80 % is imposed, while in the Netherlands and the Scandinavian countries, a maximal fresh water consumption of 60 - 70 L a car is enforced. Also in Belgium, a recycling percentage of 70 % will be needed in the future to obtain an environmental license (Huybrechts *et al.*, 2002). Nowadays, nearly 15 % of the Belgian carwashes already purifies and re-uses 55 % of the wastewater by using different techniques such as sand filtration, adsorption or biological treatment. However, these systems

are not satisfactory enough to recycle wastewater in high-quality applications like for example in the main washing process. A possible solution could be the introduction of membrane processes.

In literature, membrane research in the carwash industry is limited to the use of ultrafiltration (Hamada and Miyazaki, 2004; Urbanski *et al.*, 2002; Jönsson and Jönsson, 1995). The main problems when using ultrafiltration were membrane fouling (resulting in very low permeate fluxes) and very low retentions for small components (like surfactants or COD), which do not allow to recycle the wastewater. As the second problem is intrinsic to ultrafiltration, more attention was given in literature to the first problem, i.e., membrane fouling. Panpanit and Visvanathan (2001) tried to decrease membrane fouling by adding bentonite to the wastewater. An experimental comparison between the performance of different ultrafiltration and nanofiltration membranes also pointed out that applying nanofiltration to recycle wastewater would result in less fouling in combination with higher retentions (Karakulski and Morawski, 2003; Panpanit *et al.*, 2000).

This chapter aims to test the (short-term) performance of nanofiltration membranes when filtering wastewater of a typical automatic carwash during a working day. Because the carwash wastewater is, however, a complex mixture of several components (among which surfactants), the interpretation of the fouling results is hampered. Therefore, this chapter focuses firstly on the flux decline of various nanofiltration membranes caused by (synthetic) surfactant solutions in different conditions, representative for the carwash wastewater.

6.2 Surfactant fouling of nanofiltration membranes

6.2.1 Introduction

Surfactants are a class of industrially very important amphiphilic substances, consisting of a hydrophilic head-group to which a hydrocarbon chain is connected. One of the characteristic properties of amphiphilic substances is that they tend to

assemble at interfaces. They are therefore often referred to as surface-active agents. Another characteristic property of amphiphilic substances is the formation of large aggregates (micelles). In these micelles, the hydrophilic heads are directed towards the aqueous solution, while the hydrophobic tails are turned to the inside. Surfactants are categorized into four groups depending on the charge of the head-group: nonionic, anionic, cationic and zwitterionic surfactants.

In literature, membrane fouling during filtration of surfactant solutions is studied mainly in the case of ultrafiltration. The phenomenon of decreasing permeate flux as a function of time (at constant pressure) is thought to be caused by concentration polarisation and adsorption (Byhlin and Jönsson, 2002; Rögener *et al.*, 2002). Concentration polarization can be minimized by applying a turbulent flow in the membrane module (Urbanski *et al.*, 2002). Adsorption on the other hand is dependent on the solution chemistry and on both membrane and surfactant properties (Bandini, 2005; Gomes *et al.*, 2005; Paria and Khilar, 2004; Matsui *et al.*, 2002). In the case of nonionic surfactants, a more hydrophobic membrane surface and/or surfactant result in more adsorption and hence in more membrane fouling. In the case of ionic surfactants, not only the hydrophobicity but also the charge of the membrane and the surfactant are important characteristics to explain the adsorbed amount and membrane fouling (Doulia *et al.*, 1997; Jönsson and Jönsson, 1991). In the absence of micelles, the retention of surfactants in ultrafiltration is very low (Kowalska *et al.*, 2004). In applications where an almost complete retention is required (Wendler *et al.*, 2002; Meindersma and Kuczynski, 1996), nanofiltration instead of ultrafiltration is preferred.

Fouling studies during nanofiltration of surfactant solutions are rather scarce in literature. Wendler *et al.* (2002b), Yeom *et al.* (2000) and Archer *et al.* (1999) studied the performance of different nanofiltration membranes during filtration of an anionic surfactant. Archer *et al.* (1999) concluded that the best separation of an anionic surfactant can be achieved by a strong hydrophilic, negatively charged nanofiltration membrane. Yeom *et al.* (2000) came to the same conclusion by comparing the performance of negatively, positively and uncharged membranes in

the presence of anionic surfactants. Cornelis *et al.* (2005) focused on the nanofiltration of nonionic surfactants; their study indicated that adsorption of nonionic surfactants on the membrane surface and in the membrane pores is the main mechanism of membrane fouling. A systematic and thorough fouling study of nanofiltration with surfactant feed solutions is currently lacking in literature.

The aim of this study is to determine and to explain membrane fouling of different nanofiltration membranes when solutions of different types of surfactants in different conditions are filtered. As in some studies in literature, a relation between membrane fouling and adsorption is assumed (Cornelis *et al.*, 2005; Van der Bruggen *et al.*, 2002; Mietton-Peuchot and Ranisio, 1997), static adsorption experiments were performed for each solution to check this statement. After the adsorption experiments, the hydrophobicity of the membrane surface was determined again to get an idea about the orientation of the adsorbed surfactants (Dutschk *et al.*, 2003). Since surfactants can adsorb either by their hydrophobic tails or by their hydrophilic heads (Jönsson and Jönsson, 1991), the top layer of the membrane may become more hydrophilic or hydrophobic.

Three different types of surfactants were selected: an ethoxylated alcohol (neodol 91-5E, nonionic), sodium dodecylbenzenesulfonate (SDBS, anionic) and hexadecyltrimethylammonium bromide (cetrimide, cationic) of which the characteristics and the structures were summarized in Table 2.6 and Appendix II, respectively. The membranes NFPE10, NTR7450, Desal51HL and NF270 were selected for this study. As already discussed in Chapter 4 (Table 4.3), NFPE10 and NTR7450 have the most hydrophobic top layer; NFPE10 also has the highest cut-off and the smallest charge at neutral pH. NF270 is the most hydrophilic membrane with the lowest cut-off. The surface charge of NF270 at neutral pH is very large and comparable to the surface charge of NTR7450. The characteristics of Desal51HL are situated between the other membranes.

Firstly, (adsorption and filtration) experiments were performed to study the influence of the type of surfactant on fouling and surfactant retention. The fouling

degree of the membranes was presented by the relative flux (section 2.1), which is defined as the ratio of the permeate flux to the respective pure water flux. The effect of increasing surfactant concentration and the effect of adding electrolyte to the solution were also studied. Experiments at different pH were then carried out, as both the membrane charge and the surfactant charge depend on the pH of the solution. In all cases, the difference in performance between the different nanofiltration membranes was explained by the difference in membrane characteristics.

6.2.2 Effect of the type of surfactant

The performance of the nanofiltration membranes was studied when filtering a feed solution of neodol, SDBS or cetrimide. As it is mentioned in literature (Van der Bruggen *et al.*, 2002) that flux decline is related to the adsorbed amount, the results of the adsorption experiments are described firstly.

6.2.2.1 Effect of the type of surfactant on adsorption and hydrophobicity

The results of the adsorption experiments for a feed solution of 600 mg L⁻¹ of neodol, SDBS or cetrimide at neutral pH (without addition of NaCl) are summarized in Table 6.1. In the adsorption experiments, a feed volume of 50 mL with a concentration of 600 mg L⁻¹ is exposed to a membrane surface of 19.625 cm², which implies that around 40.8 mmol m⁻² surfactant is present and available for adsorption. Comparing the adsorbed amount (Table 6.1) with this total amount available for adsorption reveals that the highest adsorption observed (cetrimide-NF270) corresponds with half of the surfactant amount, available during adsorption.

Table 6.1: Adsorbed amount (mmol m⁻²) of the surfactants neodol, SDBS and cetrimide (feed concentration = 600 mg L⁻¹, neutral pH, without salt addition)

	NF270	Desal51HL	NTR7450	NFPES10
neodol	0.7	7.4	5.9	14.0
SDBS	0.0	1.5	2.6	2.6
cetrimide	23.0	14.0	17.7	19.1

For the nonionic surfactant neodol, adsorption is influenced by hydrophobic interactions rather than electrostatic interactions. Neodol adsorbed the most on NFPE10, as the top layer of this membrane is the most hydrophobic. A further explanation for the high adsorption on this membrane is that neodol can fold its chains and can penetrate and adsorb in the large pores of NFPE10. Although NTR7450 has the same hydrophobicity as NFPE10, neodol adsorbs less on NTR7450 due to the lower cut-off of this membrane. The most hydrophilic membrane NF270 has the lowest adsorption for neodol. Similar conclusions were taken by Cornelis *et al.* (2005) and Doulia *et al.* (1997).

In contrast to neodol, electrostatic interactions play an important role in the adsorption of SDBS and cetrime. SDBS adsorbs significantly less than cetrime and neodol on all membranes, due to repulsive interactions between this anionic surfactant and the negatively charged membranes. Electrostatic attractions between cetrime and the membranes cause a very high adsorption. These electrostatic attractions are even stronger than the hydrophobic interactions of neodol, as indicated by the higher amount of adsorption of cetrime on all membranes (Table 6.1).

A comparison between the different membranes shows that NF270, NFPE10 and NTR7450 have the most adsorption for cetrime. This was explained by the largely negative surface charge, in the case of NF270 and NTR7450. The high adsorption of cetrime on the hydrophobic membrane NFPE10 indicates that in addition to electrostatic interactions, hydrophobic interactions are also important.

After the adsorption experiments, the hydrophobicity of the membrane surface was determined again to study the orientation of the adsorbed surfactants on the membranes. The contact angles before and after adsorption are given in Table 6.2. Since it is known in literature (Jönsson and Jönsson, 1991) that surfactants can adsorb either by their hydrophobic tails or by their hydrophilic charged heads, the top layer of the membrane may become more hydrophilic or hydrophobic.

Table 6.2: Contact angles (°) of the different membranes before and after surfactant adsorption (feed concentration = 600 mg L⁻¹, neutral pH, without salt addition)

	NF270	Desal51HL	NTR7450	NFPES10
pure water	27	47	70	72
neodol	29	36	57	78
SDBS	29	35	65	77
cetrimide	33	40	71	60

Table 6.2 indicates that the membrane surface of Desal51HL and NTR7450 becomes more hydrophilic after adsorption of SDBS and neodol, in spite of the low adsorption of the former. The increase in hydrophilicity after adsorption of neodol and SDBS was explained by hydrophobic and electrostatic repulsive interactions with the membrane surface, respectively. This implies that the hydrophobic tails of the surfactants are oriented towards the membrane surface and that the hydrophilic (charged in the case of SDBS) heads are oriented towards the aqueous phase, resulting in a more hydrophilic membrane surface (Figure 6.1).

However, both for neodol and SDBS, the top layer of NFPES10 becomes more hydrophobic after adsorption. A possible explanation for this could be that neodol positions itself parallel with the membrane surface (as was also suggested by Jönsson and Jönsson (1991)), so that maximal interactions between the hydrophobic tails and the hydrophobic membrane surface could take place (Figure 6.1). The same phenomenon also occurs for SDBS, due to the high hydrophobicity of NFPES10 on the one hand and to the small negative surface charge on the other hand. Due to the very low adsorption of neodol and SDBS on NF270 (Table 6.1), no significant difference in contact angle (Student *t* test) was observed.

For cetrimide, one would expect that the hydrophilic positively charged heads of this surfactant would orient to the negative membrane surface, resulting in a more hydrophobic surface. However, Table 6.2 indicates that the membrane surface of Desal51HL and NFPES10 becomes more hydrophilic when exposed to a solution

of cetrimide. This can be explained by the concept of hemimicelle formation. As described by Paria and Khilar (2004), Childress and Elimelech (1996) and Somasundaran and Fuerstenau (1966), hemimicelles are two-dimensional aggregates that form at the solid-solution interface above the critical hemimicelle concentration (lower than CMC). They are a result of surfactant ions associating with each other to remove their hydrocarbon chains from the bulk water and, hence, to reduce the free energy of the system.

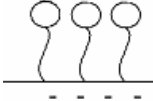
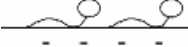
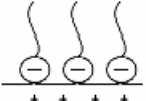
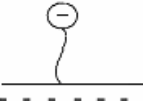
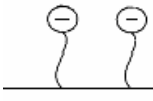

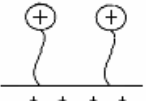
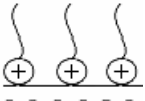
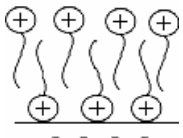
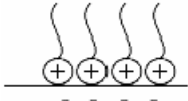
	pH 3	pH 6		pH 10
neodol		Desal51HL, NTR7450	NFPES10	
				
SDBS		Desal51HL, NTR7450	NFPES10	
				
cetrimide		Desal51HL, NFPES10	NF270	
				

Figure 6.1: Proposed scheme of the orientation of neodol, SDBS and cetrimide on the membrane top layer at different pH

The formation of these hemimicelles for cationic surfactants on negatively charged surfaces was already visualized in literature using AFM imaging (Nishimura *et al.*, 1995; Radmacher *et al.*, 1994). Because the surfactant concentration used in the

present case (600 mg L^{-1}) is high enough (Childress and Elimelech (1996) proposed the mechanism of hemimicelle formation already at a concentration of only 35 mg L^{-1}), hemimicelle formation could explain the increased hydrophilicity of the membrane surface after adsorption of cetrimide (Figure 6.1).

Only for NF270 a more hydrophobic surface was obtained after adsorption of cetrimide. This could mean that hemimicelle formation does not occur in this case because of the largely negative surface charge, which pulls all positively charged heads to the top layer of NF270. For NTR7450, hemimicelle formation (resulting in a more hydrophilic surface) and the strong attraction between cetrimide and the negative surface (resulting in a more hydrophobic surface) counteract, so that no significant difference in contact angle was observed.

6.2.2.2 Effect of the type of surfactant on fouling and retention

Relative fluxes and surfactant retentions obtained after two hours of filtration of a 40 mg L^{-1} feed solution of neodol, SDBS or cetrimide are given in Table 6.3.

Table 6.3: Relative flux (a, in %) and surfactant retention (b, in %) after filtration of a solution of 40 mg L^{-1} of neodol, SDBS or cetrimide (neutral pH, without salt addition)

	NF270	Desal51HL	NTR7450	NFPES10
neodol	88	86	30	55
SDBS	95	87	91	62
cetrimide	68	89	1	81

(a)

	NF270	Desal51HL	NTR7450	NFPES10
neodol	86	84	41	23
SDBS	100	98	97	91
cetrimide	89	97	17	21

(b)

For neodol, the lowest relative fluxes were observed for the hydrophobic membranes NTR7450 and NFPES10. NTR7450 has the lowest relative flux in

comparison with NFPE10, in spite of the lower adsorption and the smaller contact angle after adsorption for NTR7450. The very low relative flux for NTR7450 can, however, be explained by the fact that the cut-off of NTR7450 (310 Da) is of the same order of magnitude as neodol (387 Da), which results in a strong pore blocking effect during filtration. This was also observed by Cornelis *et al.* (2005) and Van der Bruggen *et al.* (2002). The relative flux of Desal51HL and NF270 during filtration of neodol is high and comparable, as both membranes have a hydrophilic top layer and a low cut-off, through which adsorption in the pores is minimized. The low cut-off of Desal51HL and NF270 also causes a very high retention of neodol (Table 6.3b). The lowest retention is observed for NFPE10, the membrane with the highest cut-off.

It can be concluded that for neodol, only the hydrophobicity and the cut-off of the membrane are important to explain flux decline and retention. However, when filtering ionic surfactants, electrostatic interactions with the membrane surface and hence the membrane surface charge are important to understand the membrane performance. A comparison between the relative flux of neodol and SDBS (Table 6.3a) indeed indicates that less flux decline is observed for SDBS. Due to these electrostatic repulsive interactions, SDBS is also retained more than neodol for all membranes (Table 6.3b).

During filtration of SDBS, the lowest relative flux is observed for NFPE10, which can be explained by a combination of several phenomena. Firstly, NFPE10 has the smallest surface charge at neutral pH. The repulsion forces between the membrane surface and SDBS are hence very small, as a result of which the surfactants can easily block the membrane pores. Secondly, the top layer of NFPE10 is very hydrophobic and even becomes more hydrophobic after adsorption (Table 6.2), which is favourable for hydrophobic interactions to occur. Adsorption also occurs in the pores of NFPE10 during filtration due to the high cut-off.

The relative flux of Desal51HL when filtering SDBS is higher than for NFPE10, but lower than for NTR7450 and NF270. The former was explained by the larger

surface charge, the lower cut-off and the smaller contact angle for Desal51HL in comparison with NFPES10.

The highest relative flux for SDBS is observed for the two membranes with the largest surface charge at neutral pH: NTR7450 and NF270. Although both membranes have the same surface charge and hence the same strong repulsion forces, there is a small difference between the relative flux of NTR7450 and NF270, as NTR7450 has a lower relative flux. This was explained by the higher cut-off (more pore blocking) and the larger contact angle of NTR7450 after adsorption (more hydrophobic interactions). Just as with neodol, the lowest retention for SDBS was observed for NFPES10 (high cut-off and small surface charge). The other three membranes show a very high and similar retention for SDBS.

Electrostatic attractive interactions become relevant when filtering an aqueous solution of cetrimide. Table 6.3a indicates that complete pore blocking occurs for NTR7450 (relative flux only 1 %). This was explained by two effects. Firstly, the molecular mass of cetrimide is close to the cut-off of NTR7450 (cf. neodol), so that a large influence on the permeate flux was expected. Secondly, because of the large surface charge of NTR7450, large electrostatic attraction forces occur between the membrane surface and the surfactant resulting in a high amount of adsorption (Table 6.1). Although NF270 has the same surface charge as NTR7450, a higher relative flux is observed for NF270 due to the lower cut-off (less pore blocking).

The highest relative fluxes for cetrimide were observed for the membranes with the smallest surface charge at neutral pH: Desal51HL and NFPES10. The higher relative flux for Desal51HL in comparison with NFPES10 follows from the higher hydrophilicity (before and after adsorption, Table 6.2) and from the lower adsorption (Table 6.1).

Table 6.3b shows that the retentions of cetrimide are the lowest for NFPES10 and NTR7450, due to the high cut-off (especially for NFPES10) and to the attraction between the negative surface and the cationic cetrimide (especially for NTR7450). In spite of the large surface charge, NF270 still has a relatively high retention for

cetrimide because of the low cut-off. Desal51HL with a low cut-off and a small membrane surface charge at neutral pH, has the highest retention for cetrimide.

It can be concluded that the type of surfactant has an important influence on adsorption and hence on membrane flux decline. Neodol shows the lowest relative fluxes for the most hydrophobic membranes (NTR7450 and NFPE10), while the membranes with the largest surface charge (NTR7450 and NF270) foul the most and the least when filtering cetrimide and SDBS, respectively. Pore blocking plays a secondary role.

6.2.3 Effect of the surfactant concentration

Filtration experiments were performed with aqueous solutions containing different concentrations of surfactant in the range of 20 mg L⁻¹ to 70 mg L⁻¹. These concentrations were selected on the basis of the composition of wastewater in the carwash industry (Stubbe, 2006). It should also be noticed that the concentration range of neodol, SDBS and cetrimide is below the critical micelle concentration (CMC, Table 2.6), so that the presence of micelles could be neglected.

The surfactant concentration has an influence on membrane flux decline. Because adsorption generally increases with increasing concentration and because of the relation between adsorption and relative flux (section 6.2.2), the relative flux decreases with increasing surfactant concentration. In literature, this was also reported by Kavitskaya (2005) and Van der Bruggen *et al.* (2002). This is given in Figure 6.2a for the hydrophilic membrane Desal51HL after filtering neodol, SDBS and cetrimide. The results for the other membranes (not given) were comparable.

The influence of increasing concentration on the retention is given in Figure 6.2b for NFPE10 (a hydrophobic membrane with a high cut-off); the results for the other membranes were comparable. Taking into account the 10 % error on the retention (due to the complex chemical analysis of the surfactants), it was concluded that the retention of SDBS and cetrimide does not change significantly and that the retention of the nonionic surfactant neodol decreases with increasing

concentration, as is already stated in general in literature (Bellona *et al.*, 2004) for uncharged organic components.

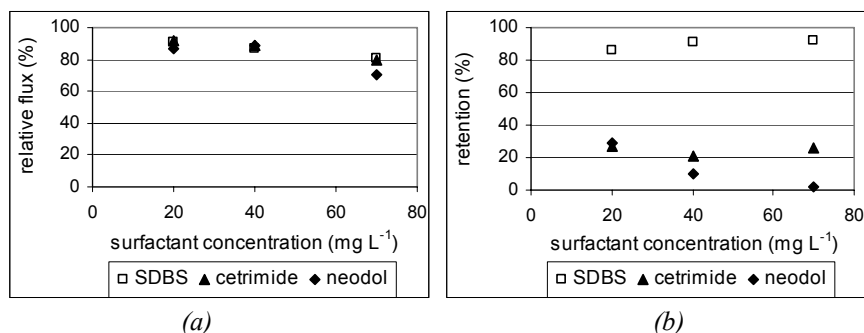


Figure 6.2: Influence of the surfactant concentration on (a) the relative flux (%) (shown for Desal51HL) and on (b) the surfactant retention (shown for NFPE10) (neutral pH, without salt addition)

6.2.4 Effect of the addition of salt

Salts can be present in the wastewater of the carwash industry, especially during wintertime. The influence of salts in wastewater was simulated by adding NaCl to the 40 mg L⁻¹ solutions of neodol, SDBS and cetrimide. The presence of sodium chloride changes both the membrane and the surfactant characteristics. For the surfactants, a decrease in electrostatic repulsions between the charged heads allows to form micelles at lower concentrations, as indicated by the lower CMC of SDBS and cetrimide in Table 2.6.

6.2.4.1 Effect of the addition of salt on adsorption and hydrophobicity

Table 6.4 compares the results of the membranes NF270, Desal51HL and NFPE10 for the static adsorption experiments and the hydrophobicity after adsorption of a surfactant solution with and without 0.1 M NaCl. These experiments were not performed with NTR7450, due to problems with availability of this membrane.

For the nonionic surfactant neodol, no influence of NaCl is expected. However, Table 6.4 indicates that the adsorption of neodol increases. This is explained in literature (Doulia *et al.*, 1997) by an increased hydrophobicity of nonionic

surfactants in the presence of salts. As it is commonly (Braeken *et al.*, 2005c) accepted that more adsorption occurs for more hydrophobic components, adsorption of neodol in the presence of salt can be larger.

Table 6.4: Adsorbed amount (q , in mmol m^{-2}) and contact angle (θ , in $^\circ$) for NF270, Desal51HL and NFPES10 after exposure to a feed solution of 600 mg L^{-1} of neodol, SDBS and cetrimide with and without 0.1 M NaCl (at pH 6)

	NF270		Desal51HL		NFPES10	
	q	θ	q	θ	q	θ
neodol	0.7	29	7.4	36	14.0	78
neodol 0.1 M NaCl	3.0	28	6.6	36	18.5	76
SDBS	0.0	29	1.5	35	2.6	77
SDBS 0.1 M NaCl	0.0	24	0.6	34	0.0	73
cetrimide	23.0	33	14.0	40	19.1	60
cetrimide 0.1 M NaCl	8.0	41	8.8	29	5.8	59

It is also mentioned in literature (Paria and Khilar, 2004) that, for ionic surfactants after addition of an electrolyte, adsorption increases or decreases depending on whether the charge of the membrane surface is equal or opposite to that of the surfactant. Table 6.4 indeed indicates that for cetrimide, the adsorption decreases in the presence of NaCl, while for SDBS the adsorption remains very low and constant. In spite of the constant adsorption of SDBS, the membrane surfaces become more hydrophilic. This was explained by the weaker repulsion forces between the heads of the surfactants, which allows a better packing of the surfactants on the membrane, resulting in a more hydrophilic surface (Figure 6.1).

Also for cetrimide, the membrane surfaces (with exception of NF270) become more hydrophilic. This was explained by the presence of salt, as not only the attraction forces between the surfactants and the membrane surface (which resulted in a lower amount of adsorption), but also the repulsion forces between the charged heads of the surfactants decrease. In the case of Desal51HL and NFPES10, hydrophobic interactions between the tails of the surfactants become more

important in the formed hemimicelles (Figure 6.1), so that more hydrophilic heads of cetrimide orient towards the aqueous phase, resulting in a more hydrophilic membrane surface (in comparison with cetrimide without salt addition).

The absence of hemimicelles in the case of NF270 (section 6.2.2.1) causes the decreased amount of surfactants on the surface (as indicated by the lower adsorption) to orient more parallel to the membrane surface giving rise to a more hydrophobic surface. This phenomenon can be compared with the adsorption of neodol and SDBS on NFPE10 at neutral pH (Figure 6.1).

6.2.4.2 Effect of the addition of salt on fouling and retention

The influence of the salt concentration on the relative flux for Desal51HL (after correcting for the osmotic pressure) and on the surfactant retention for NFPE10 is given in Figure 6.3. The results for the other membranes were comparable.

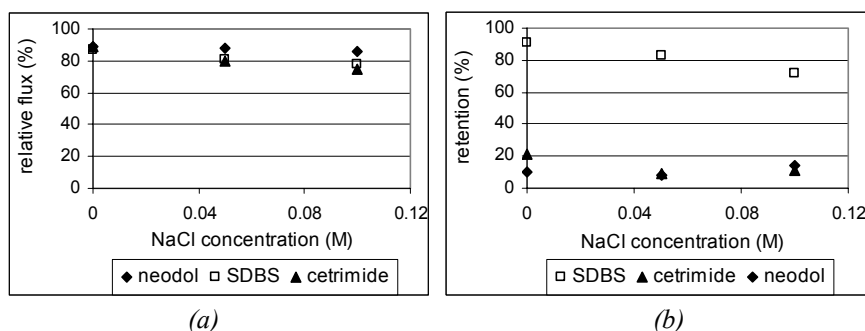


Figure 6.3: Influence of the salt concentration on (a) the relative flux (%) (shown for Desal51HL) and on (b) the surfactant retention (shown for NFPE10) (neutral pH, feed concentration = 40 mg L⁻¹)

For the nonionic surfactant neodol, no significant difference in relative flux or surfactant retention is observed by adding salt to the surfactant solution, in correspondence with Archer *et al.* (1999).

Both for SDBS and cetrimide, the relative flux and the surfactant retention decrease with increasing salt concentration. For SDBS, the decreased repulsion forces between the membrane and the surfactant in the presence of NaCl allow a better packing of the surfactants on the membrane surface and in the membrane pores, resulting in more pore blocking and hence in more flux decline. For

cetrimide, the relative flux also decreases because of the weaker electrostatic attraction forces, in spite of the lower adsorption and the increase in hydrophilicity in the presence of NaCl (Table 6.4).

6.2.5 Effect of pH of the surfactant solution

Several surfactants are used in the carwash industry, some of which are very alkaline or acid, which makes that the pH of the wastewater can deviate from neutral pH. A lower or a higher pH influences strongly the membrane performance, as the membrane surface charge and hence the electrostatic interactions are dependent on pH.

To characterize these influences, experiments were performed with 40 mg L⁻¹ solutions of SDBS and cetrimide at different pH. The presence of a sulfonic group ($-SO_3^-$) in SDBS and an ammonium group ($-N^+R_3$) in cetrimide (Appendix II) causes the charge of these surfactants to be pH independent.

6.2.5.1 Effect of pH of the surfactant solution on adsorption and hydrophobicity

The adsorbed amounts and the contact angles after adsorption of SDBS and cetrimide at different pH are given in Table 6.5 for NF270, Desal51HL, NTR7450 and NFPES10. For reference, the contact angles at different pH of the unfouled membranes were also included (Table 5.2). No pH effect on the contact angle of the unfouled membrane NF270 is observed. The hydrophilicity increases at pH 10 and pH 3 for Desal51HL and NTR7450, respectively, while NFPES10 becomes more hydrophilic both at pH 10 and at pH 3. These results are needed as reference to compare with the contact angles at different pH after adsorption of SDBS and cetrimide.

Table 6.5 indicates that adsorption of SDBS decreases and that the hydrophilicity of the membrane surface increases with increasing pH. This was explained by electrostatic attraction forces between the positive membrane surface and SDBS at low pH and by electrostatic repulsion forces between the negative membrane surface and SDBS at high pH (Figure 6.1).

Table 6.5: Adsorbed amount (q , in mmol m^{-2}) and contact angle (θ , in $^\circ$) after exposure to a feed solution of 600 mg L^{-1} of SDBS and cetrimide at different pH (without salt addition). For reference, the contact angles at different pH of the unfouled membranes are also included.

		NF270		Desal51HL		NTR7450		NFPES10	
		q	θ	q	θ	q	θ	q	θ
unfouled	pH 3	-	29	-	46	-	66	-	69
	pH 6	-	27	-	47	-	70	-	72
	pH 10	-	30	-	35	-	71	-	66
SDBS	pH 3	4.1	55	2.9	54	3.4	72	3.3	77
	pH 6	0.0	29	1.5	35	2.6	65	2.6	77
	pH 10	0.0	25	0.0	33	0.5	47	0.8	62
cetrimide	pH 3	6.6	32	2.7	27	0.4	62	0.2	58
	pH 6	23.0	33	14.0	40	17.7	71	19.1	60
	pH 10	13.9	58	15.6	49	3.8	69	13.3	63

The opposite trend was expected for the positively charged surfactant cetrimide. At low pH, electrostatic repulsion forces result in less adsorption and a more hydrophilic surface, as given in Table 6.5. It is expected that at high pH, when the membrane surface charge is very large, electrostatic attraction forces cause the adsorption to increase. However, Table 6.5 indicates that the adsorption decreases from pH 6 to pH 10. This was explained by the fact that the formation of hemimicelles is hindered (Figure 6.1). The positive surfactants are so strongly attracted to the membrane surface at pH 10 that no second layer was formed. The increase in hydrophobicity from pH 6 to pH 10 seems to support this hypothesis. The same phenomenon of hindered hemimicelle formation and increased hydrophobicity was also observed for NF270 at neutral pH (section 6.2.2.1).

However, it should be kept in mind that the presented hypotheses are based only on contact angle measurements, which are in the context of this chapter useful to get a first idea of the orientation of the surfactants. To verify the presented mechanisms, another technique (like for example AFM) should be selected.

A comparison between the contact angles of the unfouled and fouled membranes indicates that the behavior of the contact angle in the presence of a surfactant is different from the behavior of the contact angle as a function of the pH of the unfouled membranes. This implies that the observed changes in contact angles are not the result of the intrinsic effect of pH on hydrophobicity.

6.2.5.2 Effect of pH of the surfactant solution on fouling and retention

The relative fluxes and the surfactant retentions after two hours filtering of a 40 mg L^{-1} solution of SDBS and cetrimide at different pH are given in Figure 6.4 for Desal51HL and NFPE10. The results for the other membranes were comparable. In the absence of surfactants (Table 5.2), the relative flux stays close to 100 % with varying pH. Only for NTR7450 and NFPE10 at pH 3, a lower relative flux of 59 % was observed. As these lower relative fluxes at pH 3 were not observed for neither SDBS nor cetrimide, it was concluded that the measured changes in the relative fluxes are a result of surfactant interactions with the membranes.

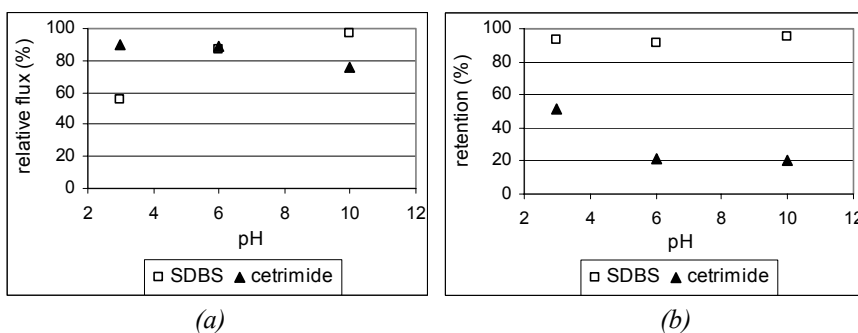


Figure 6.4: Influence of pH on (a) the relative flux (%) (shown for Desal51HL) and on (b) the surfactant retention (%) (shown for NFPE10) (feed concentration = 40 mg L^{-1} , without salt addition)

Considering SDBS, the relative flux increases with increasing pH due to the decrease in adsorption and the increased hydrophilicity (Table 6.5). Figure 6.4a shows the opposite trend for cetrimide. The decrease in flux from pH 3 to pH 6 was explained by the higher amount of adsorption and the more hydrophobic membrane surface at pH 6. However, from pH 6 to pH 10, two opposite effects

occur: a decrease in adsorption and an increase in hydrophobicity. It seems that the second effect is the most important one, as the flux decreases from pH 6 to pH 10.

In spite of the different types of electrostatic forces between the membrane surface and SDBS, the retention of SDBS does not change significantly with pH. SDBS is retained very well, independently of the pH of the feed solution. For cetrimide, Figure 6.4b indicates that the retention decreases slightly with pH due to the strong electrostatic attraction forces between this surfactant and the membrane surface at high pH.

6.2.6 Effect of a mixture of surfactants

During the washing process in a carwash, different types of surfactants are used, which all are mixed into the wastewater. Furthermore, in a carwash, groundwater or tap water is used instead of distilled water. To study the effect of a mixture of surfactants and the effect of tap water on the performance of nanofiltration, filtration experiments with two different mixtures were performed. Mixture 1 contains 20 mg L⁻¹ neodol, 20 mg L⁻¹ SDBS and 20 mg L⁻¹ cetrimide dissolved in distilled water, mixture 2 contains the same components dissolved in tap water (with a hardness of 41 °F). Filtration experiments were done for the hydrophilic membrane NF270 and the hydrophobic membrane NFPE10, of which the results are given in Table 6.6.

Table 6.6: Relative flux (%) and retention (%) for NFPE10 and NF270 after filtering a mixture of surfactants in distilled water (mixture 1) and in tap water (mixture 2) (feed concentration = 20 mg L⁻¹ of each surfactant, neutral pH, without salt addition)

		relative flux (%)	retention (%)		
			neodol	SDBS	cetrimide
mixture 1	NFPE10	1	79	-	-
	NF270	8	95	73	98
mixture 2	NFPE10	2	65	-	79
	NF270	26	93	80	94

-: analysis not possible due to small permeate volume

Comparing the relative fluxes in Table 6.6 with the ones in Table 6.3a shows that (much) more flux decline occurs when filtering a mixture, due to several reasons. Firstly, the total concentration of surfactant is higher in the mixture, which results in a lower relative flux as described in section 6.2.3. Secondly, not only interactions between the membrane and the surfactants, but also between the different surfactants occur resulting in more pore blocking and hence in more flux decline. For example, the presence of both SDBS and cetrimide in the mixture results in a neutralisation effect in the form of (visible) flakes, which can block the pores severely. From Table 6.6, it becomes also visible that mixture 2 (in tap water) fouls less than mixture 1 (in distilled water).

Comparing the retentions in Table 6.6 with the ones in Table 6.3b indicates that the retention of a surfactant is dependent on the presence of other surfactants: the retention of SDBS is lower, while the retention of cetrimide and neodol is higher in the mixture than in the one-component-solution. The difference in retention of SDBS and cetrimide was explained by the interactions between these two surfactants. As SDBS and cetrimide carry an opposite charge, they are associated in the mixture. Due to this connection, SDBS is pulled through the negative membrane by cetrimide (resulting in a lower retention of SDBS), while cetrimide is hindered to pass through the membrane by the negative SDBS (resulting in a higher retention of cetrimide). The higher retention of neodol in the mixtures can be explained by the presence of the other surfactants, which block the pores already so much, that neodol has more difficulties to pass through the membrane. However, this higher retention should be interpreted taking into account the analytical overestimation of the concentration of neodol in mixtures (section 2.6.1.3).

6.2.7 Conclusion

Surfactant solutions cause flux decline of nanofiltration membranes, but this flux decline depends strongly on the type of surfactant and feed conditions. To reduce membrane flux decline to a minimum, adsorption of the surfactant has to be

minimized and the surfactants should orient in such a way that the membrane surface becomes more hydrophilic (Figure 6.1).

The least flux decline is observed for SDBS. At neutral pH, cetrimide fouls the membranes the most because of the opposite charge of membrane and surfactant. Furthermore, the surfactant concentration plays a crucial role, as the membrane performance decreases with increasing concentration. The presence of electrolytes also has a negative influence on the membrane performance. Changing the pH can have both a positive as well as a negative influence on the relative flux depending on the surfactant type: for cetrimide the least flux decline is observed at low pH, while a high pH is favourable for SDBS.

6.3 Applicability of nanofiltration in the carwash industry

6.3.1 Description of the selected carwash

To study the applicability of nanofiltration in the carwash industry, a typical carwash was selected. This carwash, situated in Leuven (Belgium) with a capacity of 36,000 cars a year, is an automatic carwash, in which the car is pulled through the washing installation.

6.3.1.1 Use of surfactants

Different surfactants are used depending on the washing program and on the stage in the washing process. The anionic surfactant Turtle Wax HP11 is used in several stages during the washing of the car: in a low concentration for the initial manual soaping of the car, in a higher concentration when the car is hosed with the high-pressure spraying pistol before entering the washing installation and finally in a very high concentration in the washing brushes.

A rim cleaner is used to hose the rims, before entering the washing installation. Depending on the washing program, an alkaline rim cleaner from Rumler (cheap washing program) or an acid rim cleaner (more expensive washing program) is employed.

The Turtle Wax HP20/21/22 or Triple Shine is also an optional surfactant, which is applied by the washing brushes and provides extra glow.

At the end of the washing program, the wax is provided to the car. Depending on the washing program, a cheap wax (Turtle Wax HP19 Poly Glaze) or an expensive wax (Cherry Polish) can be chosen. Both waxes are dissolved in ultrapure water to avoid dirty spots on the car. In the carwash, ultrapure water was obtained by the use of ion exchange. This technique was preferred to reverse osmosis, because of the low amount of deionised water needed.

From these surfactants, the Turtle Wax HP11, the rim cleaner from Rumler and the Triple Shine occur in the highest concentrations in the wastewater. Besides the filtration of the wastewater, pure solutions of these three surfactants were filtered to study their individual effect on membrane fouling.

6.3.1.2 Actual wastewater purification installation

A schematic presentation of the actual wastewater purification installation for the selected carwash is given in Figure 6.5.

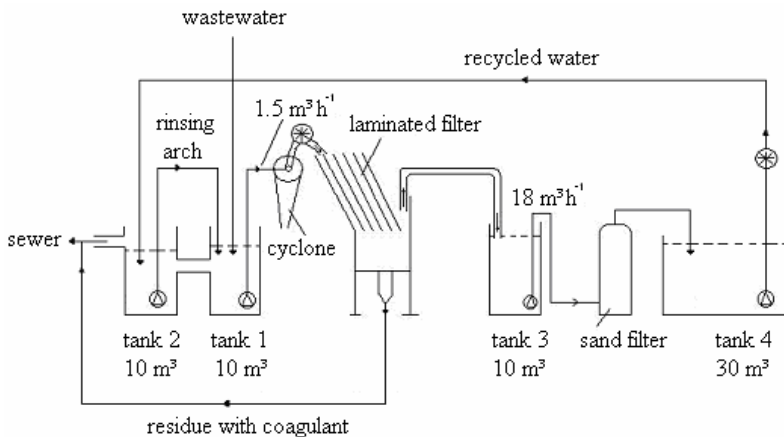


Figure 6.5: Actual wastewater purification installation of the carwash

The wastewater flows, together with the circulation water from the rinsing arch, to the first tank of 10 m³. A flow of 1.5 m³ h⁻¹ water leaves this tank to the purification installation, which is composed of a cyclone, a laminated filter and a sand filter. To obtain a good sedimentation in the laminated filter, a coagulant

(Sachtofloc, Brenntag, Germany) is added. The residue from the laminated filter together with the coagulant arrive finally in the sewer. After the laminated filter, the water is collected in tank 3, from which the water is pumped to the sand filter. This sand filter removes sand particles, as they are abrasive resulting in undesired scratches on the cars. After the sand filter, water is collected in tank 4, from which the recycled water is pumped to tank 2. Tank 2 also receives the overflow of tank 1; the overflow of tank 2 on its turn arrives in the sewer. From tank 2, water is pumped with a flow of $15 \text{ m}^3 \text{ h}^{-1}$ to the rinsing arch, after which the circulation water flows back in tank 1.

The recycled water is currently only used to rinse the cars in the rinsing arch after the washing process. This means that 160 L fresh water is still needed for one car. To obtain this fresh water, the carwash uses groundwater. As the use of groundwater will become more and more restricted in the future, the carwash is searching for solutions to diminish the amount of groundwater needed. One solution is to use the recycled water not only during the rinsing, but also during the washing of the cars. Additional water purification is therefore needed, which can possibly be obtained by nanofiltration.

6.3.2 Analysis of the wastewaters

Wastewater was collected on several days (March, 2006) on two different places in the water purification: after the cyclone and after the sand filter (Figure 6.5). The analysis results for these wastewaters and for the three surfactants, that occur in the highest concentrations in the wastewater (Turtle Wax HP11, Triple Shine and the rim cleaner from Rumler) are given in Table 6.7, together with the Flemish standards.

It was seen that the wastewater composition varies with time over one week: on Monday, the wastewater was most fouled, while the least fouling was observed on Friday. The fouling degree of the wastewater was related to the number of cars washed on the respective days (35 cars on Friday versus 135 cars on Monday).

Regeneration of carwash wastewater by nanofiltration

Table 6.7: Analysis results for the wastewaters, collected on several days after the cyclone (C) and after the sand filter (SF), and for the three surfactants, that occur in the highest concentrations in the wastewater (Turtle Wax HP11, Triple Shine, rim cleaner from Rumler) together with the Flemish standards

	Flemish standards	Monday		Saturday		Friday		HP11	Triple Shine	rim cleaner
		C	SF	C	SF	C	SF			
suspended solids (mg L ⁻¹)	< 60 mg L ⁻¹	136	140	94	126	78	60	0	0	0
settleable solids (mL L ⁻¹)	< 0.5 mL L ⁻¹	3.5	3.5	6.0	5.5	1.0	1.0	0	0	0
COD (mg O ₂ L ⁻¹)	< 125 mg O ₂ L ⁻¹	296	382	351	347	248	208	2,720	4,760	51,000
BOD ₅ ²⁰ (mg O ₂ L ⁻¹)	< 25 mg O ₂ L ⁻¹	109	140	95	102	75	63	513	898	9,620
pH	6.5 < pH < 9	7.6	7.6	7.5	7.6	7.6	7.5	7.5	7.7	12.7
conductivity (mS cm ⁻¹)	< 1 mS cm ⁻¹	1.1	1.1	1.0	1.0	0.8	0.8	0.7	1.0	28.6
nonionic surfactants (ppm)	sum < 3 ppm	50	51	37	39	29	32	27	450	13,000
anionic surfactants (ppm)		2.3	2.5	0.7	0.8	0.8	0.7	42.6	9.9	0.1
cationic surfactants (ppm)		4.0	3.7	4.2	4.3	-	1.7	0.2	531	90

However, no influence of the sand filter on the composition of the wastewater was observed, as the wastewaters after the cyclone and after the sand filter are almost similar. This was attributed to the current uncontrolled dosage of the coagulant in the laminated filter (Figure 6.5), which makes that suspended and settleable solids are still present after the sand filter. As these solids have a negative influence on the membrane performance, the wastewater was firstly filtered with a cellulose filter (MN 713 ¼, Macherey-Nagel, Germany) before nanofiltration, to minimize the suspended and the settleable solids in the feed solution. There was no influence of the cellulose filter on the other wastewater characteristics.

Both the COD and the BOD are too high to discharge the wastewater in surface water. The ratio between COD and BOD is on average 3.3, which is only slightly higher than for domestic wastewater (COD/BOD = 2.5). The pH of the wastewaters is almost neutral and lies within the acceptable region. A comparison with the conductivity of tap water (0.75 mS cm^{-1}) indicates that the conductivity of the wastewaters is only slightly higher. The lower conductivity on Friday was explained by the higher night temperatures, as a result of which less salt was present on the roads and hence on the cars.

For the interpretation of the surfactant concentrations, the discussion about the analysis methods should be taken into account (section 2.6.1.3 and Table 2.7). This means that the concentration of nonionic surfactants in the wastewater is overestimated (due to the presence of cationic surfactants) and that the low concentrations of anionic and cationic surfactants were explained by the fact that these two surfactants form neutral complexes with each other (which cannot be determined by the analysis methods).

For the three surfactants that occur in the highest concentrations in the wastewater, a remarkably high value of COD and BOD was noticed, especially for the strongly alkaline rim cleaner. This rim cleaner also has a very high conductivity and an extremely high concentration of nonionic surfactants. Table 6.7 indicates that the surfactant HP11 is mainly composed of anionic surfactants, which corresponds

with the information given by the manufacturer (HP11 is composed for 75 – 95 % of the anionic surfactant sodium olefin sulfonate). The highest concentrations of nonionic and cationic surfactant are observed for Triple Shine, as this surfactant is mentioned (by the manufacturer) to be composed of quaternary ammonium components and lauramide oxide (and various other components).

6.3.3 Filtration experiments of the different wastewaters

Filtration experiments during a period of 9 hours were performed with the membranes NF270 and NFPE10 (Table 4.3) for the wastewaters after the cyclone and after the sand filter. This time span was chosen to simulate the operation of a nanofiltration membrane during a whole day in the carwash. Both the relative fluxes and the retentions were stable after 9 hours filtration: the relative fluxes stayed almost constant after 6 hours filtration (Figure 6.6), while the retentions were already stable after one hour filtration. This knowledge was used when filtering the three surfactants, which occur in the highest concentrations in the wastewater, as these filtration experiments were ended after 6 hours filtration.

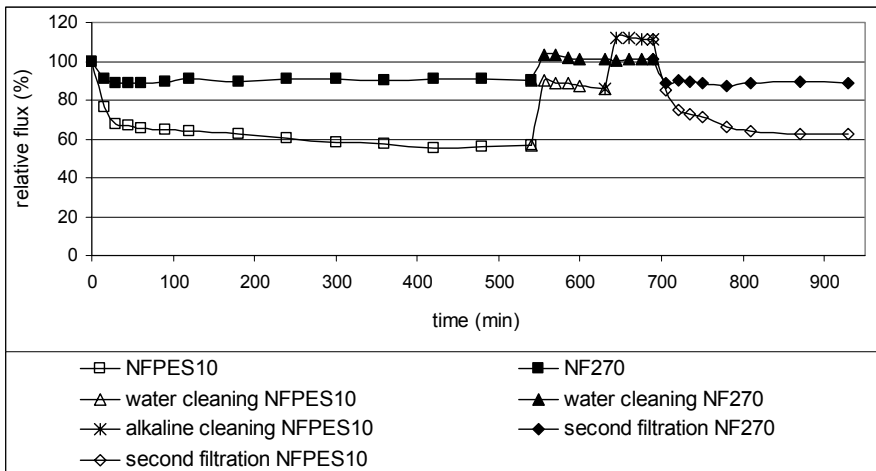


Figure 6.6: Evolution of relative flux (%) for the membranes NF270 and NFPE10 during filtration of the wastewater after the sand filter on Friday, during cleaning with water and with alkaline products (only for NFPE10) and during the second filtration with the same wastewater

6.3.3.1 Fouling results during filtration of carwash wastewater

The relative fluxes are given in Table 6.8. The relative fluxes after cleaning will be discussed in section 6.3.4; the wastewater taken after the sand filter on Friday (*SF (2)*) is filtered a second time after the membrane cleaning, as will also be discussed in section 6.3.4. These relative fluxes were already corrected for the osmotic pressure (retention of conductivity was 25 % for NFPE10 and 75 % for NF270).

Table 6.8: Relative flux (%) for the membranes NF270 and NFPE10 after filtering the wastewater (both after the cyclone (C) and after the sand filter (SF)), after filtering Turtle Wax HP11, Triple Shine and the rim cleaner from Rumler, and after cleaning

		NF270		NFPE10		
		after filtration	after water cleaning	after filtration	after water cleaning	after alkaline cleaning
Monday	<i>C</i>	92	99	34	57	78
	<i>SF</i>	84	95	49	71	115
Saturday	<i>C</i>	89	100	56	93	111
	<i>SF</i>	87	105	57	83	115
Friday	<i>SF</i>	90	101	56	86	111
	<i>SF (2)</i>	91	-	63	-	-
HP11		90	121	61	124	-
Triple Shine		92	105	27	76	106
rim cleaner		51	134	56	35	86

Table 6.8 indicates that the relative flux of NFPE10 is lower than the relative flux of NF270. This was explained by the fact that NFPE10 has a more hydrophobic top layer and a higher cut-off. For the filtration experiments on Monday, when the wastewater was the most fouled (Table 6.7), lower relative fluxes were observed for NFPE10. The absolute permeate fluxes were comparable for both membranes (around 50 L m⁻² h⁻¹).

For the relative fluxes for HP11, Triple Shine and the rim cleaner, the highest relative fluxes were found when filtering HP11, since HP11 is mainly composed of anionic surfactants. As the pH of the wastewater is situated around 7.5, electrostatic repulsion forces occur between the membrane surface and the anionic surfactants, resulting in less pore blocking and less flux decline (section 6.2.2.2). Another reason for the higher relative flux of HP11 in comparison with the other two surfactants (Triple Shine and the rim cleaner), is the lower total concentration of surfactants in the wastewater, as it is known that the relative fluxes decrease with increasing surfactant concentration (section 6.2.3).

The hydrophilic membrane NF270 is less sensitive to flux decline from Triple Shine than NFPE10. This was explained by the fact that Triple Shine is composed of very hydrophobic components (information given by the manufacturer), which mainly cause strong flux decline on hydrophobic membranes, in this case on NFPE10 (section 5.2.1).

The lowest relative fluxes were found for both NFPE10 and NF270, when filtering the rim cleaner from Rumler. Hypothetical explanations are the high concentration of nonionic and cationic surfactants, the large amount of organic components (as indicated by the large value of COD and BOD) and the high conductivity of this wastewater (Table 6.7). All these parameters give rise to a low relative flux, as discussed in section 6.2. As this alkaline rim cleaner has the most negative influence on membrane flux decline, it should be avoided during the washing process and be replaced by another (less fouling) rim cleaner.

6.3.3.2 Retention results during filtration of carwash wastewater

The retentions of surfactants and COD at the end of the filtration are given in Table 6.9; the wastewater taken after the sand filter on Friday (*SF (2)*) is filtered a second time after the membrane cleaning, as will be discussed in section 6.3.4. The highest retentions were observed for NF270, consistent with the fact that this membrane has the lowest cut-off. The anionic surfactants are best retained (section 6.2.2.2), followed by the nonionic and cationic surfactants.

Table 6.9: Retentions of the surfactants and COD (%) for the membranes NF270 and NFPE10 after filtering the wastewater (both after the cyclone (C) and after the sand filter (SF)), and after filtering Turtle Wax HP11, Triple Shine and the rim cleaner from Rumler

		NF270				NFPE10			
		surfactants			COD	surfactants			COD
		nonionic	anionic	cationic		nonionic	anionic	cationic	
Monday	<i>C</i>	98	98	97	78	51	85	50	36
	<i>SF</i>	99	98	99	100	43	83	37	47
Saturday	<i>C</i>	98	93	98	95	54	71	48	65
	<i>SF</i>	97	95	95	95	45	79	51	49
Friday	<i>SF</i>	97	94	100	98	50	80	27	70
	<i>SF (2)</i>	98	94	-	98	54	80	-	76
HP11		93	85	-	91	91	53	-	78
Triple Shine		98	99	96	76	46	87	70	55
rim cleaner		93	100	83	88	30	100	71	33

For the surfactant and COD retentions when filtering HP11, Triple Shine and the rim cleaner, some differences with the results of the real wastewater (after cyclone and sand filter) become visible, especially for NFPE10 (the membrane with the highest cut-off). When filtering a solution of HP11, a significantly higher and lower retention for the nonionic and anionic surfactants, respectively, was observed. This was explained by the high concentration of anionic surfactants present in the feed solution (Table 6.7), as an increase in concentration leads to a decrease in the retention. Due to the strong electrostatic repulsions between the anionic surfactants and between the surfactants and the membrane surface, the nonionic surfactants are also prevented to pass through the membrane (section 6.2.6), as indicated by the high retention.

In the solution of Triple Shine and the rim cleaner, a high concentration of nonionic and cationic surfactants was detected (Table 6.7). This results in an expected low retention of the nonionic surfactants, but in an unexpectedly high retention of the cationic surfactants. A possible explanation could be that these cationic surfactants form micelles in the feed, which are (because of their size) better retained. Also for Triple Shine and the rim cleaner, a very low COD retention is obtained, due to the very high COD of the feed solution.

6.3.4 Cleaning procedure

After filtration during one working day, the membranes were cleaned to recover their initial performance. The cleaning was done in two steps, as was proposed by Weis *et al.* (2003). Firstly, the reversible part of flux decline was removed by rinsing with water. Secondly, some chemical cleaning was needed to remove the irreversible part of flux decline (fouling). After these two steps, the original pure water flux (or a relative flux of 100 %) should be obtained. Chemical cleaning was done with the alkaline P3-Ultraperm 091 WT product and the acid P3-Ultraperm 075 WT product (Henkel). Several cleaning procedures were tested. The optimal cleaning procedure consists of a rinse with water during 15 minutes at 8 bar and 293 K, followed by an alkaline chemical cleaning of pH 12.9 (1 % solution of P3-

Ultraperm 091 WT) during 30 minutes at 4 bar and 313 K. After each cleaning step, the pure water flux was again determined at 8 bar and 293 K.

The results of this cleaning procedure are given in Table 6.8 and Figure 6.6. For NF270, the rinse with water was already sufficient to remove the reversible flux decline, as also observed by Cornelis *et al.* (2005). However, for the hydrophobic membrane NFPE10, an additional alkaline cleaning is required. According to the manufacturer, the membrane will not be damaged by this alkaline solution, as NFPE10 is stable until pH 14 (Table 2.1). Table 6.8 shows that the initial pure water flux of the NFPE10 membrane is again obtained after these two cleaning steps. An additional chemical cleaning with the acid Ultraperm product is therefore not necessary.

After cleaning with water (and with the alkaline Ultraperm product in the case of NFPE10), membrane fouling is completely removed. Table 6.8 indicates that the relative flux is even higher than 100 %, which means that the pure water flux after cleaning is higher than the original pure water flux. This phenomenon was also observed by Cornelis *et al.* (2005). As a high relative flux was particularly the case for NFPE10 after alkaline cleaning, it is possible that the alkaline product has adsorbed on the membrane surface resulting in a more negatively charged membrane surface and hence in stronger repulsion forces between the membrane surface and distilled water.

To check whether the membranes are not damaged during cleaning, a filtration experiment with the same wastewater was performed with the cleaned membranes to control if the degree of fouling and the retentions were the same before and after cleaning. The results of the relative flux and the retention after filtering the wastewater (taken after the sand filter on Friday) with the cleaned membranes are shown in Table 6.8 and 6.9, respectively (named as *SF (2)*). The results indicate that both the relative flux and the retention of surfactants and COD are the same during the first and second filtration (after cleaning). This proves that the membranes are not damaged during cleaning.

6.4 Conclusion

The experimental results indicate that nanofiltration can be applied to recycle wastewater in the carwash industry. For good operation, a high water permeability, a high relative flux and a high retention are required. For this purpose, a hydrophilic nanofiltration membrane with small pores should be selected, like NF270. With this membrane, permeate fluxes of $45 \text{ L m}^{-2} \text{ h}^{-1}$ are obtained that contain less than 5 % of the original concentrations of surfactants and organic components. Another advantage of this hydrophilic membrane is that the original pure water flux was obtained after cleaning with water during only 15 minutes. No further chemical cleaning is needed. It is also shown that after cleaning, the membrane is not damaged.

If nanofiltration would be implemented in the future to recycle wastewater in the carwash industry, it is advised to keep the concentration of the surfactants as low as possible and to make a study of the composition of the individual surfactants. Surfactants composed of a very high concentration of nonionic or cationic components, should be avoided or replaced by other less fouling surfactants.

Summary and General Conclusions

A breakthrough of nanofiltration (NF) in new applications is hampered by the phenomenon of membrane fouling which results in an undesirable flux decline. From the literature, it is known that membrane fouling is an interplay between different parameters: the feed composition, membrane characteristics and operating conditions. The latter can be controlled by using a cross-flow setup in combination with a high feed velocity and an optimal cleaning frequency. The former two parameters (i.e., feed composition and membrane characteristics) are interrelated, as the composition of the feed determines which membrane characteristics are crucial to prevent fouling.

The aim of this work was to study the membrane performance (i.e., flux decline and retention) on the basis of membrane characteristics. In a first part, representative NF membranes were characterized thoroughly for both chemical and physical properties.

Commercially available NF membranes from different manufacturers and with a wide range of properties were selected: UTC20 (Toray), NF270 (DOW/FilmTec), Desal51HL and Desal5DL (GE Osmonics), N30F and NFPE10 (Nadir), and NTR7450 (Nitto-Denko).

In addition to these commercial membranes, nanoporous polyethersulfone (PES) membranes were prepared by DIPS (Diffusion Induced Phase Separation). These membranes have a well-known composition of the top layer (i.e., PES), in contrast to the scarce information given by the manufacturer about the commercial membranes.

Optimizing the preparation conditions during synthesis led to four different types of membranes: D13 and D71 (for a 32 % PES/DMF solution cast on FO2413 and FO2471, respectively), and N13 and N71 (for a 30 % PES/NMP solution cast on FO2413 and FO2471, respectively). As non-solvent, the best results were obtained for a distilled water bath at 293 K in combination with a relative humidity of 40 %

during casting of the polymer solution and without addition of components to the non-solvent bath or to the polymer solution.

Under these conditions, PES membranes with a good reproducibility and a water permeability comparable with commercial NF membranes, were obtained. For N13 and N71, even a higher water permeability was observed.

The roughness, the hydrophobicity and the behavior of the surface charge as a function of pH of the top layer of these laboratory-made membranes were comparable with commercial membranes, in contrast to the cut-off (i.e., the molecular mass of a component with 90 % retention).

In spite of the higher cut-off for the laboratory-made membranes, the retention of charged components was remarkably high and especially during filtration of small, positively charged components. This was explained by the smaller negative surface charge (less electrostatic attraction forces) of the laboratory-made membranes. In spite of the higher retentions, flux decline for the laboratory-made membranes was comparable to the commercial membranes, which in combination with the higher water permeability (for N13 and N71), leads to higher permeate fluxes.

The laboratory-made and the selected commercial NF membranes were characterized for their chemical composition and for some physical characteristics, which (possibly) play a role in membrane fouling. PAS (Positron Annihilation Spectroscopy), a relatively novel characterization technique in nanofiltration, was also applied on the different membranes.

Chemical characterization of top and support layer was performed with ATR-FTIR (Attenuated Total Reflectance – Fourier Transform InfraRed) and XPS (X-ray Photoelectron Spectroscopy), which allowed to distinguish two different membrane classes:

- a class of membranes with a polyamide top layer (Desal51HL, Desal5DL and NF270), which consisted of (minimum) three layers: a thin top layer of polyamide, an intermediate layer and a polyester support layer;

- a class of membranes with a polyethersulfone top layer (N30F, NFPE10, NTR7450, D71 and N13), which consisted of (minimum) two layers: a top layer of poly(phenylenesulfone ether) or the more general structure poly(arylenesulfone ether) in the case of NTR7450, and a support layer. In this second membrane class, small chemical differences were observed between the commercial and the laboratory-made membranes, which were attributed to the use of additives or post-treatments by the manufacturers.

The physical characteristics studied were cut-off, surface roughness (determined by non-contact and tapping mode AFM, Atomic Force Microscopy), surface hydrophobicity (determined by tapping mode AFM and contact angle measurements), surface charge (determined by measurements of the streaming potential) and thickness of the top layer (determined by PAS). The same membrane classes were distinguished for these characteristics, as the polyamide class has the lowest cut-off and the roughest, thinnest and most hydrophilic top layer.

In this top layer, the pore size distribution was observed by PALS (Positron Annihilation Lifetime Spectroscopy) to be a bimodal instead of the well-accepted log-normal function, with pore sizes between 0.125 – 0.155 nm and 0.320 – 0.395 nm (depending on the membrane). Moreover, the cut-off did not correlate with the pore size, but rather with the ratio of the volume fraction of the large pores to the volume fraction of all pores. This indicates that transport through NF membranes depends more on the relation between the different pores than on the absolute pore size.

In a second part, the membrane characteristics of the commercial NF membranes were, by means of multiple linear regression, coupled to the experimental results of relative flux (i.e., relation of permeate flux to pure water flux), retention and adsorbed amount, obtained during experiments with three different feed solutions:

- aqueous solutions containing dissolved uncharged organic components;
- aqueous solutions containing dissolved charged organic components;
- colloidal dispersions.

It was concluded that in order to minimize fouling during filtration of aqueous feed solutions containing dissolved organic components, a membrane with a low volume fraction of small pores in the top layer should be selected. When the organic components are charged, a membrane with a large surface charge and a high hydrophilicity is also favourable. Not only the membrane, but also the feed characteristics control the degree of fouling: the best results during filtration of dissolved uncharged or charged components were obtained with hydrophilic or negatively charged components, respectively.

Dissolved organic components were best retained by membranes with a low cut-off. In addition, uncharged organic components should be hydrophilic and large to obtain a high retention, while the interplay between membrane and component charge is crucial during filtration of dissolved charged organic components.

To minimize fouling during filtration of colloidal dispersions, the hydrophobicity of the membrane surface should be minimal. Only when small colloids are filtered, a hydrophilic and smooth membrane was needed to prevent the phenomenon of “valley clogging”. For the colloid characteristics, the least membrane fouling was observed (at neutral pH and without the addition of salt) for large, negatively charged colloids. Depending on the pore size of the membrane, increasing the ionic strength of the solution (at neutral pH) was also advantageous to minimize colloidal fouling.

The results indicate that for each type of feed solution, a specific membrane needs to be selected. However, interactions between different components (like e.g., in a real wastewater) were not taken into account. This implies that filtration experiments with (representative) mixtures of components are still needed to fine-tune the understanding of membrane performance in real applications. Moreover, experiments with other nanofiltration membranes (other polymeric ones or anorganic ones) are needed to extend the conclusions made to the whole nanofiltration world.

Another suggestion for further research is membrane modification. For example, PES membranes have a better thermal and chemical stability but also a higher hydrophobicity, which is shown to be disadvantageous for membrane fouling. More hydrophilic PES membranes can be obtained by making the polymer more hydrophilic (e.g., by sulfonating or by adding a more hydrophilic polymer during the synthesis process) or by making the membrane surface more hydrophilic (e.g., by grafting).

On the other hand, the polyamide membranes have the advantage of being hydrophilic, but the disadvantage of being rough (which causes problems during filtration of small colloids). This can (possibly) be solved by changing the preparation conditions during interfacial polymerisation.

The results of the present study were applied to evaluate wastewater recycling in the carwash industry with NF. For that purpose, filtration experiments were performed, firstly with synthetic surfactant solutions. It was concluded from these experiments that, to reduce membrane fouling to a minimum, adsorption of the surfactants should be minimized and that the surfactants should orient in such a way that the membrane surface becomes more hydrophilic. The latter can be realized by a proper choice of membrane and surfactant in combination with the right conditions of pH and ionic strength.

During filtration of carwash wastewater, the best results were obtained with a hydrophilic membrane with small pores, as this gives a high permeate flux which contains only a small fraction of the initial concentrations of surfactants and dissolved organic components. An additional advantage of such a membrane is that a cleaning step with water during 15 minutes was already sufficient to reach the original pure water flux.

References

- Abbe JCH, Duplatre G, Maddock AG, Talamoni J, Haessler A, 1981. Correlation between pulse radiolysis and positron annihilation techniques data. *Journal of Inorganic and Nuclear Chemistry* 43: 2603-2610
- Aerts P, Genné I, Leysen R, Jacobs PA, Vankelecom IFJ, 2006. The role of the nature of the casting substrate on the properties of membranes prepared via immersion precipitation. *Journal of Membrane Science* 283: 320-327
- Agenson KO, Oh JI, Urase T, 2003. Retention of a wide variety of organic pollutants by different nanofiltration/reverse osmosis membranes: controlling parameters of process. *Journal of Membrane Science* 225: 91-103
- Aimar P, Meireles M, Sanchez V, 1990. A contribution to the translation of retention curves into pore size distributions for sieving membranes. *Journal of Membrane Science* 54: 321-338
- Akbari A, Desclaux S, Rouch JC, Aptel P, Remigy JC, 2006. New UV-photografted nanofiltration membranes for the treatment of coloured textile dye effluents. *Journal of Membrane Science* 286 (1-2): 342-350
- Algers J, Sperr P, Egger W, Kögel G, Maurer FHJ, 2003. Median implantation depth and implantation profile of 3-18keV positrons in amorphous polymers. *Physical Review B* 67: 125404
- Ang WS, Lee SY, Elimelech M, 2006. Chemical and physical aspects of cleaning of organic-fouled reverse osmosis membranes. *Journal of Membrane Science* 272: 198-210
- Archer AC, Mendes AM, Boaventura RAR, 1999. Separation of an anionic surfactant by nanofiltration. *Environmental Science and Technology* 33: 2758-2764
- Ariza MJ, Benavente J, Rodriguez-Castellon E, Palacio L, 2002. Effect of hydration of polyamide membranes on the surface electrokinetic parameters: surface characterization by X-ray photoelectronic spectroscopy and atomic force microscopy. *Journal of Colloid and Interface Science* 247: 149-158

- Ariza MJ, Rodriguez-Castellon E, Rico R, Benavente J, Munoz M, Oleinikova M, 2000. X-Ray photoelectron spectroscopy analysis of di-(2-ethylhexyl) phosphoric acid activated membranes. *Journal of Colloid and Interface Science* 226: 151-158
- ATHAS Data Bank, 1994. <http://web.utk.edu/~athas/databank>
- Baik KJ, Kim JY, Lee JS, Kim SC, Lee HK, 2001. Morphology of membranes formed from polysulfone/polyethersulfone/N-methyl-2-pyrrolidone/water system by immersion precipitation. *Korea Polymer Journal* 9 (5): 285-291
- Bandini S, 2005. Modelling the mechanism of charge formation in NF membranes: Theory and application. *Journal of Membrane Science* 264 (1-2): 75-86
- Bargeman G, Vollenbroek JM, Straatsma J, Schroën CGPH, Boom RM, 2005. Nanofiltration of multi-component feeds: interaction between neutral and charged components and their effect on retention. *Journal of Membrane Science* 247: 11-20
- Barth C, Wolf BA, 2000. Evidence of ternary interaction parameters for polymer solutions in mixed solvents from headspace-gas chromatography. *Polymer* 41: 8587-8596
- Barth C, Gonçalves MC, Pires ATN, Roeder J, Wolf BA, 2000b. Asymmetric polysulfone and polyethersulfone membranes: effects of thermodynamic conditions during formation on their performance. *Journal of Membrane Science* 169: 287-299
- Barton BF, Reeve JL, McHugh AJ, 1997. Observations on the dynamics of nonsolvent-induced phase inversion. *Journal of Polymer Science B: Polymer Physics* 35: 569-585
- Bas C, Alberola ND, Barthe MF, De Baerdemaeker J, Dauwe C, 2004. Positron interactions in polymers. *International Journal of Modern Physics A* 19: 3951-3959
- Beckstein O, Sansom MSP, 2004. The influence of geometry, surface character and flexibility on the permeation of ions and water through biological pores. *Physical Biology* 1: 42-52
- Beamson G, Briggs D, 1992. High resolution XPS of organic polymers: the Scienta ESCA300 database. John Wiley & Sons, England

- Bellona C, Drewes JE, 2005. The role of membrane surface charge and solute physico-chemical properties in the rejection of organic acids by NF membranes. *Journal of Membrane Science* 249: 227-234
- Bellona C., Drewes JE, Xu P, Amy G, 2004. Factors affecting the rejection of organic solutes during NF/RO treatment: a literature review. *Water Research* 38: 2795-2809
- Benavente J, Vazquez MI, 2004. Effect of age and chemical treatments on characteristic parameters for active and porous sub layers of polymeric composite membranes. *Journal of Colloid and Interface Science* 273: 547-555
- Bhattacharjee S, Elimelech M, 1997. Surface element integration: a novel technique for evaluation of DLVO interaction between a particle and a flat plate. *Journal of Colloid and Interface Science* 193: 273-285
- Blackadder DA, Ghavamikia H, 1979. Crystallinity in polyethersulfone: problem of definition. *Polymer* 20 (11): 1432-1434
- Bowen WR, Doneva TA, Stoton JAG, 2002. Protein deposition during cross-flow membrane filtration: AFM studies and flux loss. *Colloids and Surfaces B* 27: 103-113
- Bowen WR, Welfoot JS, 2002b. Modelling the performance of membrane nanofiltration: critical assessment and model development. *Chemical Engineering Science* 57: 1121-1137
- Bowen WR, Doneva TA, 2000. AFM studies of nanofiltration membranes: surface morphology, pore size distribution and adhesion. *Desalination* 129: 163-172
- Braeken L, 2005. Influence of fouling by dissolved organic compounds in aqueous solution on the performance of nanofiltration. PhD thesis, K.U.Leuven, Belgium
- Braeken L, Ramaekers R, Zhang Y, Maes G, Van der Bruggen B, Vandecasteele C, 2005b. Influence of hydrophobicity on retention in nanofiltration of aqueous solutions containing organic compounds. *Journal of Membrane Science* 252 (1-2): 195-203

- Braeken L, Boussu K, Van der Bruggen B, Vandecasteele C, 2005c. Modeling of the adsorption of organic compounds on polymeric nanofiltration membranes in solution containing two compounds. *ChemPhysChem* 6: 1606-1612
- Braeken L, Van der Bruggen B, Vandecasteele C, 2004. Regeneration of brewery waste water using nanofiltration. *Water Research* 38: 3075-3082
- Brant JA, Childress AE, 2002. Membrane-colloid interactions: comparison of extended DLVO predictions with AFM force measurements. *Environmental Engineering Science* 19: 413-427
- Byhlin H, Jönsson AS, 2002. Influence of adsorption and concentration polarisation on membrane performance during ultrafiltration of a nonionic surfactant. *Desalination* 151: 21-31
- Cao H, Yuan JP, Zhang R, Sundar CS, Jean YC, Suzuki R, Ohdaira T, Nielsen B, 1999. Free volumes and holes near the polymer surface studied by positron annihilation. *Applied Surface Science* 149: 116-124
- Capelle N, Moulin P, Charbit F, Gallo R, 2002. Purification of heterocyclic derivatives from concentrated saline solution by nanofiltration. *Journal of Membrane Science* 196 (1): 125-141
- Carbonez A, 2004. Regression and Variance Analysis. Course taught in October, 2004 at the University Centre of Statistics of K.U.Leuven
- Chaturvedi BK, Ghosh AK, Ramachandhran V, Trivedi MK, Hanra MS, Misra BM, 2001. Preparation, characterization and performance of polyethersulfone ultrafiltration membranes. *Desalination* 133: 31-40
- Childress AE, Elimelech M, 2000. Relating nanofiltration membrane performance to membrane charge (electrokinetic) characteristics. *Environmental Science and Technology* 34: 3710-3716
- Childress AE, Elimelech M, 1996. Effect of solution chemistry on the surface charge of polymeric reverse osmosis and nanofiltration membranes. *Journal of Membrane Science* 119: 253-268

- Chun MS, Park WC, 2004. Time evolution of electrokinetic flow-induced streaming potential and flux in dead-end and cross-flow filtration of colloids through nanopores. *Journal of Membrane Science* 243: 417-424
- Chun MS, Cho HI, Song IK, 2002. Electrokinetic behaviour of membrane zeta potential during the filtration of colloidal suspension. *Desalination* 148: 363-367
- Clesceri LS, Greenberg AE, Trussel RR, 1989. Standard methods for the examination of water and wastewater. American Public Health Association, Washington D.C.
- Cleveland CT, Seacord TF, Zander AK, 2002. Standardized membrane pore size characterization by polyethylene glycol rejection. *Journal of Environmental Engineering* 128: 399-407
- Colowick SP, Kaplan NO, 1957. *Methods in Enzymology*. Academic Press Inc., New York
- Cornelis G, Boussu K, De Vreese I, Van der Bruggen B, Vandecasteele C, 2005. Nanofiltration of nonionic surfactant solutions: effect of molecular weight cut-off and hydrophilicity on flux behavior. *Industrial Engineering and Chemistry Research* 44: 7652-7658
- Costa AR, de Pinho MN, 2005. Effect of membrane pore size and solution chemistry on the ultrafiltration of humic substances solutions. *Journal of Membrane Science* 255: 49-56
- Crittenden JC, Trussell RR, Hand DW, Howe KJ, Tchobanoglous G, 2005. *Water Treatment: Principles and Design*. John Wiley & Sons, New Jersey
- Cyna B, Chagneau G, Bablon G, Tanghe N, 2002. Two years of nanofiltration at the Méry-sur-Oise plant, France. *Desalination* 147: 69-75
- Davey M, Landman K, Perera JM, Stevens GW, Lawrence ND, Iyer M, 2004. Measurement and prediction of the ultrafiltration of whey protein. *AIChE Journal* 50: 1431-1437

De Florio L, Giordano A, Mattioli D, 2005. Nanofiltration of low-contaminated textile rinsing effluents for on-site treatment and reuse. *Desalination* 181 (1-3): 283-292

Dlubek G, Gupta AS, Pionteck J, Häßler R, Krause-Rehberg R, Kaspar H, Lochhaas KH, 2005. Glass transition and free volume in the mobile (MAF) and rigid (RAF) amorphous fractions of semicrystalline PTFE: a positron lifetime and PVT study. *Polymer* 46: 6075-6089

Dlubek G, Alam MA, 2002. Studies of the positron lifetime and Doppler-broadened annihilation radiation of polypropylene-polystyrene alloys. *Polymer* 43: 4025-4031

Douliat D, Gekas V, Trägårdh G, 1997. Interaction behaviour in ultrafiltration of nonionic surfactants, part II: static adsorption below CMC. *Journal of Membrane Science* 123: 133-142

Drioli E, 2002. An international report on Membranes Science and Technology, perspectives and needs. Prepared and discussed at the International Conference on Membranes (ICOM 2002) held in Toulouse on July 7-12

Dubois M, Gilles KA, Hamilton JK, Rebers PA, Smith F, 1956. Colorimetric method for determination of sugars and related substances. *Analytical Chemistry* 28 (3): 350-356

Dutschk V, Sabbatovskiy KG, Stolz M, Grundke K, Rudoy VM, 2003. Unusual wetting dynamics of aqueous surfactant solutions on polymer surfaces. *Journal of Colloid and Interface Science* 267: 456-462

Elimelech M, Zhu X, Childress AE, Hong S, 1997. Role of membrane surface morphology in colloidal fouling of cellulose acetate and composite aromatic polyamide reverse osmosis membranes. *Journal of Membrane Science* 127: 101-109

Ernst M, Bismarck A, Springer J, Jekel M, 2000. Zeta-potential and rejection rates of a polyethersulfone nanofiltration membrane in single salt solutions. *Journal of Membrane Science* 165: 251-259

- Faibish RS, Elimelech M, Cohen Y, 1998. Effect of interparticle electrostatic double layer interactions on permeate flux decline in crossflow membrane filtration of colloidal suspensions: an experimental investigation. *Journal of Colloid and Interface Science* 204: 77-86
- Fairbrother F, Mastin H, 1924. Studies in electro-endosmosis. *Journal of the Chemical Society* 125: 2319
- Faupel F, Kanzow J, Gunther-Schade K, Nagel C, Sperr P, Kögel G, 2004. Positron Annihilation Spectroscopy in polymers. *Materials Science Forum* 445-446: 219-223
- Fievet P, Sbai M, Szymczyk A, Magnenet C, Labbez C, Vidonne A, 2004. A new tangential streaming potential setup for the electrokinetic characterization of tubular membranes. *Separation Science and Technology* 39: 2931-2949
- Freger V, Gilron J, Belfer S, 2002. TFC polyamide membranes modified by grafting of hydrophilic polymers: an FT-IR/AFM/TEM study. *Journal of Membrane Science* 209: 283-292
- Gaid A, Bablon G, Turner G, Franchet J, Protais JC, 1998. Performance of 3 years' operation of nanofiltration plants. *Desalination* 117: 149-158
- Gardella JA, Ferguson SA, Chin RL, 1986. $\pi^* \leftarrow \pi$ shakeup satellites for the analysis of structure and bonding in aromatic polymers by X-Ray Photoelectron Spectroscopy. *Applied Spectroscopy* 40: 224-232
- Geens J, Hillen A, Bettens B, Van der Bruggen B, Vandecasteele C, 2005. Solute transport in non-aqueous nanofiltration: effect of membrane material. *Journal of Chemical Technology and Biotechnology* 80 (12): 1371-1377
- Gelman Sciences Inc., 1993. Hydrophilic membranes prepared from polyethersulfone/poly-2-oxazoline/polyvinylpyrrolidone blend. European Patent WO/1993/005871. 1993-04-01
- Gomes AC, Goncalves IC, de Pinho MN, 2005. The role of adsorption on nanofiltration of azo dyes. *Journal of Membrane Science* 255: 157-165

- Goodwin J, 2004. Colloids and interfaces with surfactants and polymers. John Wiley & Sons, Chichester
- Gumi T, Valiente M, Khulbe KC, Palet C, Matsuura T, 2003. Characterization of activated composite membranes by solute transport, contact angle measurements, AFM and ESR. *Journal of Membrane Science* 212: 123-134
- Hamada T, Miyazaki Y, 2004. Reuse of carwash water with a cellulose acetate ultrafiltration membrane aided by flocculation and activated carbon treatments. *Desalination* 169:257-267
- Han MJ, Nam ST, 2002. Thermodynamic and rheological variation in polysulfone solution by PVP and its effect in the preparation of phase inversion membrane. *Journal of Membrane Science* 202: 55-61
- Han MJ, 1999. Effect of propionic acid in the casting solution on the characteristics of phase inversion polysulfone membranes. *Desalination* 121: 31-39
- Han MJ, Bummer PM, Jay M, Bhattacharyya D, 1995. Phase transitions of polysulfone solution during coagulation. *Polymer* 36 (24): 4711-4714
- Han MJ, Bhattacharyya D, 1994. Morphology and transport study of phase inversion polysulfone membranes. *Chemical Engineering Communications* 128: 197-209
- He C, Suzuki T, Hamada E, Kobayashi H, Kondo K, Shantarovich VP, Ito Y, 2003. Characterization of polymer films using a slow positron beam. *Materials Research Innovations* 7: 37-41
- Hilal N, Al-Zoubi H, Darwish NA, Mohammad AW, Arabi MA, 2004. A comprehensive review of nanofiltration membranes: treatment, pre-treatment, modelling and atomic force microscopy. *Desalination* 170: 281-308
- Hilal N, Bowen WR, 2002. AFM study of the rejection of colloids by membrane pores. *Desalination* 150: 289-295
- Ho AK, Perera JM, Dunstan DE, Stevens GW, Nyström M, 1999. Measurement and theoretical modelling of protein mobility through membranes. *AIChE Journal* 45: 1434-1450

- Hoek EMV, Agarwal GK, 2006. Extended DLVO interactions between spherical particles and rough surfaces. *Journal of Colloid and Interface Science* 298: 50-58
- Hoek EMV, Bhattacharjee S, Elimelech M, 2003. Effect of membrane surface roughness on colloid-membrane DLVO interactions. *Langmuir* 19: 4836-4847
- Hoek EMV, Kim AS, Elimelech M, 2002. Influence of cross-flow membrane filter geometry and shear rate on colloidal fouling in reverse osmosis and nanofiltration separations. *Environmental Engineering Science* 19: 357-372
- Howell JA, Sanchez V, Field RW, 1993. *Membranes in bioprocessing: Theory and Applications*. Elsevier Science Publishers Inc.
- Hubert M, 2004. *Regression Techniques*. Acco, Leuven
- Huisman IH, Pradanos P, Hernandez A, 2000. The effect of protein-protein and membrane-protein interactions on membrane fouling in ultrafiltration. *Journal of Membrane Science* 179: 79-90
- Huisman IH, Dutré B, Persson KM, Trägårdh G, 1997. Water permeability in ultrafiltration and microfiltration: viscous and electroviscous effects. *Desalination* 113: 95-103
- Hummel DO, Scholl F, 1978. *Atlas of polymer and plastics analysis: Polymers, structures and spectra*. Hanser, München
- Huybrechts D, De Baere P, Van Espen L, Wellens B, Dijkmans R, 2002. Best available techniques for carwash and truckwash. BBT study VITO: <http://www.emis.vito.be>
- Jean YC, Mallon PE, Schrader DM, 2003. *Principles and Applications of positron and positronium chemistry*. World Scientific Publishing Co. Pte. Ltd., Singapore
- Jiao B, Cassano A, Drioli E, 2004. Recent advances on membrane processes for the concentration of fruit juices: a review. *Journal of Food Engineering* 63: 303-324
- Jönsson C, Jönsson AS, 1995. The influence of degreasing agents used at carwashes on the performance of ultrafiltration membranes. *Desalination* 100: 115-123

- Jönsson AS, Jönsson B, 1991. The influence of nonionic and ionic surfactants on hydrophobic and hydrophilic ultrafiltration membranes. *Journal of Membrane Science* 56: 49-76
- Karakulski K, Morawski AW, 2003. Treatment of wastewater from carwashes by ultrafiltration. *Fresenius Environmental Bulletin* 12: 343-348
- Kastelan-Kunst L, Dananic V, Kunst B, Kosutic K, 1996. Preparation and porosity of cellulose triacetate reverse osmosis membranes. *Journal of Membrane Science* 109: 223-230
- Kaul A, 1987. ESCA analysis of the surface oxidation of polyphenylene sulphide powder in a slurry reaction. *Abstracts of papers of the American Chemical Society* 193: 229-231
- Kavitskaya AA, 2005. Separation characteristics of charged ultrafiltration membranes modified with the anionic surfactant. *Desalination* 184: 409-414
- Khulbe KC, Matsuura T, 2000. Characterization of synthetic membranes by Raman spectroscopy, electron spin resonance and AFM; a review. *Polymer* 41: 1917-1935
- Kilburn D, Dlubek G, Pionteck J, Bamford D, Alam MA, 2005. Microstructure of free volume in SMA copolymers, II Local free volume from PALS. *Polymer* 46: 869-876
- Kim IC, Yoon HG, Lee KH, 2002. Formation of integrally skinned asymmetric PEI NF membranes by phase inversion process. *Journal of Applied Polymer Science* 84 (6): 1300-1307
- Kim JH, Lee KH, 1998. Effect of PEG additive on membrane formation by phase inversion. *Journal of Membrane Science* 138: 153-163
- Kim JY, Lee HK, Kim SC, 2000. Liquid-liquid phase separation during PSf membrane preparation. *Korean Journal of Chemical Engineering* 17 (5): 564-569
- Kim KJ, Fane AG, Nyström M, Pihlajamäki A, Bowen WR, Mukhtar H, 1996. Evaluation of electro-osmosis and streaming potential for measurement of electric charges of polymeric membranes. *Journal of Membrane Science* 116: 149-159

- Kim SH, Kwak SY, Suzuki T, 2005. Positron Annihilation Spectroscopic evidence to demonstrate the flux-enhancement mechanism in morphology-controlled thin-film-composite membrane. *Environmental Science and Technology* 39: 1764-1770
- Kimura K, Amy G, Drewes J, Watanabe Y, 2003. Adsorption of hydrophobic compounds onto NF/RO membranes: an artefact leading to overestimation of rejection. *Journal of Membrane Science* 221: 89-101
- Kiso Y, Sugiura Y, Kitao T, Nishimura K, 2001. Effects of hydrophobicity and molecular size on rejection of aromatic pesticides with nanofiltration membranes. *Journal of Membrane Science* 192: 1-10
- Koros WJ, Ma YH, Shimizu T, 1996. Terminology for membranes and membrane processes – IUPAC recommendations 1996. *Journal of Membrane Science* 120: 149-159
- Kosmulski M, 2003. A literature survey of the differences between the reported IEP and their discussion. *Colloids and Surfaces A* 222: 113-118
- Kowalska I, Kabsch-Korbutowicz M, Majewska-Nowak K, Winnicki T, 2004. Separation of anionic surfactants on ultrafiltration membranes. *Desalination* 162: 33-40
- Kruse J, Kanzow J, Ratzke K, Faupel F, Heuchel M, Frahn J, Hofmann D, 2005. Free volume in polyimides: positron annihilation experiments and molecular modelling. *Macromolecules* 38: 9638-9643
- Kuan WH, Lo SL, Wang MK, 2000. pH effect on the surface and bulk characteristics of metallic cations/SiO₂ suspensions. *Water Science and Technology* 42: 441-446
- Kull KR, Steen ML, Fisher ER, 2005. Surface modification with nitrogen-containing plasmas to produce hydrophilic low-fouling membranes. *Journal of Membrane Science* 246: 203-215

- Kwak S, Yeom M, Roh IJ, Kim DY, Kim J, 1997. Correlations of chemical structure, AFM morphology and reverse osmosis characteristics in aromatic polyester high-flux reverse osmosis membranes. *Journal of Membrane Science* 132: 183-191
- Lafreniere LY, Talbot FDF, Matsuura T, Sourirajan S, 1987. Effect of polyvinylpyrrolidone additive on the performance of polyethersulfone ultrafiltration membranes. *Industrial & Engineering Chemistry Research* 26 (11): 2385-2389
- Lee S, Cho J, Elimelech M, 2005. Combined influence of natural organic matter and colloidal particles on nanofiltration membrane fouling. *Journal of Membrane Science* 262: 27-41
- Lee S, Cho J, Elimelech M, 2004. Influence of colloidal fouling and feed water recovery on salt rejection of reverse osmosis and nanofiltration membranes. *Desalination* 160: 1-12
- Liikanen R, Yli-Kuivila J, Laukkanen R, 2002. Efficiency of various chemical cleanings for nanofiltration membrane fouled by conventionally-treated surface water. *Journal of Membrane Science* 195: 265-276
- Lin DJ, Chang CL, Chen TC, Cheng LP, 2002. Microporous PVDF membrane formation by immersion precipitation from water/TEP/PVDF system. *Desalination* 145: 25-29
- Linder C, Kedem O, 2001. Asymmetric ion exchange mosaic membranes with unique selectivity. *Journal of Membrane Science* 181: 39-56
- Lopes CN, Petrus JCC, Riella HG, 2005. Color and COD retention by nanofiltration membranes. *Desalination* 172: 77-83
- Marchese J, Ponce M, Ochoa NA, Pradanos P, Palacio L, Hernandez A, 2003. Fouling behaviour of polyethersulfone UF membranes made with different PVP. *Journal of Membrane Science* 211: 1-11

- Marchese J, Almandoz C, Amaral M, Palacio L, Calvo JI, Pradanos P, Hernandez A, 2000. Fabrication and characterization of microfiltration tubular ceramic membranes. *Boletín de la Sociedad Española de Cerámica y Vidrio* 39: 215-219
- Marletta G, Pignataro S, Toth A, Bertoti I, Szekely T, Keszler B, 1991. X-ray, electron and ion beam induced modifications of polyethersulfone. *Macromolecules* 24: 99-105
- Matsui Y, Knappe D, Takagi R, 2002. Pesticide adsorption by granular activated carbon adsorbents. 1. Effect of natural organic matter preloading on removal rates and model simplification. *Environmental Science and Technology* 36 (15): 3426-3431
- McHugh AJ, Miller DC, 1995. The dynamics of diffusion and gel growth during nonsolvent-induced phase inversion of polyethersulfone. *Journal of Membrane Science* 105: 121-136
- Médout-Marère V, 2000. A simple experimental way of measuring the Hamaker constant A_{11} of divided solids by immersion calorimetry in apolar liquids. *Journal of Colloid and Interface Science* 228: 434-437
- Meindersma GW, Kuczynski M, 1996. Implementing membrane technology in the process industry: problems and opportunities. *Journal of Membrane Science* 113 (2): 285-292
- Meylan WM, Howard PH, 2000. Estimating log P with atom/fragments and water solubility with log P. *Perspectives in Drug Discovery and Design* 19: 67-84
- Merkel TC, Freeman BD, Spontak RJ, He Z, Pinnau I, Meakin P, Hill AJ, 2002. Ultraporous, reverse-selective nanocomposite membranes. *Science* 296: 519-522
- Mietton-Peuchot M, Ranisio O, 1997. Study of the behavior of membranes in the presence of anionic or nonionic surfactants. *Filtration and Separation* 34: 883-886
- Miller JN, 1984. *Statistics for analytical chemistry*. Ellis Horwood Limited, West Sussex

- Moresi M, Lo Presti S, 2003. Present and potential applications of membrane processing in the food industry. *Italian Journal of Food Science* 15 (1): 3-34
- Mosqueda-Jiminez DB, Narbaitz RM, Matsuura T, 2004. Manufacturing conditions of surface-modified membranes: effects on ultrafiltration performance. *Separation and Purification Technology* 37: 51-67
- Mulder M, 1996. *Basic principles of membrane technology*. Kluwer Academic Publishers, The Netherlands
- Mänttari M, Viitikko K, Nyström M, 2006. Nanofiltration of biologically treated effluents from the pulp and paper industry. *Journal of Membrane Science* 272 (1-2): 152-160
- Mänttari M, Pihlajamaki A, Nyström M, 2006b. Effect of pH on hydrophilicity and charge and their effect on the filtration efficiency of NF membranes at different pH. *Journal of Membrane Science* 280 (1-2): 311-320
- Mänttari M, Nyström M, 2004. Ultrafiltration and nanofiltration in the pulp and paper industry using cross-rotational (CR) filters. *Water Science and Technology* 50: 229-238
- Mänttari M, Puro L, Nuortila-Jokinen J, Nyström M, 2000. Fouling effects of polysaccharides and humic acid in nanofiltration. *Journal of Membrane Science* 165: 1-17
- Möckel D, Staude E, Dal-Cin M, Darcovich K, Guiver M, 1998. Tangential flow streaming potential measurements: hydrodynamic cell characterization and zeta potentials of carboxylated polysulfone membranes. *Journal of Membrane Science* 145: 211-222
- Nishimura S, Scales PJ, Biggs SR, Healy TW, 1995. AFM studies of amine surfactant hemimicelle structures at the mica-water interface. *Colloids and Surfaces A* 103 (3): 289-298
- Nghiem LD, Schäfer AI, Elimelech M, 2005. Nanofiltration of hormone mimicking trace organic contaminants. *Separation Science and Technology* 40 (13): 2633-2649

- Nghiem LD, Schäfer AI, Elimelech M, 2004. Removal of natural hormones by nanofiltration membranes: measurement, modelling and mechanisms. *Environmental Science and Technology* 38: 1888-1896
- Nghiem LD, Schäfer AI, Waite TD, 2002. Adsorptive interactions between membranes and trace contaminants. *Desalination* 147: 269-274
- Norde W, 2003. *Colloids and interfaces in life sciences*. Dekker, New York
- Nuortila-Jokinen J, Mänttari M, Huuhilo T, Kallioinen M, Nyström M, 2004. Water circuit closure with membrane technology in the pulp and paper industry. *Water Science and Technology* 50 (3): 217-227
- Nyström M, Kaipia L, Luque S, 1995. Fouling and retention of nanofiltration membranes. *Journal of Membrane Science* 98: 249-262
- Nyström M, Lindström M, Matthiasson E, 1989. Streaming potential as a tool in the characterization of ultrafiltration membranes. *Colloids and Surfaces* 36: 297-312
- Osmonics Inc., 2000. Preparation of polyethersulfone membranes. US Patent 6,056,903. 2000-05-02
- Oshima H, 2001. Approximate analytic expression for the electrophoretic mobility of a spherical colloidal particle. *Journal of Colloid and Interface Science* 239: 587-590
- Ozaki H, Li H, 2002. Rejection of organic compounds by ultra-low pressure reverse osmosis membrane. *Water Research* 36: 123-130
- Panpanit S, Visvanathan C, 2001. The role of bentonite addition in UF flux enhancement mechanisms for oil/water emulsion. *Journal of Membrane Science* 184: 59-68
- Panpanit S, Visvanathan C, Muttamara S, 2000. Separation of oil-water emulsion from carwashes. *Water Science and Technology* 41: 109-116
- Paria S, Khilar KC, 2004. A review on experimental studies of surfactant adsorption at the hydrophilic solid-water interface. *Advances in Colloid and Interface Science* 110: 75-95

- Paul DR, 2004. Reformulation of the solution-diffusion theory of reverse osmosis. *Journal of Membrane Science* 241: 371–386
- Pavia DL, Lampman GM, Kriz GS, 1996. *Introduction to Spectroscopy: a guide for students of organic chemistry*. Saunders, Philadelphia
- Petersen RJ, 1993. Composite reverse-osmosis and nanofiltration membranes. *Journal of Membrane Science* 83 (1): 81-150
- Pihlajamäki A, Väisänen P, Nyström M, 1998. Characterization of clean and fouled polymeric ultrafiltration membranes by Fourier transform IR spectroscopy – attenuated total reflection. *Colloids and Surfaces A* 138: 323-333
- Puglisi O, Fragala ME, Lynn KG, Petkov M, Weber M, Somoza A, Dupasquier A, Quasso F, 2001. Study of ion beam induced depolymerization using positron annihilation techniques. *Nuclear Instruments and Methods in Physics Research B* 175-177: 605-609
- Qin JJ, Oo MH, Wai MN, Wong FS, 2003. Effect of feed pH on an integrated membrane process for the reclamation of a combined rinse water from electroless nickel plating. *Journal of Membrane Science* 217: 261-268
- Rabinovich-Guilatt L, Couvreur P, Lambert G, Goldstein D, Benita S, Dubernet C, 2004. Extensive surface studies help to analyze zeta potential data: the case of cationic emulsions. *Chemistry and Physics of Lipids* 131: 1-13
- Radmacher M, Fritz M, Cleveland JP, Walters DA, Hansma PK, 1994. Imaging adhesion forces and elasticity of lysozyme adsorbed on mica with the atomic-force microscope. *Langmuir* 10 (10): 3809-3814
- Ren J, Li Z, Wong FS, 2006. A new method for the prediction of pore size distribution and MWCO of ultrafiltration membranes. *Journal of Membrane Science* 279: 558–569
- Robinson JP, Tarleton ES, Ebert K, Millington CR, Nijmeijer A, 2005. Influence of cross-linking and process parameters on the separation performance of poly(dimethylsiloxane) nanofiltration membranes. *Industrial and Engineering Chemistry Research* 44: 3238-3248

- Roudman AR, DiGiano FA, 2000. Surface energy of experimental and commercial nanofiltration membranes: effects of wetting and natural organic matter fouling. *Journal of Membrane Science* 175: 61-73
- Round AN, Miles MJ, 2004. Exploring the consequences of attractive and repulsive interaction regimes in tapping mode AFM of DNA. *Nanotechnology* 15: 176-183
- Rousseeuw PJ, Leroy AM, 2003. *Robust Regression and Outlier Detection*. John Wiley & Sons Inc., New York
- Rögener F, Willems M, Mavrov V, Chmiel H, 2002. The influence of cleaning additives on rejection and permeability in nanofiltration and ultrafiltration of bottle washing solutions. *Separation and Purification Technology* 28: 207-217
- Santos JLC, Montesinos AH, Karpinsky A, Velizarov S, Crespo JG, 2006. Modelling of solute and solvent transport through nanofiltration membranes. *Desalination* 199: 448-450
- Santos NC, Castanho M, 2004. An overview of the biophysical applications of AFM. *Biophysical Chemistry* 107: 133-149
- Santos JLC, de Beukelaar P, Vankelecom IFJ, Velizarov S, Crespo JG, 2006. Effect of solute geometry and orientation on the rejection of uncharged compounds by nanofiltration. *Separation and Purification Technology* 50: 122-131
- Satyanarayana SV, Subrahmanyam VS, Verma HC, Sharma A, Bhattacharya PK, 2006. Application of positron annihilation: study of pervaporation dense membranes. *Polymer* 47: 1300-1307
- Schaep J, Vandecasteele C, 2001. Evaluating the charge of nanofiltration membranes. *Journal of Membrane Science* 188: 129-136
- Schaep J, Van der Bruggen B, Vandecasteele C, Wilms D, 1998. Influence of ion size and charge in nanofiltration. *Separation and Purification Technology* 14: 155-162

- Schoeberl P, Brik A, Braun R, Fuchs W, 2005. Treatment and recycling of textile wastewater-caste study and development of a recycling concept. *Desalination* 171: 173-183
- Schwarzenbach RP, Stierli R, Folsom BR, Zeyer J, 1988. Compound properties relevant for assessing the environmental partitioning of nitrophenols. *Environmental Science and Technology* 22 (1): 83-92
- Schäfer AI, Fane AG, Waite TD, 2005. *Nanofiltration: principles and applications*. Elsevier Advanced Technology, United Kingdom
- Schäfer AI, Fane AG, Waite TD, 2001. Cost factors and chemical pre-treatment effects in the membrane filtration of waters containing natural organic matter. *Water Research* 36: 1509-1517
- Shaalán HF, Ghaly MY, Farah JY, 2007. Techno-economic evaluation for the treatment of pesticide industry effluents using membrane schemes. *Desalination* 204 (1-3): 265-276
- Shaalán HF, 2002. Development of fouling control strategies pertinent to nanofiltration membranes. *Desalination* 153: 125-131
- Shimazu A, Miyazaki T, Katayama S, Ito Y, 2003. Permeability, permselectivity and penetrant-induced plasticization in fluorinated polyimides studied by Positron Lifetime measurements. *Journal of Polymer Science B* 41: 308-318
- Shimazu A, Ikeda K, Miyazaki T, Ito Y, 2000. Application of positron annihilation technique to reverse osmosis membrane materials. *Radiation Physics and Chemistry* 58: 555-561
- Singh G, Song L, 2005. Quantifying the effect of ionic strength on colloidal fouling potential in membrane filtration. *Journal of colloid and Interface Science* 284: 630-638
- Somasundaran P, Fuerstenau DW, 1966. Mechanisms of alkyl sulfonate adsorption at the alumina-water interface. *Journal of Physical Chemistry* 70: 90-96

- Song W, Ravindran V, Koel BE, Pirbazari M, 2004. Nanofiltration of natural organic matter with H₂O₂/UV pretreatment: fouling mitigation and membrane surface characterization. *Journal of Membrane Science* 241: 143-160
- Spricigo CB, Petrus JCC, Machado RAF, Sarmiento LAV, Bolzan A, 2002. Preparation and characterization of polyethersulfone membranes for use in supercritical medium. *Journal of Membrane Science* 205: 273-278
- Stubbe L, 2006 (Carwash Stubbe BVBA, Turnhout). Personal communication
- Susanto H, Ulbricht M, 2005. Influence of ultrafiltration membrane characteristics on adsorptive fouling with dextrans. *Journal of Membrane Science* 266 (1-2): 132-142
- Swinyard BT, Barrie JA, 1988. Phase separation in non-solvent/dimethylformamide/polyethersulfone and non-solvent/dimethylformamide/polysulfone systems. *British Polymer Journal* 20: 317-321
- Syracuse Research Corporation, 2003. Interactive LogKow (KowWin) Demo, http://www.syrres.com/esc/est_kowdemo.htm
- Szpała S, Petkov MP, Lynn KG, 2002. A simple positron lifetime spectrometer for a magnetically guided low-energy beam. *Review of Scientific Instruments* 73: 147-155
- Tam CM, Tremblay AY, 1991. Membrane pore characterization: comparison between single and multicomponent solute probe techniques. *Journal of Membrane Science* 57: 271-287
- Tarabara VV, Koyuncu I, Wiesner MR, 2004. Effects of hydrodynamics and solution ionic strength on permeate flux in cross-flow filtration: direct experimental observation of filter cake cross-sections. *Journal of Membrane Science* 241: 65-78
- Teixeira MR, Rose MJ, Nyström M, 2005. The role of membrane charge on nanofiltration performance. *Journal of Membrane Science* 265 (1-2): 160-166

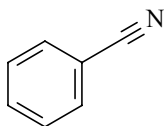
- Timmer JMK, Speelmans MPJ, van der Horst HC, 1998. Separation of amino acids by nanofiltration and ultrafiltration membranes. *Separation and Purification Technology* 14: 133-144
- Tkacik G, Zeman L, 1987. Component mobility analysis in the membrane-forming system water/N-methyl-2-pyrrolidone/polyethersulfone. *Journal of Membrane Science* 31: 273-288
- Tsai FJ, Kang D, Anand M, 1995. Thin-film-composite gas separation membranes – on the dynamics of thin-film formation mechanism of porous substrates. *Separation Science and Technology* 30 (7-9): 1639-1652
- Tsubouchi M, Yamasaki N, Yanagisawa K, 1985. Two-phase titration of Poly(oxyethylene) non-ionic surfactants with tetrakis(4fluorophenyl)borate. *Analytical Chemistry* 57: 783-784
- Urbanski R, Goralska E, Bart HJ, Szymanowski J, 2002. Ultrafiltration of surfactant solutions. *Journal of Colloid and Interface Science* 253: 419-426
- Van der Bruggen B, Segers D, Vandecasteele C, Braeken L, Volodin A, Van Haesendonck C, 2004. How a microfiltration pretreatment affects the performance in nanofiltration. *Separation Science and Technology* 39: 1443-1459
- Van der Bruggen B, Kim JH, DiGiano FA, Geens J, Vandecasteele C, 2004b. Influence of microfiltration pre-treatment on nanofiltration performance for aqueous solutions containing particles and an organic foulant. *Separation and Purification Technology* 36: 203-213
- Van der Bruggen B, Braeken L, Vandecasteele C, 2002. Flux decline in nanofiltration due to adsorption of organic compounds. *Separation and Purification Technology* 29 (1): 23-31
- Van der Bruggen B, Vandecasteele C, 2001. Flux decline during nanofiltration of organic components in aqueous solution. *Environmental Science and Technology* 35: 3535-3540
- Van der Bruggen B, 2000. Removal of organic compounds from aqueous solutions by nanofiltration. PhD thesis, K.U.Leuven, Belgium

- Van der Bruggen B, Schaep J, Wilms D, Vandecasteele C, 2000b. A comparison of models to describe the maximal retention of organic molecules in nanofiltration. *Separation Science and Technology* 35 (2): 169-182
- Van der Bruggen B, Schaep J, Wilms D, Vandecasteele C, 1999. Influence of molecular size, polarity and charge on the retention of organic molecules by nanofiltration. *Journal of Membrane Science* 156: 29-41
- Van der Meeren P, Saveyn H, Kassa SB, Doyen W, Leysen R, 2004. Colloid-membrane interaction effects on flux decline during cross-flow ultrafiltration of colloidal silica on semi-ceramic membranes. *ChemPhysChem* 6: 1408-1412
- Van de Witte P, Dijkstra PJ, Van den Berg JWA, Feijen J, 1996. Phase separation processes in polymer solutions in relation to membrane formation. *Journal of Membrane Science* 117: 1-31
- Vankelecom IFJ, 2002. Polymeric membranes in catalytic reactors. *Chemical Reviews* 102 (10): 3779-3810
- Vilaseca M, Mateo E, Palacio L, Pradanos P, Hernandez A, Paniagua A, Coronas J, Santamaria J, 2004. AFM characterization of the growth of MFI-type zeolite films on alumina substrates. *Microporous and mesoporous materials* 71: 33-37
- Violleau D, Essis-Tome H, Habarou H, Croue JP, Pontie M, 2005. Fouling studies of a polyamide nanofiltration membrane by selected natural organic matter : an analytical approach. *Desalination* 173 (3): 223-238
- Vrijenhoek EM, Hong S, Elimelech M, 2001. Influence of membrane surface properties on initial rate of colloidal fouling of reverse osmosis and nanofiltration membranes. *Journal of Membrane Science* 188: 115-128
- Väisänen P, Bird MR, Nyström M, 2002. Treatment of ultrafiltration membranes with simple and formulated cleaning agents. *Food and Bioproducts processing* 80: 98-108
- Wang Z, Zhao YY, Wang JX, Wang SC, 2005. Studies on nanofiltration membrane fouling in the treatment of water solutions containing humic acids. *Desalination* 178: 171-178

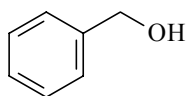
- Wang KY, Chung TS, 2005b. The characterisation of flat composite NF membranes and their applications in the separation of Cephalexin. *Journal of Membrane Science* 247: 37-50
- Wang ZF, Wang B, Qi N, Ding XM, Hu JL, 2004. Free volume and water vapour permeability properties in polyurethane membranes studied by positrons. *Materials Chemistry and Physics* 88: 212-216
- Warczok J, Ferrando M, Lopez F, Güell C, 2004. Concentration of apple and pear juices by nanofiltration at low pressures. *Journal of Food Engineering* 63: 63-70
- Wavhal DS, Fisher ER, 2002. Hydrophilic modification of polyethersulfone membranes by low temperature plasma-induced graft polymerization. *Journal of Membrane Science* 209: 255-269
- Weis A, Bird MR, Nyström M, 2003. The chemical cleaning of polymeric UF membranes fouled with spent sulphite liquor over multiple operational cycles. *Journal of Membrane Science* 216: 67-79
- Wendler B, Goers B, Wozny G, 2002. Nanofiltration of solutions containing surfactants: prediction of flux decline and modeling of mass transfer. *Desalination* 147: 217-221
- Wendler B, Goers B, Wozny G, 2002b. Regeneration of process water containing surfactants by nanofiltration: investigation and modeling of mass transport. *Water Science and Technology* 46: 287-292
- Wiesendanger R, 1994. *Scanning probe microscopy and spectroscopy: Methods and applications*. University Press, Cambridge
- Winberg P, DeSitter K, Dotremont C, Mullens S, Vankelecom IFJ, Maurer FHJ, 2005. Free volume and interstitial mesopores in silica filled poly(1-trimethylsilyl-1-propyne) nanocomposites. *Macromolecules* 38: 3776-3782
- Wu AG, Yu LH, Li ZA, Yang HM, Wang EK, 2004. AFM investigation of large-circle DNA molecules. *Analytical Biochemistry* 325: 293-300
- Xiarchos I, Doulia D, 2006. Effect of nonionic surfactants on the solubilization of alachlor. *Journal of Hazardous Materials* 136 (3): 882-888

- XPS Peak 4.1, 2001. <http://www.phy.cuhk.edu.hk/~surface/XPSPEAK/>
- Yamazaki M, 1998. Medicinal Chemistry: Today and Tomorrow. Blackwell Science Ltd., Japan
- Yeom CK, Lee SH, Lee JM, 2000. Effect of the ionic characteristics of charged membranes on the permeation of anionic solutes in reverse osmosis. *Journal of Membrane Science* 169: 237-247
- Yiantsios SG, Karabelas AJ, 1998. The effect of colloid stability on membrane fouling. *Desalination* 188: 143-152
- Yoon Y, Westerhoff P, Snyder SA, Wert EC, Yoon J, 2007. Removal of endocrine disrupting compounds and pharmaceuticals by nanofiltration and ultrafiltration membranes. *Desalination* 202 (1-3): 16-23
- Zachee P, Snauwaert J, Vandenberghe P, Hellemans L, Boogaerts M, 1996. Imaging red blood cells with the atomic force microscope. *British Journal of Haematology* 95 (3): 472-481
- Zhang M, Song L, 2000. Mechanisms and parameters affecting flux decline in cross-flow microfiltration and ultrafiltration of colloids. *Environmental Science and Technology* 34: 3767-3773
- Zhang SH, Jian XG, Dai Y, 2005. Preparation of sulfonated poly(phthalazinone ether sulfone ketone) composite nanofiltration membrane. *Journal of Membrane Science* 246 (2): 121-126
- Zhu XH, Elimelech M, 1997. Colloidal fouling of reverse osmosis membranes: measurements and fouling mechanisms. *Environmental Science and Technology* 31: 3654-3662
- Zhu XH, Elimelech M, 1995. Fouling of reverse osmosis membranes by aluminum oxide colloids. *Journal of Environmental Engineering* 121: 884-892

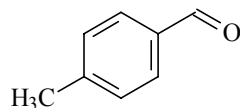
Appendix I: Chemical structure of uncharged organic components



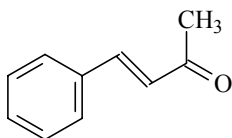
benzonitrile



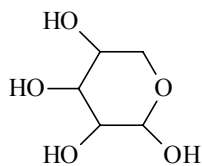
benzylalcohol



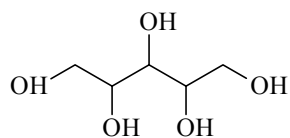
p-tolualdehyde



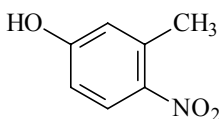
benzylidene acetone



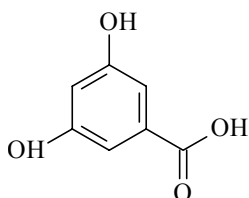
xylose



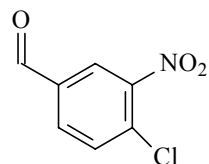
xylitol



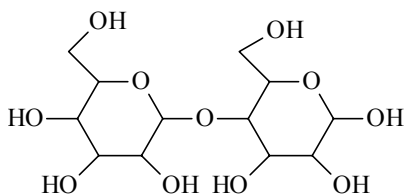
3,4-methylnitrophenol



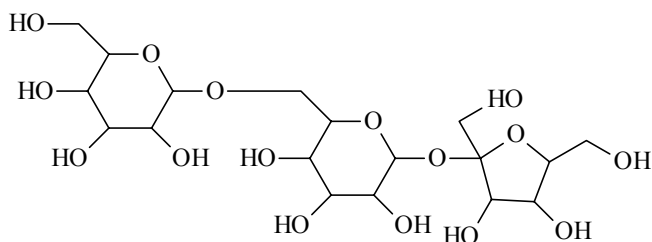
3,5-dihydroxybenzoic acid



4,3-chloronitrobenzaldehyde

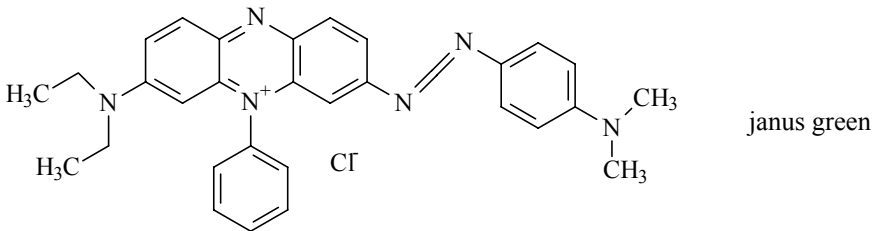
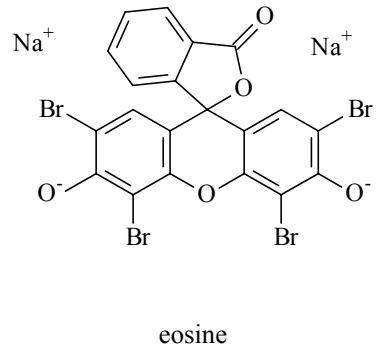
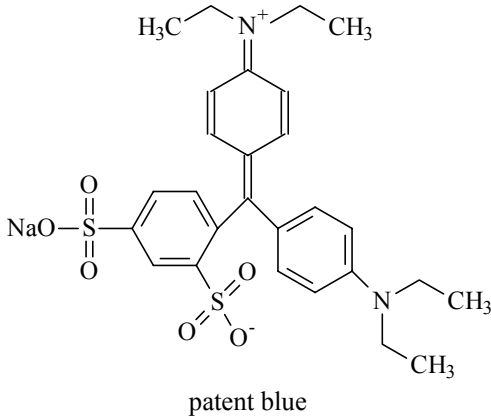
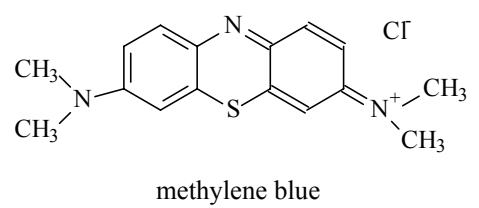
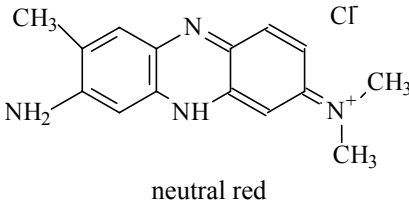
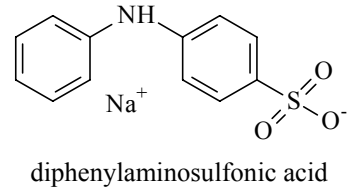
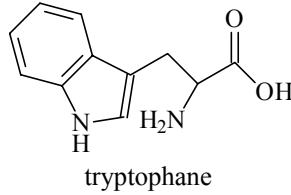
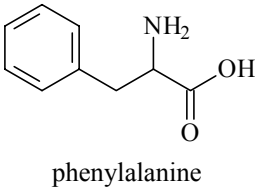
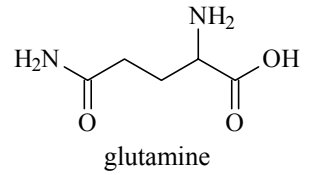
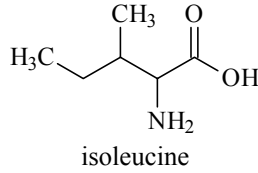
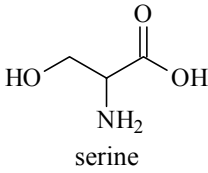


maltose

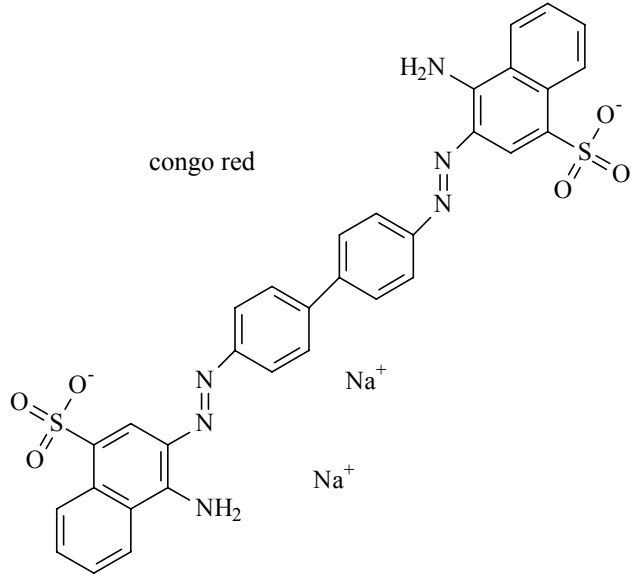
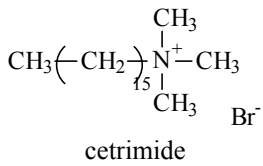
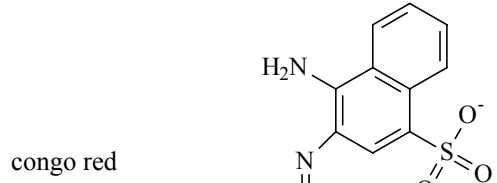
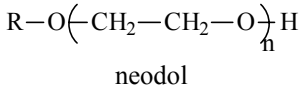
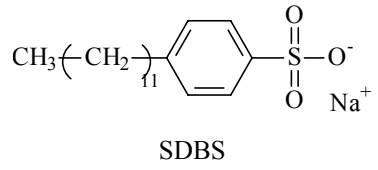
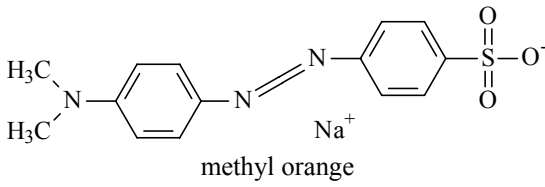


raffinose

Appendix II: Chemical structure of charged organic components



Appendix II



List of publications

Publications in peer-reviewed international journals

First author

Boussu K, Vandecasteele C, Van der Bruggen B, 2007. Relation between membrane characteristics and performance in nanofiltration. Submitted for publication

Boussu K, Van Baelen G, Coolen W, Eelen D, Vanassche S, Vandecasteele C, Van der Bruggen B, 2007. Technical and economical evaluation of water recycling in the carwash industry with membrane processes. Submitted for publication

Boussu K, Kindts C, Vandecasteele C, Van der Bruggen B, 2007. Surfactant fouling of nanofiltration membranes: measurements and mechanisms. *ChemPhysChem* 8: 1836-1845

Boussu K, De Baerdemaeker J, Dauwe C, Weber M, Lynn G, Depla D, Aldea S, Vankelecom IFJ, Vandecasteele C, Van der Bruggen B, 2007. Physico-chemical characterization of nanofiltration membranes. *ChemPhysChem* 8: 370-379

Boussu K, Belpaire A, Volodin A, Van Haesendonck C, Van der Meeren P, Vandecasteele C, Van der Bruggen B, 2007. Influence of membrane and colloid characteristics on fouling of nanofiltration membranes. *Journal of Membrane Science* 289: 220-230

Boussu K, Kindts C, Vandecasteele C, Van der Bruggen B, 2007. Applicability of nanofiltration in the carwash industry. *Separation and Purification Technology* 54: 139-146

Boussu K, Zhang Y, Cocquyt J, Van der Meeren P, Volodin A, Van Haesendonck C, Martens JA, Van der Bruggen B, 2006. Characterization of polymeric nanofiltration membranes for systematic analysis of membrane performance. *Journal of Membrane Science* 278: 418-427

Boussu K, Vandecasteele C, Van der Bruggen B, 2006. Study of the characteristics and the performance of self-made nanoporous polyethersulfone membranes. *Polymer* 47: 3464-3476

Boussu K, Van der Bruggen B, Volodin A, Van Haesendonck C, Delcour JA, Van der Meeren P, Vandecasteele C, 2006. Characterization of commercial nanofiltration membranes and comparison with self-made polyethersulfone membranes. *Desalination* 191 (1-3): 245-253

Boussu K, Van der Bruggen B, Vandecasteele C, 2006. Evaluation of self-made nanoporous polyethersulfone membranes, relative to commercial nanofiltration membranes. *Desalination* 200: 416-418

Boussu K, Van der Bruggen B, Volodin A, Snauwaert J, Van Haesendonck C, Vandecasteele C, 2005. Roughness and hydrophobicity studies of nanofiltration membranes using different modes of AFM. *Journal of Colloid and Interface Science* 286: 632-638

Co-author

De Baerdemaeker J, Boussu K, Dauwe C, Weber M, Lynn KG, Van der Bruggen B, 2007. Revealing nanofiltration principles using positronium atoms. Submitted for publication

De Baerdemaeker J, Boussu K, Djourelov N, Van der Bruggen B, Dauwe C, Weber M, Lynn KG, 2007. Investigation of nanopores in nanofiltration membranes using slow positron beam techniques. *Physica Status Solidi C* 4 (10): 3804-3809

Van der Bruggen B, Jansen JC, Figoli A, Geens J, Boussu K, Drioli E, 2006. Characteristics and performance of a "universal" membrane suitable for gas separation, pervaporation, and nanofiltration applications. *Journal of Physical Chemistry B* 110 (28): 13799-13803

Geens J, Boussu K, Vandecasteele C, Van der Bruggen B, 2006. Modelling of solute transport in nonaqueous nanofiltration. *Journal of Membrane Science* 281 (1-2): 139-148

Braeken L, Bettens B, Boussu K, Van der Meeren P, Cocquyt J, Vermant J, Van der Bruggen B, 2006. Transport mechanisms of dissolved organic compounds in aqueous solution during nanofiltration. *Journal of Membrane Science* 279 (1-2): 311-319

Braeken L, Boussu K, Van der Bruggen B, Vandecasteele C, 2005. Modelling of the adsorption of organic compounds on polymeric nanofiltration membranes in solutions containing two compounds. *ChemPhysChem* 6: 1606-1612

Cornelis G, Boussu K, De Vreese I, Van der Bruggen B, Vandecasteele C, 2005. Nanofiltration of nonionic surfactant solutions: effect of molecular weight cut-off and hydrophilicity on flux behaviour. *Industrial and Engineering Chemistry Research* 44: 7652-7658

Van der Bruggen B, Boussu K, De Vreese I, Van Baelen G, Willemse F, Goedemé D, Colen W, 2005. Industrial process water recycling: principles and examples. *Environmental Progress* 24: 417-425

Contribution to international conferences

Oral presentations

Boussu K, Van Baelen G, Coolen W, Eelen D, Vanassche S, Vandecasteele C, Van der Bruggen B, 2007. Technical and economical evaluation of water recycling in the carwash industry with membrane processes. The 6th Conference on Wastewater Reclamation and Reuse for Sustainability (WRRS 2007), Antwerp (Belgium), October 9-12

De Baerdemaeker J, Boussu K, Djourellov N, Van der Bruggen B, Dauwe C, Weber M, Lynn KG, 2006. Investigation of nanopores in nanofiltration membranes using slow positron beam techniques. The 14th International Conference on Positron Annihilation (IPCA 14), Hamilton (Canada), July 23-28

Boussu K, Van der Bruggen B, Volodin A, Van Haesendonck C, Delcour JA, Van der Meeren P, Vandecasteele C, 2005. Characterization of commercial nanofiltration membranes and comparison with self-made polyethersulfone membranes. International Congress on Membranes (ICOM), Seoul (Korea), August 21-26, Proceedings Volume I, 217-218

Boussu K, Braeken L, Van der Bruggen B, Vandecasteele C, 2004. Fouling of nanofiltration membranes: experimental observation and modelling of adsorption of organic compounds. The VII CST Workshop: Fouling and Critical Flux (FCF '04), Lappeenranta (Finland), June 16-18

Poster presentations

Boussu K, Van der Bruggen B, Vandecasteele C, 2006. Study of the characteristics and the performance of self-made and commercial polyethersulfone nanofiltration membranes. Poster presented at Euromembrane, Messina (Italy), September 24-28

Boussu K, Van der Bruggen B, Vandecasteele C, 2005. Study of the characteristics and the performance of self-made and commercial polyethersulfone nanofiltration membranes. Poster presented at the Annual NMG meeting, Ede (The Netherlands), October 27

Scientific award

European Membrane Society (EMS) award for the Best Young Scientist's Presentation "Fouling of nanofiltration membranes: experimental observation and modelling of adsorption of organic compounds" at the VII CST Workshop: Fouling and Critical Flux '04, Lappeenranta University of Technology, Lappeenranta, Finland, June 16-18, 2004

Publications in national journals

Cornelis G, Boussu K, De Vreese I, Van der Bruggen B, Vandecasteele C, 2005. Nanofiltratie voor zuivering van afvalwaters die niet-ionische surfactanten bevatten. Afvalwaterwetenschap jaargang 4: 77-85

Curriculum vitae

Katleen Boussu was born on August 30th, 1980 in Hasselt (Belgium). She followed her secondary education at Humaniora Virga Jesse (Hasselt) and got her degree in Sciences and Mathematics in 1998. From 1998 till 2003, she attended the Katholieke Universiteit Leuven, from which she obtained a Chemical Engineering degree at the Faculty of Engineering summa cum laude with felicitations of the jury. She performed her master thesis in the Laboratory of Applied Physical Chemistry and Environmental Technology supervised by professor Bart Van der Bruggen and professor Carlo Vandecasteele. In 2003, she started a PhD in the same research group under the same supervisors with a fellowship of the Institute for Promotion of Innovation by Science and Technology in Flanders (IWT-Vlaanderen). The experimental work on the fouling degree of nanofiltration membranes resulted in the present thesis.

